



Leibniz University of Hannover
Institute of Photogrammetry
and GeoInformation (IPI)



Landcover Mapping of Banda Aceh, Indonesia, using Optical and SAR Satellite Imagery

Diploma Thesis
of the study course
Geodesy and Geoinformatics

by
Marc Schmitz
Matr.-No.: 2292830

Tutor:

Dr.-Ing. Peter Lohmann

Prof. Dr.-Ing. Uwe Sörgel

In cooperation with the Federal Institute for Geosciences and Natural Resources (BGR)



Summary

Currently the Federal Institute for Geosciences and Natural Resources (BGR) processes at the present time a project of technical cooperation with Indonesia with the objective of the geoscientific support of sustainable reconstruction for the region of Banda Aceh. The main discussion topics are among ground ratings, georisk management (landslides, volcanic eruptions, earthquakes, floods and tsunami), natural resources analysis and hydrogeological workings. Remote sensing is used to support the mentioned tasks with relevant data.

In this diploma thesis it has to be shown how far a land use classification can be improved by the fusion (pixel- und object-based) of optical and SAR remote sensing data. Thereby has showed that the combination of optical data and SAR radar offers difficulties.

In the pixel-based approach it could be demonstrated that beside two common fusion methods (PCA and Multiplicative) and a newer fusion technique from Ehlers (2005) no improvements could be obtained in comparison to the optical SPOT 5 data, which was used as reference, as well spectrally as in the classification result. The Ehlers Fusion is able to preserve the spectral and radiometric features as best, but the whole potential of this fusion technique could not be exploited mainly because of the high requirements of coregistration in the geocoding process (subpixel accuracy). The PCA Transform seems to be an alternative of the common fusion methods, but it is presented that it is advantageous, if the SAR data show a high correlation to the optical data as much as possible. The simply multiplication is the worst alternative as well spectrally as in the classification result.

In case of the object-based approach it has been shown that a global improvement in the classification result by using additional radar information is hardly to reach and only in case of good conditions, for example at same acquisition time. The use of Haralick texture features of the SAR data in eCognition caused rather a degradation in the classification result due to the fact that the texture features are only calculated in the segments, which size is limited. This is a real disadvantage for a data set with lower resolution, as it could be demonstrated in the data set of ASTER and Envisat ASAR. The feature of the standard deviation offered a good alternative in case of this data set, because a global improvement could be obtained.

Nethertheless, it has to be mentioned that the classification result of the SPOT 5 reference data set was quite good and therefore the potential of improvement for radar data is quite low, especially by the use of additional information as artificial bands. Here, it could be displayed that the result could be improved by using additional information, for example elevation information. Thus a classification gain could be obtained as well in the pixel-based as in the object-based approach. In comparison to each other it could be shown that the segment-based indicates more benefits caused by the fact that additional features like shape and class relations can be used. In this case the object-based classification offers the best way to achieve an improvement in the classification by the use of additional radar information.

Zusammenfassung

Die Bundesanstalt für Geowissenschaften und Rohstoffe (BGR) bearbeitet gegenwärtig ein Projekt der technischen Zusammenarbeit mit Indonesien mit dem Ziel der geowissenschaftlichen Unterstützung des sicheren Wiederaufbaus der Region Banda Aceh. Schwerpunktthemen sind dabei unter anderem Baugrundbewertungen, allgemeine Risiken und Gefahren (Hangrutschungen, seismische und vulkanische Risiken, Überschwemmungen, Tsunamis, etc.), rohstoffwirtschaftliche Analysen und hydrogeologische Arbeiten. Die Fernerkundung wird eingesetzt, um die genannten Themenbereiche mit relevanten Informationen zu unterstützen.

Im Rahmen des Diplomarbeitsthemas soll untersucht werden, inwieweit eine Landnutzungsklassifizierung (pixel- und objektbasiert) durch Verschneidung von optischen Daten und Radardaten effizienter und genauer gestaltet werden kann. Dabei hat sich gezeigt, dass die Kombination von optischen Daten und SAR Radardaten sich als sehr schwierig erweist.

Im pixelbasierten Ansatz konnte demonstriert werden, dass neben zweier gewöhnlicher Fusionsmethoden (PCA und Multiplicative) und einer neueren Fusionsmethode von Ehlers (2005) im Vergleich zu einem rein optischen Referenzdatensatz keine Verbesserungen sowohl radiometrisch als auch im Klassifizierungsergebnis erreicht werden konnte. Die Ehlers Fusion erhält die radiometrischen Eigenschaften am besten, jedoch konnte die ganze Bandbreite dieses Ansatzes aufgrund von hohen Genauigkeitsansprüchen bei der Geocodierung nicht umfassend getestet werden. Die PCA Transformation erscheint für gewöhnliche Fusionsmethoden eine Alternative zu sein, jedoch zeigt sich, dass es vorteilhaft ist, wenn die SAR Daten eine möglichst hohe Korrelation zu den optischen Daten aufweisen. Die einfache Multiplikation ist die schlechteste Alternative sowohl radiometrisch als auch im Klassifizierungsergebnis.

Bei der objektbasierten Klassifizierung hat sich ebenfalls erwiesen, dass eine globale Verbesserung im Klassifizierungsergebnis durch zusätzliche Radarinformationen nur sehr schwer zu erreichen ist und das nur bei günstigen Bedingungen beispielsweise gleicher Aufnahmezeit. Die Einbeziehung von Texturmerkmalen der SAR-Daten nach Haralick in eCognition verursachte eher eine Verschlechterung im Klassifizierungsergebnis aufgrund der Tatsache, dass die Texturmerkmale nur in den Segmenten berechnet werden, deren Größe begrenzt ist. Gerade bei einem Datensatz mit gröberer Auflösung ist dies von Nachteil, wie sich beim Datensatz von ASTER und ENVISAT ASAR gezeigt hat. Das Merkmal der Standardabweichung erwies sich jedoch bei diesem Datensatz als eine gute Alternative, da hiermit eine globale Verbesserung erzielt wurde.

Jedoch muss auch erwähnt werden, dass allein mit dem optischen SPOT-5 Referenzdatensatz ein gutes Klassifizierungsergebnis erreicht wurde und dadurch das Verbesserungspotenzial durch Radardaten eher gering war, insbesondere bei der Einbeziehung von zusätzlichen wissensbasierten Informationen aus künstlichen Kanälen. Hierbei hat sich gezeigt dass durch zusätzliche Informationen wie beispielsweise Höheninformationen das Ergebnis deutlich verbessert werden kann. So konnte sowohl im pixelbasierten als auch im objektbasierten Ansatz eine Verbesserung erreicht werden. Im Vergleich der beiden Ansätze untereinander konnte gezeigt werden, dass der objektbasierte Ansatz besser abschneidet, aufgrund der Tatsache, dass zusätzliche Merkmale im Bezug auf die Form, Gestalt und Nachbarschaftsbeziehungen zu anderen Klassen eingesetzt werden können. Die objektbasierte Klassifizierung erweist sich in diesem Fall als die beste Möglichkeit, eine Genauigkeitssteigerung bei der Klassifizierung unter Verwendung zusätzlicher Radarinformationen zu erreichen.

Declaration

Certified herewith I declare that I have made this Diploma Thesis self dependent and by the using of the employment of the bibliographical reference and resources.

Hannover, May 2007

(Marc Schmitz)

Acknowledgement

I wish to thank Mr. Dr. F. Kühn in the Department of Remote Sensing of the Federal Institute for Geosciences and Natural Resources who offered this cooperation with the BGR and provided the satellite imagery.

Also I wish to thank Mr. Dr. U. Schäffer and Mr. F. Schwonke who have assisted me in the Department of Remote Sensing during this thesis.

A special thank be valid to Mr. A. Hoffmann-Rothe, who gave me the chance to run a project in Banda Aceh and who always sides with me in difficulties and formalities.

Furthermore I wish to thank Mr. T. Rehmann and his colleague they have regrets by my sojourn in Banda Aceh and as well as the local assistants of the bureau of BGR in Banda Aceh.

Index

1	Introduction	4
1.1	Sumatra-Andamanen Earthquake	4
1.2	Management of Georisks in the Province Aceh	4
1.3	Aim of this thesis	5
1.4	Test area of Band Aceh	5
2	Basics.....	7
2.1	Land cover and land use	7
2.2	Optical and multi-spectral remote sensing data.....	7
2.2.1	Radiometric features.....	7
2.2.2	Factors influencing radiometric features	7
2.3	Basics of Radar remote sensing.....	8
2.3.1	Introduction into Radar remote sensing	8
2.3.2	Imaging Radar	9
2.3.3	Side-looking Radar	9
2.3.4	Synthetic Aperture Radar	10
2.3.5	Characteristics of SAR	12
2.3.6	Special characteristics of microwaves.....	15
3	Digital image fusion	19
3.1	Definition.....	19
3.2	Applications of image fusion.....	19
3.3	Level of image fusion.....	20
3.4	Pixel-based image fusion techniques.....	20
3.4.1	RGB Band combination	20
3.4.2	Arithmetic combination.....	21
3.4.3	Colour-space transforms.....	22
3.4.4	Statistical methods.....	22
3.4.5	Spatial transforms.....	23
3.5	Problems of image fusion techniques.....	24
4	Data used and Pre-processing.....	25
4.1	Optical sensor	25
4.1.1	ASTER	25
4.1.2	SPOT	26
4.2	SAR Sensor	27
4.2.1	Envisat ASAR	27
4.2.2	Radarsat	27
4.3	Initial data set	28
4.3.1	Initial optical data set.....	28
4.3.2	Initial SAR data set.....	28
4.3.3	Ancillary data	29
4.3.4	Overview of all scenes.....	30
4.4	Data pre-processing	30
4.4.1	Pre-processing of the optical data.....	31
4.4.2	Pre-processing of the SAR data.....	33
4.5	Data preparation	35
4.5.1	First data set of January / April / May 2005	35
4.5.2	Second data set of January 2005	36
5	Generation of the classification system.....	37
5.1	Classification systems	37
5.2	Definition of the classification system	37

5.3	Definition of the map scale.....	37
5.4	Definition of the categories and classes	38
5.5	Description of the classes	39
5.5.1	A - Agriculture	39
5.5.2	U – Urban	42
5.5.3	S - Soil	48
5.5.4	V – Vegetation.....	52
5.5.5	W – Waterbodies	56
6	Pixel-based image fusion of optical and SAR data	59
6.1	Multi-spectral classification of the optical SPOT 5 data.....	59
6.1.1	Optical SPOT 5 data.....	59
6.1.2	Classes	59
6.1.3	Supervised Classification	61
6.1.4	Selection of samples	61
6.1.5	Analysis of spectral signature.....	62
6.1.6	Maximum-Likelihood-Classification	63
6.1.7	Additional knowledge-based information	63
6.2	Pixel-based image fusion.....	66
6.2.1	Selection of image fusion methods.....	66
6.2.2	Knowledge-based classification	69
6.2.3	Visual comparison	70
6.2.4	Statistical comparison.....	71
6.2.5	Absolute accuracy assessment.....	71
6.3	Discussion of the fusion methods.....	76
6.4	Fusion of the second data set.....	77
7	Object-based Classification	80
7.1	Segmentation and classification in eCognition	80
7.1.1	Segmentation in eCognition	80
7.1.2	Classification in eCognition	82
7.2	Object-based Classification of the SPOT 5 Data.....	84
7.2.1	Segmentation	84
7.2.2	Supervised Classification with Nearest Neighbour	84
7.2.3	Knowledge-based information with Membership Function.....	88
7.2.4	Modelling of the knowledge-based rules.....	89
7.3	Object-based Classification with additional Radarsat SAR data.....	95
7.3.1	Integration of optical data and Radarsat data by segmentation.....	95
7.3.2	Integration of radar texture features into Nearest Neighbour.....	96
7.3.3	Accuracy Assessment.....	98
7.3.4	Evaluation of the results	101
7.4	Integration of radar texture features into Membership Function.....	102
7.4.1	Modelling	102
7.4.2	Accuracy Assessment.....	104
7.5	Object-based Classification of the ASTER and Envisat data.....	105
7.5.1	Object-based Classification of the optical ASTER data.....	105
7.5.2	Radarsat data integration into Nearest Neighbour.....	105
7.5.3	Accuracy Assessment.....	105
7.5.4	Evaluation of the results	106
8	Ground check and final map.....	108
8.1	Reason for a ground check	108
8.2	Local ground check	108
8.3	Analysis of the ground check	109

8.4	Results of the ground check	109
8.5	Editing the final map	110
9	Evaluation of the classification results	111
10	Prospects	113
11	References	114
12	Annex	119
12.1	Spectral signatures of the pixel-based approach (SPOT 5)	119
12.2	Rules and criteria in the pixel-based approach	124
12.3	Results of the pre-calculation for the IHS Transform	126
12.4	Results of the PCA Transform (SPOT, Radarsat)	127
12.5	Results of the PCA Transform (ASTER, Envisat)	128
12.6	Results of the pixel-based classification approach	129
12.7	Results of the object-based classification approach	136
12.8	Knowledge-based rules of the object-based classification	143
12.9	Confusion Matrices of the Object-based approach with 17 classes	145

1 Introduction

1.1 Sumatra-Andamanen Earthquake

On 26th December in 2004 at 1.58 Central European Time the *Sumatra-Andamanen Earthquake* hit with a magnitude of 9.0 (BGR, 2006) the Indonesian island Sumatra. The epicentre was located about 250 km south of the city Banda Aceh underneath the Sunda trench in the Eastern Indian Ocean, where two of the earth's tectonic plates meet (Fig.1.1, yellow star). The undersea earthquake caused a series of devastating water waves, so-called *Tsunami*, (jap.: *tsu* = Harbour, *nami* = Wave), which struck in addition to the Indonesian islands Sumatra also the coasts of Thailand, Malaysia, India, Sri Lanka and even East-Africa. The waves destructed areas near the coast. A lot of material damage and damage to persons had been complained.

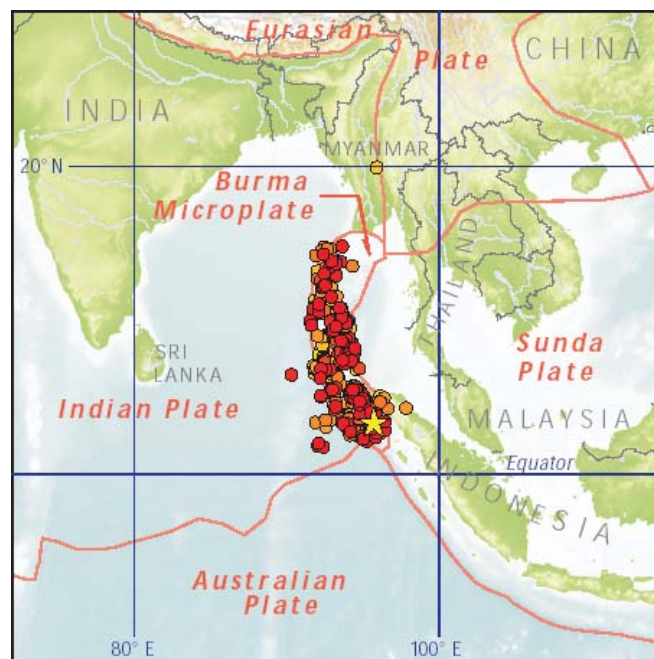


Figure 1.1: Location of the epicentre of the earthquake of 26th December 2004 (yellow star) and of the more than 100 aftershocks with a magnitude > 5.0 (orange and red dots) (BGR, 2006)

1.2 Management of Georisks in the Province Aceh

The Tsunami-disaster struck the city of Banda Aceh at Northern Sumatra very hard. It caused the loss of life of more than 120,000 people, the missing of more than 110,000 people and the destruction of about 80 % of all private houses, basic infrastructure and public facilities in the coastal region of Aceh Province (BGR, 2006).

The Banda Aceh Project *Management of Georisks in the Province Aceh* is an international cooperation between the Federal Institute for Geosciences and Natural Resources (BGR) and several Indonesian institutions where geological background information and guidelines for sustainable local disaster reduction will be given to regional and town planners. This includes information about georisk assessment (floods, volcanic eruptions, landslides, earthquakes and tsunami), construction of raw materials with identification of suitable building materials (e.g. sand, limestone) and hydrogeology for the identification of freshwater resources. Remote sensing is used to support the mentioned tasks with relevant data.

1.3 Aim of this thesis

As support and additional information for the georisks management in the Province Banda Aceh a land use map based on remote sensing data is to be generated. The land use map serves as decision guidance concerning the sustainable reconstruction of settlement areas and geological questions. In addition to the optical remote sensing data SAR remote sensing data are to be implemented.

In this diploma thesis it has to be shown how far a land use classification can be improved by the fusion of optical and SAR remote sensing data. In the first step it is attempted to investigate and analyse several data fusion methods for optical and SAR data in a pixel-based approach supported by additional knowledge-based information. In the second step it is intended, in a object-based approach also by using additional knowledge-based information, to accomplish the actual land use classification on the test area. In the third step the results have to be verified and improved by a local ground check. The end product is an updated analogue and digital land use map of Banda Aceh und region. The digital map is to be integrated in a Geographic Information System (GIS).

1.4 Test area of Band Aceh

The province Aceh with the capital Banda Aceh is located in Northern Sumatra (Indonesia). The maximum extension is about 85 x 70 km. According to the given original and reference data a part of this region with extensions of 26.85 x 25.5 km (Fig. 1.2, red square) was chosen as test area. It includes the city of Banda Aceh and ranges in north-south direction from the north coast to a big cement factory and in west-east direction from the west coast to the airport and foothills.



Figure 1.2: Test area for the classification at Northern Sumatra (Google Map, 2007)

The city Banda Aceh is located at the mouth of the river Aceh into the Indian Ocean (Fig.1.2). The delta area of the river Aceh, which is bounded by the last foothills of the Barisan range in the east and west, is characterized by a mixture of tropical evergreen forest, plantations, paddy fields and sparse settlement. At the flat coast dense settlement is dominating. The west foothills are mostly covered with dense rainforest while the east foothills are signified by rather mixed and sparse vegetation including areas of slash and burn.

The agriculturally used area is multipurpose. The plantations which are mostly located near the river Aceh and the foothills are cultivated with coconuts, mangos, melons and bananas. On the plantations itself smaller cattle-breeding is not unusual. But the biggest part of the agriculture in the Province Aceh is used for the cultivation of paddy. The paddy fields are in general segmented in small (about 10 x 10 to 30 x 30 m) rectangle plots (Fig.1. 3, right). So-called wet rice is grown, that means the paddy is cultivated on plane ground first and then later flooded. Rice itself is not a water plant, but it has been adapted to this type of farming by breeding, because of the flooding weed and pest can be avoided. The rice plant belongs to the category of sweet grass (*Poaceae*) with wide leaves and long panicles (Fig. 1.3, left). The rice seeds are located inside the panicles, which can be harvested up to three times a year.



Fig. 1.3: left: Rice plant with panicles, right: typical plot structure for paddy fields in the province Aceh

The cultivation of paddy can be distinguished into five periods:

- sowings of the germ buds in a save, dry bed
- mixture of the soil of the planned paddy field with water
- moving of the seedling from the bed and planting into the paddy field by hand
- regular flood irrigation of the paddy field during the growing and maturity time
- harvest of the panicles

Because of the different periods the paddy fields show very different spectral behaviour, for example, in case of wet and dry paddy fields or in different stages of maturation of the plant. This has to be considered during a classification process.

2 Basics

2.1 Land cover and land use

In the domain of classification with remote sensing data two expressions are often been used interchangeably: *land cover* and *land use*. But it is important to be aware that these two expressions are not necessarily the same. Land cover is restricted to the natural and artificial compositions covering the earth's surface at a certain location (Avery and Berlin, 1992), while potential meaning of the area for human applications is not considered. The latter aspect is covered by the term land use, beyond the pure physical characteristics and meanings of a surface (Geßner, 2005). In most cases the land cover can be detected in remote sensing data directly. However, during mapping of classes land use aspects can be inferred indirectly based on context knowledge of the interpreter.

During this work a distinction between these expressions was made by defining the classes and generating the map. Thus the generated map is not an absolute land use map but rather a mixture of land use and land cover map.

2.2 Optical and multi-spectral remote sensing data

2.2.1 Radiometric features

Basic elements of optical and multi-spectral data are the characteristics of radiometric features. Such remote sensing data include information about the radiation in several different wavelengths which is received by the sensor. The spectrum of the wavelengths reaches from visible (VIS), near infrared (NIR) and short-wave infrared (SWIR) to thermal infrared (TIR). The single spectral ranges are called bands. Every band can be displayed as one layer whereas every pixel of this layer can be assigned to one radiance or reflection value of the relative wavelength. In case of optical remote sensing visual and infrared spectrum are covered.

2.2.2 Factors influencing radiometric features

The radiometric information content of optical remote sensing data is affected by several factors of influence. Besides sensor features, such as spectral and spatial resolution, the reflection of the detected object, the geometry of monitoring and illumination as well as transport of radiation through the atmosphere between object and sensor are important. In the following only the reflection of the detected object is briefly discussed.

The figure 2.1 shows, for example, the reflectance spectrum of several surface types for the wavelength interval between 410 nm and 910 nm. The typical qualitative characteristics of reflection of vegetation are easy to understand by the displayed spectral signature. In the visible spectrum between 400 nm and 700 nm the reflectance is significant low because of the absorption of leaf pigments like chlorophyll a and b. The relative maximum at the range of 550 nm is caused by less absorption of green wavelength by chlorophyll. In the range of near-infrared between 700 nm and 1300 nm the reflection of plants is high. In this range the reflected radiation depends on the cell structure and their orientation with respect to the incoming radiation direction (Reinartz, 1998).

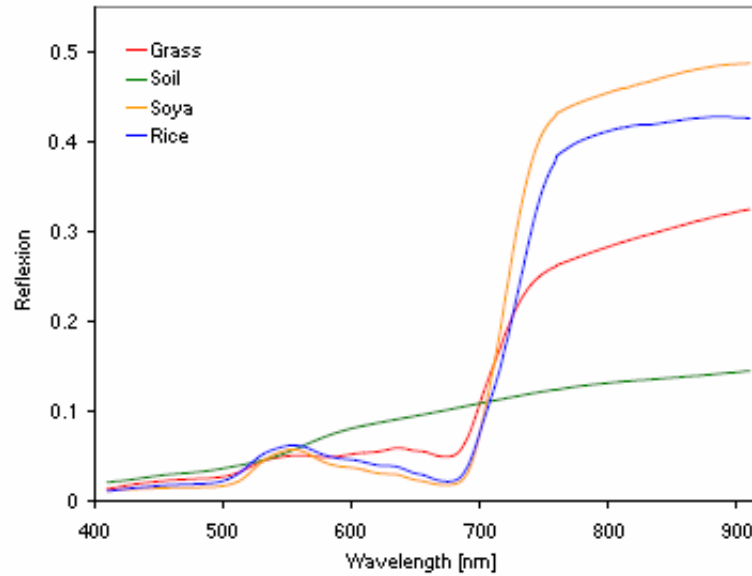


Figure 2.1: Spectrum of reflection of different land cover types (Geßner, 2005)

The characteristics of reflection of objects from the earth's surface are influenced by material, physical condition and surface nature. In order to distinguish between different types of land cover by using satellite images, significant variations of the reflection of the separate objects have to be measured. For example in figure 2.1 the spectral signatures of soil and grass vary significantly so that they can be distinguished. On the other hand paddy and soya are very similar to each other. In cases like this difficulties in multi-spectral classification processes are to be expected. These difficulties can be reduced by increasing the spectral resolution. This can be achieved by using additional multi-spectral bands in case of a spectrometer or bands from the microwave spectrum by the use of radar images.

2.3 Basics of Radar remote sensing

2.3.1 Introduction into Radar remote sensing

The term *RADAR* was coined in 1941 as an acronym for *Radio Detection and Ranging*. It is in contrast to optical remote sensing an active system. Generating electromagnetic waves by itself, a radar unit transmits short pulses or bursts of microwave radiation and then receives the reflection of the signal from the scene. The reflected component is called *echo* or *backscatter* (Avery and Berlin, 1992). The transmitted radiation is in the microwaves domain in a frequency range between 1 and 100 cm (Fig. 2.2). The spectrum of the microwaves is divided into bands (e.g. X-Band). Signal of larger wavelength (starting from approximately 3 cm, X-Band) is virtual independent from the weather and able to penetrate clouds, steam and smoke. This is a big advantage in contrast to the optical remote sensing systems. Another advantage is the fact that the radiation of the microwaves is able to penetrate partly into natural materials of the surface. Furthermore, surface roughness and the moisture content of the scattering medium can be examined.

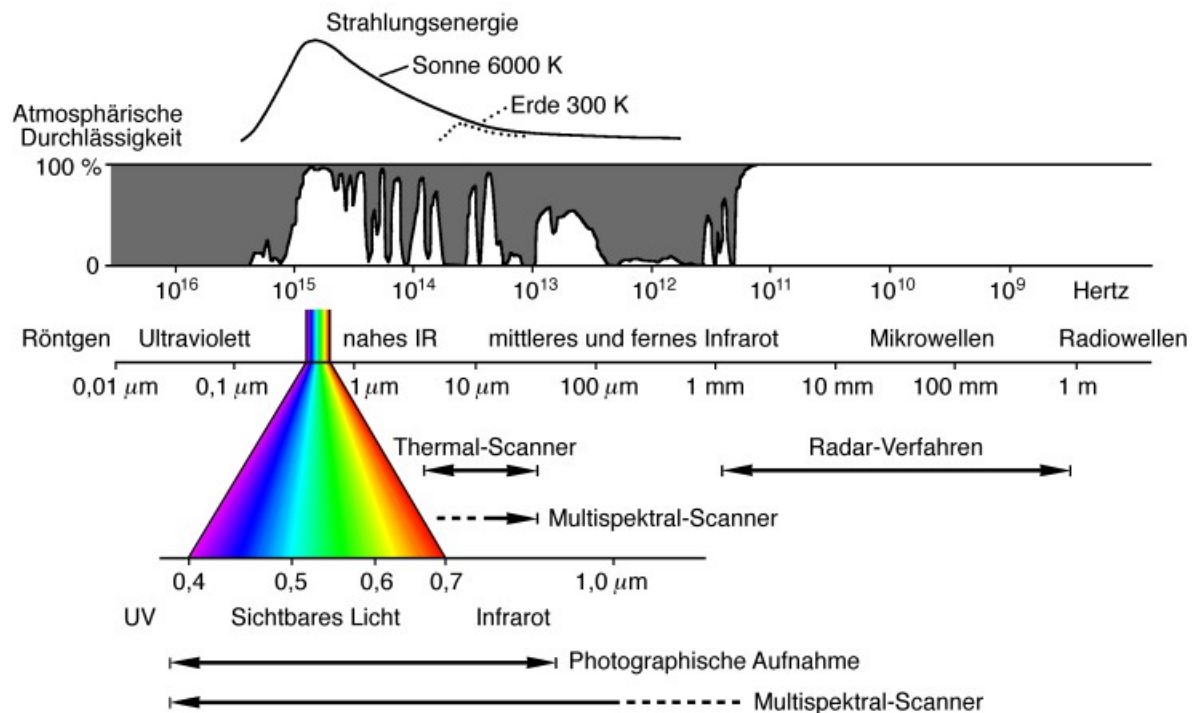


Fig. 2.2: Electromagnetic spectrum (Albertz, 2001)

2.3.2 Imaging Radar

Imaging Radar is able to provide two-dimensional images of the scene. Important information about roughness, geometric structure and electric features of the Earth's surface and underneath can be derived from the backscatter.

Although both methods use electromagnetic waves, imaging radar systems differ basically from optical systems. Optical systems image like the human eye in a central perspective. Radar systems use a very different physical principle. The sensor transmits with a beam antenna vertical to flight direction (across-track) short waves of electromagnetic radiation. The part of the signal reflected from an object back towards the sensor is sampled. The distance from the sensor to the object is calculated from the signal time of flight between transmit and receive, in the directivity of the antenna defines *range direction* which coincides with the first image coordinate of the objects position. The second image coordinate, the position of the object in *azimuth direction* (along-track), is generated by simultaneous motions of the sensor in flight direction and constant transmitting of further signals. All the objects in the image are scattering a part of the incoming energy of the radar signal back to the sensor. After signal processing an individual backscatter intensity value can be assigned to every picture element.

2.3.3 Side-looking Radar

In contrast to optical systems the radar sensor is side-looking because of the large diffraction cone resulting from the long wavelength that is several orders of magnitude larger compared to visible domain. The radar pulse passes with the speed of light c (approximately 300,000 km/s) the distance from the sensor to the scattering object and backwards. Different objects can only be distinguished, if they are separated for enough in range and azimuth direction. In case of the same distance between two different objects a distinction it is no longer possible.

The resolution δ_r in range direction depends only on the effective length of the pulse τ or from the bandwidth W of the transmitted signal:

$$\delta_r = \frac{c \cdot \tau}{2} = \frac{c}{W \cdot 2}, \quad \tau \cdot W \approx 1 \quad (2.1)$$

Because of the geometric conditions the resolution in range direction, projected on the ground range, depends on the located illumination angle or incidence angle θ which is defined here between the nadir point of the sensor and the object (Fig. 2.3):

$$\delta_r = \frac{c \cdot \tau}{2 \cdot \sin \theta} \quad (2.2)$$

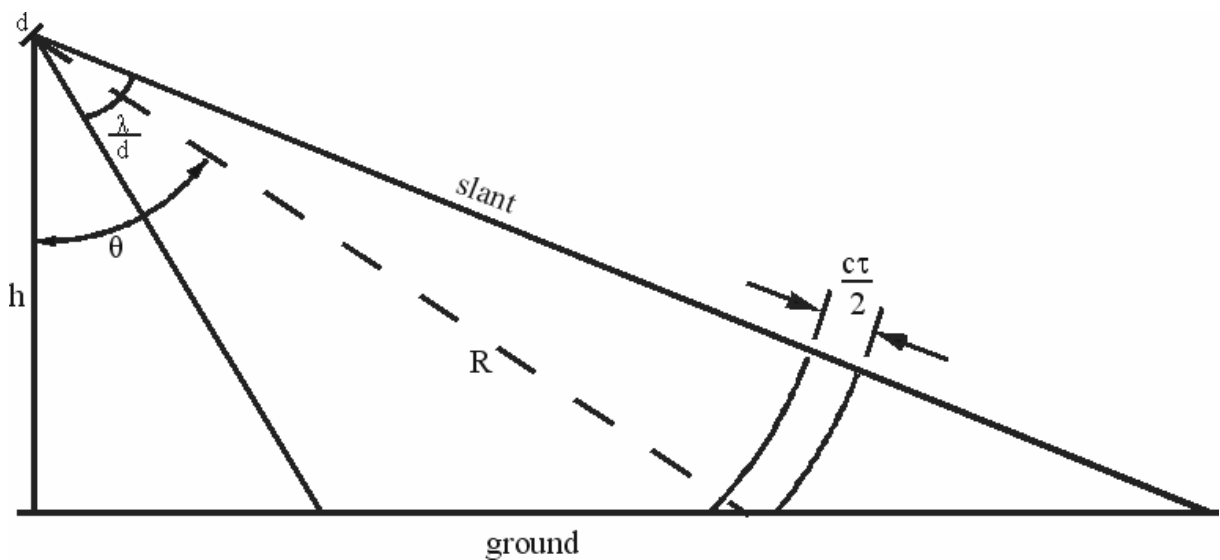


Figure 2.3: Resolution in range of a side-looking radar (Sörgel, 2003)

The resolution in azimuth on ground range δ_{ra} is given by the product of the angle resolution θ_a (diffraction) with the distance r . The given equation is only true for conventional Radar with Real Aperture (RAR).

$$\delta_{ra} = \theta_a \cdot r \approx \frac{\lambda \cdot r}{D} \quad \text{with} \quad \theta_a \approx \frac{\lambda}{D} \quad (2.3)$$

λ = Wavelength

D = Antenna size in Azimuth

2.3.4 Synthetic Aperture Radar

An improvement of the resolution in azimuth direction for a given range can be achieved either by reducing the wavelength or by enlarging the antenna. Both factors can only be adjusted at limited degree to ensure all-weather capability the minimum wavelength suitable for remote sensing is approximately 1 cm and antenna size is bounded by the physical dimensions of the sensor carrier.

Synthetic Aperture Radar (SAR) is a technique to achieve high azimuth resolution despite using a small antenna. By signal processing of many radar pulses a virtual long antenna is synthetically established. Alternating microwave pulses are transmitted across the track with pulse repetition frequency (PRF) and the received signals are stored. Thus an object on the ground, as long as it is inside of the illuminated area, is irradiated several times (Sörgel, 2003), like it is shown in figure 2.4. During processing the pulses gathered separately along sensor track can be treated as signals of different antenna elements of a very long antenna located at the related sensor positions each. The received signals are correlated twice with the transmit pulse, from these so-called in-phase and quadrature elements the relative Doppler frequency shift of the resulting phasor can be derived. This shift is used to integrate all signal contributions of an individual point scatter into the correct range/azimuth image pixel. The frequencies of the radar echo are higher as long as the sensor is approaching to the object and lower when heading away of it compared to the transmitted radar pulse (Bayer, 1990). At the moment of pass by the object the Doppler frequency shift is null. If the phase relations between the pulses are stable and known (coherent radar), a synthetic aperture can be calculated from all signals.

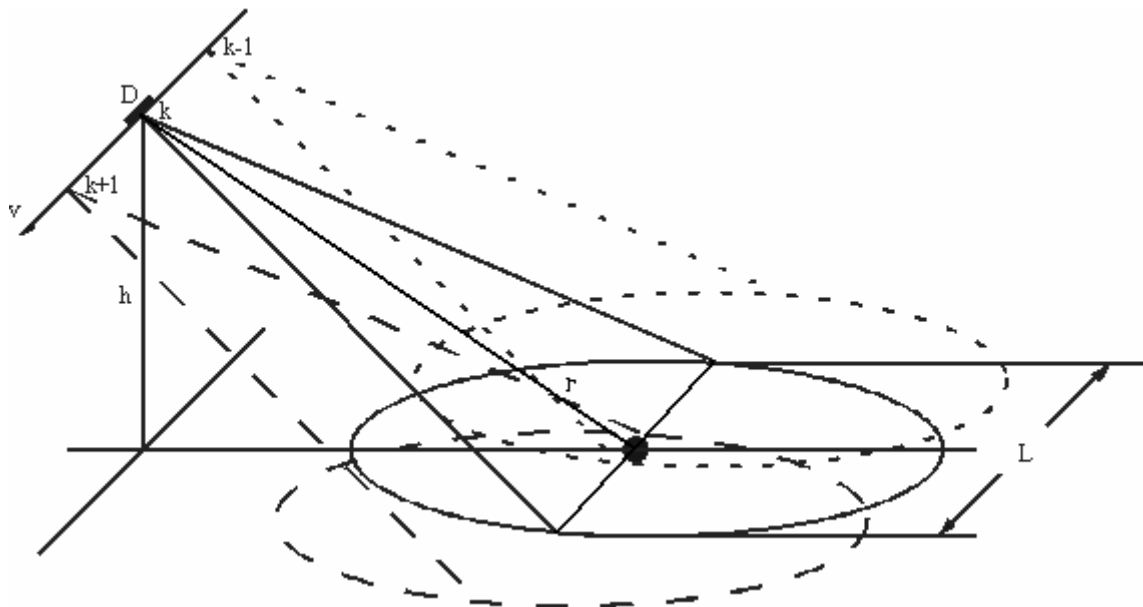


Figure 2.4: Resolution in azimuth in case of a SAR (Sörgel, 2003)

The maximum length L_s of the synthetic aperture coincides to the width of the real aperture antenna footprint that is shifted pulse per pulse over the scene. Thus, L_s is equal to the product of the angle resolution of the real aperture δ_{ra} and the distance r :

$$L_s = \delta_{ra} \approx \frac{\lambda \cdot r}{D} \quad (2.4)$$

In the case of real aperture radar an object in the far field is illuminated by a planar phase front, the phase gradient is only generated on the way back to the sensor (from target to sensor), whereas for SAR the single elements (i.e. the real antenna) are transmitting separately and one after the other. Therefore, the way from sensor to target has to be considered, too, and the phase shift is twice as big as against the real aperture case.

$$\theta_{SAR} = \frac{\lambda}{2 \cdot L_s} \quad (2.5)$$

The maximum angle resolution of the synthetic aperture θ_{SAR} is derivable from the two equations above (2.4 and 2.5). The length of the synthetic aperture is proportional to the distance of the scatter and reverse proportional to the real aperture length:

$$\theta_{SAR} = \frac{D}{2 \cdot r} \quad (2.6)$$

Because of the synthetic aperture length's, L_s , linear dependency of range r , the distance term cancels out in the equation for the azimuth resolution of SAR (Fig. 2.7).

$$\delta_{SAR} = \theta_{SAR} \cdot r \approx \frac{\lambda \cdot r}{2 \cdot L_s} \approx \frac{D}{2} \quad (2.7)$$

Thus the maximum resolution of the synthetic aperture δ_{SAR} corresponds to the maximum resolution of SAR in azimuth direction δ_a and is equal to the half length of the antenna in azimuth. direction. It is independent from the distance.

2.3.5 Characteristics of SAR

Geometric aspects

As mentioned before, the synthetic aperture radar principle requires side-looking illumination (Albertz, 2001). In a simplified manner SAR can be described as a distance measurement with high resolution in range and azimuth coordinates, but poor resolution in elevation (along a circle of different viewing angles θ). The position of the area element F is defined by the time of the transmitting and receiving waves from which the slant range between antenna and the target is derived. Thus, the distance is shortened in slant range (Fig. 2.5, a). For a non distorted projection in ground range the following equation can be used considered the case of ideal conditions:

$$y = \sqrt{S^2 - h_g^2} \quad (2.8)$$

where y is the coordinate of ground range, S the slant range distance and h_g sensor altitude. In case of strong terrain height undulations (e.g. mountains) additional distortion due to terrain arises in the form of *Foreshortening*, *Layover* and *Radar Shadows*. In case of Foreshortening (Fig. 2.5, b) the mountain side distance \overline{AB} that is oriented towards the radar sensor is shortened to $\overline{A_1B_1}$ in the radar image. Additionally, the area $\overline{A_1B_1}$ appears bright, because the entire energy of \overline{AB} is integrated there. If the slope angle α of the mountain side \overline{AB} equals or even becomes bigger than the angle of illumination, the distance from the sensor to the top of the mountain side B is shorter then the distance to the base point A. Thus the point B_1 is imaged in slant range in front of point A_1 , so that objects \overline{AB} appear in reverse order $\overline{B_1A_1}$. This effect is called Layover (Fig. 2.5, c). The third effect (Fig. 2.5, d) is called Radar Shadow. It occurs if a steep mountain side \overline{BC} (steeper then the angle of illumination) is

turned away from the radar sensor. Therefore, it can not be illuminated and not be imaged and the area between B and D appears black in the image.

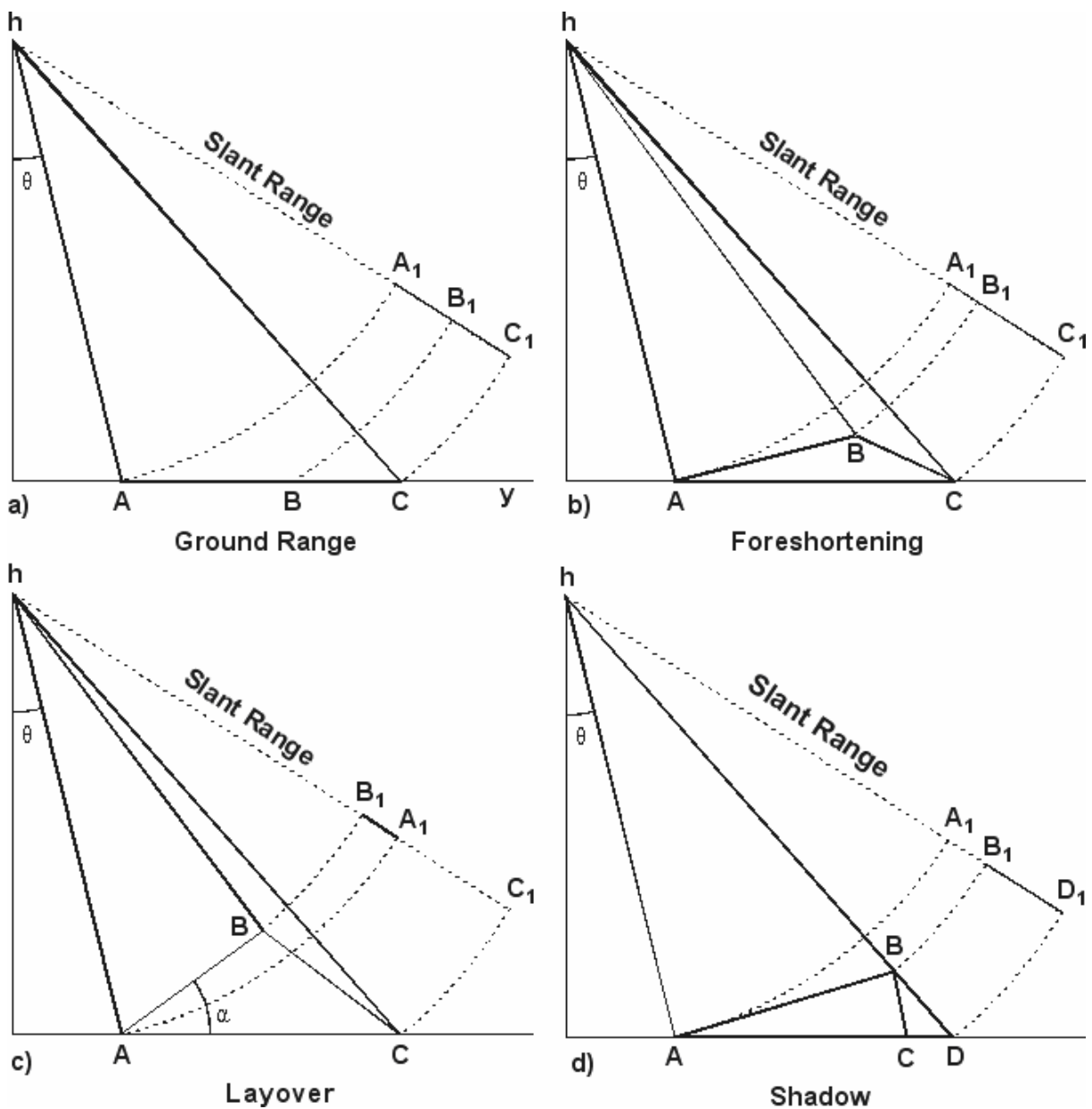


Figure 2.5: Geometric characteristics of SAR (Sörgel, 2003)

Scattering at the surface

Concerning the interaction of the signal with the Earth's surface two different scattering mechanisms are considered: *surface scattering* and *volume scattering*.

The former describes the reflections at the border surface of two media (i.e. air and soil) with different material features, such as conductivity and roughness (Ulaby et al., 1982). The microwaves are partly reflected, absorbed, and transmitted. Depending on the soil roughness, the observed reflection can be of any type inside the range of two extreme cases, namely specular reflection at mirror-like surfaces and diffuse (*Lambertian*) reflection (Hochschild, 1995).

Volume scattering differs fundamentally from surface scattering. Such model is required if a significant part of the signal propagates through the surface and penetrates into a 3D medium, which is inhomogeneous in terms of type, distribution, geometry or conductivity of objects inside. Two factors are mainly determining the kind and the strength of the volume scattering, namely the heterogeneity of the medium and the penetration of the wave. Furthermore, the scattering process is influenced by the incidence angle and the signal polarisation. In contrast to the surface scattering the incidence angle is less important compared to polarisation. Due to multiple scattering in inhomogeneous medium, the cross polar entries of the scattering matrix are usually large in the case of volume scattering. This effect is often exploited for land cover classification.

The general behaviour of different important surface types is shown in figure 2.6. The examples *a*, *b*, *f* and *h* demonstrate a special case of the surface scattering, the *Corner-Reflection* here: *double bounce*. Because of two or multiple specular reflection a huge amount of transmitted radiation comes back to the sensor. The effect depends strongly on the aspect angle and is often observed at buildings like in case *h*. The volume scattering is shown in sketch *c*. It is predominant for vegetation, ice and sand. In case of *g* the backscatter is lower because the transmitted radiation penetrates into the ground and the bigger part is absorbed by the material. The examples *d* and *e* represent surface scattering. Often at flat surfaces the backscatter is much less as in case of the volume scatter especially for *e*. Here the surface acts like a mirror. This is typical for water bodies and planar anthropogeneous surfaces such as streets. In case *d* the backscatter is higher because of the higher roughness of the surface. The example of *i* shows the geometric effect of the shadow of radar which was mentioned before.

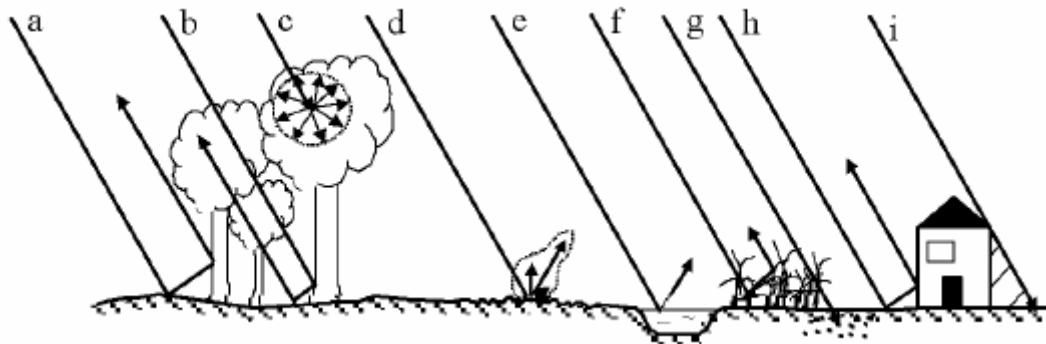


Figure 2.6: Characteristics of different scatter of radar radiation (Raney, 1998)

Speckle

The signal can be considered as the coherent superposition of contributions of different scatters present in the resolution cell (Fig. 2.7), dependent on the system and surface parameters (Schmullius, 1992). The individual backscatter vectors of the scattering centres are summed up coherently at the receiver. If a large number of such sub-scatters are present in the resolution cell, which are mutual independent, randomly distributed, and contribute in comparable amounts to the measured signal, the central limit theorem of probability holds. Hence, the amplitude A of the resulting phasor follows a *Rayleigh-distribution* while the phase φ is distributed equal in ideal case.

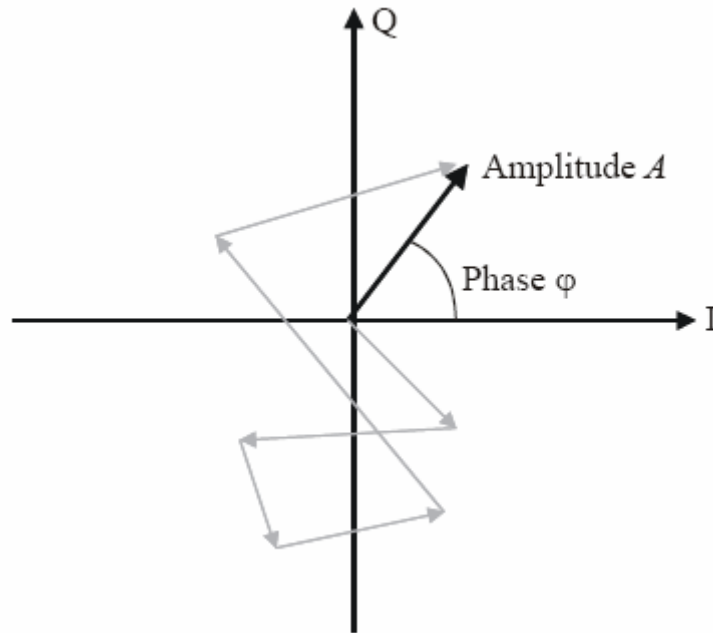


Figure 2.7: Development of a radar signal for an area target (Müllenhoff, 2004)

Since the distribution of sub-scatters is individual and not spatially correlated even for neighbouring pixels of natural surfaces, the appearance of “homogeneous” surfaces, such as grass, is rather salt-and-pepper alike. However, different surface types reveal different parameters of the pdf (such as expectation value μ and standard deviation σ). This grainy texture is called *Speckle* and is statistical independent from the underlying texture of the viewed area. Even though it is no noise, but the signal, speckle is often modelled to be some form of multiplicative noise. This is due to the effect, that the salt-and-pepper appearance burdens the interpretation both from human operators as well as automatic image analysis methods. The scene texture and the speckle composite the image texture (Raney, 1998). In order to reduce the speckle effect different methods are applied, all of them result in reduced spatial resolution for the sake of improved radiometric resolution:

- *Multi-looking*: The bandwidth in range and/or in azimuth is split into non-overlapping parts and several SAR images of lower resolution are processed. By incoherent averaging of the independent images, the grainy appearance is suppressed.
- *Averaging in the single look image*: First, a single SAR image is processed using the full signal bandwidth. In this image the speckle is reduced by spatial averaging.
- *Adaptive Filtering*: Image processing filters tailored to speckle effect are applied, which consider local image statistics or focus on geometric constraints.

2.3.6 Special characteristics of microwaves

The interaction of the microwaves with the surface depends on different parameters of the imaging system and of the detected target. All these factors are described in the radar equation. In this equation the power of the transmitted and received pulse are considered as well as the parameter of signal wavelength, antenna characteristics, and object features.

$$P_E = \frac{P_S \cdot G^2 \cdot \lambda^2 \cdot \sigma}{(4\pi)^3 \cdot r^4 \cdot L_v} \quad (2.9)$$

with:

P_E : received energy [W];

r : Range [m];

P_S : transmitting energy [W];

σ : radar cross section [m²];

G : antenna gain;

L_v : factor of system loss

λ : wavelength [m];

In the following the fundamental parameters are shortly introduced.

Wavelength

The wavelength determines the part of the scattering at the surface of the object, the penetration and the absorbability of the signal in vegetation or at the ground. Thus it influences the volume scattering of the overall backscattering on the Earth's surface (Bayer, 1990). The wavelength influences the backscatter by two ways. On the one way the effective roughness can be determined by the relation between the wavelength and the roughness of the surface, the wavelength determinates the penetration depth of the electromagnetic wave inside the medium. Long wave radar signal, such as L- and P-band, are in many cases able to penetrate through vegetation to the soil in contrast to short wave radiation like the X-Band , which is more useful to reveal information about the canopy (Fig. 2.8).

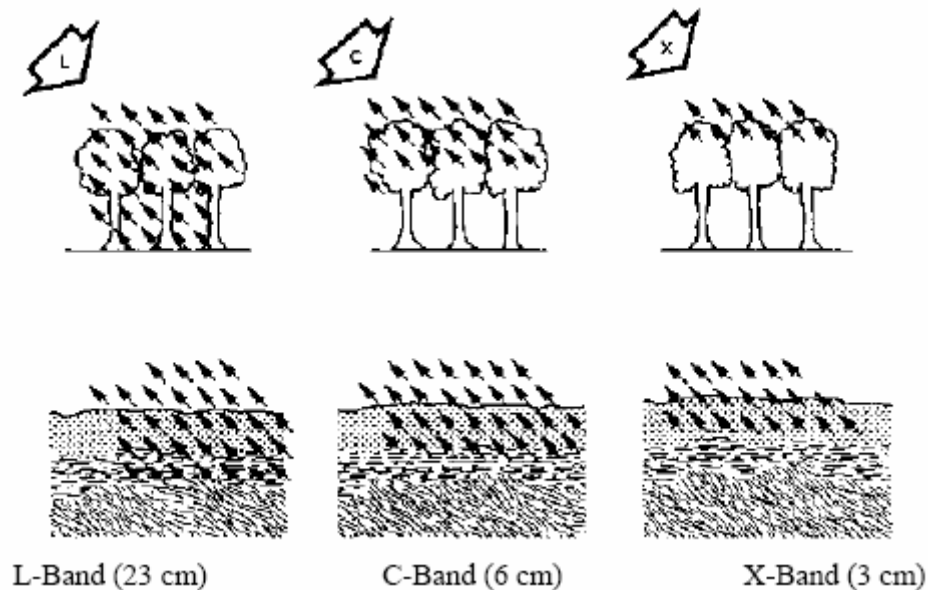


Figure 2.8: Illustration of the penetration of different microwaves (Schättler, 1992)

Roughness

An important factor for the characteristic of the reflection is the roughness of the surface. If the roughness is low (e.g. waterbodies) in comparison to the wavelength of the radiation the microwaves are reflected like on a mirror and no signal can be received by the sensor (Fig. 2.9, case a). If the roughness is in the order of the wavelength, the area appears like a diffuse reflector and there are mixtures of reflection (Fig. 2.9, case b and c).

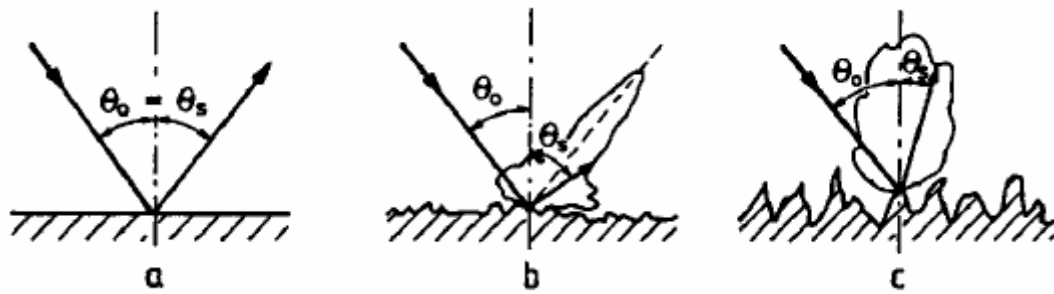


Figure 2.9: Parts of coherent and diffuse scattering for different roughness (Schanda, 1986)

The relative roughness of a reflected surface is described by the *Rayleigh-Criterion*. A threshold of average height variation h of the microrelief shows the dependency of the wavelength λ and the incidence angle θ , if a surface can be regarded as flat.

$$h < \frac{\lambda}{8 \cdot \cos \theta} \quad (2.10)$$

Polarisation

The transmitted electromagnetic radiation of the radar consists of an electric and magnetic field which are in phase, orthogonal to each other, and orthogonal to the direction of propagation (*transversal waves*). The state of a wave is described by its amplitude, phase, and polarization. The polarisation describes the plane in which of the electronic field vector oscillates. In remote sensing usually linear polarised signals are used, e.g. horizontal (H) or vertical (V) polarisation (Fig. 2.10).

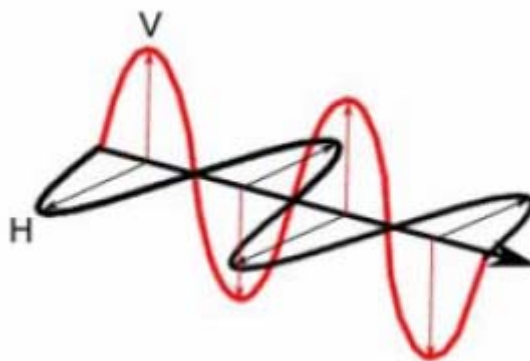


Figure 2.10: Illustration of the horizontal (H) and vertical (V) polarisation of waves (Müllemhoff, 2003)

The signal polarisation is steered either mechanically, for example by the antenna shape, or electronically. The generation of horizontal polarisation is for example achieved using a horizontal dipole, or vertical polarisation by a vertical dipole. In the same manner during receive the antenna is able to detect either horizontal or respectively vertical signal polarisation components. The signal polarisation can be changed by reflection on the object, depending on incidence angle and the characteristics of the object. Radar sensors are able to transmit and receive different polarisation. It can be distinguished between *parallel-* or *like-*

polarised and *cross-polarised* systems. Parallel-polarised systems are transmitting and receiving only in the same polarisation (e.g. vertical transmit, vertical receive [VV]). But the most common design is the complementary HH (Avery and Berlin, 1992). Cross-polarised systems are able to transmit either in horizontal or vertical direction and to receive respectively in a different polarisation (e.g. transmit horizontal, receive vertical [HV] or the complementary [VH]).

Sophisticated systems acquire dual-polarized data or even the entire scattering matrix. Dependent on the characteristics of the object different polarised radiation leads to different characteristic of the backscatter. Equal-polarised radar radiation show different backscatter in dependency of the horizontal and vertical structure of the illuminated surface of target. The cross-polarised systems are recording the backscattered depolarised radiation, which mostly occurs in case of multiple reflection and diffuse scattering. In general, the backscatter intensity is much less than in the equal-polarised systems.

Dielectric constant

The dielectric constant describes the characteristic of a surface to absorb and reflect energy or how far microwaves are able to penetrate into this surface. In case of natural surfaces this constant depends basically on the moisture. Normally the penetration of microwaves into the surface is decreasing by increasing degree of moisture. Waterbodies, for example, offer few penetration of microwave. Also wet soil is scattering mostly at the surface and in the first centimetres of the surface (Klenke, 1999). In case of dry soil the microwaves are able to penetrate up to several decimetres (Müllenhoff, 2001).

3 Digital image fusion

With the availability of multi-sensor, multi-temporal, multi-resolution and multi-frequency image data from operational earth observation satellites, the fusion of digital image data has become a valuable tool in remote sensing image evaluation. The aim of the image fusion is to integrate complementary data in order to obtain more information that can be derived from single data (Pohl, 1996). To benefit from the increasing number of remote sensing platforms, which offer different spatial and spectral resolution image fusion methods are required in order to combine these data. In the following chapter different image fusion methods are introduced.

3.1 Definition

A general definition of image fusion is given by Van Genderen and Pohl (1994), “Image fusion is the combination of two or more different images to form a new image by using a certain algorithm”. In this definition the image fusion is described as a combination. Other definitions use expressions like *image merging* (Carper et al., 1990), *image integration* (Welch and Ehlers, 1988) and *multi-sensor data fusion* (Franklin and Blodgett, 1993). Often the expressions ‘data’ and ‘image’ are used as a synonym. The expression ‘data’ includes not only remote sensing images but further ancillary data such as topographic and thematic maps, GPS coordinates, geophysical information contribute to the resulting image (Harris et al., 1989). In the context of Geographic Information Systems the term of *data integration* is also used (Ehlers, 1993). The replacement of one of the three channels in the Red-Green-Blue (RGB) colour space, or parts of it, with an image from another data source is called *substitution* (Suits et al., 1988). This method is typical for a false colour image with green, red and near infrared band (VNIR). It is also possible simply append all image bands in a layer stack which represents the whole image. This is called *supplement*.

3.2 Applications of image fusion

The applications of image fusion are manifold. A common one is *image sharpening* or *pan sharpening* by a high-resolution image fusion. This method for example is used to merge high spatial resolution data (e.g. SPOT panchromatic: ‘PAN’) with low spatial but high spectral resolution data (e.g. SPOT multi-spectral: ‘XS’ or Landsat Thematic Mapper: ‘TM’) in order to combine the high spatial and spectral resolution of both images in one image. Another application is the *synergy of optical and radar data* (mostly SAR data) in order to improve classification. Therefore the benefits of the radar data (e.g. cloud penetration, sensitivity with respect to surface roughness, object shape and moisture content of the observed ground cover are exploited. A further application is *change detection* in case of multi-temporal data in order to detect temporal changes inside a certain area that may have occurred. This detection can be done by data of one sensor or by multi-sensoral data. In case of multi-sensoral data the data sets must be calibrated and adjusted to each other. A detailed list and description of further applications is given by Pohl (1996).

3.3 Level of image fusion

The original images are the input parameter for any kind of image fusion, image integration or image merging. Normally they do have different attributes in spatial, spectral and temporal resolution. The image fusion is performed according to Pohl (1996) at three different levels according to the stage at which fusion takes place:

1. pixel-based,
2. feature-based or
3. based on a decision level.

The pixel-based method accomplishes the fusion at the lowest level. It is applied on raster data, in which every pixel and its grey value are examined. The values are modified by mathematical calculations and operators. It is the most common method. Fusion at feature level requires the extraction of objects recognized in the various data sources, like the use of segmentation procedures (Pohl, 1996). Features correspond to characteristics extracted from the initial images which depend on their environment, such as the characteristics dimension, shape and neighbourhood. These similar objects from multiple sources are assigned to each other and then fused for further assessment using statistical approaches. Decision- or interpretation level fusion represent methods that use value-added data where the input images are processed individually for information extraction. The information obtained is combined applying Bayes or Dempster-Shafer's rule to reinforce common interpretation and resolve differences for a better understanding of the objects observed (Shen, 1990).

3.4 Pixel-based image fusion techniques

The pixel-based image fusion techniques can be divided after Rencz (1999) into five classes:

1. RGB band combinations
2. Arithmetic combinations,
3. Colour-space transforms,
4. Statistical transforms and
5. Spatial transforms (wavelet transform, high-frequency filter transforms)

3.4.1 RGB Band combination

The RGB band combination is no real fusion technique. As mentioned before in section 3.1 it is rather a band substitution. A combination of different band can be made in case of more than three bands (e.g. Landsat). It is possible to select the bands which are most suitable for a certain application. Also other external data could be integrated by band selection.

A simply addition of all available bands in a layer stack, is also possible. In most software packages for image processing the image can only be viewed using three bands. But the representation of an image must not be limited on three bands (for every RGB channel one image band). Today software for image processing is available where more than three bands can be used to visualise one image. In this case more than one band is assigned to one RGB channel. Thus, the colour composition of the resulting image is changed, but all bands can be integrated.

3.4.2 Arithmetic combination

Another combination method is the arithmetic combination of different images. The multiplicative method is a commonly applied. It is a simple multiplication of two raster images. This transformation does not mainly preserve the radiometry, but also leads to minor radiometric changes (Crippen, 1989a). Difference or ratio images are also used. The most common applications are in change detection (ratio of 1 = no change) and the calculating of different vegetation indices like the *Normalized Differenced Vegetation Index* (NDVI). A mixture of multiplication and ratio methods is the *Synthetic Variable Ratio* method (SVR). Here, the multi-spectral bands are multiplied with the intensity band (e.g. panchromatic band) and then divided by a synthetic intensity band which is derived by low resolution multi-spectral bands.

$$XSP_i = Pan_H \cdot \frac{XS_{Li}}{Pan_{LSyn}} \quad (3.1)$$

Where XSP_i is the grey value of the i th band of the merged high-resolution image, Pan_H is the grey value of the original intensity image, the XS_{Li} is the grey value of the i th band of the multi-spectral image modified to have the same pixel size as the original intensity image Pan_H and Pan_{LSyn} is the grey value of the high-resolution synthetic intensity image.

In a modified approach of Zhang (1999) the synthetic intensity band is generated by following equation:

$$Pan_{LSyn} = \sum \varphi_i \cdot XS_{Li} \quad (3.2)$$

where φ_i are the parameters, which are calculated directly through multiple regression analysis of the original intensity image Pan_H and the original multi-spectral bands XS_{Li} formulated in the next equation:

$$Pan_H = \sum \varphi_i \cdot XS_{Li} \quad (3.3)$$

A new advanced approach of the SVR method, the *Block-SVR Fusion* method was introduced by Yang (2006). In this case the multiple linear regression is not considered on the whole image, but rather on block regions of the image. Thus this method is able to compute quickly and to preserve spectral characteristics and enhancement of spatial and textural contents.

Another new approach in this context is the so-called $\sigma - \mu$ method of Gungor and Shan (2006). In this case a linear combination of the fused image is introduced.

$$F_{K(m,n)} = a_{(m,n)} \cdot I_{O(m,n)} + b_{(m,n)} \cdot I_{K(m,n)} \quad (3.4)$$

In the equation above the intensity image $I_{O(m,n)}$ is added with the single multi-spectral bands $I_{K(m,n)}$ to the fused image $F_{K(m,n)}$ where a and b are the weighting coefficients for pixel location (m,n) .

The coefficients control the amount of contribution from the intensity image and multi-spectral bands respectively (Gungor and Shan, 2006). The criteria for the coefficients are determined by two rules. The first rule considers the local variance σ of the fused image and intensity band which should be equal. The second rule accounts the local mean μ of the merged image and the multi-spectral bands which should be equal too. Both coefficients are determined for the centre pixel of small local windows in the image.

3.4.3 Colour-space transforms

The colour-space transforms are based on theory of colours and colour composites. Every image can only be posed by the so-called additive primary colours red, green and blue (RGB), which form a colour composite that may be displayed by conventional media or by the subtractive primaries yellow, cyan and magenta (YCM) which is more used for a plotting device. The additive primary colours can be transformed into another colour space by the so-called IHS- colour transformation. IHS is an acronym for Intensity (I), Hue (H) and Saturation (S). By this transformation the image is separated into spatial (I) and spectral (H, S) information which are equal to image channels. An inverse transformation from IHS to RGB is possible. A detailed introduction is given in Harrison and Jupp (1990).

In case of the IHS method, which is a very common image fusion method, a RGB image (e.g. SPOT MS image) is firstly transformed to the IHS components. In a second step, the intensity channel (I) is replaced by another intensity channel (I', e.g. SPOT Pan). The third and last step the IHS components are transformed back into RGB channels.

It is assumed that the intensity channel (I'), which is inserted, is equal to the intensity channel (I) obtained by the RGB image (Chavez et al, 1991). This is frequently not the case by using input image that has more than three bands or is collected by a different sensor (Gungor and Shan, 2006). The method is also limited to three bands.

A new approach with an advanced IHS fusion method was developed by Ehlers, the so-called *Ehlers Fusion*. This approach combines IHS transform with Fast Fourier Transform (FFT) and is extended to include more than the standard 3 bands (Ehlers, 2005).

First the RGB channels are transformed into the IHS colour space then the intensity channel (I) is transferred into the frequency space by a FFT and filtered by a Low Pass Filter backward. In a second step the other intensity channel (P, e.g. PAN band) is also transferred into the frequency space by a FFT and filtered by a High Pass Filter and then back again. Now, both intensity channels (I, P) are added. In the last step the new intensity channel and the H and S channel are transformed back into the RGB colour space. The process of the image fusion is shown in the figure 3.1. The Low and High Pass Filter are variable adjustable for different purpose (e.g. emphasizing of definite classes like urban or rural or minimizing the effect of colour change). Thus the resulting new intensity channel is adaptable to the local requirements of the user.

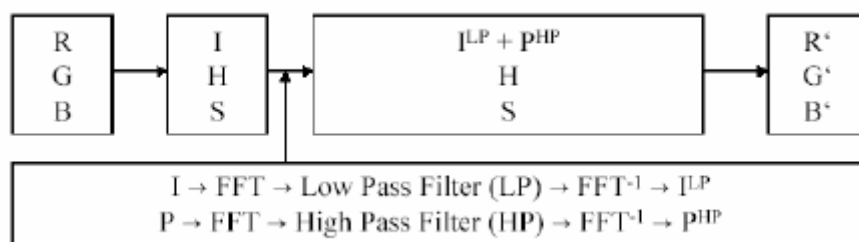


Figure 3.1: FFT based Ehlers-Fusion using a standard IHS transform (Ehlers, 2005)

3.4.4 Statistical methods

A representative statistical method is the Principal Component Analysis (PCA). The PCA transforms a multivariate data set of intercorrelated variables into a data set of new uncorrelated linear combinations of the original variables. It generates a new set of axes which are orthogonal (Yesou et al., 1993a).

First the different channels are checked for similarity. Especially neighbouring multi-spectral bands of a sensor are highly correlated. Thus the data includes redundant information. The transformation assures that the data set is reduced on the basics. Thus the method is called 'Decorrelation' (Albertz, 2001).

The figure 3.2 shows the decorrelation in case of two spectral bands. First both bands are displayed in a two-dimensional coordinate system (x, y). Caused by the correlation between two bands, a slant, stretched scatter plot is obtained. In the next step a new centre of the scatter plot is determined and a new shifted coordinate system x', y' . The axis of the new coordinate system are rotated by an angle from the origin coordinate system (x, y), so that the new axis (called the first principal component) points into the main direction (highest variation) of the scatter plot. The other axis (second principal component) is vertical to the first axis. Because of the transformation the data are decorrelated. In case of more bands the relevant information concentrates mostly on the first components. The other components contain mostly noise. For an image fusion by the PCA this assumption is exploited. The first component with the most information is replaced by an intensity band (e.g. panchromatic image) and then the components are inverse transformed into the original image space.

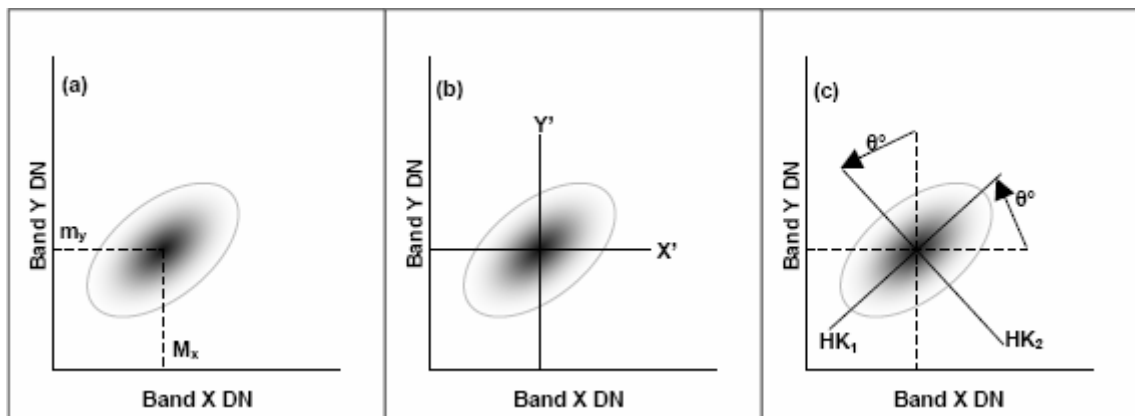


Figure 3.2: Schematic illustration of the Principal component (Drury, 1997)

3.4.5 Spatial transforms

The spatial transform transfers the image into the frequency space such as the Fast Fourier Transform. In this space the image is separated into signals which can be described by sine or cosine waves. In the next step the image is filtered by a *Low or High Pass Filter*, which filters either low or high frequencies in the image. After the filtering the image is transferred back to the original colour space by an inverse transformation.

A common approach in this context is the Wavelet transform. This transformation is similar to the Fast Fourier Transform. But instead of sine or cosine waves of intensity support in image space, short, local and discrete so-called wavelets are used. The wavelet transform can decompose the digital image into a set of wavelet coefficients for each resolution level. The wavelet coefficients for each level contain the spatial (detail) differences between two successive resolution levels (Zhang, 2000). At first, a high resolution intensity channel is decomposed into a set of low resolution images with wavelet coefficients for each level. Then one of the low resolution intensity images is replaced by a multi-spectral band at the same resolution level. In the next step a inverse wavelet transform is performed in order to convert the decomposed and replaced intensity set back to the original resolution level. The replacement and inverse transformation is done for each single multi-spectral band. A detailed description of this approach is given by Yocky (1996) and Wald et al. (1997).

3.5 Problems of image fusion techniques

A general aim of fusion methods is the integration of complementary information (e.g. spatial and spectral issues) of different images into a new image which should be qualitatively better than each of the given image. But this is often not the case, especially if the merged images are generated from different platforms with different features. A main problem of image fusion techniques in this context is the colour distortion (Zhang, 2000). It is always intended to preserve the given radiometric features of the images as good as possible. But this is quite difficult. Therefore it is needed that the merged images are highly correlated with each other. Especially the fusion of optical and SAR imagery is more difficult than the ordinary pan sharpening in case of optical data because the grey values of SAR imagery do not correlate with those of multi-spectral imagery (Yang, 2006). One reason is the mono-spectrum of radar imagery. The other reason is the fact that radar images contain only spatial information than spectral information which is typical for multi-spectral bands (Sun, 2006). Radar data describe typical surface characteristics like roughness or moisture than intensity values. Thus radar data cannot be treated as further multi-spectral bands in a multi-spectral classification where only the single grey values are considered. Here, additional texture features have to be considered in order to represent the typical surface characteristics.

The effect of non correlation can be minimized in smaller image areas as studies of Gungor and Shan (2006) and Yang (2006) showed. But a global preservation is hardly to achieve, for example, for classification purpose. Another problem is the limitation of some image fusion methods like the IHS Transform, where only three bands can be considered at the same time. It is also stated that common image fusion techniques like the IHS and the PCA Transform often create images of higher spatial resolution but usually at the cost that these transforms do not preserve the original colour or spectral characteristics of the input images (Ehlers, 2005).

4 Data used and Pre-processing

In this work several optical data sets from ASTER- and SPOT 5 and SAR data sets from Envisat ASAR- and Radarsat were available. Additionally to these data sets aerial images, a digital elevation model (DEM), a geological map and GIS data from the test area were disposable. In the following chapter the different optical and radar sensor, the different data sets, the pre-processing and the preparation of the data are introduced.

4.1 Optical sensor

4.1.1 ASTER

ASTER, an optical remote sensing system, is operated in a joint venture of the United States of America (USA) and Japan. The ASTER system was developed by the Japanese side and positioned on the American TERRA satellite. The main task of the ASTER system is to image the earth's surface temperature, emissivity and reflection as part of the earth monitoring system EOS.

The ASTER instrument provides the next generation in remote sensing imaging capabilities compared with the older Landsat Thematic Mapper and Japan's JERS-1 OPS scanner (NASA, 2004). The system consists of three separate instrument subsystems. Each subsystem operates in a different spectral region (VNIR, SWIR, TIR) and spatial resolution (15, 30, 90 meters). Overall 14 bands are available in different spectral bands. The different bands combined with the three subsystems are listed in table 4.1.

No.	Bands	Spectral range [μm]	Resolution [m]
1	Green	0.52 – 0.60	15
2	Red	0.63 – 0.69	
3	NIR	0.76 – 0.86	
4	SWIR	1.600 – 1.700	30
5		2.145 – 2.185	
6		2.185 – 2.225	
7		2.235 – 2.285	
8		2.295 – 2.365	
9		2.360 – 2.430	
10	TIR	8.125 – 8.475	90
11		8.475 – 8.825	
12		8.925 – 9.275	
13		10.25 – 10.95	
14		10.95 – 11.65	

Table 4.1: Bands of the ASTER sensor (NASA, 2004)

4.1.2 SPOT

SPOT is a series of optical remote sensing satellites from France. Since May 2002 SPOT-5 is in orbit (Fig. 4.1). The satellite is now the fifth generation following SPOT 4 and SPOT 3 to SPOT 1. It circuits the earth in a height of 822 km in a near polar, sun-synchronous orbit in 101.4 minutes cycle. Thus a complete coverage of the earth takes 26 days.



Figure 4.1: SPOT 5 satellite (CNES, 2002)

SPOT 5 is equipped with three monitoring systems, the HRG- (High Resolution Geometric), HRV- (High Resolution Visible) and HRS-instrument (High Resolution Stereo). The HRG-instrument uses the panchromatic mode with a resolution of 2.5 respectively 5 meters. The HRV-instrument is imaging in a multi-spectral mode with a resolution of 10 in case of the visual and near infrared bands respectively 20 meters for the short-wave infrared band. It offers the same bands (spectral range) and resolution as the HRG-Sensor. The different modes, bands and spectral ranges are listed in table 4.2.

Mode	Szene	Bands	Spectral range [μm]	Resolution [m]
HI-Mode (multi-spectral)	MS	Green	0,50 – 0,59	10
		Red	0,61 – 0,68	
		NIR	0,79 – 0,89	
		SWIR	1.58 – 1.75	20
HX-Mode (multi-spectral)	Color	Green	0,50 – 0,59	2,5 – 5
		Red	0,61 – 0,68	
		NIR	0,79 – 0,89	
HM-Mode (panchromatic)	PAN	PAN (G, R, NIR)	0,51 – 0,73	2,5 – 5

Table 4.2: Bands of the SPOT 5 instruments (CNES, 2002)

4.2 SAR Sensor

4.2.1 Envisat ASAR

Envisat is a remote sensing satellite of European Space Agency (ESA). It was developed for the monitoring of the climate, the ocean and ice, snow and land surface. On the satellite platform the C-Band *Advanced Synthetic Aperture Radar* (ASAR) is installed beside nine further systems and instruments.

The ASAR sensor is able to produce SAR images in five different modes, Image Mode, Wave Mode, Wide Swath Mode, Global Monitoring Mode and Alternating Polarisation Mode. In the Image Mode (IM) swaths up to 100 km and a geometric resolution of approximately 30 m x 30 m are imaged. The standard polarisation modes are HH or VV. With the Wide Swath Mode (WS) swaths up to 400 km and a resolution of about 100 m x 100 m are available. In the Global Monitoring Mode (GM) swaths are much bigger then in Wide Swath Mode but the resolution is worse with approximately 1000 m. In the Alternating Polarisation Mode (AP) three different polarisation combinations (HH and VV, HH and HV or VV and VH) are possible (ESA, 2007).

4.2.2 Radarsat

Radarsat is a commercial remote sensing satellite from the Canadian Space Agency (CSA). The main task of this instrument is the monitoring of the physical oceanography, ice and snow coverage and land surface. Its only imaging instrument is a C-Band and HH polarised Synthetic Aperture Radar (SAR).

Radarsat offers a wide variety of beam widths and range resolution in different imaging modes, which include Standard, Wide Swath, Fine Resolution, Extended and ScanSAR (Fig. 4.2). In the Standard imaging mode the incident angle is variable from about 10 ° to 60 °. The satellite orbits the earth in an elevation of about 800 km with an inclination of 98.6°. Its time of circulation are 100.7 minutes, the repetition cycle takes 24 days.

The follow-up satellite RADARSAT-2 is planned to be started in 2007. This satellite will be able to provide four polarisation modes (HH, VV, HV and VH) as well as a much better resolution (3 m) in the Fine Resolution Mode.

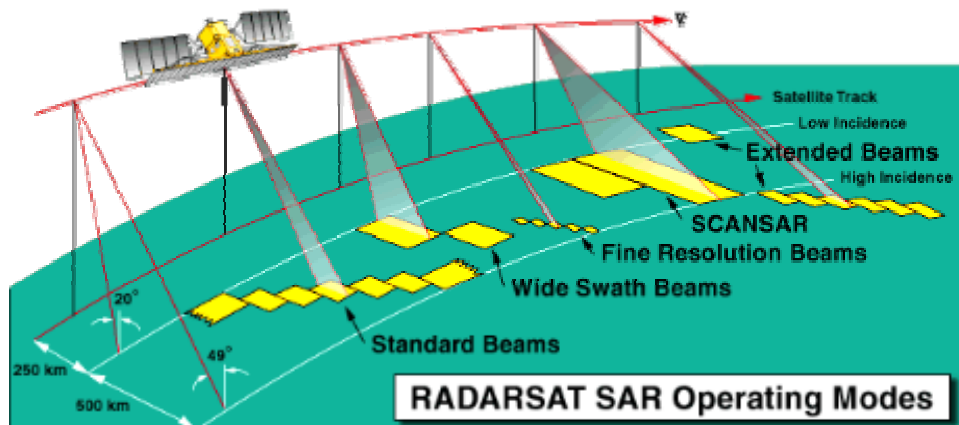


Figure 4.2: Operating modes of Radarsat (CSA, 2006)

4.3 Initial data set

The data of the different sensors used in this study with their characteristics and the additional ancillary data sets are briefly introduced.

4.3.1 Initial optical data set

The ASTER scene was available for the processing level 1B, subdivided into the three groups of bands at the acquisition time Jan., 25th, 2005 (Tab. 4.3).

Name	Bands	Resolution	Acquisition time	Short term
Subscene 1	G, R, NIR	15 m	25.01.2005	ASTER_VNIR-2501
Subscene 2	SWIR	30 m	25.01.2005	ASTER_SWIR-2501
Subscene 3	TIR	90 m	25.01.2005	ASTER_TIR-2501

Table 4.3: ASTER data divided into 3 subscenes in different resolution

From SPOT 5 three different subscenes were disposable from April, 6th, 2005 in the processing level 1A. These three scenes include a high resolution panchromatic scene, a high resolution multi-spectral scene as colour composite and a medium resolution multi-spectral scene with an additional short-wave infrared band (Tab. 4.4).

Name	Bands	Resolution	Acquisition time	Short term
SPOT 5 MS	VNIR, SWIR	10, 20 m	23.05.2005	SPOT 5 MS-2305
SPOT 5 Pan	Panchromatic	2,5 m	23.05.2005	SPOT 5 Pan-2305
SPOT 5 Color	VIS,NIR	2,5 m	23.05.2005	SPOT 5 Color-2305

Table 4.4: SPOT data including 3 subscenes in different mode and resolution

4.3.2 Initial SAR data set

From Envisat two Single Look ASAR-Scenes (SLC), one from 25th of Jan. 2005 and one from the April, 5th, 2005, were available in Image Mode and vertical polarisation (Tab. 4.5).

Mode	Polarisation	Format	Resolution	Acquisition time	Short term
Image Mode	V/V	SLC	30 m	25.01.2005	ASAR-2501
Image Mode	V/V	SLC	30 m	05.04.2005	ASAR-0504

Table 4.5: ASAR data including 2 scenes with different acquisition time

From Radarsat two Single Look ASAR-Scenes (SLC), one from Jan., 24th, 2005 and one from April, 6th, 2005, were available in Fine-Beam Mode and horizontal polarisation (Tab. 4.6).

Mode	Polarisation	Format	Resolution	Acquisition time	Short term
Fine-Beam	H/H	SLC, CEOS	8 m	24.01.2005	RSAR-2401
Fine-Beam	H/H	SLC, CEOS	8 m	06.04.2005	RSAR-0604

Table 4.6: Radarsat data including 2 scenes with different acquisition time

4.3.3 Ancillary data

An additional data set of aerial orthophotos, a digital elevation model (DEM), a geological map and GIS data were available.

Aerial ortho imagery and elevation model

An additional data set of aerial orthophotos covering the test area about June 2005 at a resolution of approximately 30 centimetres was available (Fig. 4.3, left). The data set was referenced on the WGS 84 ellipsoid and projected in *Universal Tranverse Mercator* (UTM) in *Zone 46, North*. It was used as reference because of the high resolution and good quality of the coordinates.

Additional to the aerial images a DEM was available which was derived from the aerial images together with ASTER stereo remote sensing data. The DEM was available as raster data with a ground resolution of 10 m (Fig. 4.3. right). Because of the generation with two different initial data sets (aerial and satellite image) some artefacts and errors appear.

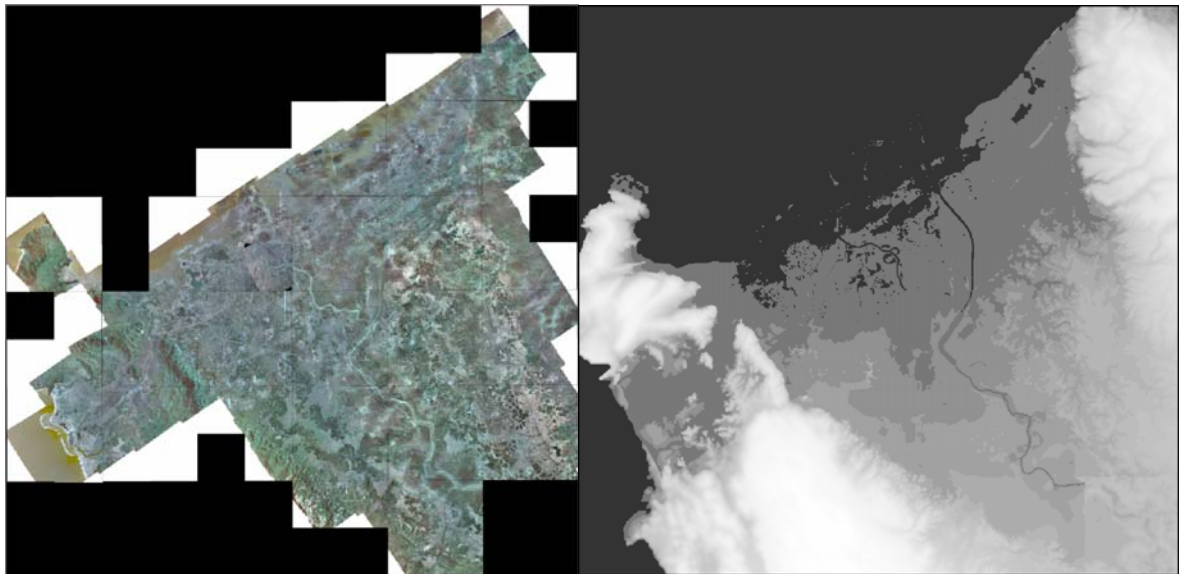


Figure 4.3: left: mosaics of the aerial orthophotos of the test area Banda Aceh, acquisition about June 2005
right: digital elevation model, derived from the aerial and ASTER image data

Geological map

To support the mapping of soil classes a geological map from 1982 with different soil coverage of the test area was used. The map was digitized and referenced to the aerial images.

GIS data

In addition to the aerial images, the DEM and the geological map GIS data were disposable. This GIS data include vector data in form of streets and borders.

4.3.4 Overview of all scenes

In the following illustration (Fig. 4.4) all data sets of the different sensor and the DEM are shown. The scenes are referenced by geographic coordinates.

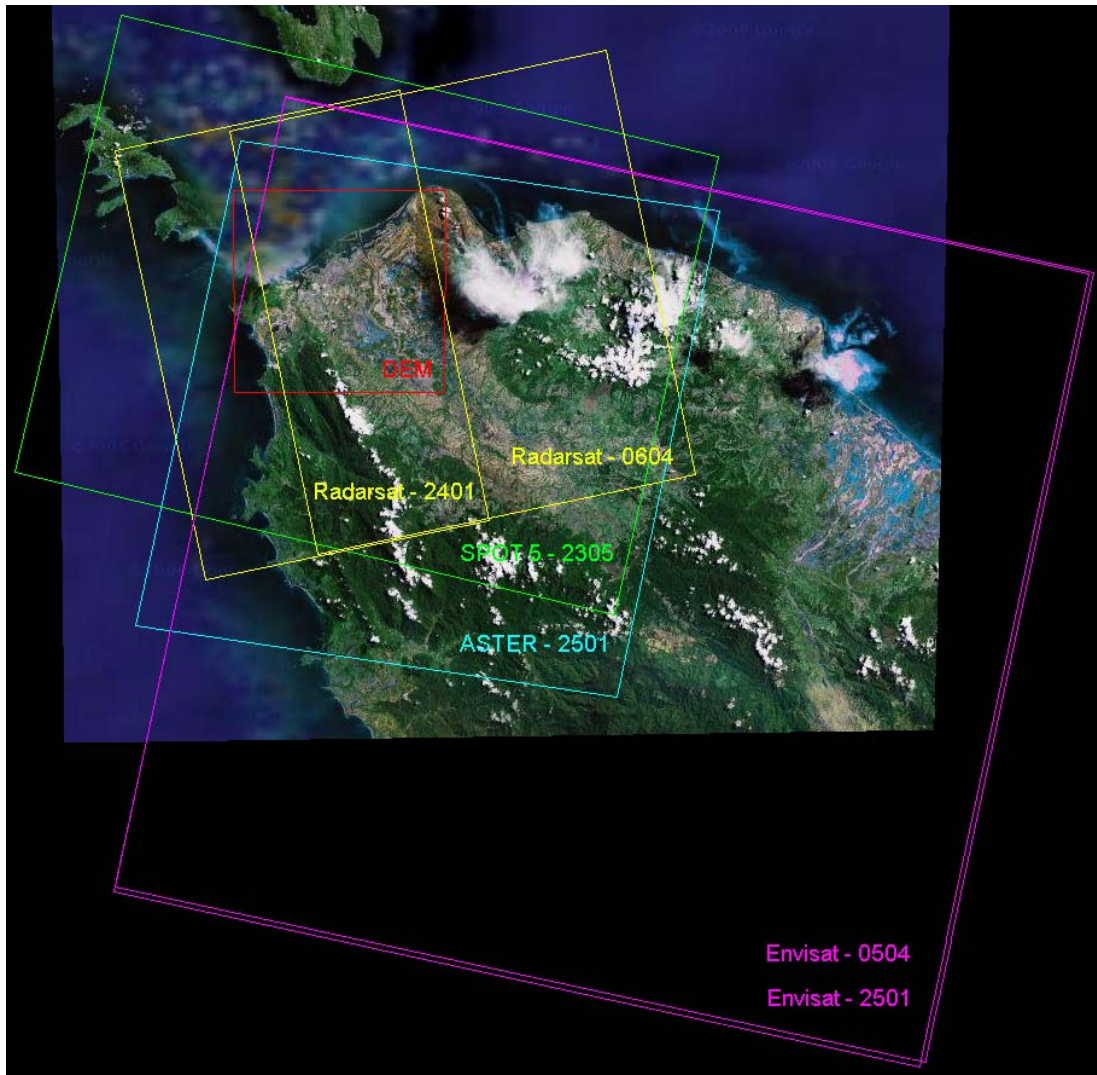


Figure 4.4: Illustration of all scenes as vector layers referenced on a satellite image (Google Map, 2007) by geographic coordinates

4.4 Data pre-processing

In order to perform an image fusion and classification on the initial images the data sets had to be pre-processed. The pre-processing for optical and SAR data is different.

The optical data needs to be corrected normally by an atmospheric calibration because it is influenced by atmosphere before geocoding (Fig. 4.5). In case of the SAR data a speckle reduction, normally a terrain correction and a conversion from 16 to 8 bit has to be done besides the geocoding process. The order of the different processing steps of the SAR data is partly disputed. Some researchers suggest first reducing speckle and then geocoding (Dallemand et al., 1992), while others perform filtering and resampling during the geocoding process in one step (Pohl, 1996).

Nethertheless it is advisable to do the conversion from 16 to 8 bit at the end of the filtering and geocoding process in order to minimize information loss. In this case the speckle reduction was done directly after the geocoding and after the conversion to 8 bit.

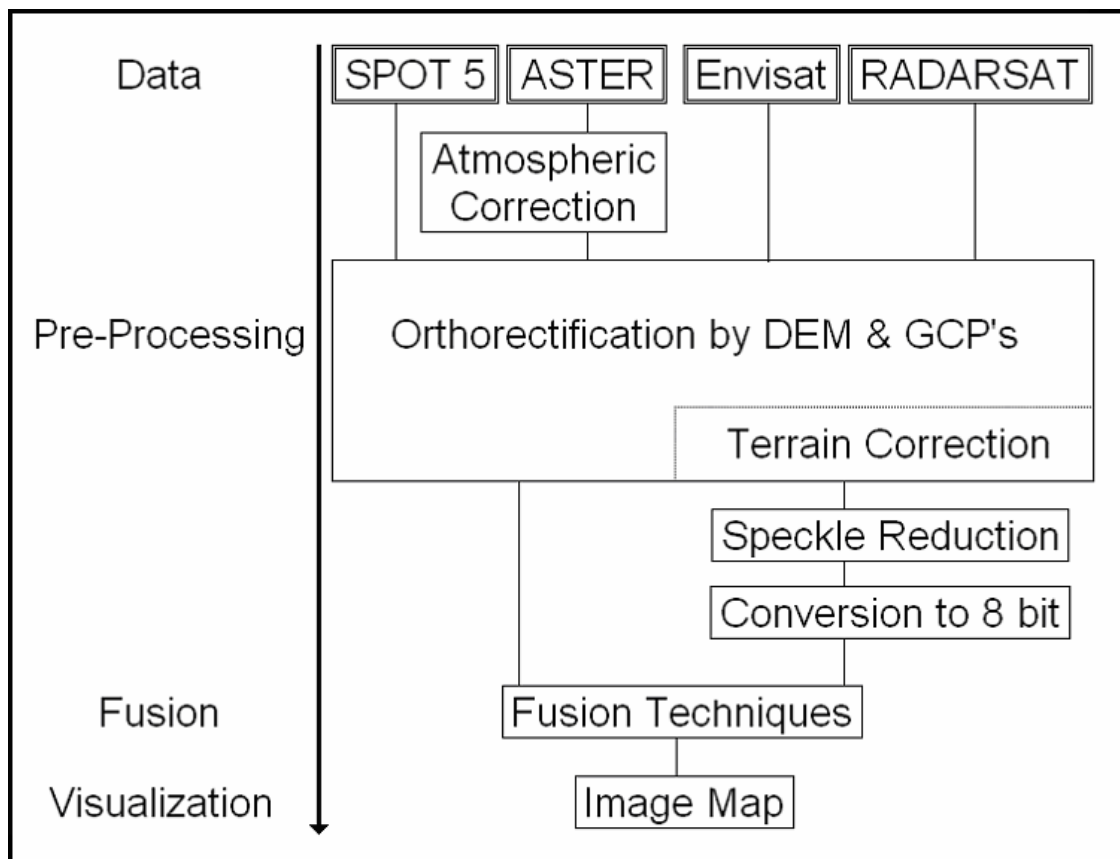


Figure 4.5: Pre-processing flow chart for pixel-based image fusion

4.4.1 Pre-processing of the optical data

In a first step the raw data of the optical scenes were pre-processed.

Radiometric calibration

Depending on the processing level a radiometric calibration during the pre-processing is necessary. In the processing level 1A the SPOT 5 data are already radiometric calibrated (SPOT Image, 2007). In case of the ASTER data a radiometric calibration was necessary because of the three different subsystems. The calibration was done with an internal module of the image processing software ERDAS Imagine during the import of the data. In this module a conversion to radiance and a transformation to 8 bit were accomplished.

The obtained result was not satisfactory for the VNIR bands, especially the green channel (Fig. 4.6, left). Thus, a radiometric enhancement was done manually. A simple reduction of the influence of the atmosphere was accomplished. Therefore, a correction value was determined on the basis of the histograms of the different bands. In this procedure it is assumed that in infrared bands the influence of the atmosphere is not as significant as in visual bands. Therefore, the histogram values of a very dark sector (e.g. dark shadow) of the infrared band are compared with the histogram values of same sector of the visual band. The

histogram values in the infrared band are usually much lower than in the visual band because they are not so bright. This shift in the histogram between the two bands can be interpreted as the correction for the influence of the atmosphere (Albertz, 2001).

The correction was done on the green band which was very pale and saturated. The correction was determined from the average of a test series of points (20) of a dark shaded area. The result (Fig. 4.6, right) is simply a reduction of the brightness of the green band.



Figure 4.6: left: ASTER1-2501 scene after the radiometric calibration by the ERDAS Imagine Import module, right: ASTER1-2501 scene after the manual radiometric enhancement

Geometric adjustment

For multi-spectral classification it is more advantageous if the processing is done on the data without any geometric adjustment in which grey values are changed caused by resampling. In case of multi-sensoral data this aim is very difficult to achieve. Due to the fact that in this work an image fusion of multi-sensoral data had to be done with orthorectified images and high resolution reference data was available in a UTM projection (WGS 84), it was reasonable to adapt the optical and SAR data to the reference data. The geometric adjustment was done by orthorectification. That means effects of the topographical relief by so-called differential displacement of each image point were considered, so that it fits onto an orthogonal projection. The orthorectification by the DEM was done as well in ERDAS Imagine as in ENVI.

The orthorectification of the SPOT scenes was carried out using an extra ERDAS module for SPOT data. For the orthorectification process a digital elevation model and ground control points (GCP) from the reference data were available. The accuracy for every scene was about 1 Pixel. A better accuracy could not be obtained because of manual measurement of the points. Nearest Neighbour was chosen as resampling method in order to preserve the grey values as good as possible. The resulting maximum resolution was chosen by 5 m. The SPOT 5 data offer a resolution of 2.5 m but this resolution is interpolated (SPOT Image, 2007). The orthorectification of the ASTER scenes was done in ENVI, because of the lack of a special orthorectification tool in ERDAS. The process was analogue to the rectification of the SPOT scenes. Here the accuracy was about 1 and 1.5 pixel because of the different resolution of the scenes. Nearest Neighbour resampling was chosen again. In this case all scenes were rectified to a maximum resolution of 15 m. Thus, the resolution of the other ASTER bands was increased artificially.

4.4.2 Pre-processing of the SAR data

In a second step the Radar data were pre-processed.

Radiometric Calibration (Terrain Correction)

The backscatter coefficient depends of the local incidence angle and terrain slope. Thus, different terrain slopes regarding to the line of sight of the SAR sensor show different backscatter (Bähr and Vögtle, 1998). This effect can be corrected theoretically during pre-processing by weighting according to the local incidence angle.

Because of the following reasons it was not carried out here:

1. The backscatter of natural surfaces is a very complex value which is composed of the overlay of many scatter. Thus it is very difficult to reduce the influence of the terrain, even if the local coverage is known very well. Because of the multitude factors such as roughness, moisture, etc. of the surface, the same conditions for the coverage of the surface which are necessary for the determination of the correction, cannot be made. (Hagemeister, 2001).
2. The correction of radiometric terrain effects relies on a high resolution digital elevation model in order to calculate correct local incidence angle. The given elevation model does only partly meet this constraint because of a low geometric resolution in some sectors and artefacts caused by mosaicing.
3. However, radiometric correction using the SARscape software and the given DEM yield only negligible enhancement (Fig. 4.7).
4. The investigated test area covers an area of approximately 68,500 ha. 77 % are plane areas with a maximum slope of 2° . Areas with a steep slope ($> 10^\circ$) are mostly covered with dense, mixed or sparse vegetation.
5. Areas for erosion potential can be detected adequate by the use of optical data, so that additional information from radar data is not absolute necessary in these areas.

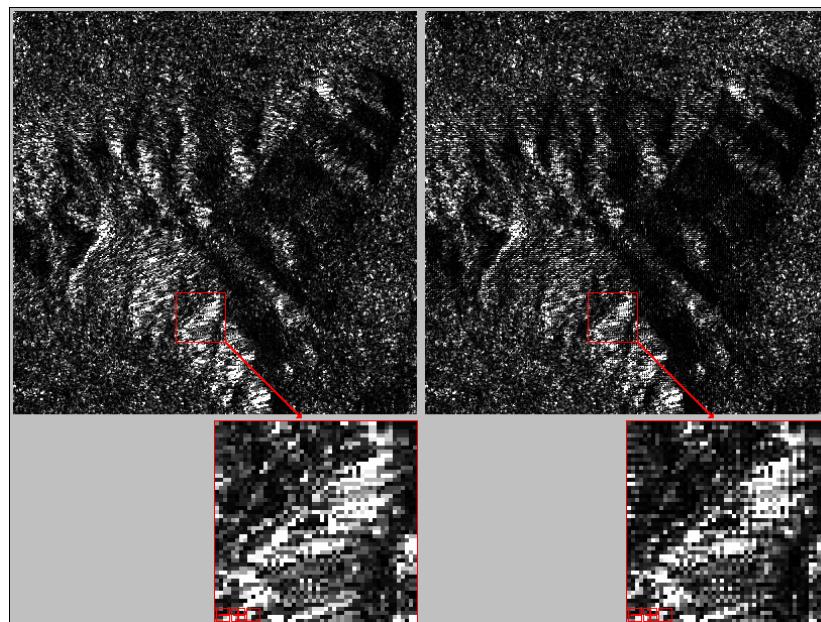


Figure 4.7: left: Sector of the Radarsat-0604 scene without terrain correction with zooming sector (4 x) below, right: Sector of the Radarsat-0604 scene with terrain correction with zooming sector (4 x) below

Geometric Adjustment

Since SAR resolution in elevation direction is poor, a direct projection on a DEM is not recommended, especially in mountainous terrain. Instead geocoding of SAR imagery is usually carried out using an indirect method (Leberl, 1990). For each 3D grid point of the DEM the related position in the SAR geometry is determined. For geometric adjustment of the SAR data a special Radar orthorectification module was used which considers the DEM and sensor parameters. For an exact registration of the radar scenes to the optical and reference data the same ground control points were used. For the resampling method Nearest Neighbour was chosen.

The Radarsat Fine Beam Mode images (8 m resolution) were interpolated on the 5 m grid of the SPOT 5 data.

the maximum resolution was specified to 5 m. In case of the Envisat scenes the maximum resolution was chosen to 15 m in order to correspond with the ASTER data. Normally the resolution of the Envisat scene is about 30 m in Image Mode.

Speckle Filtering

Speckle in SAR images is generally undesirable. However, the reduction of the speckle effect always results in lower spatial resolution of the radar image. As mentioned before, speckle reduction can be achieved by different methods: *Multi-looking*, *Averaging in the single look image* and *Adaptive Filtering*. Because of used single-look images of Radarsat and Envisat and in order to avoid averaging in single look images, the Adaptive Filtering was accomplished in the pre-processing workflow.

Two common adaptive filters are the filters from Lee (1981) and from Frost (1982). A third common filter is the so-called Gamma-Map filter (Lopes et al., 1993). This filter does a classification on the basis of the local coefficient of variation and distinguishes between homogeneous, homogeneous and textured and inhomogeneous parts of the image. Thus strong point targets are retained and only homogeneous parts are smoothed. Therefore, the speckle reduction was done by a Gamma-Map filter, which was available in ERDAS. In this tool the size of the filter mask was chosen by 5 x 5 pixel for the Radarsat and 3 x 3 pixel for the Envisat data.

Conversion to 8 bit

The radar scenes had to be converted from 16 bit or Float to 8 bit because of the image fusion and classification with the optical data that are in 8 bit format. This was arranged by the conversion tool Rescale in ERDAS. In this tool the minimum and maximum grey value range in 16 bit are specified and then converted into 8 bit.

4.5 Data preparation

After the pre-processing the different optical and SAR data sets were combined to two main data sets of different date (January 2005 and April / May 2005).

4.5.1 First data set of January / April / May 2005

The first data set contains essentially the time period of April / May 2005, but also January 2005. In this case a contemporary combination was not possible. Here, the SPOT 5 scenes SPOT5_Color-2305, SPOT5_MS-2305 (Fig. 4.8, left) and both Radarsat scenes RSAR-2401 and RSAR-0604 (Fig. 4.8, right) were combined. In case of the SPOT5_MS-2305 scene only the short-wave infrared band was used because of the redundant information (Tab. 4.7). Normally, the panchromatic band is merged with all bands of the MS scene in order to increase and enhance the spatial resolution and to preserve the spectral content of the MS scene. But this was not necessary because of the high resolution of the SPOT 5_Color-2305 scene. Because of the fact that the RSAR-0604 scene does not cover to 100 % the test area, the scene was combined with the RSAR-2401 scene in order to obtain a coverage of 100 % and to avoid gaps. Thus both scenes were merged to the scene labelled as RSAR-2401 / RSAR-0604. The Radarsat scene RSAR-2401 covers about a fourth of the test area in the western part.

Scene	Band	Resolution [m]	Acquisition time
SPOT 5_Color-2305	1, 2, 3	5	23.05.2005
SPOT 5_PAN-2305	Intensity	5	23.05.2005
SPOT 5_MS-2305	4	5 (20)	23.05.2005
RSAR-2401 / RSAR-0604	Intensity	5 (8)	24.01.2005 / 06.04.2005

Table 4.7: First data set at the time Jan. /April / May 2005

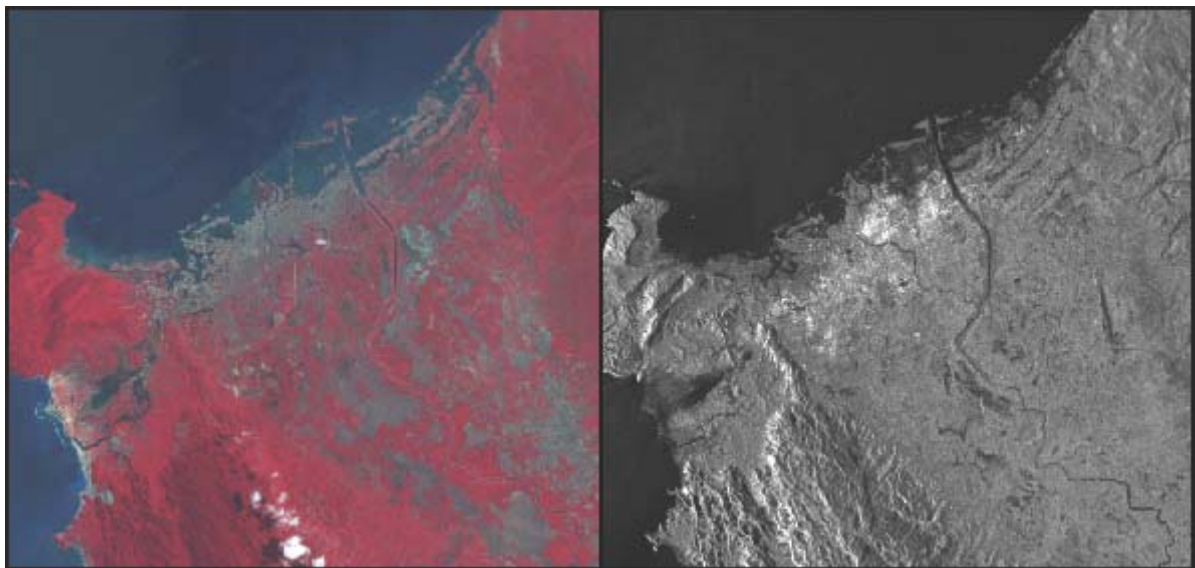


Figure 4.8: left: optical data of SPOT 5, right: Radarsat scene RSAR-2401 / RSAR-0604

4.5.2 Second data set of January 2005

The second data set contains data taken 25th of January 2005. At this date the three ASTER scenes ASTER_VNIR-2501, ASTER_SWIR-2501, ASTER_TIR-2501 (Fig. 4.9, left) and the Envisat scene ASAR-2501 (Fig. 4.9, right) was acquired. So these scenes were combined. In case of the two ASTER scenes ASTER_SWIR-2501 and ASTER_TIR-2501 only the bands 4, 7 and 12 were used in order to reduce the data set (Tab. 4.8). The spectral ranges of these bands (q. v. tab. 4.1) are very similar to each other especially the bands 5 to 9. In this case the respectively median band was chosen.

The Envisat scene ASAR-2501 does not cover the whole test area. The upper left part is missing. The Envisat scene ASAR-0504 covers exactly the same area. Thus a combination of both scenes in order to fill this gap was not possible like in the case of the two Radarsat scenes.

Scene	Band	Resolution [m]	Acquisition time
ASTER_VNIR-2501	1, 2, 3	15	25.01.2005
ASTER_SWIR-2501	4, 7	15 (30)	25.01.2005
ASTER_TIR-2501	12	15 (90)	25.01.2005
ASAR-2501	Intensity	15 (30)	25.01.2005

Table 4.8: Second data set at the time January 2005

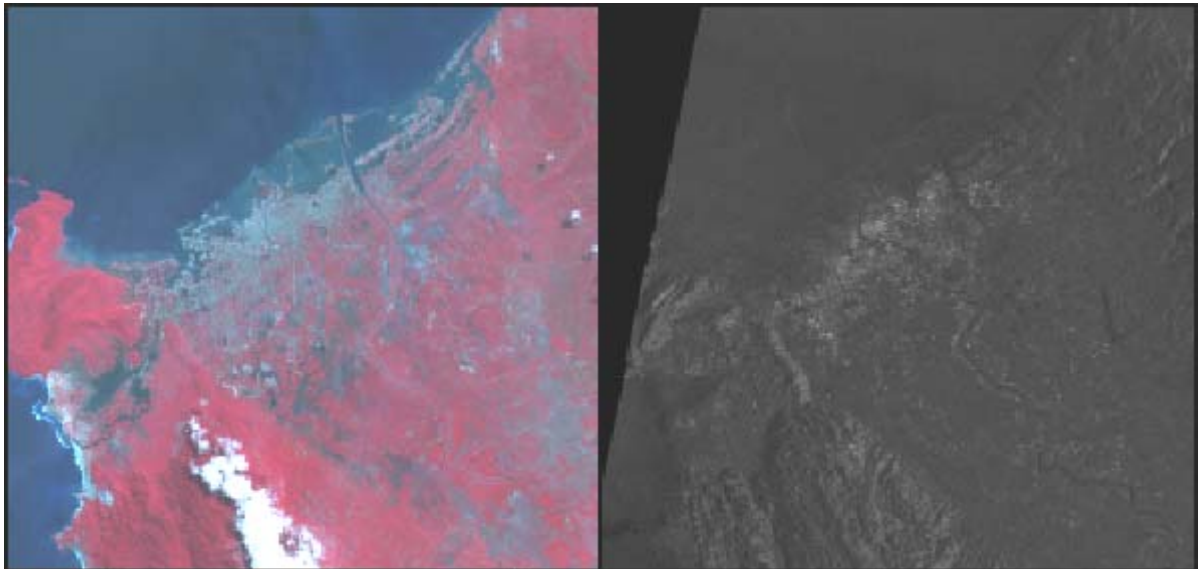


Figure 4.9: left: optical ASTER data, right: Envisat scene ASAR-2501 which covers not the western part

5 Generation of the classification system

5.1 Classification systems

A crucial issue in classification task is the choice of an adequate classification system. This classification system defines the discrete classes of a land coverage respectively land use. Often a hierarchical order is desired, so that the classes of a higher level (*category*, e.g. agriculture) contain more specialized classes of lower level (*classes*, e.g. paddy fields).

There are many classification systems which are used as well for global as for local purpose. But these systems differ beside the region also in the use of the data and resolution. A well known classification system for European regions is the classification system of *CORINE Land Cover*. This system is structured in three hierarchical ranks including land coverage classes (first and second rank) and land use classes (third rank). It was mainly developed for Landsat and SPOT data in a resolution of 20 to 30 meters (Geßner, 2004).

5.2 Definition of the classification system

Although Corine was designed for Europe and it therefore not specified for equatorial regions, it is a useful template for a class description adapted to the test area. Thus an own class description was defined and several categories and classes from the Corine classification system were adapted. Specific categories and classes for this area like *soil – limestone*, *sand*, *etc.* were new defined. The several categories and classes are described in section 5.4. For the classification system the thematic accuracy has to be defined. The thematic accuracy was determined by the counterpart of the BGR with about 90 %.

5.3 Definition of the map scale

For the plotting of the classification result in a map the scale has to be defined. The scale depends on the defined size of the map and on the size of the data. Normally the paper of a map includes a size of about 0.5 x 0.5 m. The test area covers a size of 26.850 x 25.5 km. Thus a scale of 1:50,000 was defined.

5.4 Definition of the categories and classes

In this work an own classification system was defined. It includes five categories of land coverage (Tab. 5.1) and 22 classes for land cover and land use which are grouped semantically (Tab. 5.2).

Categories
A – Agriculture
U – Urban
S – Soil
V – Vegetation
W – Waterbodies

Table 5.1: Choice of the five categories with minimum mapping size and thematic accuracy

ID	Classes	Description
Land Use Classes		
A – Agriculture		
AM	Mixed Farming	Diverse plantation for fruit-growing, grassland for cattle-breeding
AP	Paddy Farming	Paddy fields
AF	Fish Farming	Water ponds for Fish Farming
U – Urban		
UD	Urban (dense)	Continuous dense settlement and infrastructure areas
US	Urban (sparse)	Continuous sparse settlement and infrastructure areas
UR	Urban (rebuild)	Rebuild, mostly former destroyed and flooded settlement and infrastructure areas
UP	Park and sport field	Parks in residential areas with intensive interaction of sport and leisure (including cemetery)
UA	Airport	Infrastructure of air traffic
UM	Military area	Continuous settlement and infrastructure areas for military purpose
UI	Industry	Continuous infrastructure areas for industrial purpose
S – Soil		
SL	Limestone Mining	Limestone mine above ground for industrial use
SC	Clay Mining	Clay mine above ground for industrial use
Land Cover Classes		
S – Soil		
SG	Gravel	Gravelly areas, mostly flood plain near the coast
SS	Sand	Sandy areas, mostly near the coast
V – Vegetation		
VD	Vegetation (dense)	Dense rainforest and palm forest
VM	Vegetation (mixed)	Mixture of rainforest and palm trees combined with bushes
VS	Vegetation (sparse)	Separate single trees, single bushes and grass
VB	Slash and Burn	Former areas of mixed and sparse vegetation which was used for slash and burn
W – Waterbodies		
WO	Ocean	Open saline waterbodies of the ocean
WR	River	Flowing fresh waterbodies in natural and artificial riverbed
WL	Lake	Stock-still fresh waterbodies
WF	Flooding	Current stock-still waterbodies with soil and mud

Table 5.2: Choice of the 22 classes with ID and description

5.5 Description of the classes

5.5.1 A - Agriculture

AM – Mixed Farming

Primary content:	Plantation, grassland	Primary coverage:	$\geq 50 \%$
Secondary content:	Mixed, sparse vegetation and soil	Secondary coverage:	$< 50 \%$
Degree of sealing:	0 %	Use:	Diverse agriculture

Table 5.3: Content, degree of sealing, proportion and land use of the class Mixed Farming

Description:

- Diverse plantation for fruit-growing,
- Includes grassland for cattle-breeding
- Small plantation plots for different agricultural use (agriculture, grassland, fruit-growing, diverse permanent crop)
- Maximum elevation about 100 m

Land Cover:

- Agricultural crop

Land Use:

- Fruit-growing, cattle-breeding, diverse agriculture

Picture:



Figure 5.1: left: Diverse plantations for fruit-growing, right: Grassland for cattle-breeding

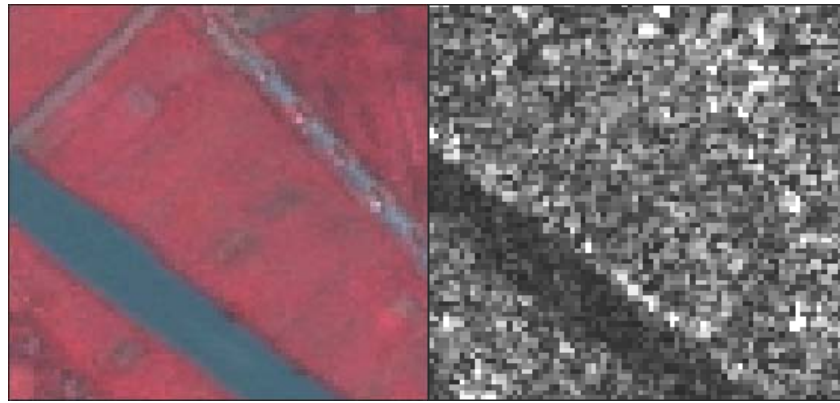


Figure 5.2: left: Plantations in the SPOT 5 scene, right: Plantations in the Radarsat scene

AP – Paddy Farming

Primary content:	Paddy fields	Primary coverage:	$\geq 50 \%$
Secondary content:	Water, clay	Secondary coverage:	$< 50 \%$
Degree of sealing:	0 %	Use:	Paddy Farming

Table 5.4: Content, degree of sealing, proportion and land use of the class Paddy Farming

Description:

- Paddy field, mixture of partly flooded, dry, bloomy and harvested paddy
- maximum elevation about 60 m, plane acreage (slope about 0°)

Land Cover:

- Agricultural crop (paddy plant), water, clay

Land Use:

- Paddy Farming

Picture:



Figure 5.3: left: Flooded paddy fields, right: paddy fields with bloomy paddy (more green)



Figure 5.4: left: Paddy fields which are ready for harvest (colour: yellow), right: dry paddy fields after harvest

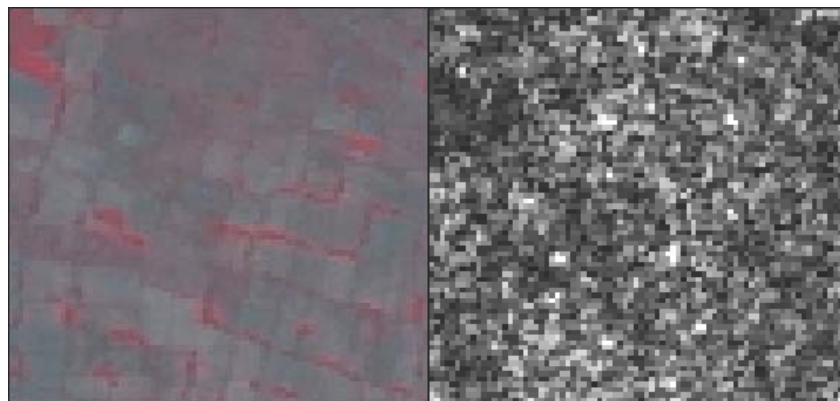


Figure 5.5: left: Paddy fields in the SPOT 5 scene, right: Paddy fields in the Radarsat scene

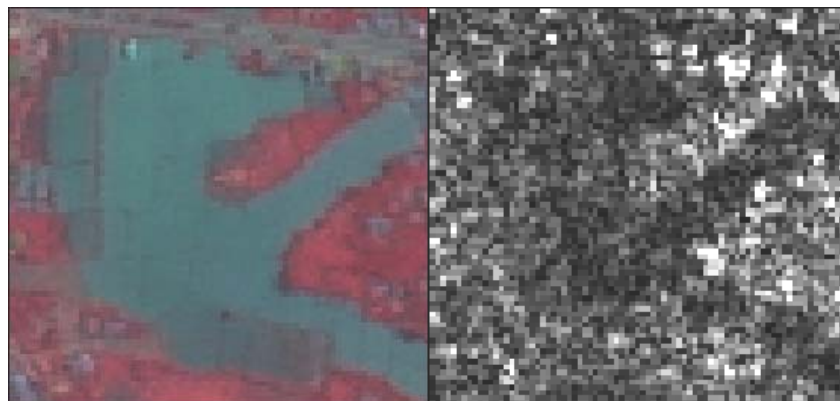


Figure 5.6: left: wet Paddy fields in the SPOT 5 scene, right: wet Paddy fields in the Radarsat scene

AF – Fish Farming

Primary content:	Waterbodies	Primary coverage:	$\geq 90 \%$
Secondary content:	Clay, sand	Secondary coverage:	$< 10 \%$
Degree of sealing:	0 %	Use:	Fish Farming

Table 5.5: Content, degree of sealing, proportion and land use of the class Fish Farming

Description:

- Water ponds for Fish Farming
- Maximum elevation about 15 m

Land Cover:

- Water ponds

Land Use:

- Fish Farming

Picture:



Figure 5.7: Water ponds for Fish Farming

5.5.2 U – Urban

UD – Urban (dense)

Primary content:	Settlement, infrastructure	Primary coverage:	$\geq 80 \%$
Secondary content:	Vegetation	Secondary coverage:	$< 20 \%$
Degree of sealing:	$\geq 80 \%$	Use:	Settlement

Table 5.6: Content, degree of sealing, proportion and land use of the class Urban (dense)

Description:

- Continuous dense settlement and infrastructure areas
- Land coverage under intensive anthropogenic interaction
- mostly near north coast
- maximum elevation about 15 m

Land Cover:

- Dense settlement and infrastructure areas
- Partly vegetated (single trees, bushes, grass)

Land Use:

- Settlement: habitation and mixed usage

Picture:



Figure 5.8: Dense settlement

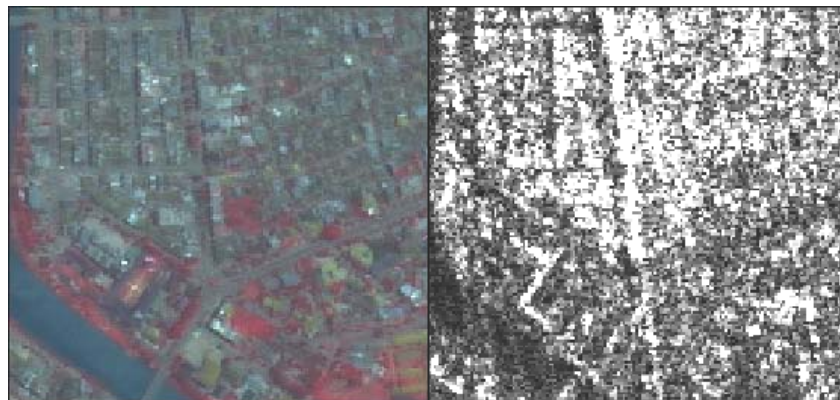


Figure 5.9: left: Dense settlement in the SPOT 5 scene, right: Dense settlement in the Radarsat scene

US – Urban (sparse)

Primary content:	Settlement, infrastructure	Primary coverage:	$\geq 50 \%$
Secondary content:	Vegetation	Secondary coverage:	$< 50 \%$
Degree of sealing:	$\geq 50 \%$	Use:	Settlement

Table 5.7: Content, degree of sealing, proportion and land use of the class Urban (sparse)

Description:

- Continuous sparse settlement and infrastructure areas
- Land coverage under intensive anthropogenic interaction
- Maximum elevation about 60 m

Land Cover:

- Sparse settlement and infrastructure areas
- Vegetation (trees, bushes, grass)

Land Use:

- Settlement: habitation and mixed usage

Picture:



Figure 5.10: left: Building of sparse settlement, right: Typical sparse settlement [aerial image]

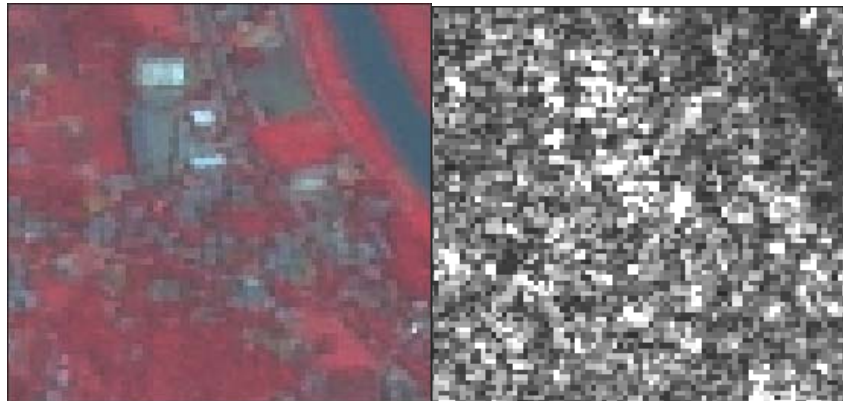


Figure 5.11: left: Sparse settlement in the SPOT 5 scene, right: Sparse settlement in the Radarsat scene

UR – Urban (rebuild)

Primary content:	Settlement, infrastructure	Primary coverage:	$\geq 50 \%$
Secondary content:	Vegetation, Gravel, Sand	Secondary coverage:	$< 50 \%$
Degree of sealing:	$\geq 50 \%$	Use:	Settlement

Table 5.8: Content, degree of sealing, proportion and land use of the class Urban (rebuild)

Description:

- Rebuild, mostly former destroyed and flooded settlement and infrastructure areas near the coast (about 90 %)
- Newly built settlement and infrastructure areas (10 %) mostly in the north east
- Partly continuous sparse settlement and infrastructure areas
- Maximum elevation of former destroyed areas about 15 m

Land Cover:

- Dense settlement and infrastructure areas
- Vegetation (trees, bushes, grass)

Land Use:

- Settlement: habitation and mixed usage

Picture:



Figure 5.12: left: Rebuilt settlement near the coast, right: Newly built settlement

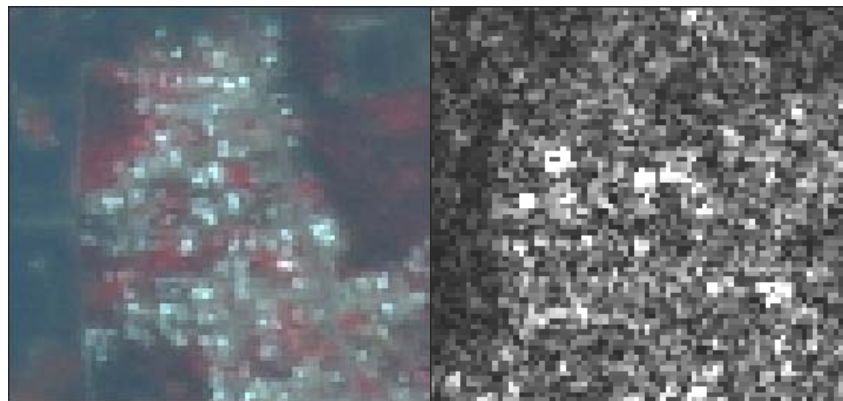


Figure 5.13: left: Destroyed settlement in the SPOT 5 scene, right: Destroyed settlement in the Radarsat scene

UP – Park and sport field

Primary content:	Parks, sport fields	Primary coverage:	$\geq 50 \%$
Secondary content:	Vegetation	Secondary coverage:	$< 50 \%$
Degree of sealing:	0 %	Use:	Leisure

Table 5.9: Content, degree of sealing, proportion and land use of the class Park, sport field

Description:

- Parks in residential areas with intensive interaction of sport and leisure
- Sport field areas with intensive interaction of sport
- Including cemetery parks
- Maximum elevation about 60 m
- Mostly near urban areas

Land Cover:

- Parks, sport ground, vegetation

Land Use:

- Leisure, sport activities

Picture:

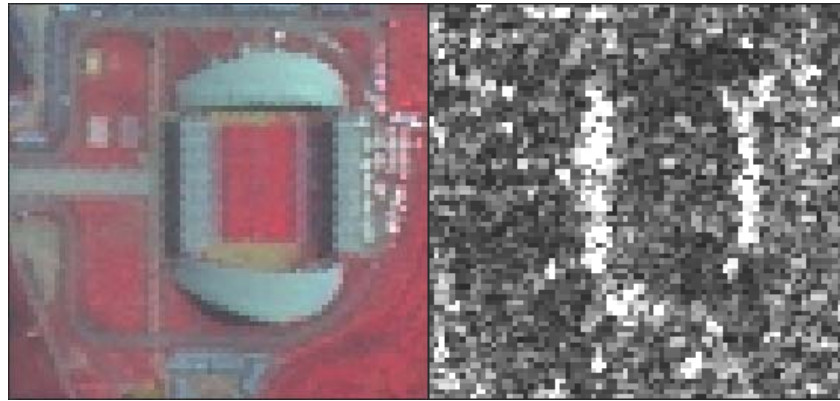


Figure 5.14: left: Park, sport field in the SPOT 5 scene, right: Park, sport field in the Radarsat scene

UA – Airport

Primary content:	Infrastructure for air traffic	Primary coverage:	$\geq 70 \%$
Secondary content:	Settlement, Vegetation	Secondary coverage:	$< 30 \%$
Degree of sealing:	$> 70 \%$	Use:	Air traffic

Table 5.10: Content, degree of sealing, proportion and land use of the class Airport

Description:

- Infrastructure of air traffic
- Domestic airport
- Maximum elevation about 25 m
- Plane runway

Land Cover:

- Infrastructure of air traffic, settlement, vegetation

Land Use:

- Air traffic

Picture:

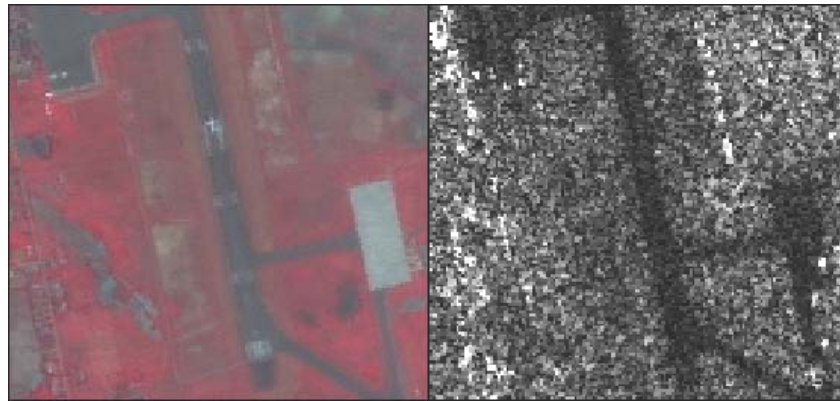


Figure 5.15: left: Airport in the SPOT 5 scene, right: Airport in the Radarsat scene

UM – Military area

Primary content:	Infrastructure for military	Primary coverage:	$\geq 70 \%$
Secondary content:	Vegetation, sand, clay	Secondary coverage:	$< 30 \%$
Degree of sealing:	$> 70 \%$	Use:	Military

Table 5.11: Content, degree of sealing, proportion and land use of the class Military

Description:

- Continuous settlement and infrastructure areas for military purpose
- Settlement: barracks
- Maximum elevation about 60 m

Land Cover:

- Settlement (barracks), vegetation, sand, clay

Land Use:

- Military

UI – Industry

Primary content:	Industrial infrastructure	Primary coverage:	$\geq 70 \%$
Secondary content:	Vegetation, sand, clay	Secondary coverage:	$< 30 \%$
Degree of sealing:	$> 70 \%$	Use:	Industry

Table 5.12: Content, degree of sealing, proportion and land use of the class Industry

Description:

- Continuous infrastructure areas for industrial purpose
- Mainly represented by a cement factory
- Maximum elevation about 60 m

Land Cover:

- Industrial infrastructure, vegetation, sand, clay

Land Use:

- Industry

Picture:



Figure 5.16: Cement factory

5.5.3 S - Soil

SL – Limestone Mining

Primary content:	Limestone	Primary coverage:	$\geq 70 \%$
Secondary content:	Vegetation	Secondary coverage:	$< 30 \%$
Degree of sealing:	0 %	Use:	Limestone Mining

Table 5.13: Content, degree of sealing, proportion and land use of the class Limestone Mining

Description:

- Limestone mine aboveground for industrial use
- Maximum elevation about 220 m

Land Cover:

- Limestone, vegetation

Land Use:

- Limestone Mining

Picture:



Figure 5.17: Limestone mine

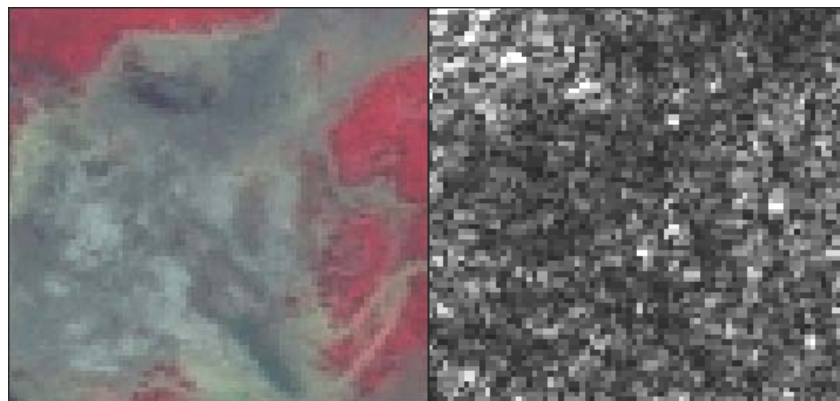


Figure 5.18: left: Limestone mine in the SPOT 5 scene, right: Limestone mine in the Radarsat scene

SC – Clay Mining

Primary content:	Clay	Primary coverage:	$\geq 70 \%$
Secondary content:	Vegetation	Secondary coverage:	$< 30 \%$
Degree of sealing:	0 %	Use:	Clay Mining

Table 5.14: Content, degree of sealing, proportion and land use of the class Clay Mining

Description:

- Clay mine above ground for industrial use
- Maximum elevation about 30 m

Land Cover:

- Clay, vegetation

Land Use:

- Clay Mining

Picture:



Figure 5.19: Clay mine

SG – Gravel

Primary content:	Gravel	Primary coverage:	$\geq 50\%$
Secondary content:	Vegetation	Secondary coverage:	$< 50\%$
Degree of sealing:	0 %	Use:	No land use

Table 5.15: Content, degree of sealing, proportion and land use of the class Gravel

Description:

- Gravelly areas, mostly former flooded plain near the coast
- Maximum elevation about 15 m

Land Cover:

- Gravel, vegetation

Land Use:

- No land use

Picture:



Figure 5.20: Gravel

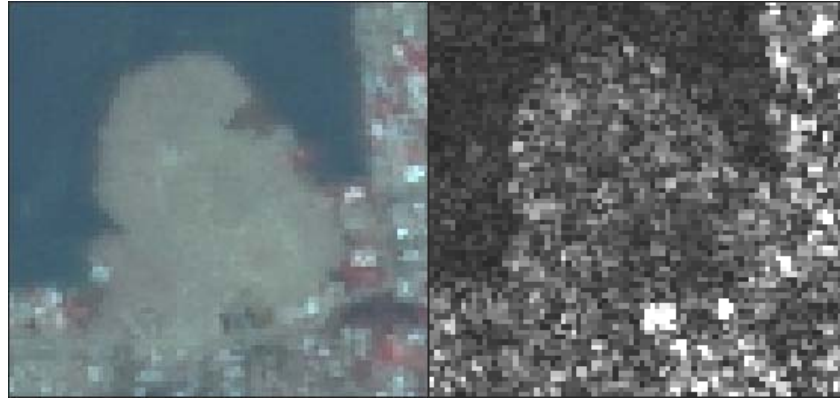


Figure 5.21: left: Gravel areas in the SPOT 5 scene, right: Gravel areas in the Radarsat scene

SG – Sand

Primary content:	Sand	Primary coverage:	$\geq 50 \%$
Secondary content:	Vegetation	Secondary coverage:	$< 50 \%$
Degree of sealing:	0 %	Use:	No land use

Table 5.16: Content, degree of sealing, proportion and land use of the class Sand

Description:

- Sandy areas, mostly near the coast
- Maximum elevation about 15 m

Land Cover:

- Sand, vegetation

Land Use:

- No land use

Picture:

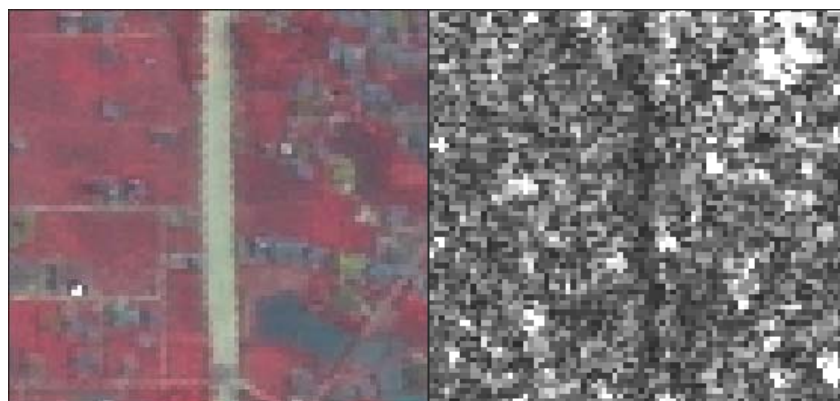


Figure 5.22: left: Sand areas in the SPOT 5 scene, right: Sand areas in the Radarsat scene

5.5.4 V – Vegetation

VD – Vegetation (dense)

Primary content:	Rainforest, palm trees	Primary coverage:	$\geq 80 \%$
Secondary content:	Bushes	Secondary coverage:	$< 20 \%$
Degree of sealing:	0 %	Use:	No explicit land use

Table 5.17: Content, degree of sealing, proportion and land use of the class Vegetation (dense)

Description:

- Dense rainforest and palm forest, evergreen forest

Land Cover:

- Dense evergreen trees (in maturation with minimum height of 5 m)

Land Use:

- Partly individual uprooting otherwise no explicit land use

Picture:



Figure 5.23: left: Evergreen forest, right: Palm forest

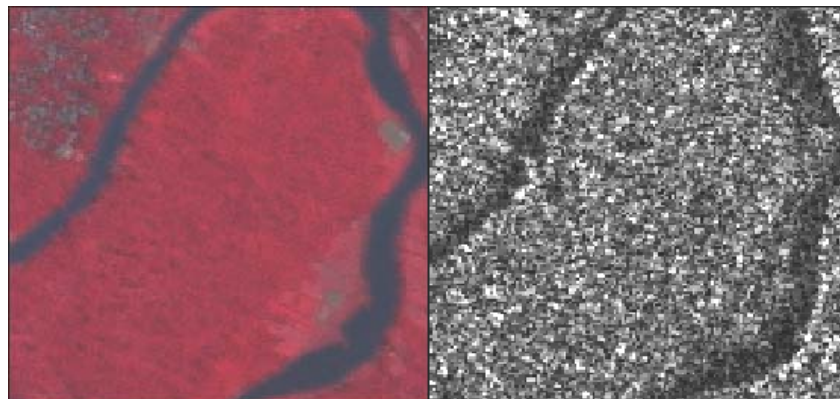


Figure 5.24: left: Dense vegetation in the SPOT 5 scene, right: Dense vegetation in the Radarsat scene

VM – Vegetation (mixed)

Primary content:	Trees, bushes	Primary coverage:	$\geq 50\%$
Secondary content:	Grass	Secondary coverage:	$< 50\%$
Degree of sealing:	0 %	Use:	No explicit land use

Table 5.18: Content, degree of sealing, proportion and land use of the class Vegetation (mixed)

Description:

- Mixture of evergreen forest and palm trees with bushes
- Partly high grass

Land Cover:

- Single evergreen trees (in maturation with minimum height of 5 m)
- Bushes (in maturation with maximum height of 3 m)

Land Use:

- Partly individual cattle-breeding otherwise no clear land use

Picture:



Figure 5.25: Mixed vegetation

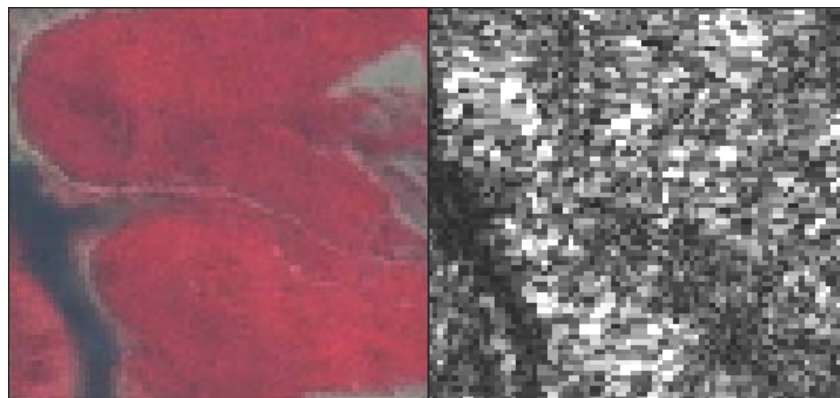


Figure 5.26: left: Mixed vegetation in the SPOT 5 scene, right: Mixed vegetation in the Radarsat scene

VS – Vegetation (sparse)

Primary content:	Grass	Primary coverage:	$\geq 50\%$
Secondary content:	Bushes, trees	Secondary coverage:	$< 50\%$
Degree of sealing:	0 %	Use:	No explicit land use

Table 5.19: Content, degree of sealing, proportion and land use of the class Vegetation (sparse)

Description:

- Grass
- Partly single bushes and separate trees

Land Cover:

- Grass (in maturation with maximum height of 2 m)
- Single bushes

Land Use:

- Partly individual cattle-breeding otherwise no clear land use

Picture:



Figure 5.27: left: Grass, right: Grass with single bushes

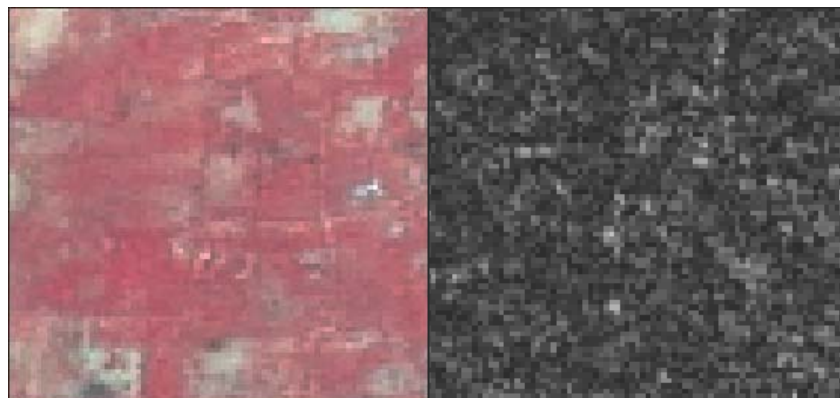


Figure 5.28: left: Dense vegetation in the SPOT 5 scene, right: Dense vegetation in the Radarsat scene

VB – Slash and Burn

Primary content:	Burned vegetation and soil	Primary coverage:	$\geq 50 \%$
Secondary content:	Trees, bushes, grass	Secondary coverage:	$< 50 \%$
Degree of sealing:	0 %	Use:	No land use

Table 5.20: Content, degree of sealing, proportion and land use of the class Slash and Burn

Description:

- Areas of mixed and sparse vegetation which was used for slash and burn
- Partly burned vegetation and soil
- Mostly recovered with sparse vegetation
- Minimum elevation about 20 m

Land Cover:

- Burned clay soil with grass and single bushes

Land Use:

- No land use

Picture:



Figure 5.29: Area of slash and burn, mostly recovered with sparse vegetation

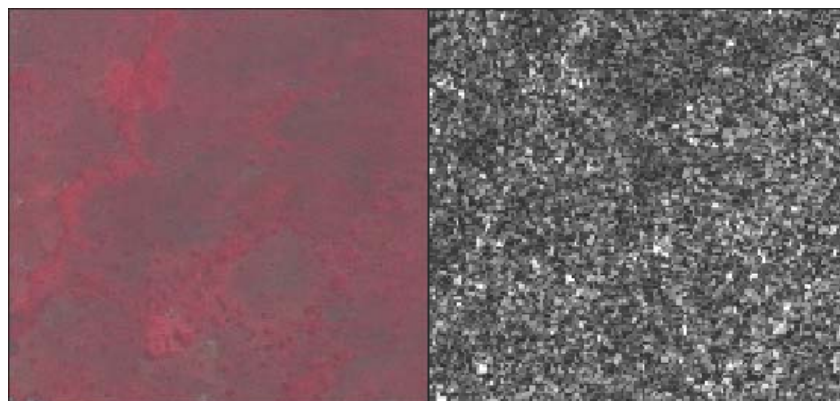


Figure 5.30: left: Dense vegetation in the SPOT 5 scene, right: Dense vegetation in the Radarsat scene

5.5.5 W – Waterbodies

WO - Ocean

Primary content:	Waterbodies	Primary coverage:	$\geq 90 \%$
Secondary content:	Vegetation, soil	Secondary coverage:	$< 10 \%$
Degree of sealing:	0 %	Use:	No explicit land use

Table 5.21: Content, degree of sealing, proportion and land use of the class Ocean

Description:

- Open saline waterbodies of the ocean
- Includes bays, strait, lagoon and reef

Land Cover:

- Water

Land Use:

- Partly individual fishing otherwise no clear land use

Picture:



Figure 5.31: left: Ocean waterbodies in the SPOT 5 scene, right: Ocean waterbodies in the Radarsat scene

WR - River

Primary content:	Waterbodies	Primary coverage:	$\geq 90 \%$
Secondary content:	Vegetation, soil	Secondary coverage:	$< 10 \%$
Degree of sealing:	0 %	Use:	No explicit land use

Table 5.22: Content, degree of sealing, proportion and land use of the class River

Description:

- Flowing fresh waterbodies in natural and artificial riverbed
- Maximum elevation about 60 m

Land Cover:

- Water

Land Use:

- Partly individual fishing otherwise no clear land use

Picture:

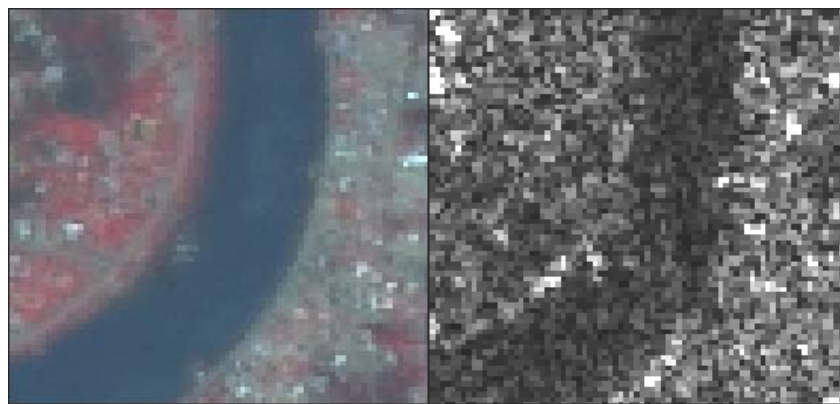


Figure 5.32: left: River waterbodies in the SPOT 5 scene, right: River waterbodies in the Radarsat scene

WR - Lake

Primary content:	Waterbodies	Primary coverage:	$\geq 90 \%$
Secondary content:	Vegetation, soil	Secondary coverage:	$< 10 \%$
Degree of sealing:	0 %	Use:	No explicit land use

Table 5.23: Content, degree of sealing, proportion and land use of the class Lake

Description:

- Stock-still fresh waterbodies
- Maximum elevation about 60 m

Land Cover:

- Water

Land Use:

- Partly individual fishing otherwise no clear land use

WF - Flooding

Primary content:	Waterbodies	Primary coverage:	$\geq 90 \%$
Secondary content:	Vegetation, soil	Secondary coverage:	$< 10 \%$
Degree of sealing:	0 %	Use:	No land use

Table 5.24: Content, degree of sealing, proportion and land use of the class Lake

Description:

- Current stock-still waterbodies with soil and mud
- Still flooded areas caused by the Tsunami
- Near the coast
- Maximum elevation about 10 m

Land Cover:

- Water

Land Use:

- No land use

Picture:



Figure 5.33: Flooding areas



Figure 5.34: left: Flooding areas in the SPOT 5 scene, right: Flooding areas in the Radarsat scene

6 Pixel-based image fusion of optical and SAR data

In the first part of this thesis a pixel-based image fusion approach was accomplished to investigate which pixel-based image fusion technique is best one for optical and SAR imagery with respect to the classification task. The first data set (SPOT 5-Color-2305, SPOT 5-MS-2305, RSAR-2401 / RSAR-0604) was used for this purpose. As classification approach a combination of supervised and knowledge-based classification was chosen. In the first step the classification was performed on the optical SPOT 5 data only. In a second step several image fusion methods for the optical and SAR data were carried out and compared to the results of the optical data set. In a third step the best fusion method was applied on the second data set.

6.1 Multi-spectral classification of the optical SPOT 5 data

The classification based on optical SPOT 5 data is used as benchmark for the fusion schemes.

6.1.1 Optical SPOT 5 data

The optical data set consists of the scenes SPOT 5-Color-2305 and SPOT 5-MS-2305 of the second data set which were introduced in section 4.5.2. An optical SPOT 5 scene is comprised to the four bands (G, R, NIR and SWIR, table 6.1).

No.	Band	Spectral range [μm]	Resolution [m]
1	Green	0,50 – 0,59	5
2	Red	0,61 – 0,68	5
3	NIR	0,79 – 0,89	5
4	SWIR	1.58 – 1.75	5 (10)

Table 6.1: Pure optical data set of SPOT 5 for the multi-spectral classification

6.1.2 Classes

The pixel-based classification in ERDAS included only land cover aspects. Thus the classification was generally done on the five categories of land coverage (Tab. 6.2). In this case the result should not be a land use map. This was done later in the object-based approach.

ID	Categories
A	Agriculture
S	Soil
U	Urban
V	Vegetation
W	Waterbodies

Table 6.2: Land cover categories for the multi-spectral classification of the SPOT 5 data

For the classification process and the selection of the samples all classes (except Industry and Military area) were used for the classification. For the analysis and the illustration only the five categories were considered.

Thus, the classes were not grouped semantically like in the classification system in chapter 5, but spectrally. For example, the class Park and sport field was referenced to the land cover category Vegetation. Fish Farming was attached to Waterbodies (Tab. 6.3). In case of the paddy fields it was also distinguished between the different kinds of paddy fields (Tab. 6.4), which were presented in section 1.4 and 5.5.1. For example, the subclass Paddy (wet) was added to Waterbodies and the other paddy fields (bloomy, harvested and dry) stayed in their semantically category Agriculture.

ID	Classes
	Agriculture
AM	Mixed Farming
AP	Paddy Farming (except wet paddy)
	Urban
UD	Urban (dense)
US	Urban (sparse)
UR	Urban (rebuild)
UA	Airport
UM	Military
UI	Industry
	Soil
SL	Limestone Mining
SC	Clay Mining
SG	Gravel
SS	Sand
	Vegetation
VD	Vegetation (dense)
VM	Vegetation (mixed)
VS	Vegetation (sparse)
VB	Slash and Burn
UP	Park, sport fields
	Waterbodies
WO	Ocean
WR	River
WL	Lake
WF	Flooding
AF	Fish Farming
APW	Paddy Farming (wet paddy)

Table 6.3: Land cover classes spectrally sorted after the Land Cover categories

ID	Subclasses
AP	Paddy Farming
APW	Paddy (wet)
APB	Paddy (bloomy)
APH	Paddy (harvested)
APD	Paddy (dry)

Table 6.4: Subclasses of the class Paddy Farming

6.1.3 Supervised Classification

Supervised Classification is a semi-automatic classification method. First, the interpreter has to define on basis of a classification system the desired thematic classes and to choose a representative training area for every class. Now statistical parameters (e.g. mean value standard deviation, covariance matrices) of the spectral characteristics of the training area are calculated and compared with each other. Based on this comparison the computer defines for every class, which has to be distinguished, a typical spectral signature, the so-called samples (Richards, 1999). Now the real classification can be started. With special algorithms, so-called classifier, every pixel is checked for similarity in all bands with the defined samples. Two common classifiers are *Maximum-Likelihood* and *Nearest-Neighbour*.

6.1.4 Selection of samples

First, for every class predefined samples were detected in the higher resolution aerial image reference data set. The geometric selection of the samples was done by polygons, so-called *Area of Interest (AOI)* in ERDAS, which could be saved and overlaid on every multi-spectral band having the same reference. These samples were overlaid on the SPOT 5 data (Fig. 6.1) and the spectral signature was calculated for each sample. Afterwards the several signatures, which represent the same class, were merged to one representative signature for the class. The mean values of the signatures for every class are given in the annex 12.1.



Figure 6.1: Selection of multiple samples for every class by so-called *AOI*

6.1.5 Analysis of spectral signature

In figure 6.2 the spectral mean values in the four bands of SPOT 5 (spectral range: 0.50 to 1.75 μm) of the five categories are illustrated. These values are derived from the merged mean values of all selected classes, which spectrally belong to this category.

All five categories show a spectral signature which is typical. Vegetation and Agriculture indicate a typical high reflection in the green band caused by absorption in the blue and red band of chlorophyll and a very high reflection in the near infrared band due to the cell structure. In the infrared band the reflectance of vegetation is much higher than the reflectance of agriculture. In the short-wave infrared band the reflectance of both categories is decreasing because of water absorption. But it is shown that these two classes are very similar to each other because of plantations. The plantations include coconut palms and banana shrubs, which are similar to evergreen bushes and trees. This can be seen by comparing the single signatures of the classes.

The category Waterbodies is significant decreasing from the green band to the short-wave infrared band. This is caused by the fact that water is only able to reflect the short visible wave like blue and green. That is why water always seems to be blue or green.

The category Soil presents a typical increasing reflectance in the short-wave infrared band like the category Urban. In the visible and near infrared band the reflectance is not so high because of iron oxide. The high reflection of soil is caused by sand and limestone which are very bright. Soil is similar to Urban caused by the fact that urban structure is normally made of stone or soil. Sparse settlement is an exception. It is more correlated with the category Vegetation because of the fact that this class is mostly surrounded by vegetation.

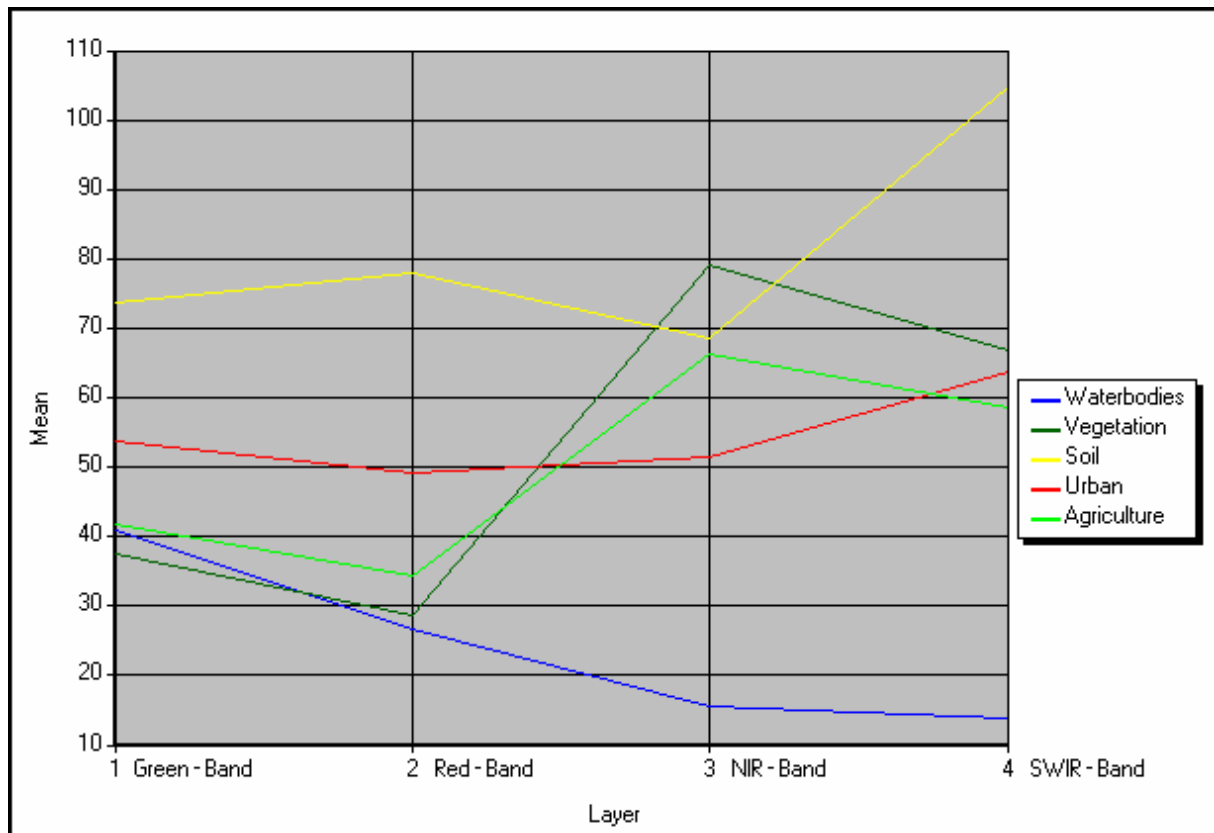


Figure 6.2: Spectral signatures in the four bands of SPOT 5 (spectral range: 0.50 to 1.75) of the five categories

6.1.6 Maximum-Likelihood-Classification

After the selection and analysis of the samples the real classification was accomplished in ERDAS. As classifier the *Maximum-Likelihood Classifier* was selected. This classifier estimates from the statistical parameters of the samples the likelihood function. This function describes the likelihood of every pixel to the class it belongs to. In this case every class in the feature space is assumed a *Gaussian Distribution* about the centre of the class. Because of correlation between the spectral bands elliptic lines of same likelihood are generated. This classifier needs a lot of time during the processing but offers normally much better results than other classifier like the *Minimum-Distance Classifier* because different ranges of dispersion of the measured values are considered (Albertz, 2001).

6.1.7 Additional knowledge-based information

Based on the supervised classification, knowledge-based information was added. Knowledge-based information is mostly given by extern, artificial data layer (e.g. digital elevation model, Ratio layer, GIS layer etc.). This information is formulated as criteria or rules mostly by *Boolean Operator* or special functions. If the condition is true, the information is assigned to this class, if it is false it is not assigned. Additional knowledge-based information normally offers better classification results. The NDV-Index for example can give more information about vegetation characteristics. Thus classes of vegetation and non vegetation can be better separated. The digital elevation model can help to correct false class assignments and limit special classes.

For modelling of the knowledge-based information the *Knowledge Classifier* of ERDAS was used. In this tool the rules and criteria were defined for every category. In this case the knowledge-based information include the *DEM layer*, a *NDVI ratio layer*, which was derived from the near infrared and red band and a *SWIR/NIR ratio layer* of the short-wave infrared and near infrared band of the SPOT 5 data.

$$NDVI = \frac{NIR - R}{NIR + R} \quad (6.1)$$

In case of knowledge-based information it can be distinguished between global and local information. Global or universal knowledge-based information includes information to be applied for any kind of data set, for example, normally vegetation shows a NDVI value which is larger than "0". Local information is only adaptable on a concrete data set, for example, in case of certain DEM information for one class. For the five categories the following rules were estimated:

Vegetation

Vegetation is easy to detect by the NDV-Index. Every NDVI value, which is larger than 0, indicates any kind of vegetation because of the high reflectance in the near infrared channel. Nevertheless the threshold was derived by observing the minimum and maximum values of the sample areas of vegetation in the NDVI layer. In the figure 6.3 it is shown that the minimum value of the vegetation class Slash and Burn is with 0.156 larger than 0.

Mostly vegetation is not limited to any elevation. This is also the case in the test area. Thus the DEM layer was not needed for this category. Considering all vegetation the value of the SWIR/NIR ratio can strongly vary from dense vegetation to sparse vegetation with some regions of soil. Thus the SWIR/NIR layer was also not considered in this case.

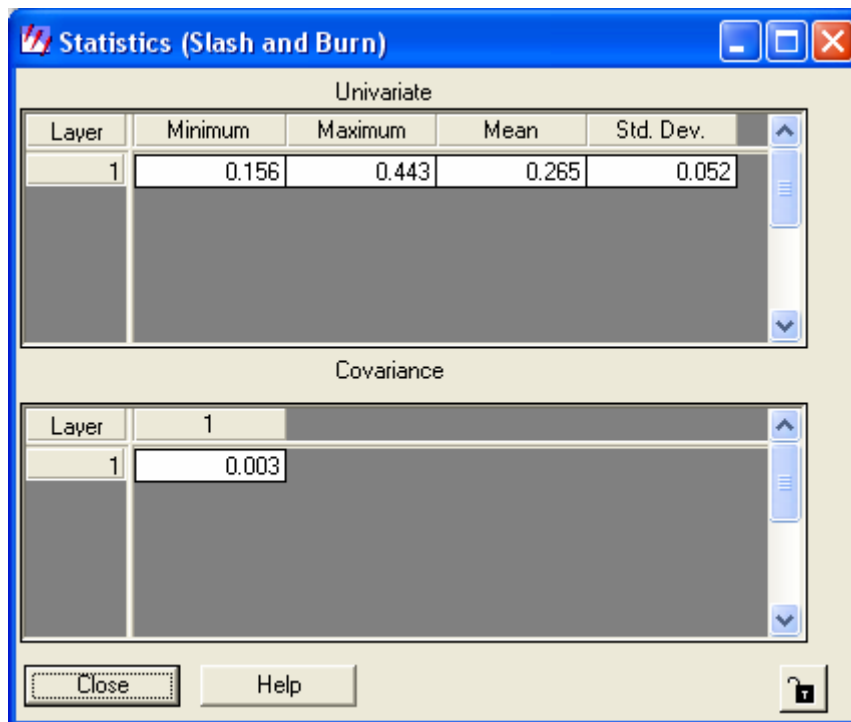


Figure 6.3: Estimating of the minimum NDVI value of the class Slash and Burn

Soil

Normally the category Soil occurs at any elevation like vegetation. But it shows in contrast to vegetation a low NDVI value which is mostly below 0. In this case the maximum border was set to 0.2 because of uncertainties of spectral mixtures with vegetation. The value of the SWIR/NIR ratio is generally quite high, mostly above 1. Thus the value of the SWIR/NIR ratio was set > 1 . The analysis of the DEM revealed that the maximum elevation in the test area of soil is in a range about 220 m.

Waterbodies

Waterbodies can appear at different elevations. The classes Ocean and Flooding are mostly at an elevation of approximately 0 or at a low surface level. In contrast to this the classes River and Lake can also occur in mountainous areas. Thus, a global rule which includes all classes cannot be found here. The maximum elevation of the category Waterbodies is in a range about 50 to 60 m. Therefore the maximum possible elevation was defined with 60 m. As general rule the NDV-Index was used. Normally any kind of waterbody shows a NDVI value < 0 . Waterbodies exhibit also a low value in the SWIR/NIR ratio. However, the class Flooding contains a high degree of soil, so that the maximum SWIR/NIR value reaches 1.4.

Agriculture

Agriculture areas behave similar to vegetation in case of the NDV-Index. But they are limited to certain elevations and slopes. Agriculture is mostly cultivated at a low slopes. Thus, a Slope rule could provide a differentiation to the correlating category vegetation. But agriculture contains also plantations, which partly occur at the foothills where the slope can be high. Additionally, the derived slope layer from the DEM presents also artefacts and error. Therefore the Slope layer was not used in this case. The maximum elevation in the test area

was estimated with about 100 m. Because of uncertainties and mixture signatures with soil the NDVI border was set > -0.1 . The SWIR/NIR layer was also not considered as in case of vegetation because of the same strong variations in this category.

Urban

Normally urban areas indicate like soil a low NDVI and a high SWIR/NIR ratio value. But in this case a suitable threshold is difficult to find, because of sparse settlement. This class is highly correlated with vegetation and agriculture because it is mostly present near these categories. The maximum NDVI and the minimum SWIR/NIR value were determined with 0.5. The maximum elevation in the test area was estimated by approximately 60 m.

To summarize the following global and local criteria were estimated:

	DEM [m]	Ratio NDVI []	Ratio SWIR/NIR []
Agriculture	< 100	> -0.1	-----
Soil	< 220	< 0.2	> 1
Urban	< 60	< 0.5	> 0.5
Vegetation	-----	> 0	-----
Waterbodies	< 60	< 0	< 1.4

Table 6.5: Rules and criteria of the knowledge-based classification

Simulation of fuzzy rules

The Knowledge Classifier in ERDAS offers only Boolean Operator (true = 1 or not true = 0). In circumstance of a containment of a class by this classifier the pixel which does not fulfil this criterion is not classified. In order to avoid an exceeding number of unlabelled pixel, these pixel were assigned to the class with the greatest correlation or further knowledge-based information.

For instance a pixel initially assigned to class urban, which is above 60 m and misclassified, will be assigned to another class, which is very common in mountainous areas, like vegetation or soil. Unclassified pixel were simply distributed to the next likely category.

First the supervised classification result of every category (e.g. water == 1) was assigned as single variable by an own rule to the same category. In the next step the single restrictions of the DEM, NDVI and SWIR/NIR layer were added as new variable to the same rule. In order to classify the untagged pixel, new rules with complementary variables were formulated (e.g. > 60 m). These rules were assigned to the category where it fits best. In case of the DEM and slope all pixel were added to the category Vegetation. In case of the NDV-Index it is difficult to assign the untagged pixel to the correct category. For example, the unclassified pixel of agriculture caused by NDVI, were assigned to waterbodies because of the correlation of the wet paddy fields to the category Waterbodies. In case of the SWIR/NIR layer the unclassified pixel of Soil were assigned to Urban because of the high correlation.

A detailed illustration of the single rules and different assignments is given in the annex 12.2.

6.2 Pixel-based image fusion

In the next step three different pixel-based image fusion methods for the fusion of optical and SAR data were applied and tested.

6.2.1 Selection of image fusion methods

In chapter 3 several image fusion methods were introduced and the problems of the image fusion were discussed.

The selection of a method depends on the data and the purpose of the image fusion. In the case of the fusion of optical and radar data it is difficult to find an adequate fusion method with respect to the preservation of spectral and spatial image characteristics. In case of pan sharpening of multi-spectral and panchromatic data of the same sensor, the panchromatic band is usually highly correlated with the multi-spectral bands. Hence, a substitution of the intensity channel in an IHS Transform or of the first component in case of a PCA Transform is justified. In general, radar images do not show comparable correlation with multi-spectral bands because radar images are different from multi-spectral images. Radar images describe more the physical object characteristics. An investigation on correlation (q.v. annex 12.3) between the optical SPOT 5 and the Radarsat SAR data has shown (Tab. 6.6) that the radar image does not correlate with one of the visual bands, but with the infrared bands. In comparison to this, the correlation between the panchromatic band and the multi-spectral bands is much higher (Tab. 6.7), especially in case of the two visual bands.

[]	Band 1 [G]	Band 2 [R]	Band 3 [NIR]	Band 4 [SWIR]	Average
SAR	-0,014	0,181	0,563	0,504	0,309

Table 6.6: Correlation between the multi-spectral bands of SPOT 5 and the Radarsat SAR scene

[]	Band 1 [G]	Band 2 [R]	Band 3 [NIR]	Band 4 [SWIR]	Average
Pan	0,980	0,978	0,142	0,373	0,618

Table 6.7: Correlation between the multi-spectral bands of SPOT 5 and the panchromatic scene

IHS Transformation

For an IHS Transformation it has to be checked, if the calculated intensity channel could be correlated with the Radarsat scene, or not. In case of the first three bands it can be stated that the Radarsat scene is not highly correlated as the panchromatic band (Tab. 6.8). But the panchromatic band shows on the other hand no high correlation with the near infrared band which does not cover the spectrum of the panchromatic band. The whole matrices are given in the annex 12.3.

[]	SPOT 5 Intensity channel [G, R, NIR]	SPOT 5 Intensity channel [R, NIR, SWIR]
Pan	0.57867	0.50444
Radarsat	0.47651	0.53168

Table 6.8: Correlation between the intensity channel of SPOT 5 and the Radarsat scene and the panchromatic band of SPOT 5

In case of the last three bands the result could be inverted because the fourth band is much more correlated with the Radarsat scene as the panchromatic scene. But these calculations are limited on three bands. The common IHS Transform cannot consider all four bands in one single processing step.

However, the Ehlers Fusion, which was introduced in section 3.4.3, is able to do this. Hence, the Ehlers Fusion was applied. This method was available as a module in ERDAS with the same name (Fig. 6.4). In this module the fusion is offered in one single step and it is possible to vary the result. There are several parameters for the used filter design which can be changed before the processing. It is possible to stress either spectral or spatial resolution or a mixture of both. Beside these special characteristics of the image content (e.g. urban or mixed, rural or other areas) can be emphasized. It is also possible to create a manual filter mask in the advanced mode. For the image fusion the spectral parameter and for the image content urban or mixed were selected in order to get the maximum spectral similarity and to emphasize the mixture of urban and rural areas. The resample mode before the IHS merge was switched off in order to obtain the original grey values as long as possible.

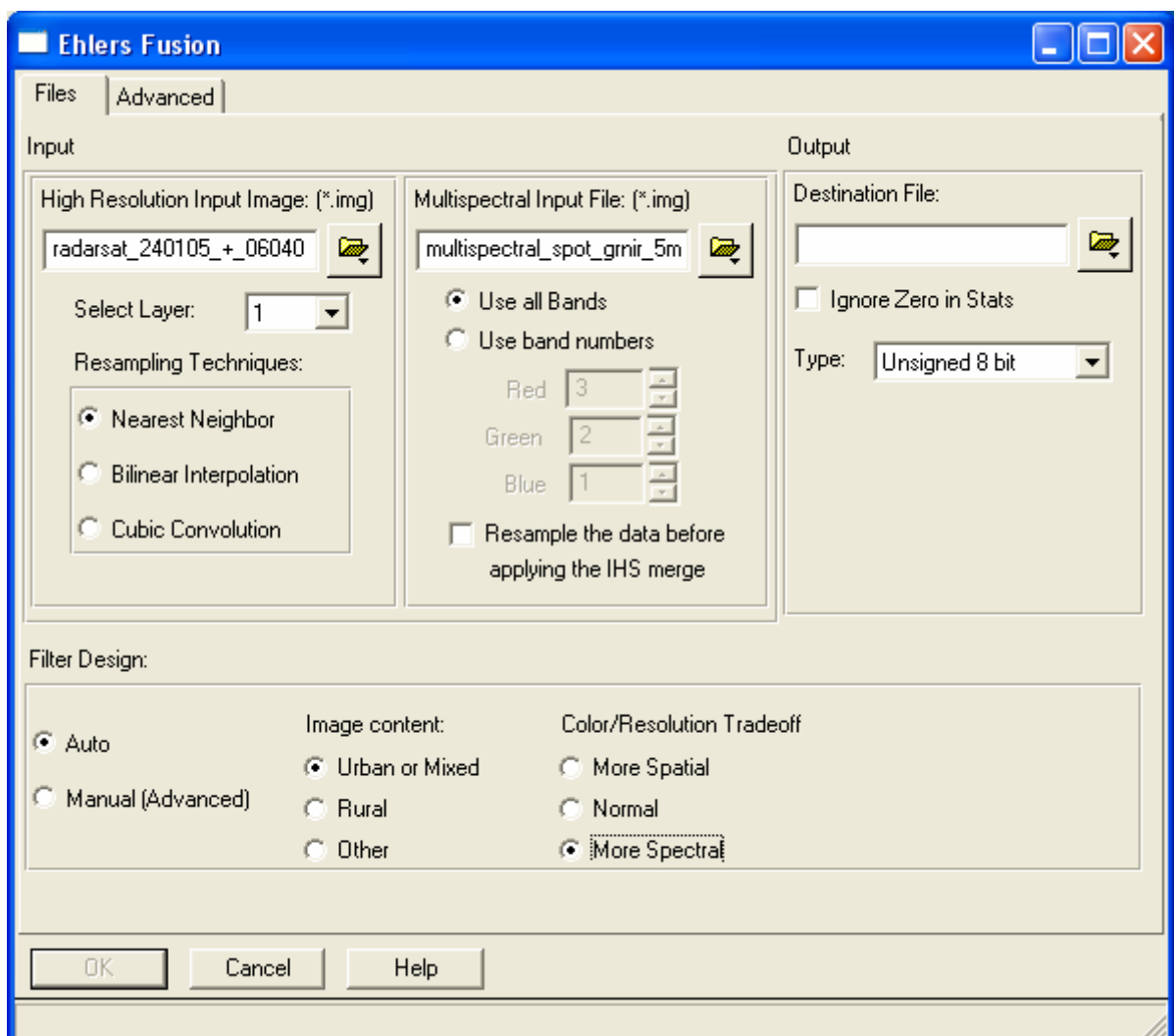


Figure 6.4: Ehlers Fusion tool in ERDAS imagine

PCA Transform

In case of the PCA transform the aspect of band correlation is similar to the IHS transform. The first component should be correlated with the intensity band. Here it can be stated that the Radarsat scene is much higher correlated with the first component as the panchromatic band (Tab. 6.9).

[]	1. PC
Pan	0.32037
Radarsat	0.55885

Table 6.9: Correlation between the first principal component and the Radarsat scene and the panchromatic band

Therefore a PCA Transform seems to promise quite good results by using the Radarsat scene. A correlation of 0.56 is not very high, but in case of a pan sharpening of the first three multi-spectral bands with the panchromatic band the correlation is not much higher. Some scientists (Gungor and Shan, 2006; Sun, 2006) stated in their investigations that the PCA Transform offers not quite satisfying results because of colour distortion. This has to be proofed. For instance, the use of the Radarsat scene should offer better results than by using the panchromatic band.

The Principal Component Analysis was done in several steps. First all multi-spectral bands of the SPOT 5 data were divided into four components by the tool *Principal Component* which is offered in ERDAS (Fig. 6.5). There the maximum number of components (4) was chosen. The *Eigen Matrix* and the *Eigenvalues* were also calculated (Annex 12.4). The Eigen Matrix gives information about the rotation of the new axis of the transformation space. The Eigenvalues represent the variance of the single components. It could be confirmed that the first component includes the most information because of the highest variance.

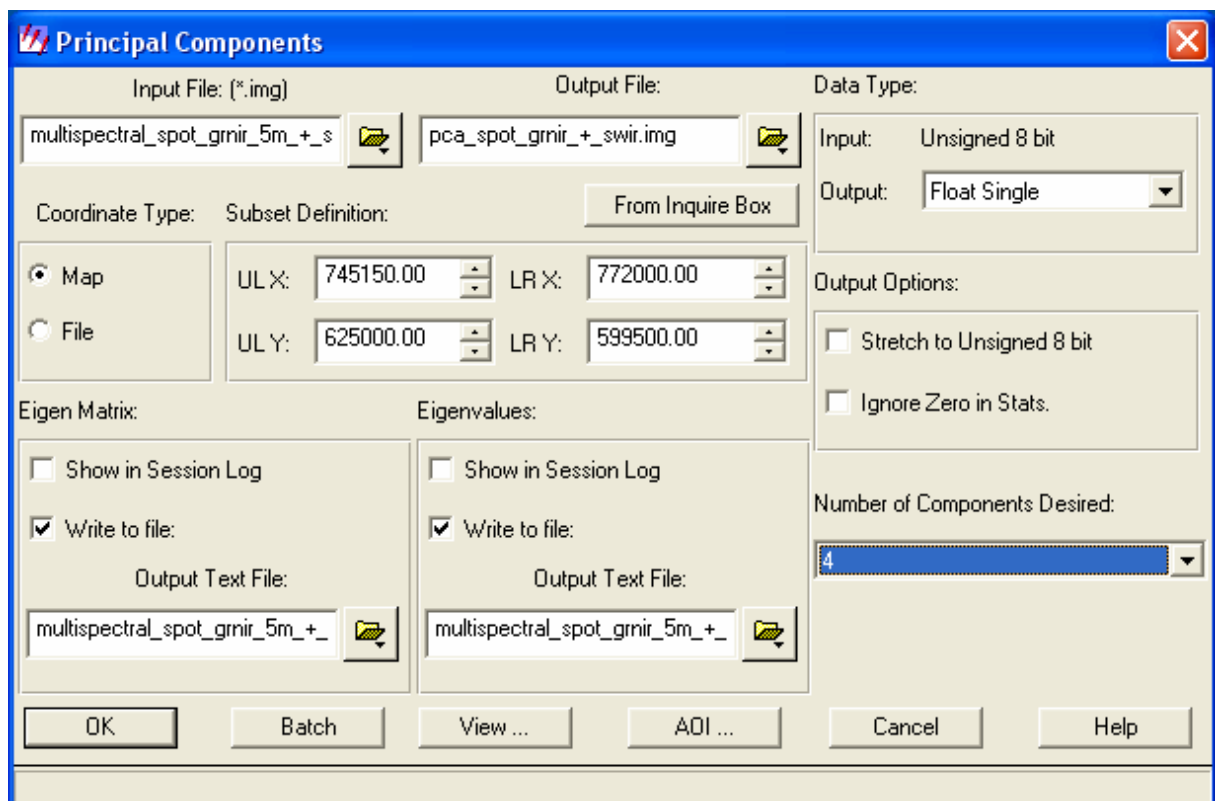


Figure 6.5: Principal Component of the optical bands of SPOT 5 and the Radarsat intensity band

After processing of the first component with the major information it was substituted by the SAR intensity band by using the *Layer Stack* tool in ERDAS. In the next step the new four components were transformed back by the tool *Inverse Principal Component*. This was analogue to the Principal Component processing. In the last step the result was also converted to 8 bit. The transformation steps were done separately by the two Principal Component tools in ERDAS in order to avoid a histogram stretching (Fig 6.6, left). In case of the resolution merge module, where a PC and inverse PC is offered in one step in ERDAS, the histogram is stretched and so the grey values are changed (Fig 6.6, right).

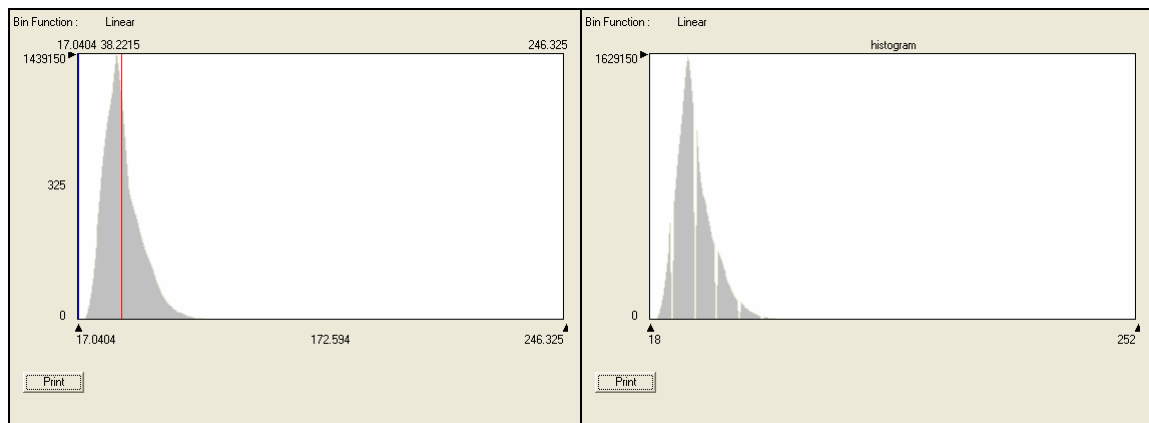


Figure 6.6: left: histogram of PCA processed in several Steps, right: histogram of PCA processed in one step

Multiplicative method

The arithmetic combinations offer four different opportunities. As noted in section 3.4.2 the Multiplicative method gains the minor radiometric changes. But this method is disputed. Rencz (1999) notes in his book that this method is an opportunity to merge optical data with SAR data and Sun (2006) could achieve good results in his investigation by this method although the original radiometry could not be retained. In contrast to this Gungor and Shan (2006) reported stated quite negative results because of high colour distortion. Therefore it is necessary to verify these results and to test the Multiplicative method.

The Multiplicative method was accomplished with the *Operator* tool in ERDAS. Here, every multi-spectral band of the SPOT 5 data was multiplied with the Radarsat intensity image. Afterwards the result was converted into 8 bit.

6.2.2 Knowledge-based classification

After the image fusion the supervised and knowledge-based classification of the three results was done analogue to the procedure applied to optical data. For the classification the same samples and knowledge-based information were used. In the Knowledge Classifier the results of the super-vised classification were simply substituted by the supervised classification results of the three fusion methods. In connection to the accuracy assessment a visual and a statistical comparison was arranged. The results in comparison with the single classification results are presented in the annex 12.6.

6.2.3 Visual comparison

In figure 6.7 a section of each image fusion result and the pure optical data is shown (upper left). In this visual comparison it is clearly visible that the colours of the multiplicative method (upper right) are changed the most, as assumed. Waterbodies or wet areas are turned black and vegetation is more coloured in magenta and not red as usual. The result of the PCA (lower left) shows also colours changes especially for vegetation. Dense and mixed vegetation is coloured more orange, grass and agriculture is darker. The result of the Ehlers Fusion (lower right) seems to preserve the colours best of all fusion methods. But a negative effect is the grainy structure of the image. This is caused by a partly imprecise geocoding. This method needs a precise geocoding in subpixel dimension. This could not be fulfilled.

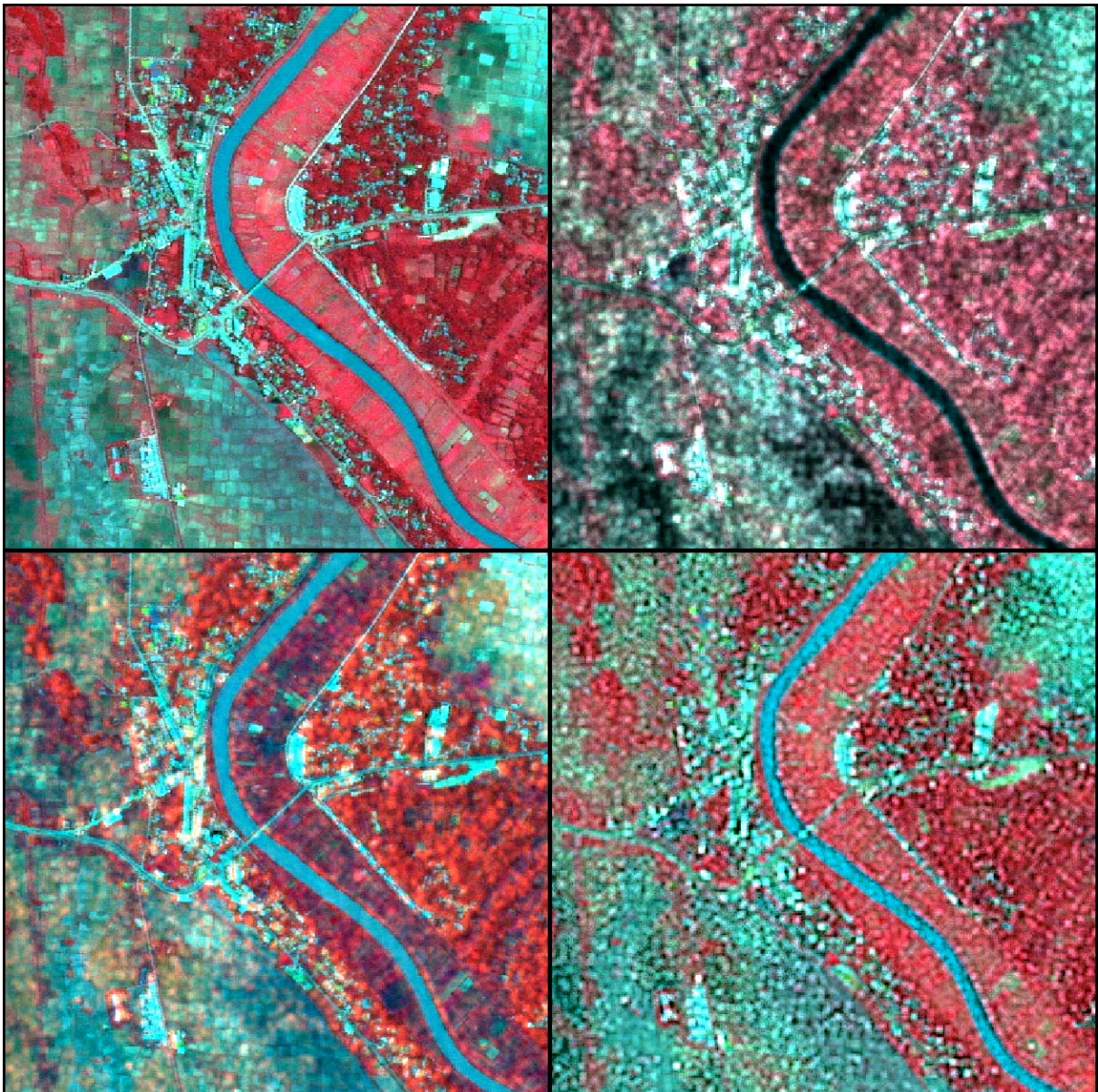


Figure 6.7: Visual comparison of the different image fusion methods in comparison to the optical data of SPOT, upper left: section of the optical SPOT data set, upper right: section of the data set of the image fusion with the Multiplicative method lower left: section of the data set of the image fusion with the Principal Component Analysis (PCA) lower right: section of the data set of the image fusion with the Ehlers Fusion

6.2.4 Statistical comparison

In the statistical comparison of the histogram values the visual impressions are confirmed (Tab. 6.10). Here, the statistical parameter minimum, maximum, mean and the standard deviation are considered. The standard deviation is a good measure for a statistical comparison because it correlates with the grey value changes.

The standard deviation values of the multiplicative fusion changed most for every band except the green band (1) in comparison to the corresponding values of the pure optical bands. The values are simply as big as the mean values. Normally the standard deviation should be less than the mean value like it is the case in the optical and other data. Thus the mean values are not determined precisely. In case of the PCA and Ehlers Fusion the values are more similar to the original values except of the short-wave infrared band (4). All together the Ehlers Fusion shows more correspondence to the optical data than the PCA.

Szene	Band	Min.	Max.	Mean	Std.-Dev.
Radarsat-SAR	1	0	255	42,541	27,132
Optical (SPOT 5-2305)	1	20	255	40,356	10,836
	2	12	255	30,618	13,003
	3	7	255	50,415	27,764
	4	3	241	42,768	24,705
Multiplicative	1	0	255	14,546	10,445
	2	0	255	11,275	9,464
	3	0	255	27,175	21,689
	4	0	255	18,584	15,352
PCA-Transformation	1	0	255	24,018	11,905
	2	0	255	28,144	14,128
	3	0	255	89,273	23,895
	4	0	255	89,605	19,718
Ehlers-Fusion	1	0	255	31,122	11,869
	2	0	255	24,225	13,250
	3	0	255	49,283	27,731
	4	0	255	48,657	28,035

Table 6.10: Statistical comparison of the histogram values of the different image fusion

6.2.5 Absolute accuracy assessment

Now the classification results of the optical and the merged data and their absolute accuracy were checked.

Visual comparison of the classification

In the visual comparison of the classification results (Fig. 6.8) it is obvious that all fusion methods cannot achieve better classification results in comparison to the result of optical data. All methods have difficulties to distinguish between the two categories Urban and Soil. A lot of urban areas (red) are classified as soil (yellow). In this case the correlation between Urban and Soil cannot be decreased by the fusion methods, but rather increased. Vegetation (dark green) is also not adequate classified in state of the Multiplicative and Ehlers fusion. In case of Waterbodies (blue) and Agriculture (green) the differences are not so high at first view.

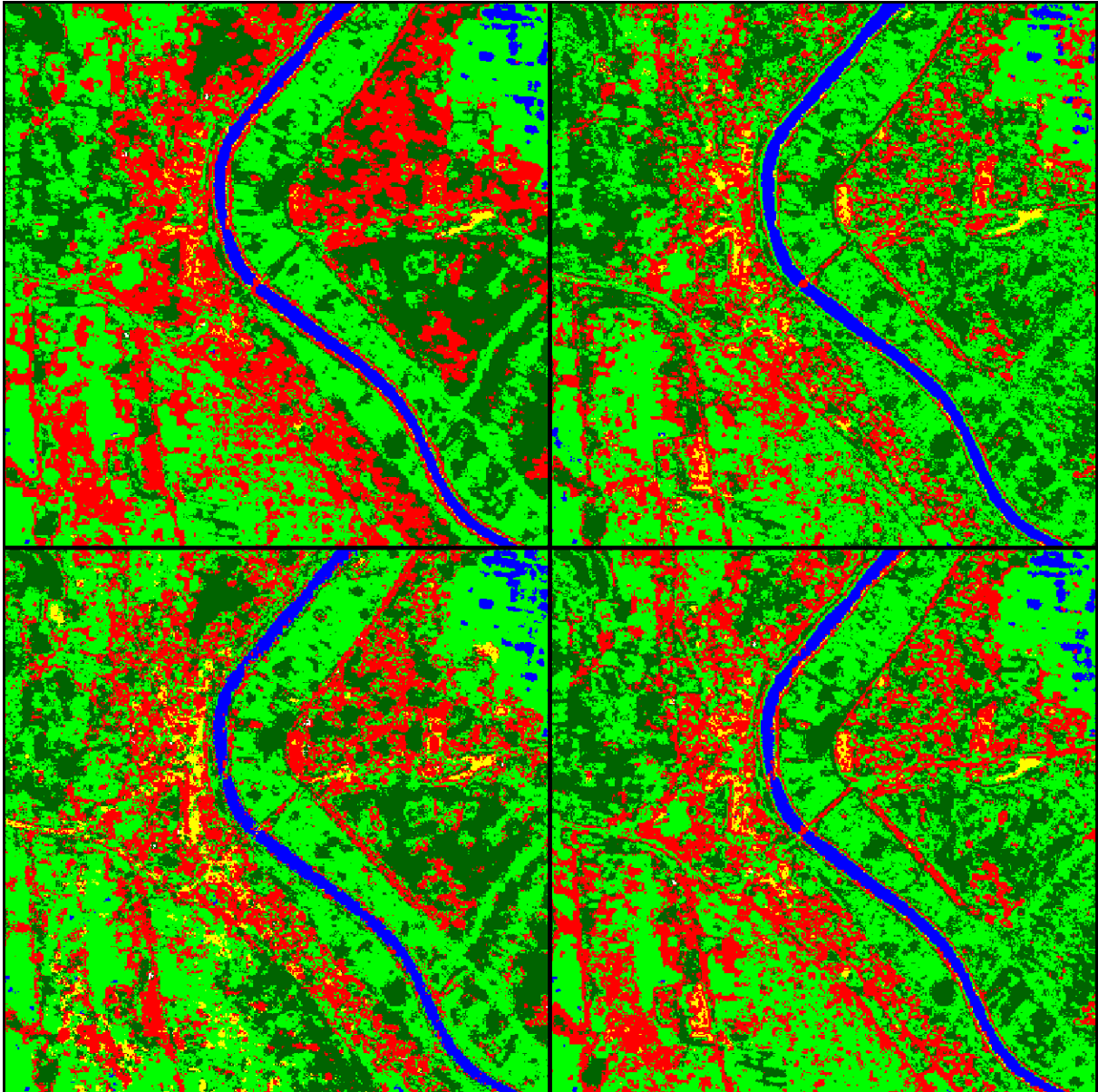


Figure 6.8: Visual comparison of the different image fusion methods in comparison to the optical data of SPOT, upper left: section of the optical SPOT data set, upper right: section of the data set of the image fusion with the Multiplicative method lower left: section of the data set of the image fusion with the Principal Component Analysis (PCA) lower right: section of the data set of the image fusion with the Ehlers Fusion

Reference points

After the visual comparison the absolute accuracy of all classification results was analysed. For an absolute accuracy assessment ERDAS offers a tool which is limited on reference points. Thus no reference areas can be chosen. In order to simulate reference areas that are bigger than one pixel, multiple small reference masks of 3 x 3 pixel were used for every class. The dimension of 3 x 3 pixel was chosen because ERDAS Imagine only considers the eight neighbouring pixel. Another reason is the fact that in a pixel-based approach most areas are not homogeneous because of the so-called “Salt and Pepper” effect. The created mask (Fig. 6.9) includes one centre point of reference (P1) which was extracted from the reference data set and ground check and its eight neighbouring pixel. Consequently nine points were generated per mask with a distance of 1 pixel. Overall 1100 reference masks were built.

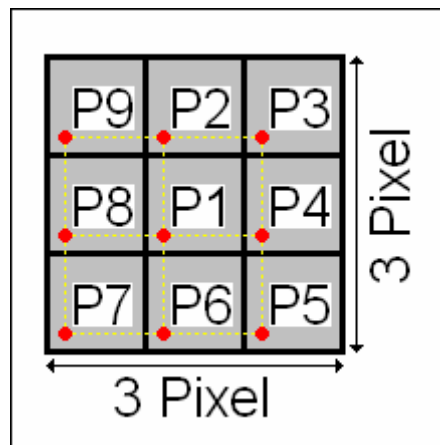


Figure 6.9: Reference mask of 3 x 3 pixel (with 9 reference points)

Accuracy assessment of the optical SPOT 5 data set

The table 6.11 shows the confusion matrix of the supervised classification without additional knowledge-based information. The error matrix gives information about the relationship and correlation between the different classes. Additionally several accuracy measures are given. The *Producer accuracy* describes the percentage how the classification fits with the reference data. While the *User accuracy* gives information how the reference data agrees with the classification. The *Kappa Coefficient* expresses the proportionate reduction in error generated by a classification process compared with the error of a completely random classification. A value of 0.82, for example, implies that the classification process is avoiding 82 percent of the errors that a completely random classification generates (ERDAS Field Guide 9.1, 2005).

Confusion Matrix [Pixel]						
User \ Reference	Waterbodies	Vegetation	Urban	Soil	Agriculture	Sum
Unclassified	0	0	0	0	0	0
Waterbodies	2149	0	0	0	40	2189
Vegetation	0	2061	6	14	102	2183
Urban	9	49	1626	195	94	1973
Soil	2	4	99	683	9	797
Agriculture	90	136	69	8	1555	1858
Sum	2250	2250	1800	900	1800	9000
Accuracy []						
Class Name	Reference Totals	Classified Totals	Number Correct	Producer [%]	User [%]	Kappa []
Undefined	0	0	0	---	---	0.0000
Waterbodies	2250	2189	2149	95.51	98.17	0.9756
Vegetation	2250	2183	2061	91.60	94.41	0.9255
Urban	1800	1973	1626	90.33	82.41	0.7802
Soil	900	797	683	75.89	85.70	0.8411
Agriculture	1800	1858	1555	86.39	83.69	0.7962
Totals	9000	9000	8074			
Total accuracy []						
Overall Accuracy	89.7					
Overall Kappa	0,869					

Table 6.11: Error Matrix and accuracy values of the optical supervised classification

Confusion Matrix [Pixel]						
User \ Reference	Waterbodies	Vegetation	Urban	Soil	Agriculture	Sum
Unclassified	0	0	0	0	0	0
Waterbodies	2134	0	8	0	41	2183
Vegetation	0	2125	6	20	102	2253
Urban	9	19	1626	191	94	1939
Soil	1	4	99	681	9	794
Agriculture	106	102	61	8	1554	1831
Sum	2250	2250	1800	900	1800	9000
Accuracy []						
Class Name	Reference Totals	Classified Totals	Number Correct	Producer [%]	User [%]	Kappa []
Undefined	0	0	0	---	---	0.0000
Waterbodies	2250	2183	2134	94.84	97.76	0.9701
Vegetation	2250	2253	2125	94.44	94.32	0.9242
Urban	1800	1939	1626	90.33	83.86	0.7982
Soil	900	794	681	75.67	85.77	0.8419
Agriculture	1800	1831	1554	86.33	84.87	0.8109
Totals	9000	9000	8120			
Total accuracy []						
Overall Accuracy	90.2					
Overall Kappa	0,875					

Table 6.12: Error Matrix and accuracy values of the optical supervised and knowledge-based classification

In table 6.12 it is shown that after the classification of the optical reference data set by using additional knowledge-based information an overall accuracy of 90.2 % could be reached. By the use of knowledge-based information in form of the DEM, NDVI and SWIR/NIR ratio layer the accuracy could be improved about 0.5 % in comparison to the pure supervised classification (Tab. 6.11). This is not so much. It is partly an improvement. One reason for this is the fact that the knowledge-based information of the NDVI and SWIR/NIR layer indicated no real accuracy improvement, because most categories except Urban were classified quite well, especially Waterbodies and Vegetation. One improvement could be attained by the DEM. In the visual classification results of the supervised and the combined (supervised and knowledge-based) classification of the SPOT 5 data (Annex 12.6, fig. 12.13 and 12.14) it is obvious that a lot of wrong classified sparse settlements in mountainous areas could be corrected by the use of the DEM. Unfortunately not so many reference points were generated in these areas because of no reference data and partly accessibility during the ground check. Thus the improvement is only about 2 %, considering the Kappa statistic. But the absolute accuracy is worse in comparison to the other categories. This is caused by the fact that Urban is correlated with all categories, especially high correlated with Soil. Agriculture is also highly correlated with other categories (Vegetation, Waterbodies and Urban), but could also be improved in comparison to the supervised classification result. The category Waterbodies achieves the best result with 97 %. The other categories are mostly similar to the supervised classification result.

Accuracy assessment of the image fusion results

In the next step the classification result of the image fusion techniques were considered. The results are listed in the tables 6.13 to 6.15.

Confusion Matrix [Pixel]						
User \ Reference	Waterbodies	Vegetation	Urban	Soil	Agriculture	Sum
Unclassified	0	0	0	0	0	0
Waterbodies	2116	0	0	0	64	2180
Vegetation	5	2097	29	27	256	2414
Urban	30	8	1350	214	55	1657
Soil	0	0	253	649	36	938
Agriculture	99	145	168	10	1389	1811
Sum	2250	2250	1800	900	1800	9000
Accuracy []						
Class Name	Reference Totals	Classified Totals	Number Correct	Producer [%]	User [%]	Kappa []
Undefined	0	0	0	---	---	0.0000
Waterbodies	2250	2180	2116	94.04	97.06	0.9609
Vegetation	2250	2414	2097	93.20	86.87	0.8249
Urban	1800	1657	1350	75.00	81.47	0.7684
Soil	900	938	649	72.11	69.19	0.6577
Agriculture	1800	1811	1389	77.17	76.70	0.7087
Totals	9000	9000	7601			
Total accuracy []						
Overall Accuracy	84.5					
Overall Kappa	0,802					

Table 6.13: Error matrix and accuracy values of the supervised and knowledge-based classification by Multiplicative method

Confusion Matrix [Pixel]						
User \ Reference	Waterbodies	Vegetation	Urban	Soil	Agriculture	Sum
Unclassified	0	0	0	0	0	0
Waterbodies	2149	0	12	0	49	2210
Vegetation	9	2097	73	29	161	2369
Urban	20	14	1406	178	48	1666
Soil	0	4	189	670	56	919
Agriculture	72	135	120	23	1486	1836
Sum	2250	2250	1800	900	1800	9000
Accuracy []						
Class Name	Reference Totals	Classified Totals	Number Correct	Producer [%]	User [%]	Kappa []
Undefined	0	0	0	---	---	0.0000
Waterbodies	2250	2210	2149	95.51	97.24	0.9632
Vegetation	2250	2369	2097	93.20	88.52	0.8469
Urban	1800	1666	1406	78.11	84.39	0.8049
Soil	900	919	670	74.44	72.91	0.6989
Agriculture	1800	1836	1486	82.56	80.94	0.7617
Totals	9000	9000	7808			
Total accuracy []						
Overall Accuracy	86.8					
Overall Kappa	0,831					

Table 6.14: Error matrix and accuracy values of the supervised and knowledge-based classification by PCA Transform

Confusion Matrix [Pixel]						
User \ Reference	Waterbodies	Vegetation	Urban	Soil	Agriculture	Sum
Unclassified	0	0	0	0	0	0
Waterbodies	2130	0	0	0	40	2170
Vegetation	0	2078	14	10	179	2281
Urban	15	9	1445	228	114	1811
Soil	7	8	219	646	10	890
Agriculture	98	155	122	16	1457	1848
Sum	2250	2250	1800	900	1800	9000
Accuracy []						
Class Name	Reference Totals	Classified Totals	Number Correct	Producer [%]	User [%]	Kappa []
Undefined	0	0	0	---	---	0.0000
Waterbodies	2250	2170	2130	94.67	98.16	0.9754
Vegetation	2250	2281	2078	92.36	91.10	0.8813
Urban	1800	1811	1445	80.28	79.79	0.7474
Soil	900	890	646	71.78	72.58	0.6954
Agriculture	1800	1848	1457	80.94	78.84	0.7355
Totals	9000	9000	7756			
Total accuracy []						
Overall Accuracy	86.2					
Overall Kappa	0,824					

Table 6.15: Error matrix and accuracy values of the supervised and knowledge-based classification by Ehlers Fusion

It is obvious that the classification results of the merged images are not quite as good as the optical reference classification as shown in the visual comparison. The overall classification accuracy is about 4 % worse in case of the PCA and the Ehlers Fusion. The Multiplicative method shows, as assumed, with about 84 % the worst result. Here, it is statistically indicated that all fusion methods have problems with correct soil detection. This is recognizable as well in the Kappa statistic as in the Error Matrix. In the Kappa statistic, for example, the accuracy deficit is about 15 to 20 %. This is quite much. The Error matrix shows that the correlation between Urban and Soil areas is increased, especially for the category Soil where the number of wrong detections of the category Urban is more than doubled. The category Agriculture is also bad detected, except by the PCA Transform where the correlation to vegetation areas is increased too. On the other hand the category Waterbodies is classified quite well in all fusion methods, especially in case of the Ehlers Fusion. But there is also no improvement in comparison to the optical data set. Using the PCA Transform urban areas are also classified quite well but only in the PCA Transform. There is also no real classification gain.

6.3 Discussion of the fusion methods

The classification results of the three investigated fusion techniques demonstrate in comparison to the optical reference classification that no global improvement could be achieved. All fusion methods indicate a decreasing overall classification accuracy. There is also no category which could be improved in comparison to optical data set. It is indicated that Waterbodies is the only category where the same accuracy could be achieved by the reference data. Thus it can be stated that none of these three fusion techniques offer an improvement in the classification results. It can be confirmed that the PCA Transform and the Multiplicative method distorts the colour as Gungor and Shan (2005) and Sun (2005) said.

But the PCA Transform seems to offer the best way of these two common approaches to combine optical with radar data as the classification result shows.

The approach of Ehlers indicates the second best classification result of the fusion techniques, but shows the best optical and statistical impression. But for this method the requirements are high. A precise geocoding (accuracy < 1 pixel) is necessary to exploit the advantages of this method. In this approach this could not be fulfilled because of the different data sets having different resolutions and the manual measurement by the ground control points.

6.4 Fusion of the second data set

Using the first data set, the results showed that additional radar information could not improve the classification result. One reason might be the fact that the optical and radar data have different acquisition times. The Radarsat scene itself consists of two different acquisition times. In case of different acquisition times it is very difficult to give a general statement about the determined accuracy. Thus it was decided to test the second data having the same acquisition time.

In a first step the optical ASTER data was classified like the optical SPOT 5 data by a supervised and knowledge-based classification. During the classification process the same samples and knowledge-based information were used. In a second step the ASTER data and the Envisat scene were merged by the PCA Transform because this transformation seems to offer the best classification results of the three tested fusion techniques. The fusion was accomplished analogue to the fusion with the SPOT 5 data. The determination of the correlation and the Eigenmatrix and Eigen values is given in the annex 12.5.

For the classification the test area had to be minimized because the Envisat scene does not cover the whole test area (q.v. section 4.5.2). Thus the number of samples and reference points had to be reduced too. The knowledge-based rules could be adapted.

Optical ASTER data set

The pure optical ASTER data set include the three ASTER scenes ASTER_VNIR-2501, ASTER_SWIR-2501 and ASTER_TIR-2501 with the bands 1, 2, 3, 4, 7 and 12 (Tab. 6.16).

No.	Band	Spectral range [μm]	Resolution [m]
1	Green (1)	0.52 – 0.60	15
2	Red (2)	0.63 – 0.69	15
3	NIR (3)	0.76 – 0.86	15
4	SWIR (4)	1.600 – 1.700	15 (30)
5	SWIR (7)	2.235 – 2.285	15 (30)
6	TIR (12)	8.925 – 9.275	15 (90)

Table 6.16: Pure optical data set of ASTER for the multi-spectral classification

Accuracy Assessment

After both classifications the following accuracy results were assessed:

Confusion Matrix [Pixel]						
User \ Reference	Waterbodies	Vegetation	Urban	Soil	Agriculture	Sum
Unclassified	0	0	0	0	0	0
Waterbodies	1520	0	0	25	94	1639
Vegetation	2	1575	25	16	179	1797
Urban	76	26	1437	299	122	1960
Soil	25	7	81	272	4	389
Agriculture	177	192	77	18	951	1415
Sum	1800	1800	1620	630	1350	7200
Accuracy []						
Class Name	Reference Totals	Classified Totals	Number Correct	Producer [%]	User [%]	Kappa []
Undefined	0	0	0	---	---	0.0000
Waterbodies	1800	1639	1520	84.44	92.74	0.9032
Vegetation	1800	1797	1575	87.50	87.65	0.8353
Urban	1620	1960	1437	88.70	73.32	0.6557
Soil	630	389	272	43.17	69.92	0.6704
Agriculture	1350	1415	951	70.44	67.21	0.5964
Totals	7200	7200	5755			
Total accuracy []						
Overall Accuracy	79.9					
Overall Kappa	0,742					

Table 6.17: Error matrix and accuracy values of the supervised and knowledge-based classification by pure optical ASTER data

Confusion Matrix [Pixel]						
User \ Reference	Waterbodies	Vegetation	Urban	Soil	Agriculture	Sum
Unclassified	0	0	0	0	0	0
Waterbodies	1419	0	71	112	97	1699
Vegetation	21	1491	24	18	139	1693
Urban	180	24	1362	193	68	1827
Soil	32	3	64	261	15	375
Agriculture	148	282	99	46	1031	1606
Sum	1800	1800	1620	630	1350	7200
Accuracy []						
Class Name	Reference Totals	Classified Totals	Number Correct	Producer [%]	User [%]	Kappa []
Undefined	0	0	0	---	---	0.0000
Waterbodies	1800	1699	1419	78.83	83.52	0.7803
Vegetation	1800	1693	1491	82.83	88.07	0.8409
Urban	1620	1827	1362	84.07	74.55	0.6716
Soil	630	375	261	41.43	69.60	0.6668
Agriculture	1350	1606	1031	76.37	64.20	0.5593
Totals	7200	7200	5564			
Total accuracy []						
Overall Accuracy	77.3					
Overall Kappa	0,708					

Table 6.18: Error matrix and accuracy values of the supervised and knowledge-based classification by PCA

Here, a global improvement with additional radar data could also not be obtained although the data sets were imaged at the same time. Only a small improvement in the category urban and vegetation is indicated by analysing the Kappa statistics. But this is only about 1 %. Thus a concrete statement if this is really an improvement cannot be made. In order to prove if one category or the whole classification is significant, more than one classification has to be made by using different samples with approximate same spectral characteristics. This is very time-consuming and costly. Another method is given by consideration the variance of the 3x3 pixel reference mask. Every mask offers nine classification possibilities with true or not true. If all pixel are classified correctly the variance is very low otherwise the variance is very high. One wrong classified pixel includes a deviation of about 11 %.

By comparing the difference of the mean value with the variance or standard deviation of both results a statement is possible if this comparison is significant or not. In case of the category Waterbodies it was proofed, if this high degradation is really significant. Therefore the mean value and the standard deviation were calculated of all used reference masks.

In table 6.19 it is shown that in case of the PCA Transform the standard deviation is much higher than the standard deviation of the pure optical ASTER data. But it is also indicated that the standard deviation is quite high in both methods in comparison to the difference of both mean values. Thus it can be stated that proving of significance is not needed because the variation of the measurements are so high that no general statement can be made.

Waterbodies	Mean	Standard Deviation
ASTER data	0.852	0.286
PCA Transform	0.784	0.331

Table 6.19: Mean and Standard deviation of the optical ASTER data set and the PCA Transform

One reason for this high standard deviation is the small size of the reference mask. In case of 200 reference masks and one total false mask the standard deviation is about 0.07. This is 7 % and the difference of the two mean values. In this data set of reference masks blunders were rejected. For the other classes similar results were achieved in which the standard deviation was higher than the difference of the mean value. Another reason is the fact that classification results are generally not so precise. Only few classes (e.g. waterbodies) are able to achieve good results which are above 90 %. A third reason is the fact that the available reference data is from June 2005. Thus variations in some few cases may be possible, especially in the category Agriculture.

So a proofing of significance under these conditions is very difficult but it seems so that the variations in the classification results are not significant because of the great variation in measurement of the optical reference data and the investigated data with additional radar information.

7 Object-based Classification

The pixel-based approach showed that no global improvement could be obtained by additional radar data in both data sets. It could be shown that the knowledge-based classification presents difficulties by defining the rules with Boolean operators. Therefore a new approach, a object-based classification, was arranged in order to fuse optical and radar information in a combination of supervised and knowledge-based classification by fuzzy rules.

7.1 Segmentation and classification in eCognition

The object-based classification was performed via the image processing software eCognition offering an object-based multi-spectral classification.

7.1.1 Segmentation in eCognition

The segmentation process in eCognition, also called *Multiresolution Segmentation*, is a threshold-based optimisation method for image objects (segments). The threshold is defined as the maximum acceptable heterogeneity for the objects. Pixel or objects are simply merged, if the heterogeneity is below the threshold. The heterogeneity of an object is composed in principle from colour and shape heterogeneity (eCognition User Guide 4, 2004). This can be adjusted according to a parameter called *Shape Factor* (Fig. 7.1).

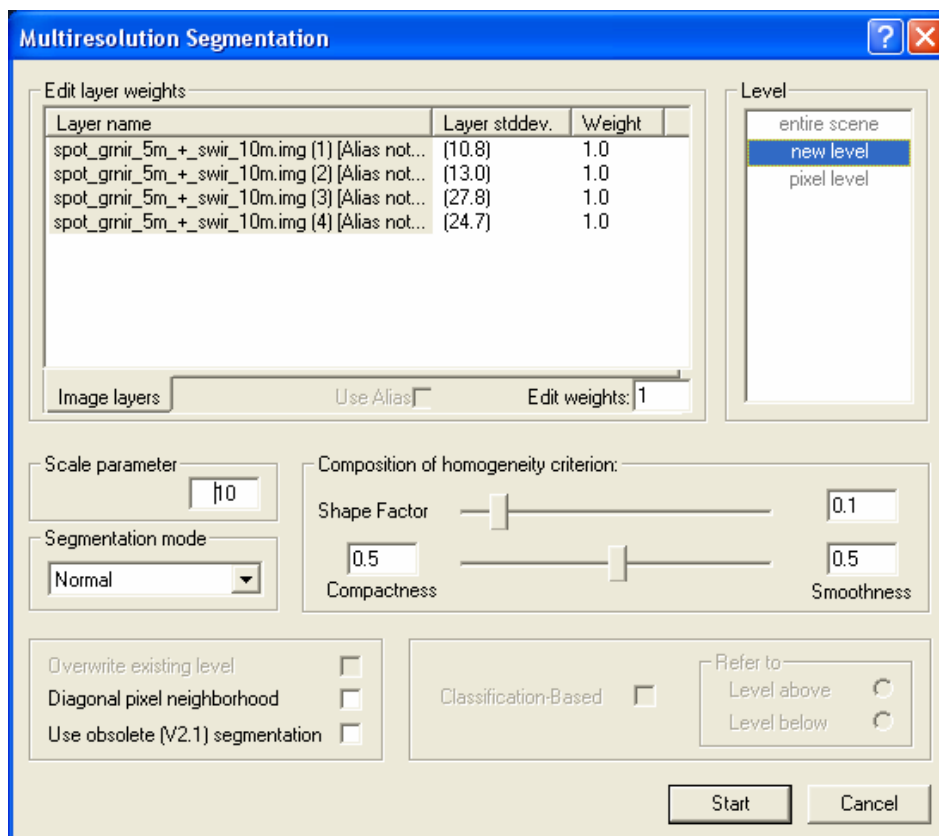


Figure 7.1: Settings of the Multiresolution Segmentation in eCognition

The shape heterogeneity is determined by two values, the *compactness*, which can be derived by the object extent l and the size n , and the *smoothness*, which is given by the object extent l and the extent of the minimum surrounded rectangle b , parallel to the image raster.

$$h_{compact} = \frac{l}{\sqrt{n}} \quad (7.1)$$

$$h_{smooth} = \frac{l}{b} \quad (7.2)$$

The colour heterogeneity is given by following equation:

$$h_{colour} = \sum_{c=1}^n w_c \cdot \sigma_c \quad (7.3)$$

whereas c is the n band, σ_c the spectral standard deviation of the band c and w the weighting of the n band analogue to the equation above.

Hence, the fusion value f can be determined from the colour and shape heterogeneity by a different weighting by following equation:

$$f = w \cdot h_{colour} + (1 - w) \cdot h_{shape} \quad (7.4)$$

The weighting is between 0 and 1.

Every potential fusion of two pixel or objects it is tested, if in case a the heterogeneity of the new object after the fusion is underneath the defined threshold (*Scale Parameter*) and in case b the potential fusion of neighbouring objects shows a minimum of heterogeneity for the new object. Neighbouring pixel or objects are simply merged if the heterogeneity offers a minimum and the Scale Parameter is smaller. The Scale parameter SP is squared (eCognition User Guide 4, 2004) as it is shown in the following equation:

$$SP \geq \sqrt{f} \quad (7.5)$$

The Scale Parameter is an abstract size and describes more the maximum possible heterogeneity of the resulting segments. This means, that segments are smaller in heterogeneous parts and bigger in homogeneous parts. But the size depends on the pixel size of the data. Thus it has to adapt to different resolution of data sets. If the resolution is much lower in contrast to another data set, the Scale Parameter should be minimized.

7.1.2 Classification in eCognition

Nearest Neighbour

The Classification in eCognition is based on the so-called *Fuzzy Logic*, a generalisation of the two-valued *Boolean Logic*. The Fuzzy Logic does not distinguish between two values true (1) or false (0), but considers also additional interim values (e.g. 0.5). Thus the Fuzzy Logic is based on the human knowledge and it is possible to assign an object to several classes. The classes are defined by features (e.g. mean, standard deviation, shape features) which build a feature space for every class. The dimension of the feature space is increasing by the number of available features. The object is assigned to one class by the criteria in the feature space. The assignment is done by Nearest Neighbour approach in eCognition. If an object is next to one criteria of a class, it is assigned to this class (Fig. 7.2, orange line). The value 1 corresponds to the maximum and 0 the minimum assignment. The criteria are defined automatically by the interpreter by different representative *samples*.

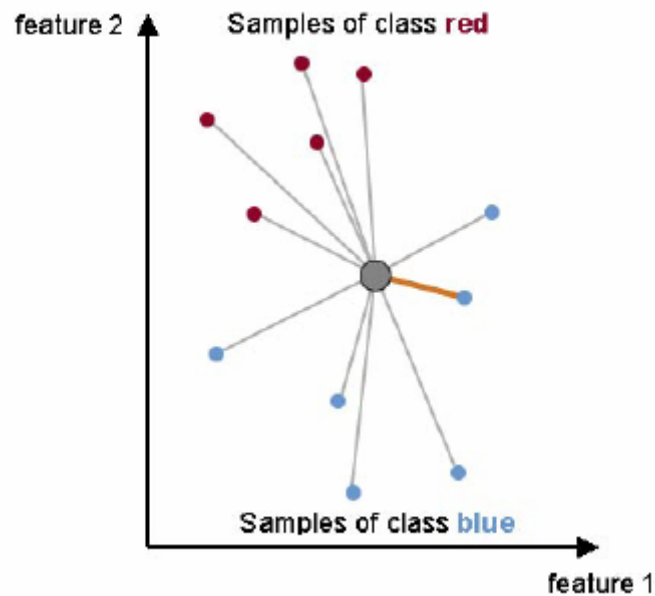


Figure 7.2: Nearest Neighbour classification in a two-dimensional feature space

The distance in the feature space between an object and a sample is calculated by the following equation:

$$d = \sqrt{\sum_f \left(\frac{v_f^{(s)} - v_f^{(o)}}{\sigma_f} \right)^2} \quad (7.6)$$

where:

- d Distance between sample object s and image object o .
- $v_f^{(s)}$ Feature value of sample object for feature f .
- $v_f^{(o)}$ Feature value of image object for feature f .
- σ_f Standard deviation of the feature values for feature f .

The distance between object and sample is standardized by the standard deviation of the values from the feature f . Thus features with varying borders can be considered in the feature space for the classification. In case of the distance 1, the distance is matched to the standard deviation of all feature values (eCognition User Guide 4, 2004).

Membership Function

The second classification method in eCognition is the so-called *Membership Function*. On basis of the distance d , a multidimensional, exponential membership function $z(d)$ is computed:

$$z(d) = e^{-k+d^2} \quad (7.7)$$

The parameter k determinates the decrease of $z(d)$. This can be defined by the parameter with the variable function slope f_s , whereby

$$k = \ln\left(\frac{1}{f_s}\right) \quad (7.8)$$

The function slope $z(f)$ equals $z(d)$ for the distance $d=1$ (Fig. 7.3). Thus, the function slope is the membership value of an image object to a class, if the closest sample object of that class has a distance to the image object which equals the standard deviation of the feature values from the closest sample object (eCognition User Guide 4, 2004). The less the parameter of the function slope, the lesser and more limited the membership function.

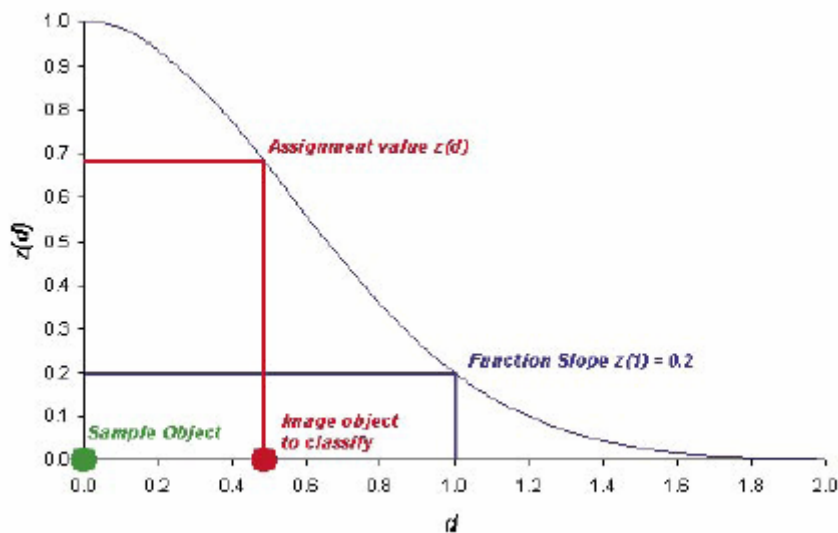


Figure 7.3: Example of a Membership Function

The Membership Function is basically designed for one-dimensional feature spaces. Thus it is a good method for a knowledge-based classification where individual, one-dimensional information is available. In contrast to this the nearest neighbour method is more favourable for fast and easy pre-classification with more classes in a multidimensional feature space. It is also easier to handle overlap areas in the feature space as in the Membership Function (eCognition User Guide 4, 2004).

7.2 Object-based Classification of the SPOT 5 Data

Like in the pixel-based approach, the same optical SPOT 5 data set was used. First a supervised classification by Nearest Neighbour was done and then based on this classification a knowledge-based classification with Membership Functions was implemented.

7.2.1 Segmentation

Before the real classification the segmentation was performed. Therefore the segmentation parameters had to be determined.

The Scale Parameter was set to 10, because this was the minimum threshold which could be derived from the available data set. The Shape Factor was selected with 0.4 in order to weight more the colour then the shape because of the given multi-spectral bands. For the shape weighting the smoothness was chosen with 0.9 very high in order to achieve consistent, rectangular segments. Every multi-spectral band was weighted with the maximum of 1.0.

7.2.2 Supervised Classification with Nearest Neighbour

In the next step the supervised classification was arranged by Nearest Neighbour.

Defining of the classes

At first the classes had to be defined. Therefore the self defined classification system with its 5 categories and 22 classes for land cover and land use was chosen and assigned.

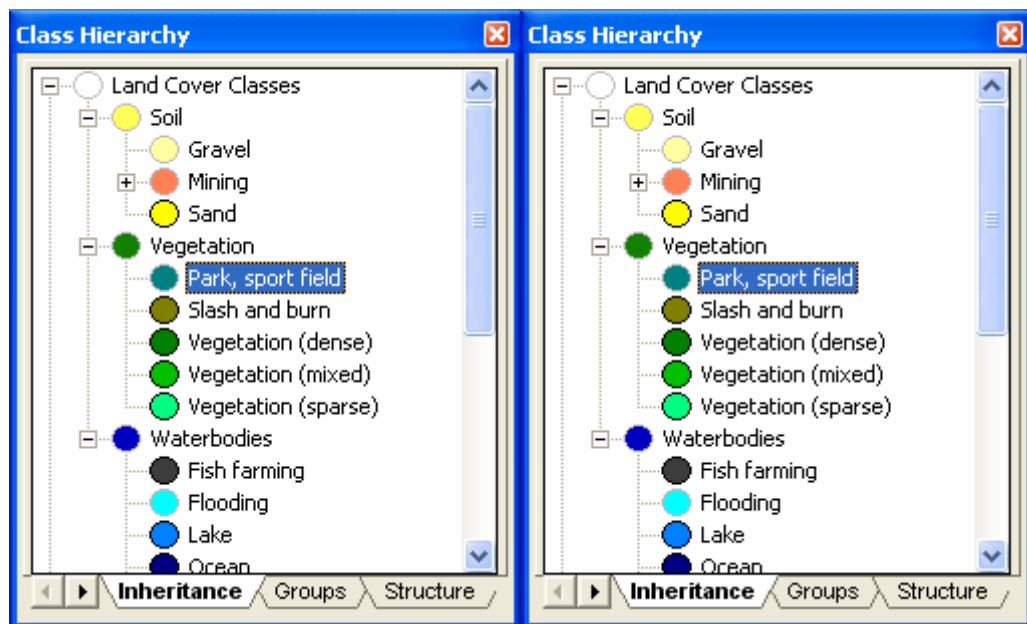


Figure 7.4: left: Classes grouped by inheritance issues including spectral relationships
right: Classes grouped by semantic issues

The classes can be illustrated differently in eCognition. On the one hand it is possible to group the classes in the 5 categories semantically like it is usual for a classification system. This can be done with *Group* (Fig. 7.4, right). It is also possible to combine the classes by their spectral relation for example the class Park, sport field is semantically assigned to Urban, but spectrally it belongs to the category Vegetation. Thus spectral information of Vegetation can be inherited to the class Park, sport field. So the classes can spectrally grouped by *Inheritance* (Fig. 7.4, left). In *Structure* the classes are grouped for the classification-based segmentation. There, it is possible to derive segmentations on single classes.

Selection of the Samples

After defining the classes the corresponding samples were chosen for the supervised classification by Nearest Neighbour. The land use classes Fish Farming, Clay Mining, Industry, Military and the Land cover class Lake were not considered during the sample selection and classification because of their small size and difficulties to distinguish from other classes. Later it is easier to edit these classes manually. The samples for the designed classes were derived from the aerial image reference data and the ground check. The single segments were assigned to the single classes and stored in *Sample Editor* (Fig. 7.5). The editor displays the whole feature range of every class in every single band. An extract of the selected segments is illustrated in figure 7.5.

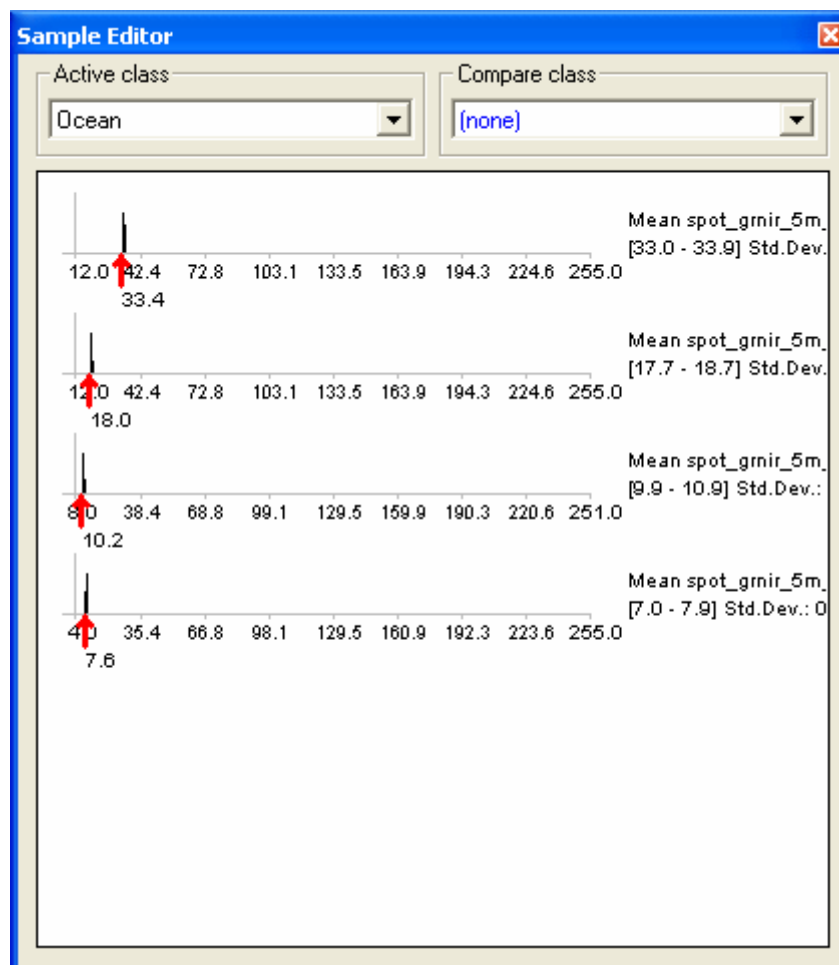


Figure 7.5: Definition and illustration of samples in the feature space in the Sample Editor

Selection of the features

In order to find well distinguishing features the *Feature Space Optimization* tool was used. This tool is able to calculate for all classes their distance in the feature space based on the samples. Thus it is able to determinate the best feature space with the best separating distance. The result depends on the given features, the maximum dimension of the feature space and of course the defined samples.

For the calculation, the common features *mean*, *standard deviation* and *ratio* were considered for every single band. The ratio of a layer in eCognition is calculated by the layer mean value of an image object divided by the sum of all spectral layer mean values. Thus, only layers containing spectral information can be used to achieve reasonable results (User Guide eCognition 4.0, 2004). The range of the feature value is between 0 and 1.

Additional the maximum feature space dimension was set to the maximum of 12. The parameters are shown in figure 7.6.

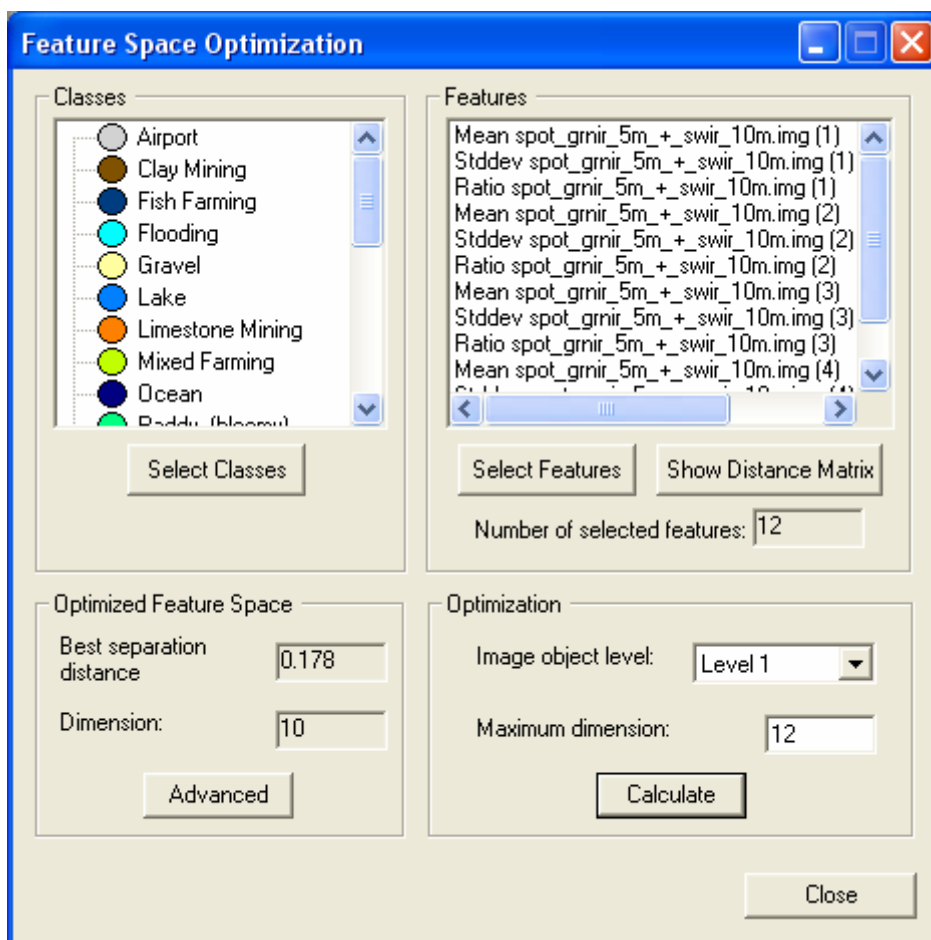


Figure 7.6: Selection of the features and the maximum dimension in the tool Feature Space Optimization

The calculated result was a feature space with a dimension of 10 and a maximum separation distance of 0.178. The single features can be taken from the figure 7.7. It can be seen in the table of the *Result Chart* that the result is almost stable after the 8th dimension. The calculated features were assumed and applied to the classes.

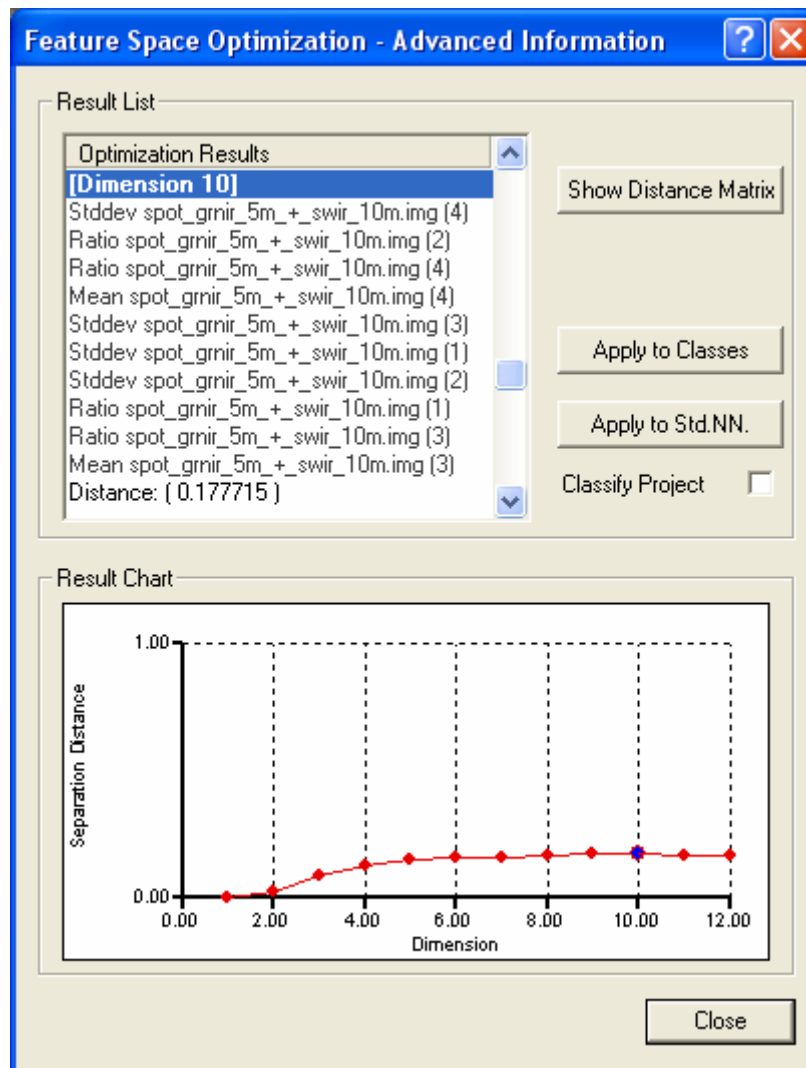


Figure 7.7: Convenient feature space with corresponding features

Classification

Now the real classification was started with *classify*. In the first step the supervised classification with Nearest Neighbour was done iterative in order to improve the feature space and thus the classification results. Therefore known, false classified segments were selected to the class they really belong to. Because of the Fuzzy Logic it is possible that one segment belongs to different classes but it can only be assigned to one class. This is the class with the minimum distance, the nearest neighbour. So it is possible that one segment belongs to 0.85 membership to the class A, but in reality it belongs to the class B although the calculated membership is only 0.80. By selection of this segment to class B the features space is changed and in the next classification the false classified segment could be classified correct. But this procedure has to be done carefully because of this change other classes could be effected negatively. This procedure was iterated carefully step by step until a satisfying result was achieved.

7.2.3 Knowledge-based information with Membership Function

In the next procedure the classification result was added by knowledge-based information. In comparison to the pixel-based approach unclassified pixel are assigned directly to the next likely class because of the Fuzzy Logic. Thus a manual assignment is not needed.

The knowledge-based features were included by Membership Functions additionally to the common features mean, standard deviation and ratio which were used in the Nearest Neighbour classification. Therefore the features of the DEM, NDVI and SWIR/NIR layer were used again. Beside the DEM, the Slope layer was used too. This layer was derived from the DEM. The NDV-Index and the SWIR/NIR layer were calculated from the corresponding multi-spectral bands by an own object feature. Additional to the pixel-based approach geometric and shape features were used. Here, the software eCognition offers a lot of different shape features (e.g. Area, Length Wide, Asymmetry etc.) which are illustrated in figure 7.8. The single features, which were used during the classification process, were inserted in the different classes as Membership Function.

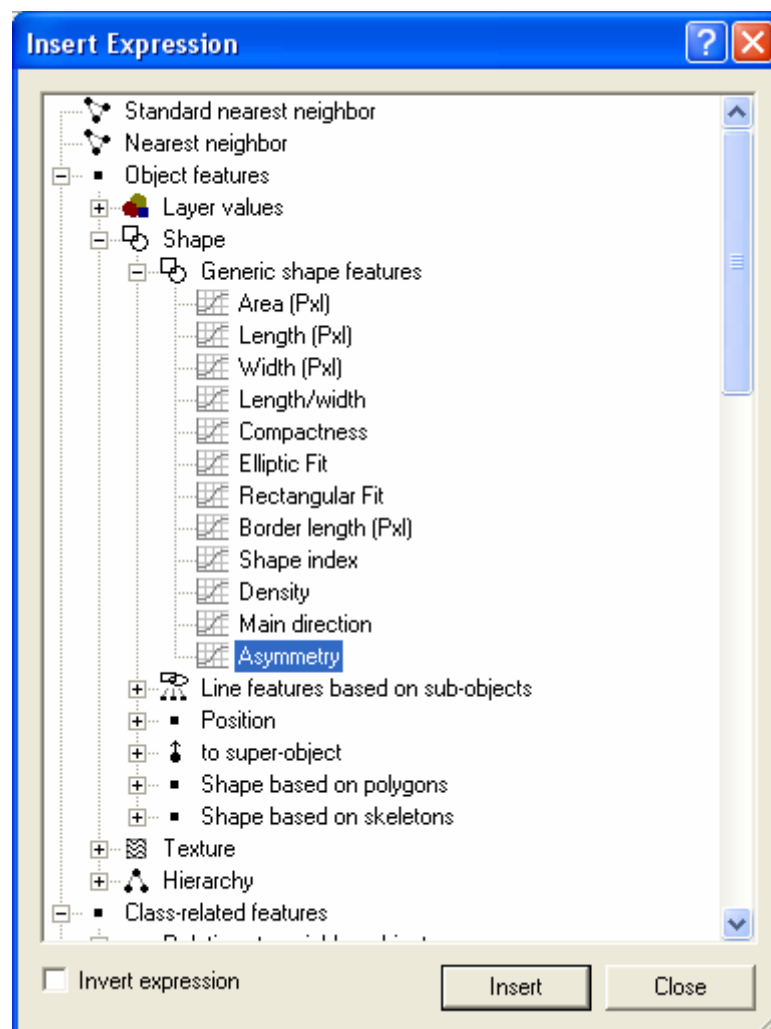


Figure 7.8: Selection of the different features by insert expression tool

7.2.4 Modelling of the knowledge-based rules

Like in the pixel-based approach before, the rules of the knowledge-based information had to be defined. Now, the several classes were considered beside the five categories. By using the DEM, NDVI and SWIR/NIR the same rules for the five categories were estimated like in the pixel-based approach. These rules were adapted to the single classes. In the following the single classes with their knowledge-based rules are introduced.

1.) Waterbodies

Ocean:

Ocean waterbodies occur mostly at an elevation about 0 m. Here, this universal rule had to be expanded to an elevation of about 15 m because of errors in the DEM. The rule is defined in the Membership Function by a Boolean range with definite borders (Fig. 7.9).

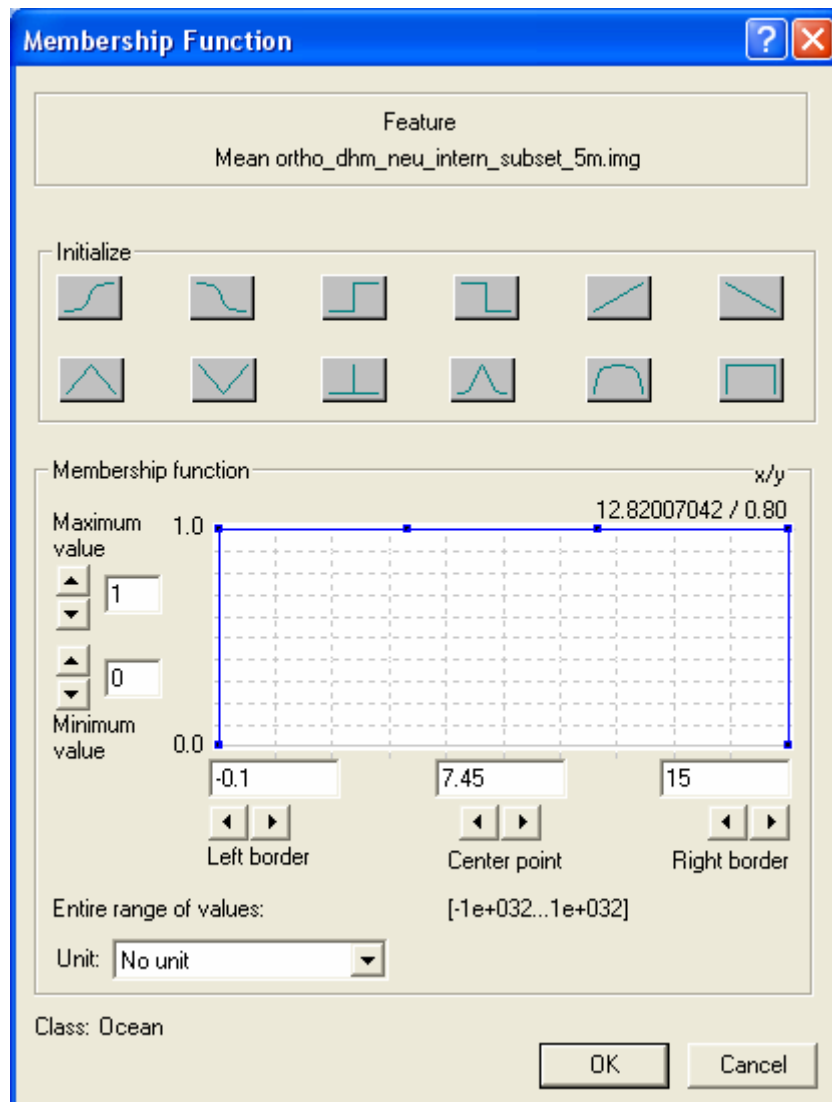


Figure 7.9: Illustration of a Membership Function for the class Ocean with Boolean range

Because of the fact that the class Ocean is mostly at the top and left border of the test area, the geometric position was defined near the image borders. The maximum distance to the borders was set to 1800 Pixel. In the right part of the test area Ocean could be excluded. Thus the maximum distance from the left image border was chosen with 4500 pixel.

River:

The class River is limited in the test area to an elevation of about 60 m. It is characterised by a special geometric feature, the asymmetry. This was exploited by defining a shape feature for this class. The range of asymmetry is between 0 and 1. At value 1 the maximum symmetry is given, at value 0 the minimum. In contrast to the classes Ocean and Flooding the asymmetry of the class River increases. Thus an according function was designed which starts slowly from 0 and reaches the maximum at 1. By this shape information the class river can easily separated from the other waterbody classes. The formulation of this rule in the Membership Function is illustrated in the figure 7.10. Areas of pure ocean waterbodies in the left side of the test area were excluded for possible assignment by a minimum distance to the left image border of 570 pixel.

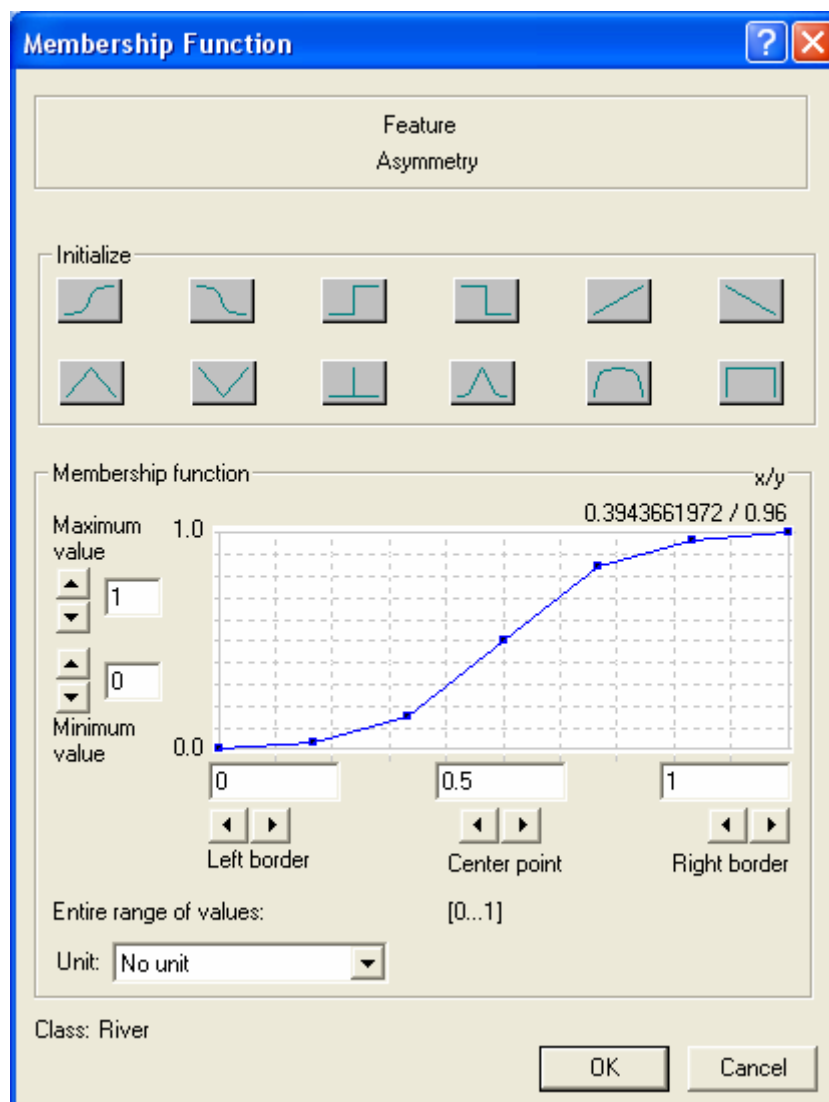


Figure 7.10: Illustration of a Membership Function for the class river in case of asymmetry

Flooding:

Flooding areas caused by ocean waterbodies are mostly near the coast and mostly in a low elevation (about 0 m). Because of artefacts and errors in the DEM the maximum elevation was set to 15 m like in case of the class ocean. The maximum distance to the class ocean was chosen with 400 Pixel because many flooding areas are also located in the inland reachable up to 2 kilometres. Like in the class Ocean the maximum distance from the left border was also chosen by 4500 pixel.

2.) Vegetation

For the classes of the category Vegetation the NDVI values of the pixel-based approach were adapted for every single class. Additionally the SWIR/NIR ratio was used. This layer indicates vegetation classes that contain a high part of soil, like sparse vegetation or slash and burn. Thus it is possible to locate land sliding in mountainous areas. Therefore the Feature View was used. This viewer shows for every segment the feature range. A bright segment represents a high, a dark segment a low range value. The Sample Editor was combined with the Feature View in order to compare the different ranges of the classes (Fig. 7.11).

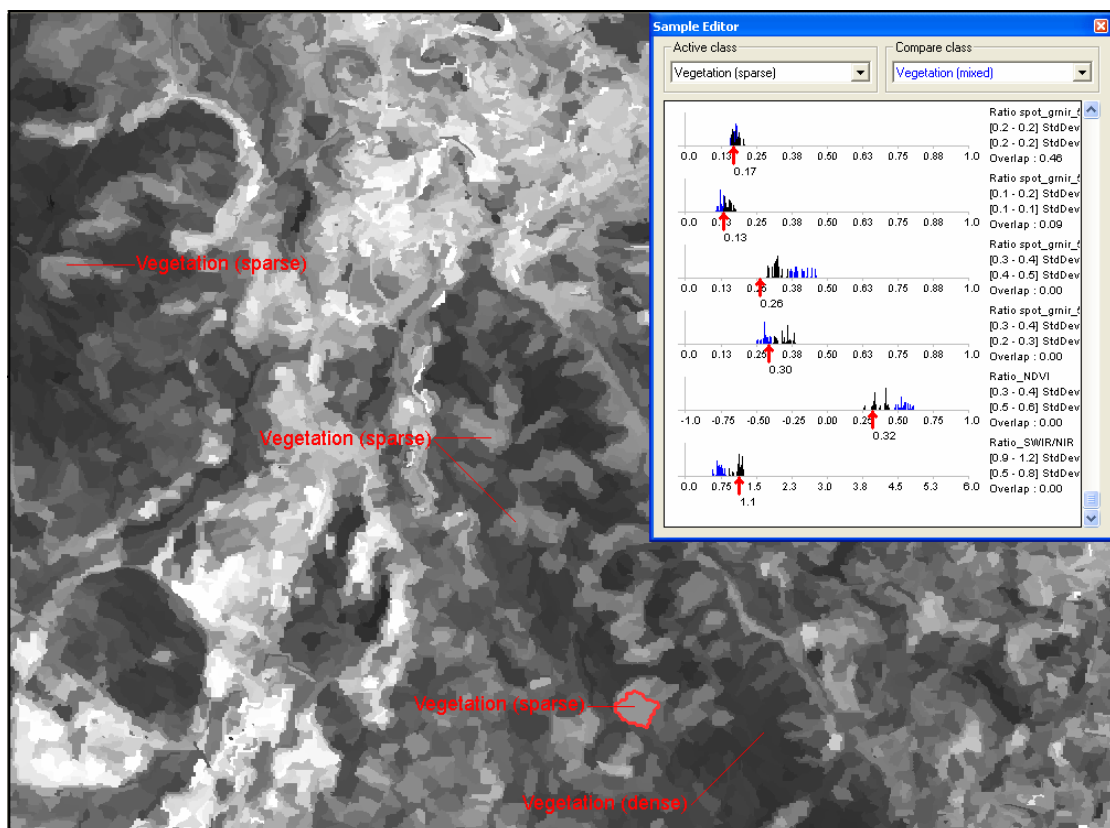


Figure 7.11: Illustration of the Feature View and the Sample Editor in eCognition

For the determination of the rules a so-called *About Range* with smooth borders was chosen (Fig. 7.12), because it is difficult to find definite borders for these classes.

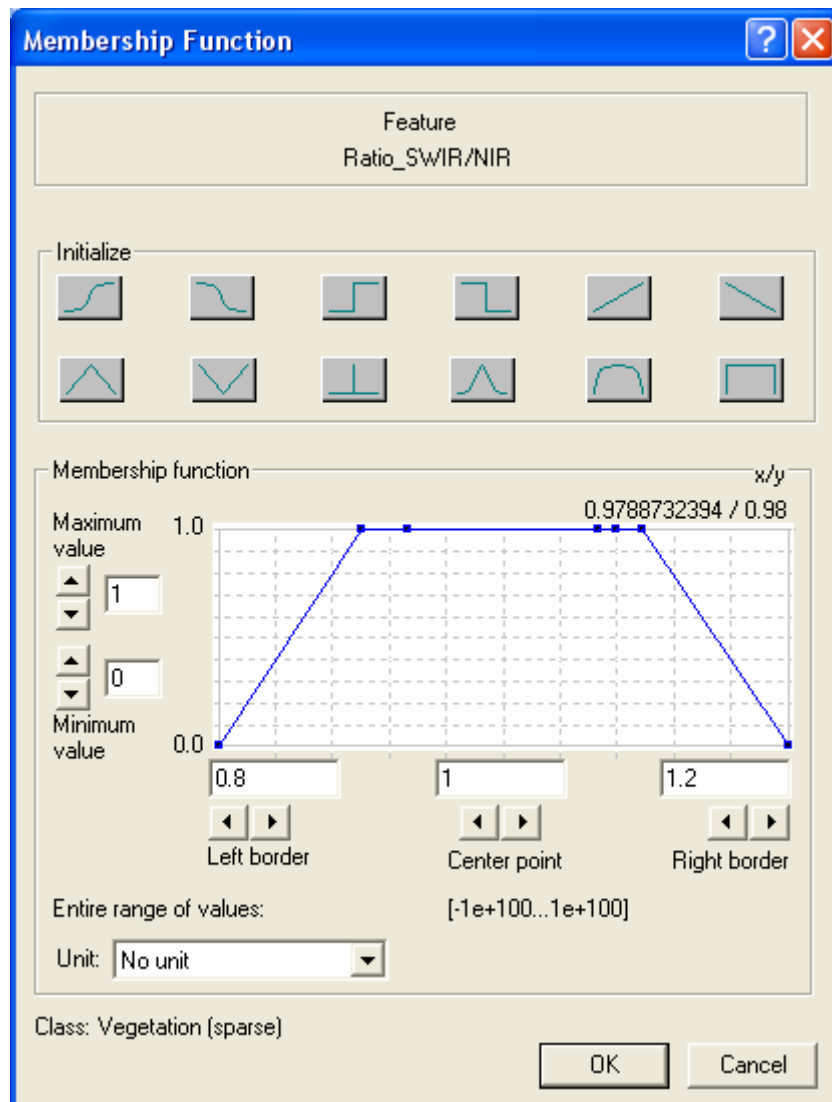


Figure 7.12: Illustration of a Membership Function for the class Vegetation (sparse) with an about range

In case of the class Slash and Burn the minimum elevation was set to 20 m because this class is only present in mountainous areas.

3.) Soil

For the category Soil the SWIR/NIR ratio values of the pixel-based approach were used again. Additionally knowledge-based information from the geological map was considered.

Limestone:

Limestone is only to find in the west foothills. Thus the areas of limestone were limited to the left border of the image by a maximum distance of 4000 Pixel and from the bottom border to a maximum distance of 3500 Pixel. The digging of limestone is limited to an elevation of approximately 220 m.

Gravel:

Gravel areas caused by the flooding are located near the coast in a maximum elevation of about 15 m. The maximum distance to the class Ocean was set to 400 Pixel, like in case of the class Flooding.

Sand:

Normally sand is also located near the coast. But the geological map displays that it is distributed area-wide in the delta of the test area. The maximum elevation is limited to approximately 60 m.

4.) Urban

The single urban areas show different kind of features which have to be considered. For example a unique NDVI or SWIR/NIR value for all classes is not available.

Urban (dense):

Urban dense describes more or less the main part of the city Banda Aceh. The position of urban dense in the test area can be limited by coordinates. It is also near the coast. The maximum elevation is about 15 m. Because of very sparse vegetation the NDVI value was set to < 0.1 . In case of the SWIR/NIR ratio layer was set to > 1 .

Urban (sparse):

Sparse urban areas are distributed all over the test area, except in the left part of the test area where only ocean waterbodies appear and in high mountainous areas. Thus the areas with ocean waterbodies were excluded. Therefore a minimum distance of 330 pixel to the left image border was set. The maximum elevation is limited to approximately 60 m. The NDVI value is quite high with maximum 0.5 because of parts of vegetation. Thus the SWIR/NIR value is < 1 .

Urban (destructured):

Former destructed urban areas are located near the cost. Thus a near distance to the class Ocean was defined. The same distance of 400 Pixel was chosen. The maximum elevation is about 15 m and the maximum NDVI and SWIR/NIR value is equal to those of sparse settlement. The geometric position was also limited by 330 pixel to the left image border because of the ocean waterbodies.

Airport:

The position of the airport can also be isolated by coordinates like the urban (dense). This was done by defining the minimum and maximum distance to the left image border ($4500 < X < 4720$) and the minimum and maximum distance to the lower image border ($2000 < X < 2600$). The elevation ranges from 15 to 25 m. The NDVI value is about 0. The exactly range was defined from -0.1 to 0.2 because of parts of vegetation near the runway. The slope is also about 0. This value was adapted to < 2 . Because of the asphalt runway the SWIR/NIR value is quite high. It was set to > 1 .

Park, sport field:

Parks and sport fields are mostly near settlement. Thus a maximum distance of 50 Pixel was chosen. The elevation limit is about 25 m. The NDVI value is above 0. The left part with ocean waterbodies was also excluded (> 330)

5.) Agriculture

The classes of Agriculture show also a variation of different features to take considered.

Mixed Farming:

Mixed Farming is distributed all over the test area except in very high mountainous regions. Thus it is limited up to an elevation of about 100 m. The NDVI value is above 0. Like in case of the urban areas the left part of the test area was excluded (> 330).

Paddy Farming:

Paddy farming is also distributed all over the test area like Mixed Farming. It is limited to an elevation of about 60 m. The NDVI value of bloomy, harvested and dry paddies is above -0.1. For wet paddies it is underneath it. The slope is normally about 0. Thus the maximum slope was set to 2° like in case of the class Airport. Here, the left part of the test area was excluded too (> 330).

The single parameters of the knowledge-based rules for every class, which were presented, are given in the annex 12.8.

Because of the class-related features (e.g. distance to another class) circular dependencies between two classes occur. This means, the classification has to be performed in minimum two cycles because at first the single segments have to be classified, then it is possible to consider the relationship between the single classes. Thus a class-related feature classification with minimum one extra cycle was performed (Fig. 7.13).

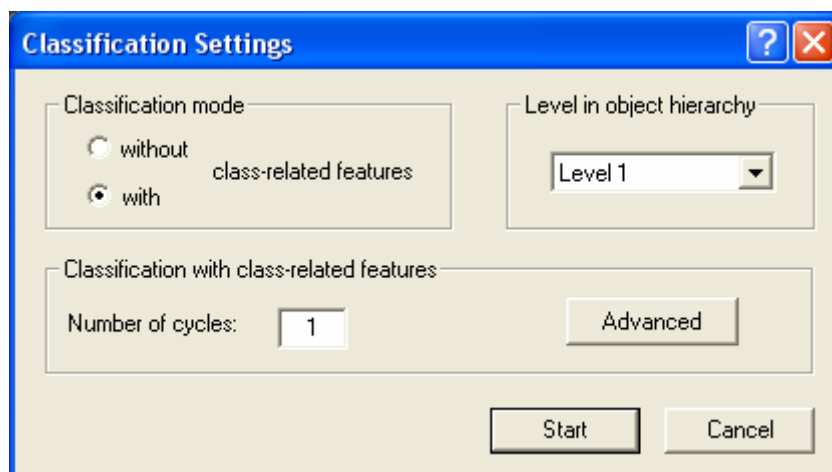


Figure 7.13: Illustration of the classification settings by using class-related features

7.3 Object-based Classification with additional Radarsat SAR data

In the next step the Radarsat SAR data was combined with the optical SPOT 5 data set. Therefore the SAR image was simply added to the optical data set and regarded as an additional band. In eCognition it is possible to add several bands and to view these bands as one image.

In the first step the radar data was combined with the optical data by a new segmentation. Then features of the radar scene were integrated into the Nearest Neighbour approach by using additionally the knowledge-based information in Membership Function (e.g. DEM, Ratio and shape information) of the supervised and knowledge-based classification of the optical data.

7.3.1 Integration of optical data and Radarsat data by segmentation

At first the Radarsat SAR scene was added as additional band to the four optical bands and a new segmentation was done. The segmentation was different to the one before. The new Radarsat scene got a smaller weight of 0.5 and the Shape factor was set to 0.5 in order to equal colour features of the multi-spectral bands and shape features of the radar image. The segmentation was also started in a new level (level 2). The new settings are shown in the figure 7.14.

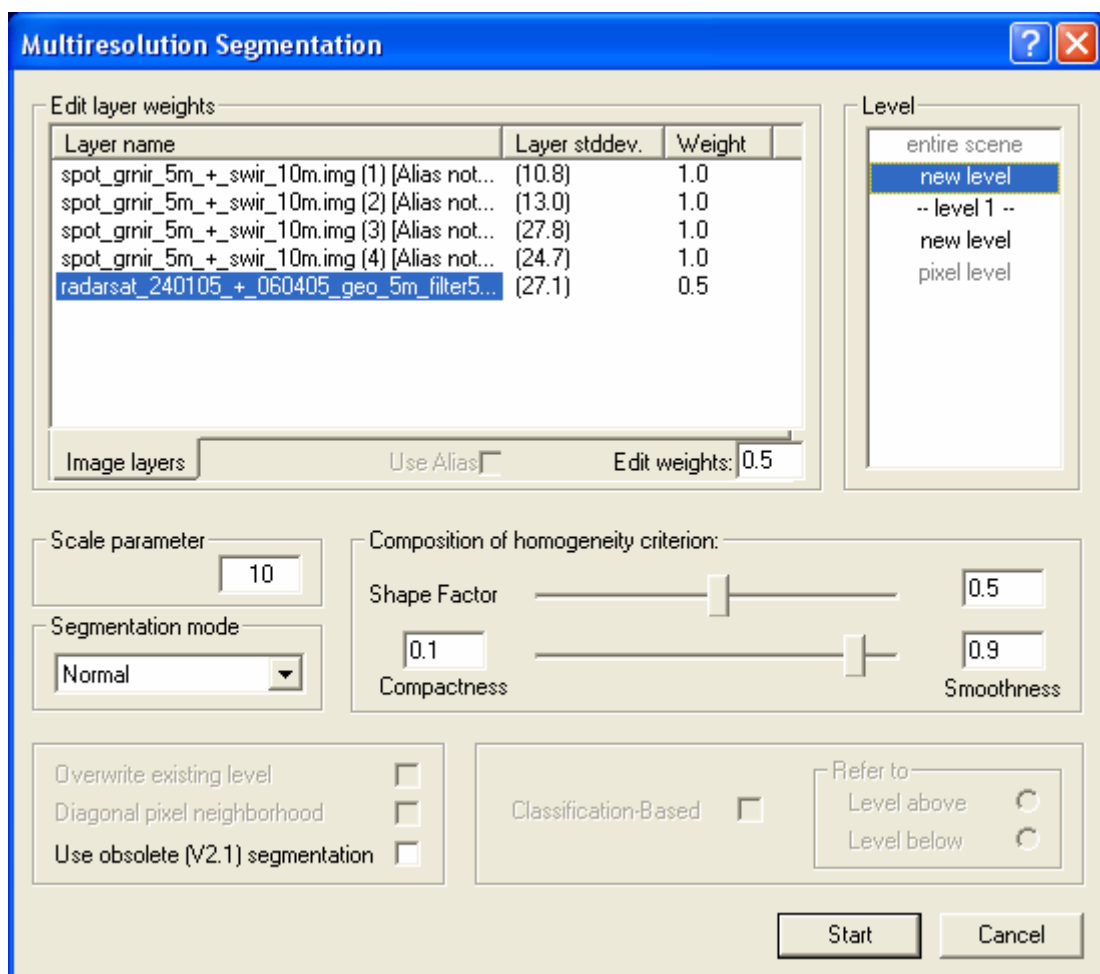


Figure 7.14: Illustration of the settings by segmentation the optical data with the radar data

The software eCognition offers the opportunity to segment and classify in several ranks. Therefore it is possible to build a hierarchical network. In the centre is level 1. From this level the user can determinate a level above with same or higher Scale parameter (Level 2) or a level beneath with lower Scale parameter until into the pixel dimension (Pixel Level). The network hierarchy is demonstrated in figure 7.15. Thus different scaling of the data and classification results is possible.

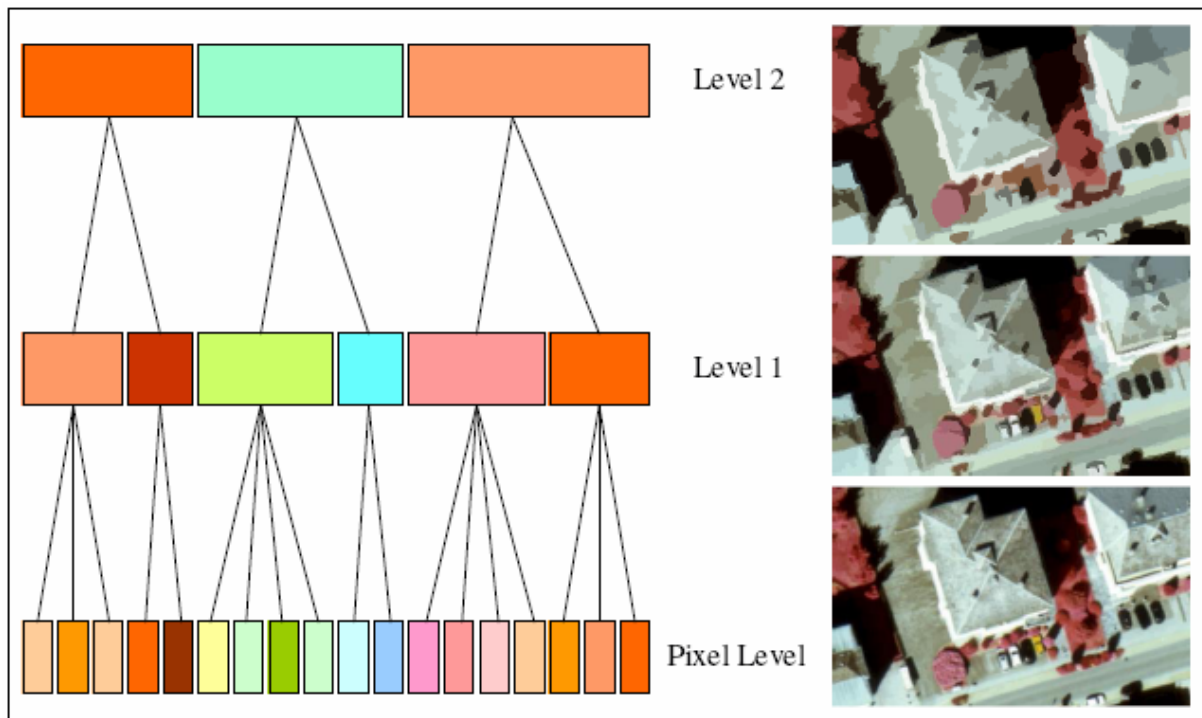


Figure 7.15: Illustration of the hierarchical network in eCognition

For the segmentation with the radar data the same Scale parameter was chosen and level 2 selected. By this method the samples which were defined in level 1 are assumed. The position is the same but the segment size can be different.

7.3.2 Integration of radar texture features into Nearest Neighbour

Beside mean and standard deviation features, texture features of the Radarsat scene were considered additionally because many objects and classes are better describable by texture characteristics in radar images than by simple grey values. Therefore texture parameters after Haralick had been calculated and integrated into the Nearest Neighbour function.

Haralick Texture

Every image is a composite of repeating elements or discrete tonal features. Texture is concerned with the spatial distribution of image intensities and discrete tonal features. In case of wide variation of discrete tonal features, the dominant property of that area is texture (Haralick, 1993). Texture can be arranged within a spectrum from stochastic to regular. The so-called *Grey Level Co-Occurrence Matrix* (GLCM) after Haralick characterizes in a stochastic approach the microtexture of an image region by measuring the dependence

between pairs of grey levels arising from pixels in a specified spatial relation. By this matrix several texture features (e.g. homogeneity, contrast, entropy etc.) can be calculated. It is simply a tabulation of how often different combinations of pixel brightness values (grey levels) occur in an image. Therefore all pixel of an image and its neighbours and beyond it have to be considered. A pixel has 8 neighbouring pixel, so 8 different directions are possible from 0° (vertical direction) to 90° (horizontal direction) and finally 315° (diagonal). Thus the calculation of all directions is very busy and needs a lot of time, especially if more then the neighbouring pixel are considered and calculated.

The Haralick features are implemented in eCognition. The texture features are calculated for every single segment in four directions that are shown in figure 7.16 below. Thus the size of the texture is limited by the size of the segment. In order to calculate a significant texture the segment size should be larger than 3 x 3 pixel.

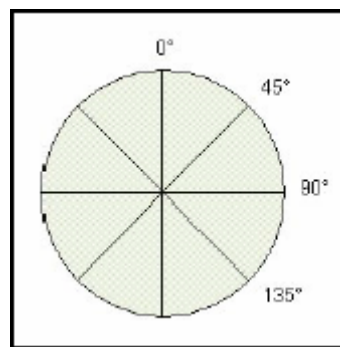


Figure 7.16: Direction of the GLCM Matrix which is calculated in eCognition

The calculated GLCM in eCognition is normalized according to the following operation:

$$P_{i,j} = \frac{v_{i,j}}{\sum_{i,j} v_{i,j}} \quad (7.8)$$

where:

i is the row number and j is the column number

i, j is the value in the cell i, j of the matrix

$v_{i,j}$ is the value in the cell i, j

$P_{i,j}$ is the normalized value in the cell i, j

N is the number of rows or columns

In eCognition overall eight Haralick features for GLCM are available. These include Contrast, Homogeneity, Dissimilarity, Entropy, Mean, Standard deviation, Correlation and Angular second moment. These features and their characteristics are described in the eCognition User Guide 4.0 (2004).

Feature Space Optimization

For the calculation of the optimised feature all eight available Haralick features by GLMC were used. Thus the calculation took very long. As result an optimum feature space of 12 features and a distance of 0.250 were determined. As best texture features Entropy, Correlation, Dissimilarity Standard deviation and Homogeneity were calculated and selected.

7.3.3 Accuracy Assessment

Reference Mask

For the determination of the absolute accuracy an absolute reference masks (TTA mask) has to be available. Thus no area-wide digital reference data set was available an own reference mask for all classes (except the smaller classes Industry, Military, Clay Mining, Fish Farming and Lake) had to be produced. This was made by accumulating several samples of all classes and save them as TTA mask. In this case a lot of samples had been selected for the reference mask and checked by the reference data and the local ground check. The mask covers about the half of the test area (Fig. 7.17). For the five land cover categories a second reference mask was build too. In this mask all classes were summarised to their categories spectrally not semantically (Fig. 7.18).

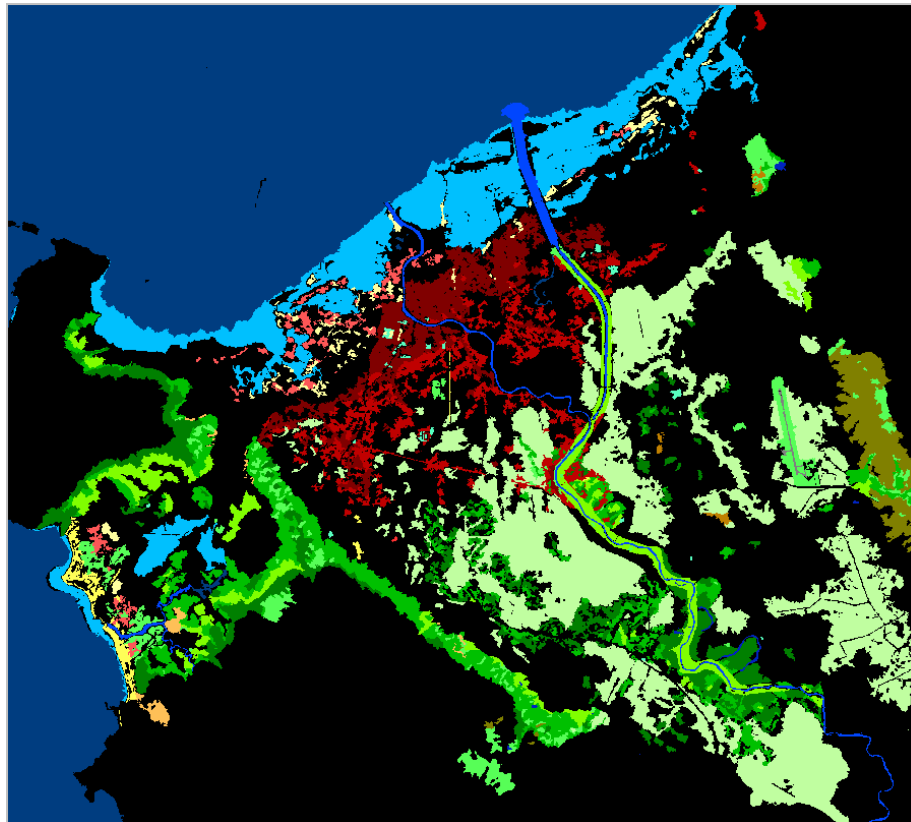


Figure 7.17: Reference mask of the test area including the reference samples for all single classes (except industry and military)

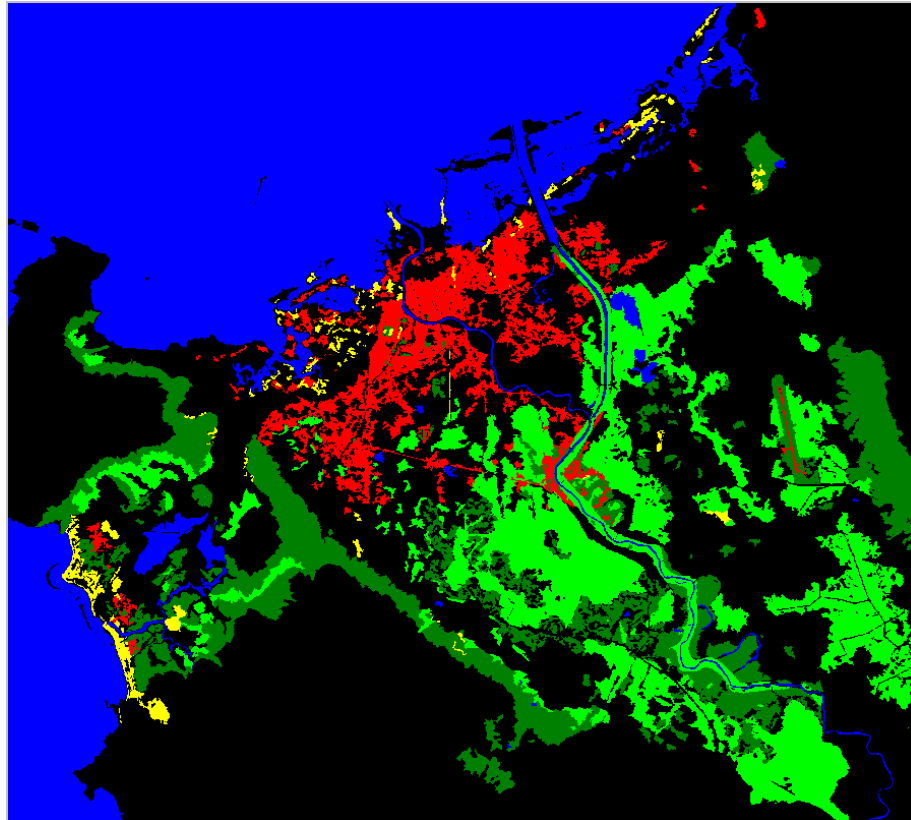


Figure 7.18: Reference mask of the test area including the reference samples of the five categories

The Accuracy measures in eCognition are derived from a Confusion Matrix (Error Matrix) where the classes of the classification result and the classes of the TTA mask are compared. This matrix is shown in the figure 7.19.

User \ Referenc...	Paddy Farming	Mixed Farming	Urban (dense)	Urban (sparse)	Urban (dest
Vegetation (mixed)	13071	111042	841	27611	0
Vegetation (sparse)	20450	21950	695	1676	1013
Slash and Burn	16581	729	370	1098	845
Ocean	0	0	0	0	0
River	2090	80	31	0	0
Flooding	11822	0	0	0	0
unclassified	99	787	446	208	1459
Sum	2226361	413386	442940	416643	97865
Accuracy					
Producer	0.8347	0.4176	0.697	0.5792	0.3102
User	0.8387	0.4640	0.5421	0.527	0.5270
Hellden	0.8367	0.4396	0.6099	0.5519	0.3905
Short	0.7193	0.2817	0.4388	0.3811	0.2426
KIA Per Class	0.8039	0.4018	0.6843	0.565	0.3073
Totals					
Overall Accuracy	0.8233				
KIA	0.7522				

Figure 7.19: Error matrix based on TTA mask in eCognition

Additional to the Kappa Index of Agreement (KIA), the Producer accuracy and the User accuracy eCognition offers the two additional accuracy measures Hellden and Short. These values are derived from different approaches of a combination of the Producer and the User accuracy. Hellden is more an optimistic, whereas Short is more pessimistic approach. But these measures are not so relevant as the KIA, Producer and User accuracy.

Results

For the accuracy assessment the Confusion Matrix and the Kappa Index were analysed for the five categories. The accuracy measures for the single 17 classes are given in the annex 12.9.

Confusion Matrix [Pixel]						
User \ Reference	Waterbodies	Vegetation	Soil	Urban	Agriculture	Sum
Waterbodies	8240034	33	65	55	141998	8382185
Vegetation	193	1739422	2791	41101	219105	2002612
Soil	2699	5571	134655	99840	28649	271414
Urban	35882	27564	32338	725842	166631	988257
Agriculture	79261	233862	10504	88724	2019119	2431470
Unclassified	4142	206	1346	5805	1047	12546
Sum	8362211	2006658	181699	961367	2576549	
Accuracy []						
Producer	0.98534	0.86683	0.74109	0.75501	0.78365	
User	0.98304	0.86858	0.49612	0.73447	0.83041	
KIA Per Class	0.96393	0.84476	0.73600	0.73653	0.73853	
Total accuracy []						
Overall Accuracy	0.912					
KIA	0.852					

Table 7.1: Accuracy results of the optical SPOT 5 data in case of the five categories without using additional knowledge-based information

Confusion Matrix [Pixel]						
User \ Reference	Waterbodies	Vegetation	Soil	Urban	Agriculture	Sum
Waterbodies	8239887	33	95	50	143999	8384064
Vegetation	650	1717289	2267	41143	211011	1972360
Soil	1118	3694	123248	69983	5092	203135
Urban	36971	23135	42955	750959	130591	984611
Agriculture	76192	262138	10798	95924	2081789	2526841
Unclassified	7393	369	2336	3308	4067	17473
Sum	8362211	2006658	181699	961367	2576549	
Accuracy []						
Producer	0.98537	0.85580	0.67831	0.78114	0.80798	
User	0.98280	0.87068	0.60673	0.76270	0.82387	
KIA Per Class	0.96387	0.83232	0.67360	0.76469	0.76601	
Total accuracy []						
Overall Accuracy	0.917					
KIA	0.858					

Table 7.2: Accuracy results of the optical SPOT 5 data in case of the five categories by using additional knowledge-based information

Confusion Matrix [Pixel]						
User \ Reference	Waterbodies	Vegetation	Soil	Urban	Agriculture	Sum
Waterbodies	8235040	18	246	53	159469	8394826
Vegetation	1701	1649635	4925	30972	231887	1919120
Soil	828	4770	108120	36933	31078	181729
Urban	42575	25525	47362	785379	175813	1076654
Agriculture	61523	314024	13095	97392	1970942	2456976
Unclassified	20544	12686	7951	10638	7360	59179
Sum	8362211	2006658	181699	961367	2576549	
Accuracy []						
Producer	0.98479	0.82208	0.59505	0.81694	0.76495	
User	0.98097	0.85958	0.59495	0.72946	0.80218	
KIA Per Class	0.96237	0.79402	0.58976	0.80179	0.71530	
Total accuracy []						
Overall Accuracy	0.905					
KIA	0.839					

Table 7.3: Accuracy results of SPOT 5 and Radarsat integration in case of the five categories by using additional information in form of additional texture features

7.3.4 Evaluation of the results

By using additional knowledge-based information the classification result of the supervised classification by Nearest Neighbour could be improved about 0.5 % in case of considering the five categories. This is not very much, but in case of considering the 17 classes (annex 12.9) an improvement of about 3 % could be achieved by additional knowledge-based information. This is quite much and indicates that their must be an improvement by using the features of the DEM, NDVI, SWIR/NIR and Slope layer.

The comparison of the classification results by using additional knowledge-based information shows that a global improvement with additional radar data could not be achieved in this data set by using additional texture features. Only the category Urban indicates a local improvement. The improvement is mainly caused by the classes Urban (sparse), Urban (destructured) and Airport as it can be seen in the Confusion Matrix of the 17 classes in the annex 12.9, tab. 12.18. Here, it is indicated that radar data are partly helpful to decrease the correlation between Urban and Soil and to improve the producer accuracy. But the category Soil could not be improved. The correlation to Urban and Vegetation increases. The result of Agriculture and Vegetation is also degraded. In case of Vegetation it is partly caused by mountainous areas which are illuminated or shaded in the radar image. Thus a lot of segments could not be classified. If the texture features are eliminated for the vegetation classes the overall classification result can be improved about 0.3 % (Tab. 7.4). This improvement is also recognizable in the visual comparison (Annex 12.7, fig. 12.22 and 12.23). In case of Agriculture a possible reason might be the case that the Radarsat scene and the SPOT 5 data were imaged at different acquisition times. Thus the agriculture could have changed during that period. Waterbodies behave mostly similar in both results. It has to be mentioned that the accuracy of the two classes Ocean and Flooding are very bad between each other by using radar texture information as it can be seen in the annex 12.9, tab. 12.18. That's why the overall accuracy is such bad. In this case the correlation between these classes is so high that the additional radar information only increases this correlation.

Confusion Matrix [Pixel]						
User \ Reference	Waterbodies	Vegetation	Soil	Urban	Agriculture	Sum
Waterbodies	8231464	18	137	53	159469	8391141
Vegetation	4365	1787025	5154	47314	318458	2162316
Soil	896	4558	108278	36704	29831	180267
Urban	45106	25148	47565	779704	174646	1072169
Agriculture	61774	189321	12869	88773	1890471	2243208
Unclassified	18606	588	7696	8819	3674	39383
Sum	8362211	2006658	181699	961367	2576549	
Accuracy []						
Producer	0.98436	0.89055	0.59592	0.81104	0.73372	
User	0.98097	0.82644	0.60065	0.72722	0.84275	
KIA Per Class	0.96134	0.87070	0.59068	0.79547	0.68330	
Total accuracy []						
Overall Accuracy	0.908					
KIA	0.845					

Table 7.4: Accuracy results of the SPOT 5 and Radarsat integration in case of the five categories by texture features without the category vegetation

7.4 Integration of radar texture features into Membership Function

The integration of radar texture features showed that a global improvement could not be obtained. Only single classes indicated a local improvement. Thus it was tested if only the use of local information could increase the overall accuracy. Therefore knowledge-based rules were formulated for these single classes by using additional radar information.

7.4.1 Modelling

For the modelling different classes of the categories Urban, Soil and Waterbodies were considered which promise to be detected quite well in radar images because of their special backscatter characteristics of microwaves.

1.) Urban

Urban (dense):

In radar images dense urban areas show generally high intensity values because of a high backscatter which comes back to the sensor because of the double bounce effect. Normally this value is very high in contrast to other classes. Thus it was exploited to use only high intensity values. The limit was set iterative by comparison to other classes which are highly correlated like Gravel. Entropy was chosen for this purpose because this feature indicated as best texture feature the fewest overlapping and best separation (8 % overlapping) to the high correlated class Gravel. Here, the Feature View was used again to display the feature range of every segment (Fig. 7.20). Bright segments represent high, dark segments low entropy values. In the centre of the image the dense settlement with bright segments can be seen. In the left upper corner waterbodies are represented by darker segments. In the middle left part the areas of gravel appear mostly in a middle grey tone.

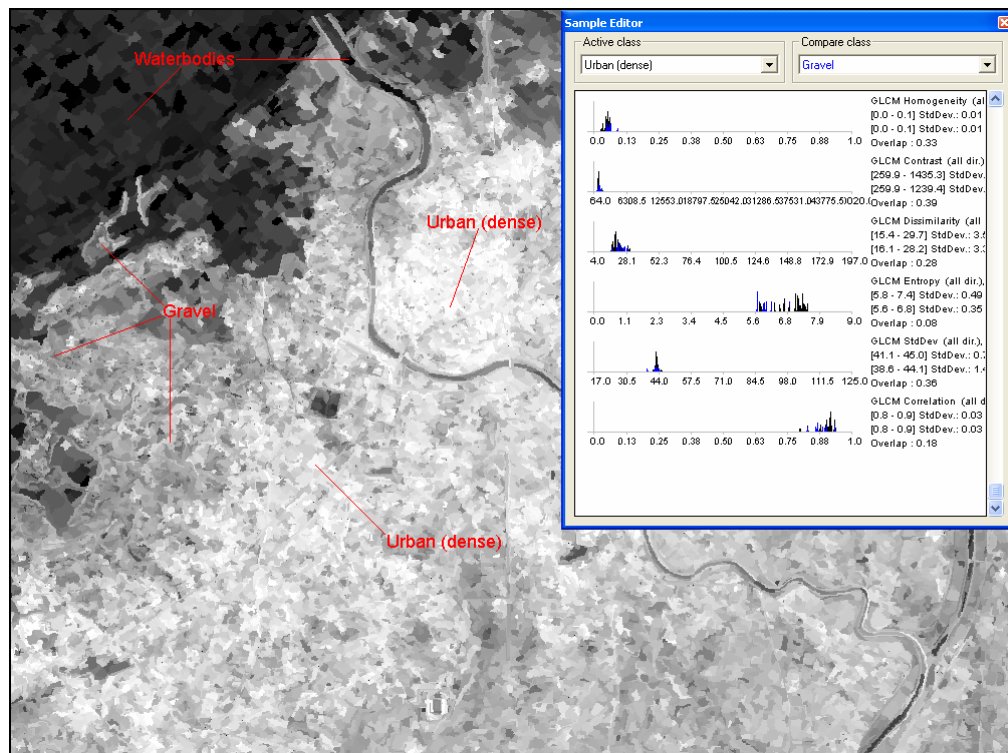


Figure 7.20: Feature view of the texture feature Entropy in eCognition

The limit was set to 6.0. All values above this limit should represent dense urban areas. In case of other texture features the overlapping was about 18 to 40 % (Fig. 7.20, Sample Editor). This is quite much. But these values must be treated carefully because these values are estimated from the given samples. This overlapping must not include that all segments of a class are considered. The variation can be much higher.

Urban (sparse):

Sparse urban settlement is generally also represented by high backscatter values, but not so high values as in case of dense settlement because of smaller buildings and mixture with vegetation. Here the same texture feature was used. The limit was set to 5.0.

Urban (destroyed):

Destroyed urban settlement is, like the other urban classes, also represented by high backscatter values. In this case the values are quite high. But the destroyed settlements are mixed with gravel and sand so that the value in the segment is much lower. Here the same texture feature was used. The limit was also set to 5.0.

Airport:

The backscatter of microwaves at runways behaves like the backscatter at waterbodies or sand. It is very low because the microwaves are totally reflected at the flat surface. Thus these areas appear very dark in the radar image. Here, the mean value of the Radarsat scene was used because this feature offered the best separation of other correlating classes. The limit was set to 30. All values above this limit were not considered.

2.) Soil

The backscatter of sand, gravel and limestone is similar to those of the airport runway. In case of the features mean, standard deviation and Entropy the values are mostly low. In this case the mean feature offered the best separation to the category urban. Thus a small mean value was considered. Here, it was set < 30 .

3.) Waterbodies

In case of waterbodies it is the same. Because of total reflection no or few signals come back to the sensor. Thus waterbodies are mostly very dark in radar images. Here, the mean value was set < 40 .

7.4.2 Accuracy Assessment

The result shows in comparison to the result of the optical reference data that the accuracy of the category Soil could be improved by additional radar information but the overall accuracy could not be increased. In comparison to this the accuracy of the category Urban was rather decreased. Reason for this is the fact that both categories are highly correlated with each other and that additional radar features are not able to decorrelate both categories. The potential gain, which was assessed in the classification by using the texture features in a global content in the Nearest Neighbour approach, of the category Urban got lost. But many restrictions have been made to the category Urban. There are many segments which belong to the category Urban, but represent not so high Entropy values, as assumed. Thus these true segments are excluded and the absolute accuracy is worse. So the given samples represent the category Urban not completely. There is still a great variation, especially in radar data which has to be considered.

Waterbodies and the other categories behave similar to the result of the reference data. There are no high differences in comparison to the result of the reference data.

Confusion Matrix [Pixel]						
User \ Reference	Waterbodies	Vegetation	Soil	Urban	Agriculture	Sum
Waterbodies	8248390	51	346	236	149786	8398809
Vegetation	1362	1731703	2466	51548	230901	2017980
Soil	3727	5650	136100	87895	4109	237481
Urban	21090	10753	27055	619900	41999	720797
Agriculture	75687	257835	12217	197119	2145488	2688346
Unclassified	11955	666	3515	4669	4266	25071
Sum	8362211	2006658	181699	961367	2576549	
Accuracy []						
Producer	0.98639	0.86298	0.74904	0.644811	0.83270	
User	0.98209	0.85814	0.57309	0.86002	0.79807	
KIA Per Class	0.96630	0.84007	0.74474	0.62566	0.79325	
Total accuracy []						
Overall Accuracy	0.915					
KIA	0.854					

Table 7.5: Accuracy results of the SPOT 5 and Radarsat integration in case of the five categories by single texture features for single classes

7.5 Object-based Classification of the ASTER and Envisat data

After the investigation with the SPOT 5 data, the second data set of ASTER and Envisat was used to perform the object-based classification in order to evaluate if in improvement could be achieved by a data set of same acquisition time. At first the optical data was used and in a second step the Envisat data were integrated into the classification.

7.5.1 Object-based Classification of the optical ASTER data

The pure optical ASTER data set include the three ASTER scenes ASTER_VNIR-2501, ASTER_SWIR-2501 and ASTER_TIR-2501 with the bands 1, 2, 3, 4, 7 and 12 as in case of the pixel-based approach.

The segmentation was analogue to those of the SPOT 5 data. In this case the Scale parameter was set to 3 because of the lower resolution of 15 m. The other parameters were retained. In case of the feature optimization the maximum dimension increased to 18 because of the 6 bands. The selection of the features was also retained. The result of the optimization was a feature space of 10 and a maximum distance of 0,255. The knowledge-based information in case of the membership function was similar to the knowledge-based information of the optical SPOT 5 data. Only the vegetation ratios in case of Vegetation (dense) and Vegetation (mixed) were different and adapted to the data set because of other grey value in the different bands. Also the number of pixel for the class-related features had to be adapted because of a greater pixel size (15 m). The detailed information of the knowledge-based rules is given in the annex 12.8.

7.5.2 Radarsat data integration into Nearest Neighbour

In the second step the Envisat scene was combined with the ASTER data and treated as additional seventh band like in case of the SPOT 5 and Radarsat data.

The pre-processing was analogue to the pre-processing of the SPOT 5 and Radarsat data by using additional texture features. In the segmentation process the Envisat scene got also a smaller weight of 0.5 and the Shape factor was also set to 0.5 in order to equal colour features of the multi-spectral bands and shape features of the radar image. In case of the feature optimization a feature space with a dimension of 10 and a distance of 0.240 was determined. The classification was performed analogue to the classification of the SPOT 5 and Radarsat data. Because of the no data values in the upper left corner of the Envisat scene features of this radar scene for the classes Waterbodies and Vegetation (dense), that were affected of the no data values in this sector, were not considered. Therefore the features of the optical data set were derived in order to classify the wholly test area and to reference with the given reference mask.

7.5.3 Accuracy Assessment

For the Accuracy assessment the same reference masks were used. Because of the fact that this mask was mostly derived from the orthophotos of June, the absolute accuracy is a little bit worse than the accuracy of the first data set. But in this case the relative accuracy between the single classification results of the second data set is much more important. The following results have been obtained:

Confusion Matrix [Pixel]						
User \ Reference	Waterbodies	Vegetation	Soil	Urban	Agriculture	Sum
Waterbodies	918538	112	1016	1122	24947	945735
Vegetation	514	160939	959	3445	45274	211131
Soil	801	379	10598	9329	93	21200
Urban	5491	4869	6158	75288	19418	111224
Agriculture	3562	55788	874	17190	196395	273809
Unclassified	2278	985	605	525	164	4557
Sum	931184	223072	20210	106899	286291	
Accuracy []						
Producer	0.98642	0.72147	0.52439	0.70429	0.68599	
User	0.97124	0.76227	0.49991	0.67690	0.71727	
KIA Per Class	0.96577	0.67812	0.51787	0.68171	0.61955	
Total accuracy []						
Overall Accuracy	0.869					
KIA	0.776					

Table 7.6: Accuracy results of the optical ASTER data in case of the five categories

Confusion Matrix [Pixel]						
User \ Reference	Waterbodies	Vegetation	Soil	Urban	Agriculture	Sum
Waterbodies	916561	194	1300	799	23385	942239
Vegetation	835	147683	534	7048	61709	217809
Soil	1839	888	8623	10469	254	22073
Urban	5870	3949	6858	66767	4376	87820
Agriculture	3353	68124	1405	18051	195604	286537
Unclassified	2726	2234	1490	3765	963	11178
Sum	931184	223072	20210	106899	286291	
Accuracy []						
Producer	0.98430	0.66204	0.42667	0.62458	0.68323	
User	0.97275	0.67804	0.39066	0.76027	0.68265	
KIA Per Class	0.96064	0.60751	0.41848	0.60230	0.61239	
Total accuracy []						
Overall Accuracy	0.852					
KIA	0.747					

Table 7.7: Accuracy results of the optical ASTER and Envisat integration by additional texture features in case of the five categories

7.5.4 Evaluation of the results

Both results show again that no global classification improvement could be obtained by additional radar information. Even in case of the same acquisition time. It can be stated that the categories Waterbodies and Agriculture were detected quite well. There is no big difference in comparison to the optical data. The accuracy of the other categories is much worse, especially Soil. One reason for the overall degradation might be the fact that the texture features are limited on the segments. In this data set the segments are very small in comparison to the pixel number because the pixel size is quite large. Thus only a small distance can be considered for the calculation of the texture feature. Therefore a third

classification was started without texture features. Only the mean and the standard deviation of the radar scene were considered as additional features, whereas the standard deviation is a quite good alternative for texture features because of the variance.

The calculated result shows that now a global improvement could be obtained. Especially the categories Urban and Soil that use to have normally smaller segments show an accuracy improvement. But this improvement is small in this case.

Confusion Matrix [Pixel]						
User \ Reference	Waterbodies	Vegetation	Soil	Urban	Agriculture	Sum
Waterbodies	919205	115	959	695	25208	946182
Vegetation	414	160052	665	5964	45434	212529
Soil	1871	590	11068	9504	262	23295
Urban	2753	4081	5496	71056	5796	89182
Agriculture	4095	56224	1098	15912	209195	286524
Unclassified	2846	2010	924	3768	396	9944
Sum	931184	223072	20210	106899	286291	
Accuracy []						
Producer	0.98714	0.71749	0.54765	0.66470	0.73071	
User	0.97149	0.75308	0.47512	0.79675	0.73011	
KIA Per Class	0.96755	0.67318	0.54083	0.64448	0.67048	
Total accuracy []						
Overall Accuracy	0.874					
KIA	0.785					

Table 7.8: Accuracy results of the ASTER and Envisat integration without additional texture features in case of the five categories

8 Ground check and final map

8.1 Reason for a ground check

In this thesis the used reference data for the determination of the absolute accuracy for the different classifications are mostly based and derived from the aerial images which were available in nearly the same time of the given remote sensing data. These images have a resolution of about 30 centimetres. A lot of classes and typical samples and areas can be recognized and referenced. But there are some areas which despite of the very high resolution need to be checked locally in order to give a precise conclusion about the area and the class it represents. A typical example of this is the class Mixed Farming. Most areas of Mixed Farming are along the river Aceh and along the foothills. But in the aerial images it is difficult to see if some areas do have a special usage for the human in form of plantations or if these areas are more or less covered with simple mixed or sparse vegetation. The defined class Mixed Farming is a rather broad class which includes several subclasses. To separate between these single subclasses would have been to complex and costly for this thesis. Most of these subclasses are very similar with respect to areas of mixed and sparse vegetation. So the ground check was necessary to exploit the possible subclasses and the areas which are really marked as a specific land use. Another case is the class Fish Farming. This class is strongly correlated to wet paddy fields and the category Waterbodies. In the aerial images it is not always to see if a wet area is more a flooded paddy field or if this is a fish pond for Fish Farming or simply a small unused lake.

8.2 Local ground check

The ground check was done in cooperation of the local bureau of the BGR in Banda Aceh. This bureau was managed in collaboration with the local agency for geology. As support for the ground check a GPS-receiver, digital camera and a workstation with a Geographical Information System (GIS) were available as well as a driver with a car.

For the check several points and areas of the test area, which were not so clear estimated, were assessed by car and checked locally by the camera and GPS coordinates (Fig. 8.1). The aerial orthophotos images from the reference data printed as analogue map were used as orientation and reference. The projection of the GPS points was adapted to projection of the maps (UTM, WGS 84, Zone 46 North).



Figure 8.1: Coordinating an imaging of an area in the test area during the ground check

In order to combine the images to the right GPS coordinates the acquisition time was adjusted to the local GPS time of the receiver. Thus the images could be assigned to the coordinates by same acquisition time. The maximum accuracy of the GPS receiver was about 5 m. But the accuracy of GPS depends on the local environment. In open areas like grassland or sparse vegetation normally the accuracy of about 6 m could be reached. In dense urban or dense vegetation areas the accuracy was often much worse (about 15 m) because of multipath effects. But mostly the accuracy was about 7 to 10 m and in some rare case over 10 m. This accuracy is sufficient for this purpose because a representative object could have the minimum size of two pixels but in this case the minimum size is about 50 to 100 m.

8.3 Analysis of the ground check

Overall about 1000 GPS points were measured. From these 1000 GPS points about 350 points could be documented by images. The coordinates from the GPS receiver were exported by the local software of the receiver and formatted into an ASCII-file which was imported to the GIS system, where the coordinates could be marked in the digital aerial image maps and the reference mask which was built in eCognition for the accuracy assessment. The reference mask was generated as vector layer. By overlaying of the GPS points, the reference mask could be adjusted to the points and improved. Therefore the attributes of the single segments were newly revised.

8.4 Results of the ground check

The ground check showed that many areas and even classes had changed dramatically during the period of about 2 years. Almost all the destructed areas near the coast which were struck by the Tsunami are rebuilt again. The estimation is about 95 % which is rebuilt. Thus the class urban (destructed) has to be renamed into urban (rebuild) in order to be actual. Also many areas, which were flooded, are now used again, for example as paddy fields, Fish Farming and other land use. Gravel areas along the coast are now mostly covered again with sparse or mixed vegetation. Also many new tall settlements had been built near the mountains in the north east of the test area in order to provide new living opportunities beside the coast for the relevant people.

The local change detections were not considered for the reference mask and accuracy assessment because the mask has to be current for the time the remote sensing data was imaged. Thus a ground check would be better shortly after the acquisition time. For the reference mask only samples and areas were considered which did not change. Thus false class assignments could be improved. The change detection was considered in a new updated land use and land cover map which is based on the result of the SPOT 5 and Radarsat data. There the changes had been inserted manually and locally. An area-wide change detection was not possible due to the single points which were measured.

8.5 Editing the final map

In the final step of this thesis the current map was generated. Therefore the result of the object-based classification by integrating local radar information in Membership Function was used as basis. Additionally the thermal band of the ASTER data set was attached in order to detect dense settlement in a better way. High grey values (> 100) in the thermal band were assigned to the class Urban (dense).

Afterwards the generated classification result was improved manually. Therefore manual editing tools in eCognition were used. These tools allow to assign false detected segments to the class they really belong to. By clicking the segment it is assigned to another class. Cutting or merging of single segments is also possible. The manually classification was done while the thematic accuracy of the five categories was reached about 90 %. The classes Industry, Military, Lake, Fish Farming and Clay Mining that were not classified during the classification process were also manually edited.

In the next step the classification result (raster layer) was exported to ERDAS Imagine. Additionally vector layer were integrated in order to represent streets and borders in the map. Finally the land use / land cover map was generated in the Map Composer of ERDAS. There the image, text, legend and scale was set. The area of the image in the map was rounded up to geographical coordinates. Thus the size was minimized a little bit. The final map (Fig. 8.2) was exported to Tif-format and then plotted.

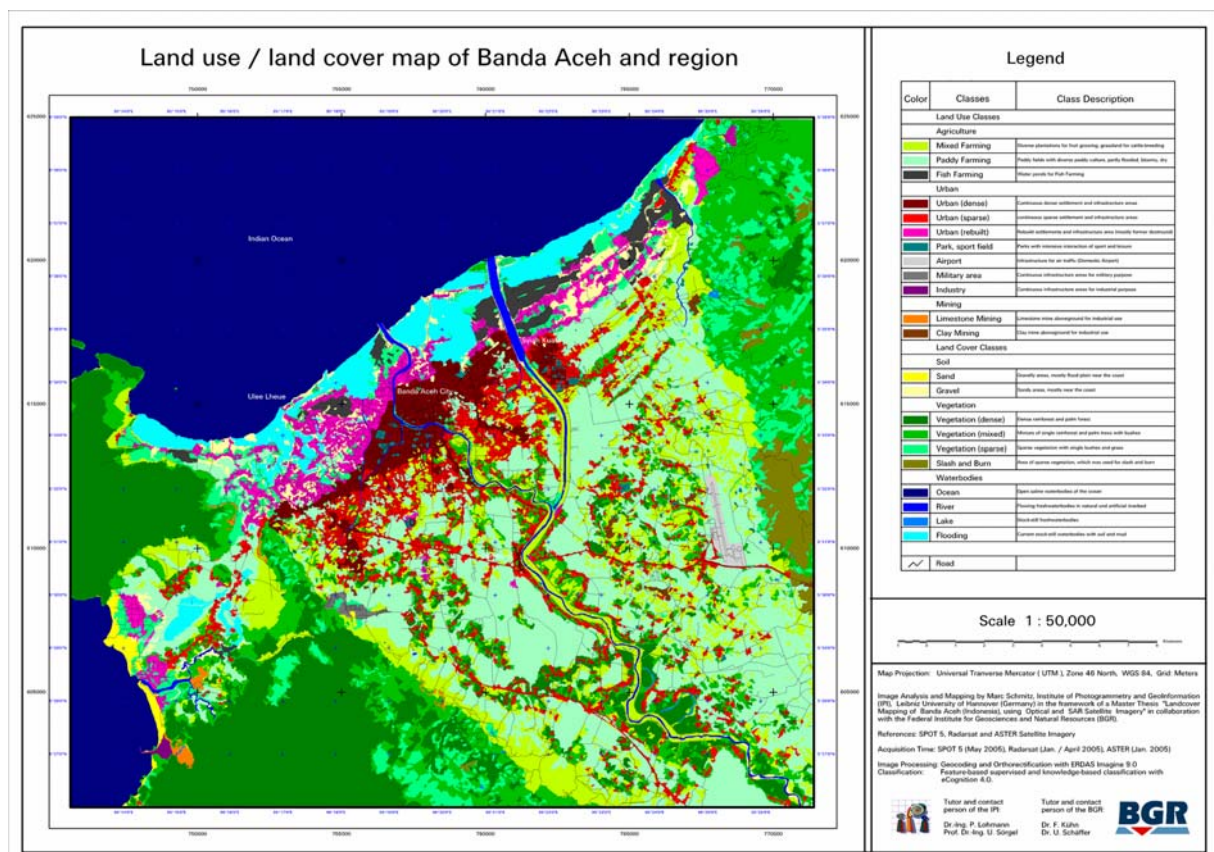


Figure 8.2: Final land use / land cover map of Banda Aceh and region

9 Evaluation of the classification results

In the pixel-based approach it could be shown that in case of the first data set (SPOT 5 and Radarsat) the selected image fusion techniques Multiplicative method, PCA Transform and Ehlers Fusion were not able to improve globally the classification result in comparison to the reference data generated from the optical data set. Neither in optical nor in statistical comparison an improvement could be assessed. But it has been exposed in the first data set that the Principle Component Analysis and the Ehlers Fusion seems to offer a quite good fusion approach in order to fusion optical with radar data. In case of the Multiplicative method it could be confirmed that this arithmetical approach indicates a great colour distortion and a degradation in the classification result.

Also in case of the second data set a global improvement in the classification result could be obtained although of same acquisition time. But here it is indicated that the degradation is not so high as in comparison to the first data set of different acquisition time. Thus it can be stated that the results of the second data indicate that with same acquisition time the best results can be achieved but not satisfying to achieve a global improvement.

The overall accuracy of the classification results by the two data sets (SPOT 5 / Radarsat and ASTER / Envisat) are illustrated in figure 9.1.

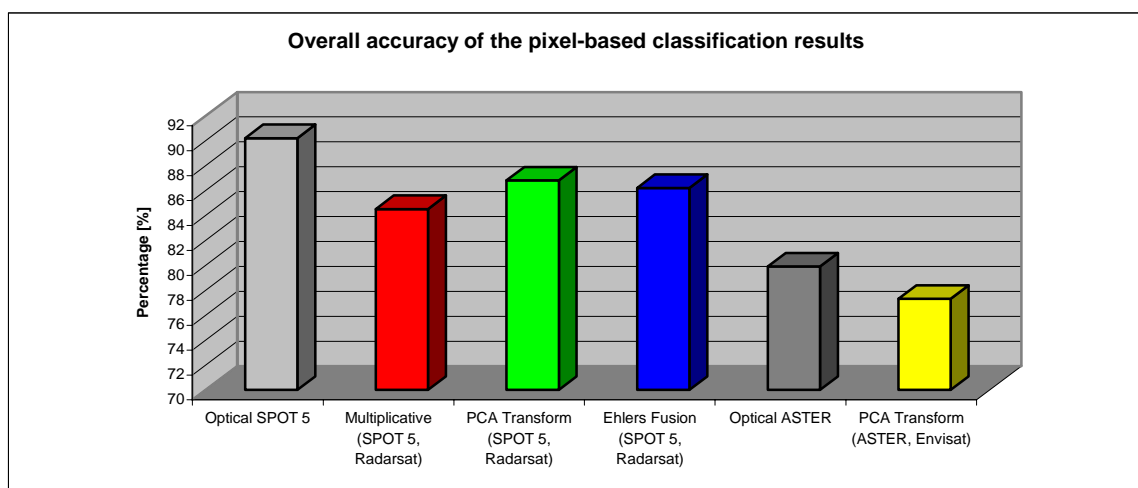


Figure 9.1: Overall accuracy of the pixel-based classification results in case of the SPOT 5 and Radarsat data

The object-based approach has also shown that hardly no global improvement could be obtained in both data sets by using additional radar information. The use of additional texture features indicated that the results become worse because of the relative small size of segments, especially in case of the second data set. The texture features show no global benefit in this case. Only in case of the category Urban a local improvement could be indicated. But this potential improvement could not be gained by an approach where local radar information was considered for the categories Urban, Soil and Waterbodies. In this case the category Soil could be improved but Urban got worse because of high correlation to Soil and partly variation in the radar scene.

For the second data set it could be indicated that a global improvement is obtainable without texture features. Therefore the standard deviation seems to offer a good alternative to the texture. But this improvement is not so high, so that no general statement can be made. Here again, it can be stated that the chances for an improvement are increased in case of same acquisition time. In the second data set with SPOT 5 and Radarsat at three different acquisition times it is obvious that the difference is much higher in case of fast changing classes like agriculture. The overall accuracy of the classification results by the two data sets (SPOT 5 / Radarsat and ASTER / Envisat) are illustrated in figure 9.2.

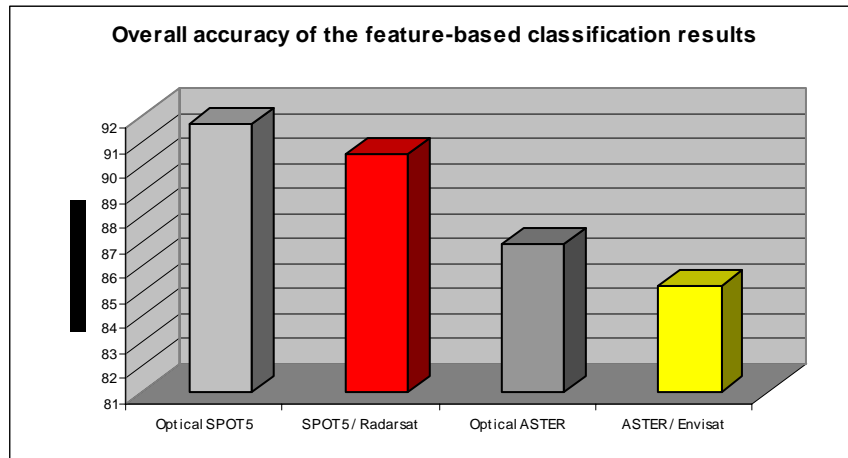


Figure 9.2: Overall accuracy of the object-based classification results in case of the SPOT 5 and Radarsat data

10 Prospects

It could be concluded that the object-based approach shows more benefits in comparison to common pixel-based approaches with several image fusion techniques. Especially the knowledge-based classification offers more advantages. It is not limited to Boolean Operators and simple pixel values like in the pixel-based approach. Especially additional standard deviation and shape features are helpful to extract better knowledge-based information out of radar images. The consideration of additional texture features has shown no improvement in the classification result because of the relative small size of the given segments. Therefore it has to be exploited in another investigation if the results could be improved by the selection of greater segments with a greater number of pixel. Generally it can be stated that a knowledge-based classification approach is necessary to improve the classification result.

In case of a pixel-based image fusion the adequate fusion method depends on the fusion purpose and data set. For the fusion of optical and radar images the Ehlers Fusion offers the best way to preserve the radiometric features. But for the purpose of classification it might not always yield better results in comparison to the original optical data. In case of the Ehlers Fusion the whole potential of this fusion technique could not be exploited mainly because of the high requirements of coregistration in the geocoding process (subpixel accuracy). Thus further investigations have to be made to give a concrete conclusion.

It has been shown by the use of different data sets that the acquisition time of both data sets to be combined is very important. Thus it can be stated that optical image data and radar data at different times do not automatically yield in better classification results, especially if radar data itself consist of two different times. Thus this special case should be avoided. But often it is not possible to receive data of same acquisition time because of different cycles of the satellites.

Generally it can be said that the object-based approach in combination of a knowledge-based classification offers a good tool to integrate optical remote sensing data with radar remote sensing data. Texture features might be the best way to describe radar images, but here these features were not really helpful because of the small size of the areas. In this case the feature standard deviation might be a good alternative for the other texture features.

11 References

Literature

Albertz J. (2001): Einführung in die Fernerkundung: Grundlagen der Interpretation von Luft- und Satellitenbildern. Darmstadt.

Bähr H.-P. and Vögtle T. (1998): Digitale Bildverarbeitung. Anwendung in Photogrammetrie, Kartographie und Fernerkundung, 3. Aufl., Wichmann.

Bayer T. (1990): Korrektur reliefbedingter radiometrischer Verzerrungen in geokodierten Seasat-A SAR Bildern am Beispiel des Szenenausschnittes Bonn und Umgebung. In: DLR Forschungsbericht; Oberpfaffenhofen.

Buckreuß S. (1994): Bewegungskompensation für flugzeuggetragene SAR-Systeme. Research Report, FB 94-17, DLR, Oberpfaffenhofen.

Carper W.J., Lillesand T.M. and Kiefer R.W. (1990): The use of Intensity-Hue-Saturation transformations for merging SPOT Panchromatic and multi-spectral image data. Photogrammetric Engineering and Remote Sensing, Vol. 56, No. 4, pp. 459-467.

Chavez P.S. Jr., Sides S.C. and Anderson J.A. (1991): Comparison of three different methods to merge multiresolution and multi-spectral data: Landsat TM and SPOT panchromatic. Photogrammetric Engineering and Remote Sensing, Vol. 57 (3), pp. 295-303.

Crippen R.E. (1989a): A Simple Spatial Filtering Routine for the Cosmetic Removal of Scan-Line Noise from Landsat TM P-Tape Imagery. Photogrammetric Engineering & Remote Sensing 55 (3): pp. 327-331.

Dallemand J.F., Lichtenegger J., Kaufmann V., Paudyal D.R. and Reichert, R. (1992): Combined analysis of ERS-1 SAR and visible/infrared RS data for land cover/land use mapping in tropical zone: a case study in Guinea. Proceedings First ERS-1 Symposium Space at the Service of our Environment, ESA SP-359, Cannes, France, 6-8 Nov., pp. 555-561.

Drury S.A. (1997): Image Interpretation in Geology. London: Chapman & Hall.

eCognition User Guide 4.0 (2004), München, Germany.

Ehlers M. (1993): Integration of GIS, remote sensing, photogrammetry and cartography: the geoinformatics approach. GIS GEO-Informationssysteme, Vol. 6, No5, October Issue, pp. 18-23.

Ehlers M. (2005): Beyond Pansharpening: Advances in data fusion for very high resolution remote sensing data.

ERDAS User Guide 9.1 (2005), Norcross, GA, USA.

Franklin S.E. and Blodgett C.F. (1993): An example of satellite multisensor data fusion. *Computers and Geoscience*, Vol. 19, No. 4, pp. 577-583.

Frost V.S., Stiles J.A., Shanmugan K.S. and Holtzman J.C. (1982): A Model for Radar Images and its Application to Adaptive Digital Filtering of Multiplicative Noise. Institute of Electrical and Electronics Engineers, Inc. (IEEE) *Transactions on Pattern Analysis and Machine Intelligence PAMI-4* (2): pp. 157-166.

Geßner U. (2005): Landbedeckungs-/Landnutzungsklassifizierung von Deutschland auf Grundlage von Daten des Sensors MERIS. Diplomarbeit im Fach Geographie, Fakultät für angewandte Informatik, Universität Augsburg.

Gungor O. and Shan J. (2006): An Optimal Fusion Approach for Optical and SAR Images. ISPRS Mid-term Symposium, Commission VII, "Remote Sensing: From Pixels to Processes", Enschede, the Netherlands, May 8-11.

Hagemeister A. (2001): Informationsgehalt von ERS-1/-2 SAR-Daten zur Erfassung der Arteninventare und des Zustandes landwirtschaftlich genutzter Böden und Vegetation. Dissertation im Fachbereich Geowissenschaften, Johannes Gutenberg-Universität Mainz.

Haralick R.M. and Shapiro L.G. (1993): *Computer and Robot Vision*, volume 2. Addison-Wesley.

Harris J.R. and Murray R. (1989): IHS transform for the integration of radar imagery with geophysical data. *Proceedings 12th Canadian Symposium on Remote Sensing*, Vancouver, Canada, pp. 923-926.

Harrison B.A. and Jupp D.L.B. (1990): Introduction to image processing. Part 2 of the microBRIAN Resource Manual, CSIRO Publications, Melbourne, Australia, 256 pages.

Hildebrandt G. (1996): *Fernerkundung und Luftbildmessung: für Forstwirtschaft, Vegetationskartierung und Landschaftsökologie*. Heidelberg.

Hochschild V. (1995): Geomorphologische Kartierung und Untersuchung der Auftaudynamik mit ERS-1-SAR-Daten im Bereich der Antarktischen Halbinsel. *Bremer Beiträge zur Geographie und Raumplanung*, Heft 28.

Klenke M. (1999): GIS gestützte Landnutzungsklassifikationen auf Grundlage von Daten passiver und aktiver Fernerkundungssensoren zur distributiven Flusseinzugsgebietsmodellierung. *Jenaer Geographische Schriften*, Band 8.

Kronberg P. (1985): *Fernerkundung der Erde*. Stuttgart.

Leberl F.W. (1990): *Radargrammetric Image Processing*. Norwood, Massachusetts: Artech House, Inc.

Lee J.E. and Walsh J.M. (1984): *Map Projections for the Use with the Geographic Information System*. U.S. Fish and Wildlife Service, FWS/OBS-84/17.

Lopes A., Nezry E., Touzi R. and Laur H. (1993): Structure detection and statistical adaptive speckle filtering in SAR images. *International Journal of Remote Sensing*, Vol. 14, No. 9, pp. 1735-1758.

Müllenhoff O. (2004): Rekonstruktion von Gewässerstrukturen im Oderbruch bei Manschnow durch multifrequente und multipolarimetrische Radarfernerkundung- und GIS-Analyse. Dissertation im Fachbereich Geowissenschaften, Mathematisch-Naturwissenschaftliche Fakultät; Westfälische Wilhelms-Universität.

Pohl C. (1996): Geometric aspects of multisensor image fusion for topographic map updating in the humid tropics. ITC Publication No. 39.

Raney R.K. (1998): Radar Fundamentals: Technical Perspective. In Henderson, F.M. und Lewis A.L. (Hrsg.): *Manual of Remote Sensing, Band 2: Principles and Applications of Imaging Radar*, Kapitel 2. Wiley, New York, USA, 3. Auflage.

Reinartz P. (1989): Untersuchungen zur multispektralen Klassifizierung von schwer trennbaren Klassen mit Beispielen aus Waldschadensgebieten. Oberpfaffenhofen.

Rencz A.N. (1999): Remote Sensing for the Earth Sciences, *Manual of Remote Sensing*. 3rd Edition, Volume 3, New York.

Richards J.A. and JIA X. (1999): *Remote Sensing Digital Image Analysis: An Introduction*. Berlin/Heidelberg.

Schanda E. (1986): *Physical Fundamentals of Remote Sensing*. Berlin.

Schättler T. (1992): Die Verarbeitung von synthetischen Aperturradardaten zu hochauflösenden Bildern der Erdoberfläche am Beispiel des ERS-1. Arbeitsunterlagen zum DLR-WT-DA SAR Workshop; Wessling.

Schmullius C. C. (1992): Radarfernerkundung landwirtschaftlicher Flächen mit einem flugzeuggetragenen L-, C- und X-Band Scatterometer, *Berliner Geowissenschaftlicher Abhandlungen, Reihe D, Band 3*, 111 S.; Berlin.

Shen S.S. (1990): Summary of types of data fusion methods utilized in workshop papers. *Proceedings Workshop Multisource Data Integration in RS*, NASA Conference Publication 3099, Maryland, USA, June 14-15, pp. 145-149.

Sörgel U. (2003): Iterative Verfahren zur Detektion und Rekonstruktion von Gebäuden in SAR und InSAR Daten. Dissertation im Fachbereich Elektrotechnik und Informationstechnik, Universität Hannover.

Suits G., Malila W. and Weller T. (1988): Procedures for using signals from one sensor as substitutes for signals of another. *Remote Sensing of Environment*, Vol. 25, pp. 395-408.

Sun X., Zhang J., Liu Z. and Zhao Z (2006): Classification from Airborne SAR Data enhanced by Optical Image using an Object-oriented Approach. *ISPRS Mid-term Symposium, Commission VII, "Remote Sensing: From Pixels to Processes"*, Enschede, the Netherlands, May 8-11.

Ulabey F., Moore R. and Fung A. (1982): Microwave Remote Sensing - Vol. II: Radar Remote Sensing and Surface Scattering and Emission Theory. Addison Wesley and Artech House.

Van Genderen J.L. and Pohl C. (1994): Image fusion: Issues, techniques and applications. Proceedings EARSeL Workshop on Intelligent Image Fusion, Genderen J.L. van and Capellini V. (Eds.), Strasbourg, France, 11 September.

Wald L., Ranchin T. and Mangolini M. (1997): Fusion of Satellite Images of Different Spatial Resolution: Assessing the Quality of Resulting Images. Photogrammetric Engineering & Remote Sensing. Vol. 63, No.6, pp. 691-699.

Welch R. and Ehlers M. (1988): Cartographic feature extraction from integrated SIR-B and Landsat TM images. International Journal of Remote Sensing, Vol. 9, No. 5, pp. 873-889.

Yang J., Zhang J., Zhao Z., Zhang Y. and Li H. (2005): Block-regression-based Fusion of Optical and SAR Imagery for Feature Enhancement. ISPRS Mid-term Symposium, Commission VII, "Remote Sensing: From Pixels to Processes", Enschede, the Netherlands, May 8-11.

Yesou H., Besnus Y. and Rolet J. (1993a): Extraction of spectral information from Landsat TM data and merger with SPOT panchromatic imagery – a contribution to the study of geological structures. ISPRS Journal of Photogrammetry and Remote Sensing, Vol. 48, No. 5, pp. 23-36.

Yocky D.A. (1996): Multiresolution Wavelet Decomposition Image merger of Landsat Thematic Mapper and SPOT Panchromatic Data. Photogrammetric Engineering & Remote Sensing. Vol. 62, pp. 1067-1074.

Zhang Y. (1999): A new merging method and its spectral and spatial effects. International Journal of Remote Sensing, Vol. 20, pp. 2003-2014.

Zhang Y. (2000): Problems in the Fusion of Commercial High-Resolution Satellite as well as Landsat 7 Images and Initial Solutions. ISPRS Journal of Photogrammetry and Remote Sensing

Internet sources

BGR (2006): Flyer Helicopter Project "Help Aceh" Indonesia
http://www.bgr.bund.de/cIn_006/nn_335066/DE/Themen/GG_Geophysik/Aerogeophysik/Downloads/flyer, 01.02.2006

CNES (2002): Instrument features. Spectral bands - Resolution - Swath
<http://spot5.cnes.fr/gb/satellite/satellite.htm>, 07. 2002

Google Map (2007):
<http://maps.google.de/>, 05.2007

NASA (2004): ASTER Characteristics.

<http://asterweb.jpl.nasa.gov/characteristics.asp>, 09. 07. 2004

SPOT IMAGE (2007): Technical Information. Processing levels and location accuracy. CNES, Toulouse, France

http://www.spotimage.fr/html/_167_224_555_234_.php, 01. 2007

SPOT IMAGE (2007): SPOT products & services. Price list. CNES, Toulouse, France

http://www.spotimage.fr/html/_167_171_172_173_.php, 01. 2007

CSA (2006): Components and Specification

<http://www.space.gc.ca/asc/eng/satellites/radarsat1/components.asp>, 11.09.2006

ESA (2007): Envisat: ASAR

<http://www.envisat.esa.int/instruments/asar/index.html>, 14.05.2007

Software index

Adobe Photoshop 7.0.1 Adobe Inc. 1990 – 2002

ENVI 4.3 ENVI Inc. 1999 - 2005

ERDAS Imagine 9.0 ERDAS Inc. 1991 - 2005

ESRI ArcGIS 9.0 ESRI Inc. 1999 – 2004

MapSource 6.0 GARMIN Inc. 1999 - 2004

SARScape 4.3 CREASO Inc. 1999 – 2007

12 Annex

12.1 Spectral signatures of the pixel-based approach (SPOT 5)

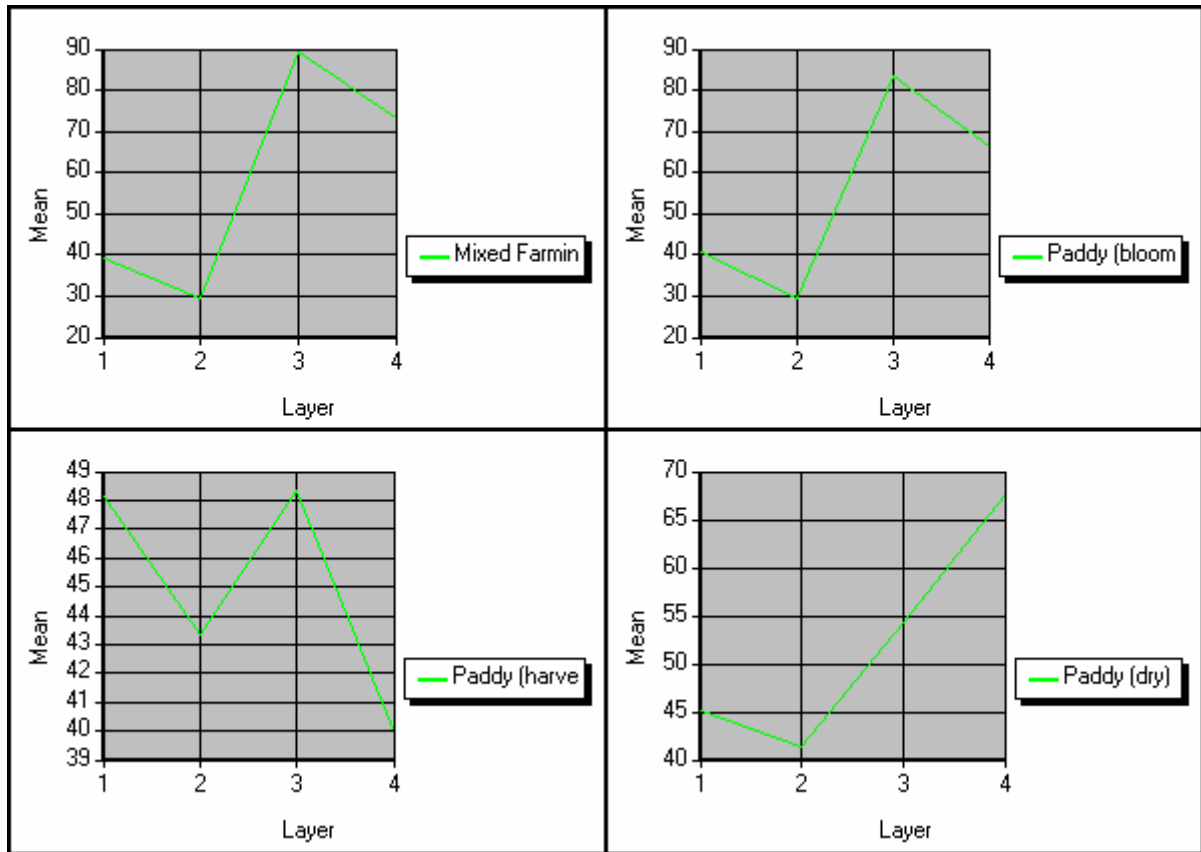


Figure 12.1: Spectral signatures of Mixed Farming, Paddy (bloomy), Paddy (harvested) and Paddy (dry)

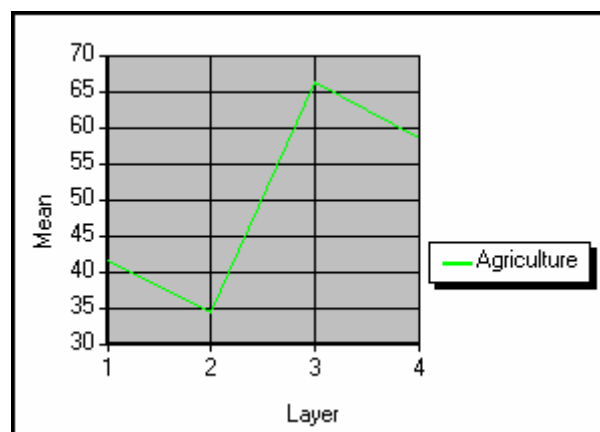


Figure 12.2: Spectral signature of the category Agriculture by merging of the signatures of the classes Mixed Farming, Paddy (bloomy), Paddy (harvested) and Paddy (dry)

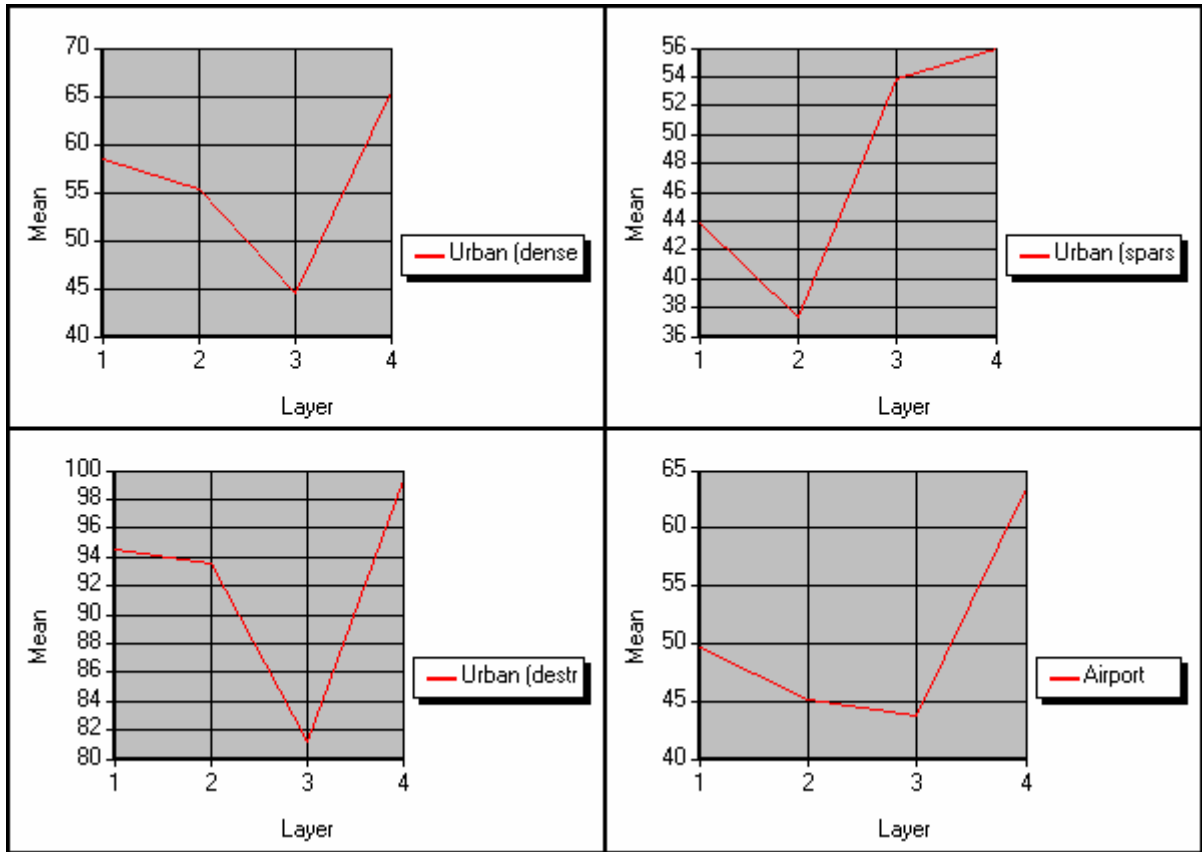


Figure 12.3: Spectral signatures of Urban (dense), Urban (sparse), Urban (destroyed) and Airport

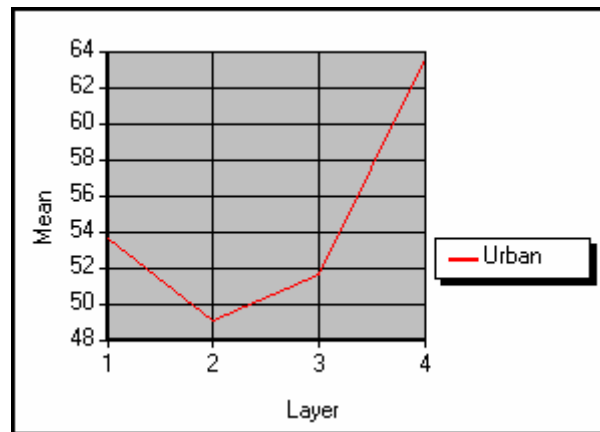


Figure 12.4: Spectral signature of the category Urban by merging of the signatures of the classes Urban (dense), Urban (sparse), Urban (destroyed) and Airport

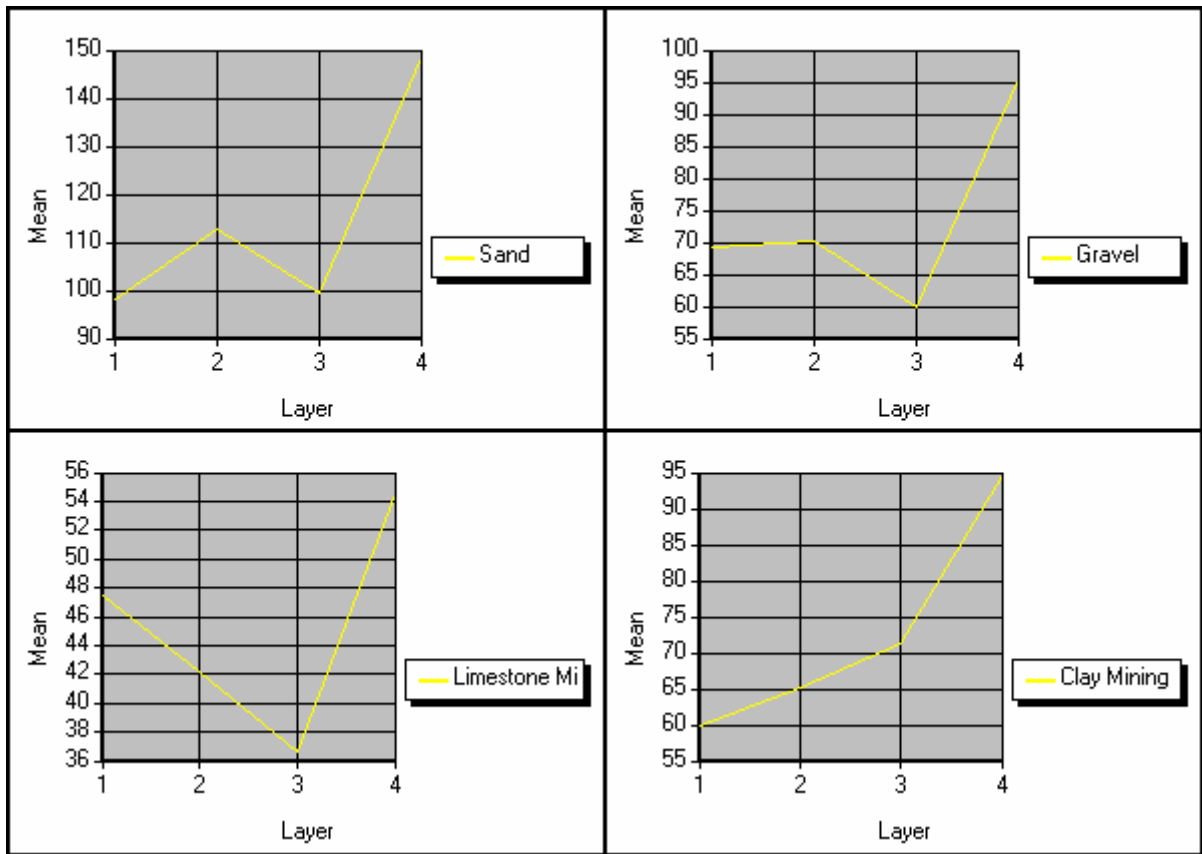


Figure 12.5: Spectral signatures of Sand, Gravel, Limestone Mining and Clay Mining

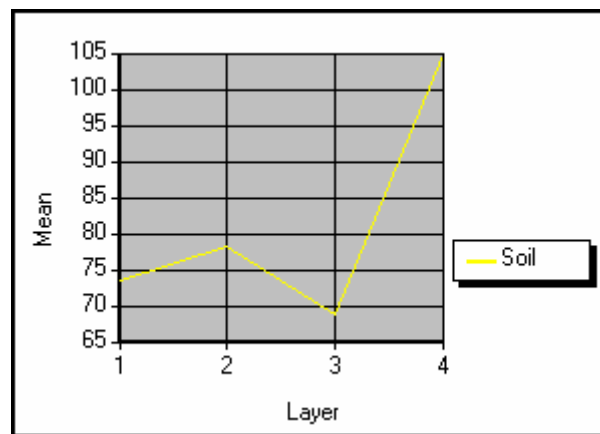


Figure 12.6: Spectral signature of the category Soil by merging of the single signatures of the classes Sand, Gravel, Limestone Mining and Clay Mining

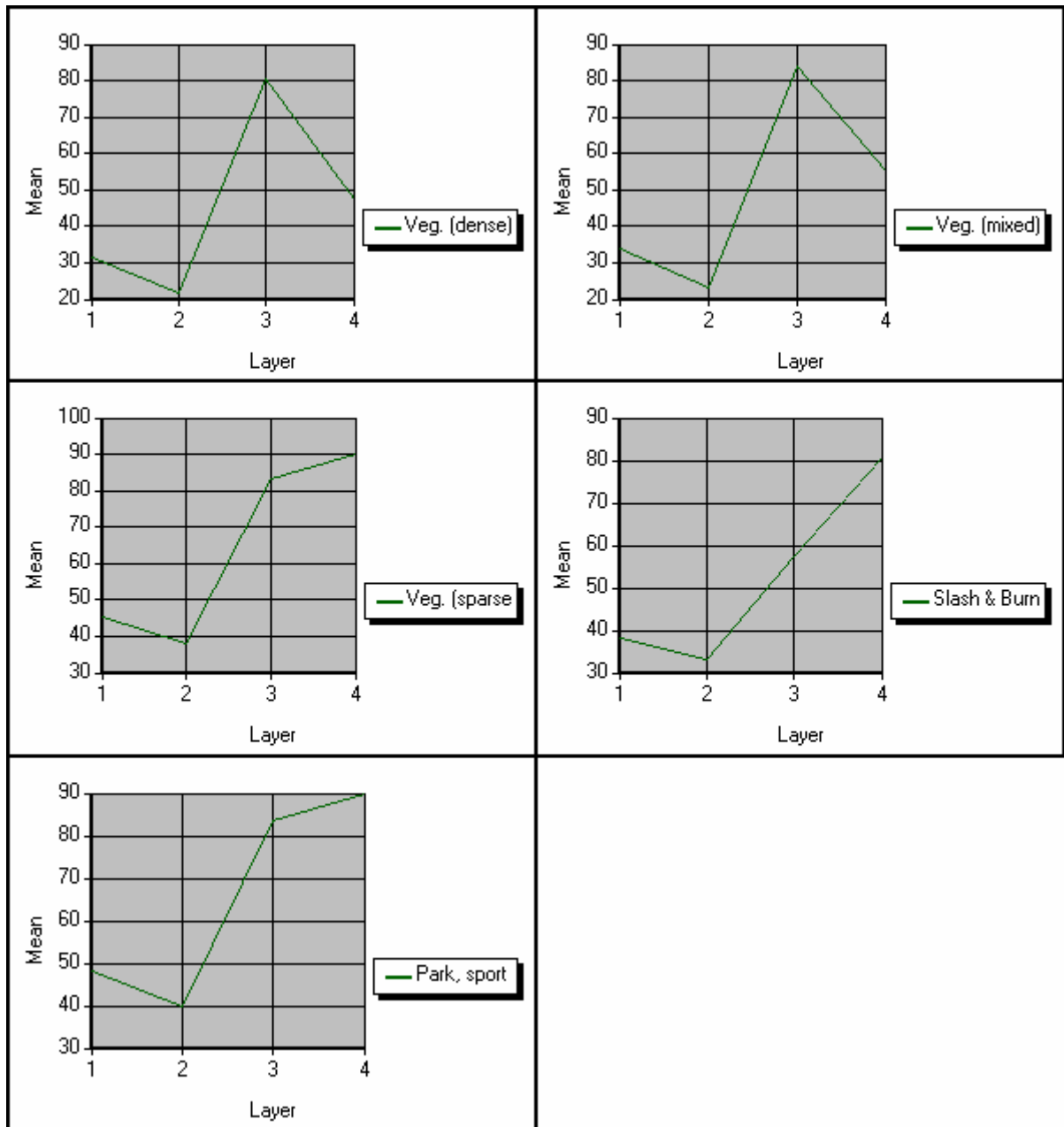


Figure 12.7: Spectral signatures of Vegetation (dense), (mixed) and (sparse), Slash and Burn, Park, sport field

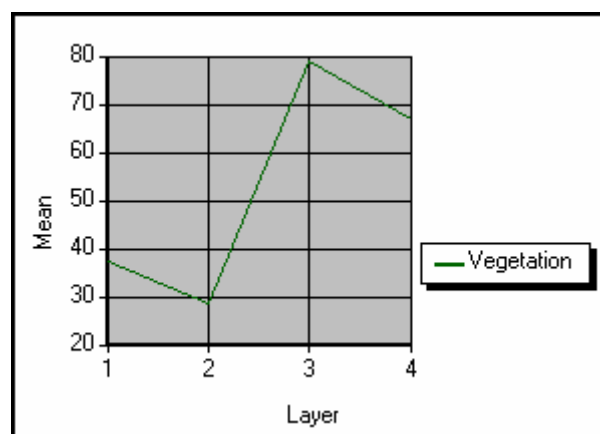


Figure 12.8: Spectral signatures of the category Vegetation by merging the signatures of the classes Vegetation (dense), (mixed) and (sparse), Slash and Burn and Park, sport field

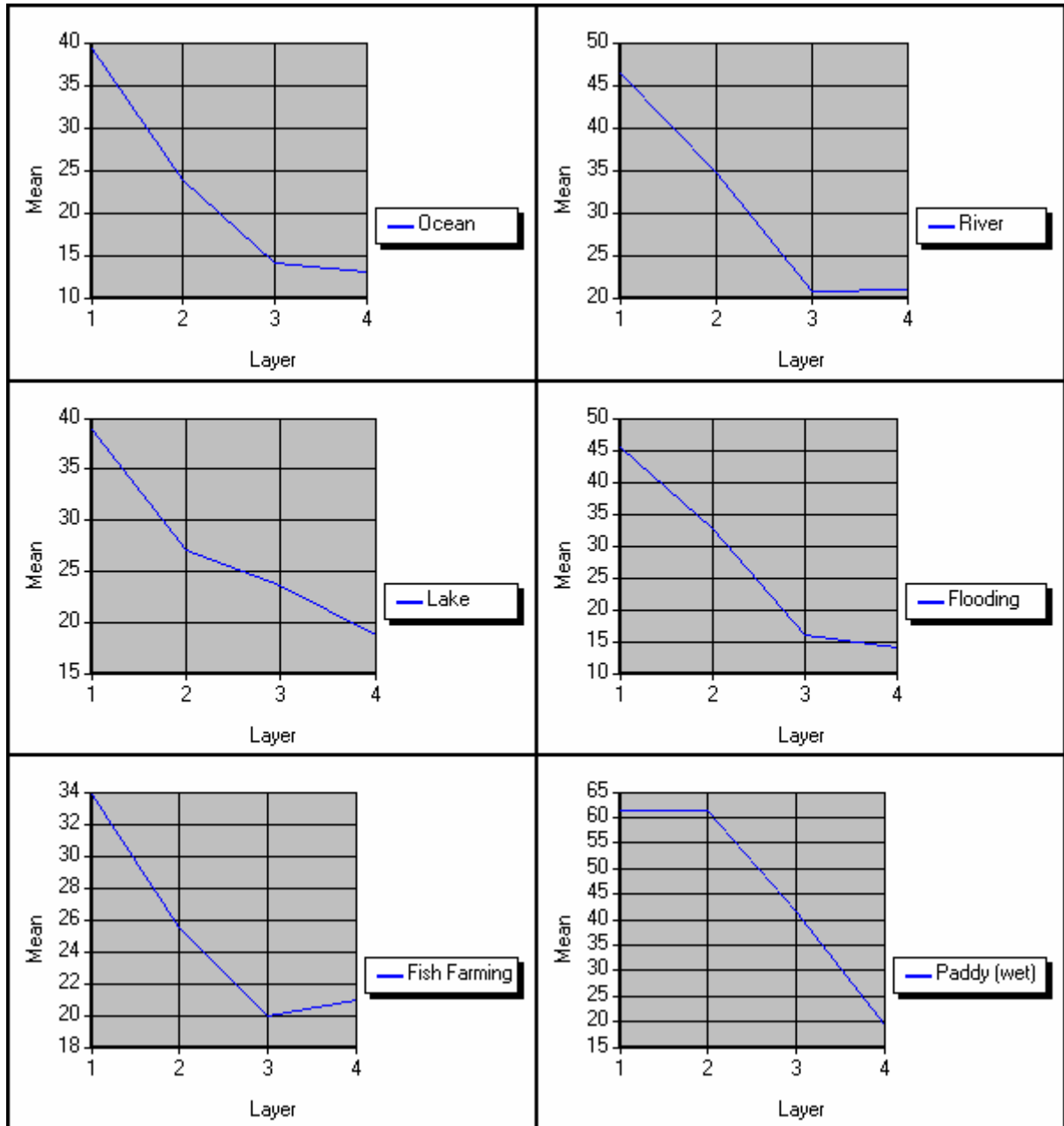


Figure 12.9: Spectral signatures of Ocean, River, Lake, Flooding, Fish Farming and Paddy (wet)

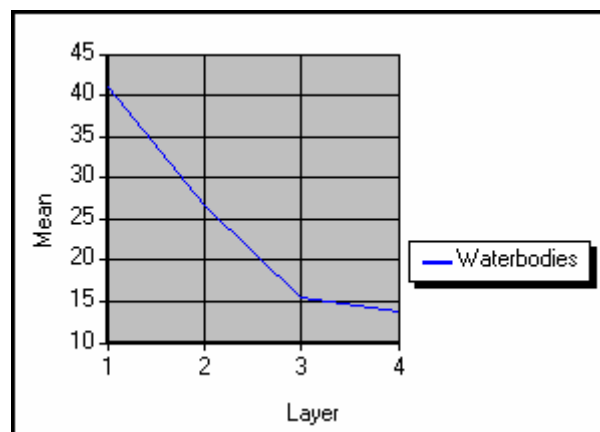


Figure 12.10: Spectral signatures of the category Waterbodies by merging the signatures of the classes Ocean, River, Lake, Flooding, Fish Farming and Paddy (wet)

12.2 Rules and criteria in the pixel-based approach

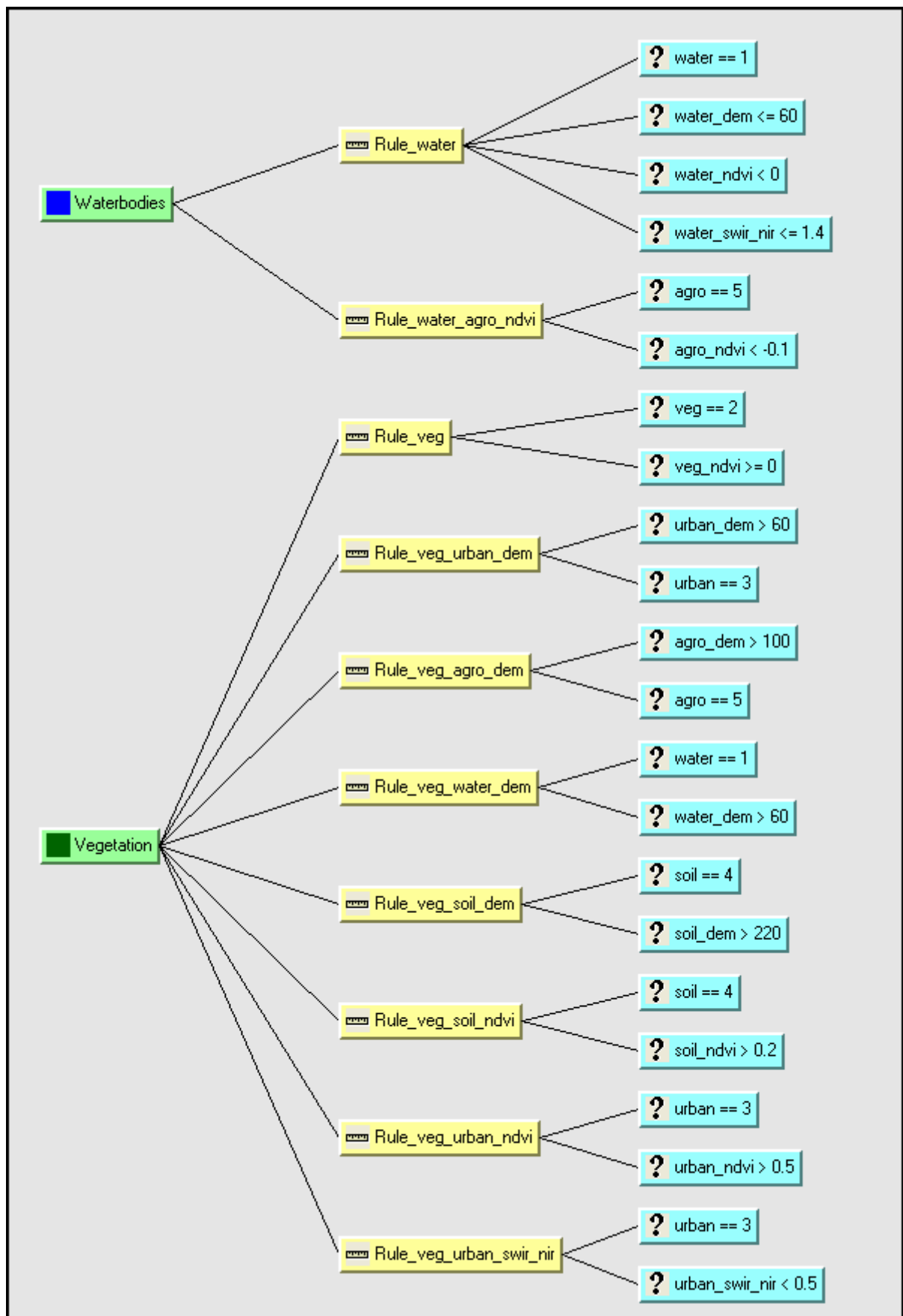


Figure 12.11: Knowledge-based rules of the pixel-based classification (categories: Waterbodies, Vegetation)

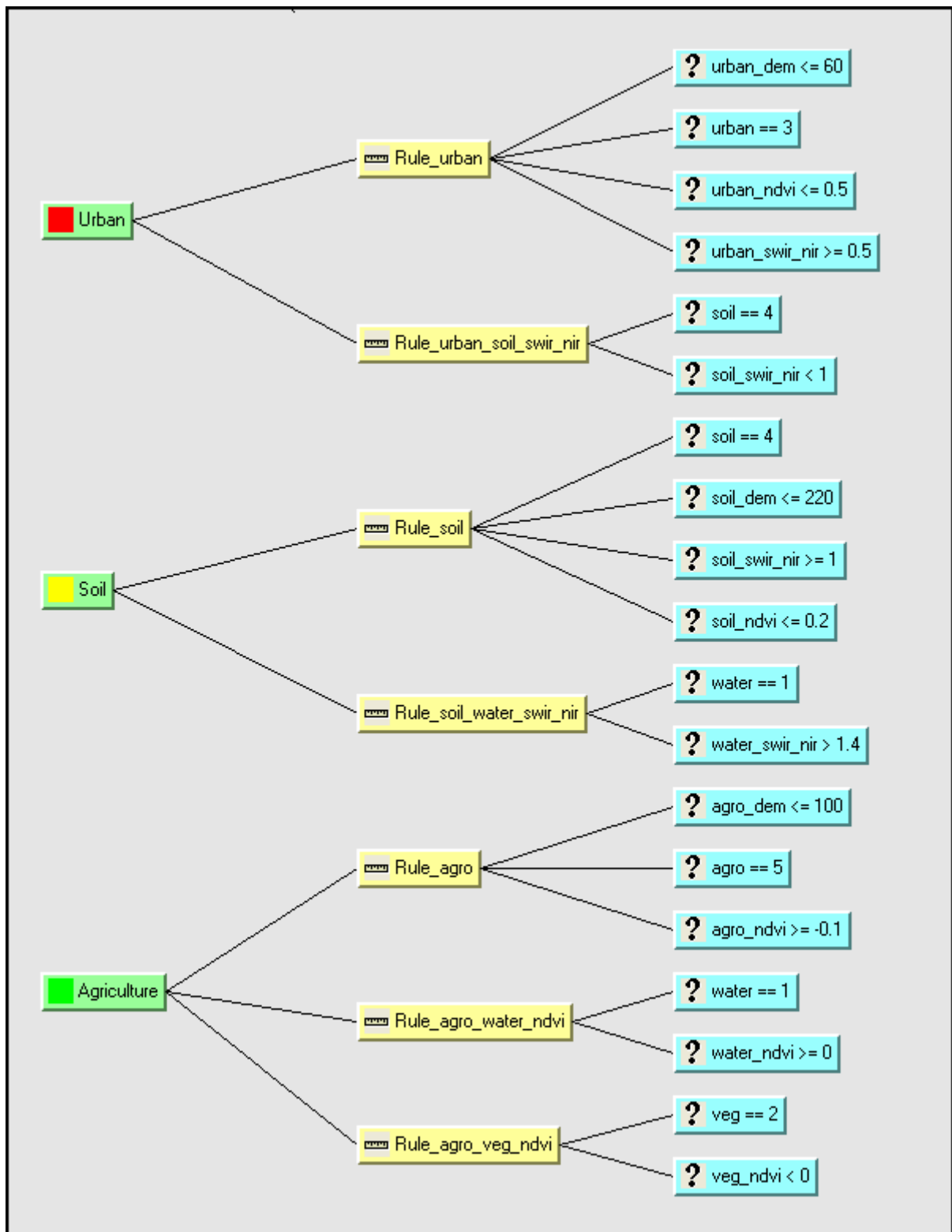


Figure 12.12: Knowledge-based rules of the pixel-based classification (categories: Urban, Soil, Agriculture)

12.3 Results of the pre-calculation for the IHS Transform

Dimension []	Radarsat	Band 1 [G]	Band 2 [R]	Band 3 [NIR]	Band 4 [SWIR]
Radarsat	1.00000	-0.01409	0.18106	0.56283	0.50420
Band 1 [G]	-0.01409	1.00000	0.93651	0.04394	0.27245
Band 2 [R]	0.18106	0.93651	1.00000	0.20941	0.45698
Band 3 [NIR]	0.56283	0.04394	0.20941	1.00000	0.82017
Band 4 [SWIR]	0.50420	0.27245	0.45698	0.82017	1.00000

Table 12.1: Correlation matrix (5x5) of the Radarsat band and the four multi-spectral bands of SPOT 5

Dimension []	Pan	Band 1 [G]	Band 2 [R]	Band 3 [NIR]	Band 4 [SWIR]
Pan	1.00000	0.97975	0.97799	0.14176	0.37339
Band 1 [G]	0.97975	1.00000	0.93651	0.04394	0.27245
Band 2 [R]	0.97799	0.93651	1.00000	0.20941	0.45698
Band 3 [NIR]	0.14176	0.04394	0.20941	1.00000	0.82017
Band 4 [SWIR]	0.37339	0.27245	0.45698	0.82017	1.00000

Table 12.2: Correlation matrix (5x5) of the panchromatic band and the four multi-spectral bands of SPOT 5

Dimension []	Pan	Intensity	Hue	Saturation
Pan	1	0.57867	0.02061	-0.67707
Intensity	0.57867	1	-0.62194	-0.27266
Hue	0.02061	-0.62194	1	0.16552
Saturation	-0.67707	-0.27266	0.16552	1

Table 12.3: Correlation matrix (4x4) of the Radarsat band and the three calculated IHS bands of SPOT 5 by using the first three bands (G, R, NIR)

Dimension []	Radarsat	Intensity	Hue	Saturation
Radarsat	1	0.47651	-0.61160	-0.25198
Intensity	0.47651	1	-0.62194	-0.27266
Hue	-0.61160	-0.62194	1	0.16552
Saturation	-0.25198	-0.27266	0.16552	1

Table 12.4: Correlation matrix (4x4) of the panchromatic band and the three calculated IHS bands of SPOT 5 by using the first three bands (G, R, NIR)

Dimension []	Pan	Intensity	Hue	Saturation
Pan	1	0.50444	-0.11187	-0.49632
Intensity	0.50444	1	-0.27299	0.20728
Hue	-0.11187	-0.27299	1	0.10252
Saturation	-0.49632	0.20728	0.10252	1

Table 12.5: Correlation matrix (4x4) of the Radarsat band and the three calculated IHS bands of SPOT 5 by using the last three bands (R, NIR, SWIR)

Dimension []	Radarsat	Intensity	Hue	Saturation
Radarsat	1	0.53168	-0.13835	0.18594
Intensity	0.53168	1	-0.27299	0.20728
Hue	-0.13835	-0.27299	1	0.10252
Saturation	0.18594	0.20728	0.10252	1

Table 12.6: Correlation matrix (4x4) of the panchromatic band and the three calculated IHS bands of SPOT 5 by using the last three bands (R, NIR, SWIR)

12.4 Results of the PCA Transform (SPOT, Radarsat)

Dimension []	Radarsat	1. PC	2. PC	3. PC	4. PC
Radarsat	1.00000	0.55885	0.09889	0.03483	-0.31690
1. PC	0.55885	1	2.074e-009	-2.998e-009	-3.359e-009
2. PC	0.09889	2.074e-009	1	4.915e-009	3.567e-009
3. PC	0.03483	-2.998e-009	4.915e-009	1	-3.430e-010
4. PC	-0.31690	-3.359e-009	3.567e-009	-3.430e-010	1

Table 12.7: Correlation matrix (5x5) of the Radarsat band and the four principal components by using the four multi-spectral bands of SPOT 5

Dimension []	Pan	1. PC	2. PC	3. PC	4. PC
Pan	1.00000	0.32037	-0.90781	0.24961	0.03087
1. PC	0.32037	1	2.074e-009	-2.998e-009	-3.359e-009
2. PC	-0.90781	2.074e-009	1	4.915e-009	3.567e-009
3. PC	0.24961	-2.998e-009	4.915e-009	1	-3.430e-010
4. PC	0.03087	-3.359e-009	3.567e-009	-3.430e-010	1

Table 12.8: Correlation matrix (5x5) of the panchromatic band and the four principal components by using the four multi-spectral bands of SPOT 5

Dimension []	1. PC	2. PC	3. PC	4. PC
1. PC	0.06568	-0.58827	0.31403	0.74229
2. PC	0.14423	-0.67973	0.27103	-0.66612
3. PC	0.73892	0.37927	0.55692	-0.00042
4. PC	0.65489	-0.21923	-0.71956	0.07273

Table 12.9: Eigen Matrix (4x4) of the 4 principal components by using all four multi-spectral bands of SPOT 5

	Eigenvalues []
1. PC	1285.04185
2. PC	289.17520
3. PC	87.94601
4. PC	6.12269

Table 12.10: Eigenvalues vector of the principal components by using all four multi-spectral bands of SPOT 5

12.5 Results of the PCA Transform (ASTER, Envisat)

Dimension []	Envisat	1. PC	2. PC	3. PC	4. PC	5. PC	6. PC
Envisat	1	0,22225	0,07465	-0,17632	-0,15149	-0,03214	0,18984
1. PC	0,22225	1	6,65E+08	-0,00013	-2,32E+10	-0,00020	-2,22E+10
2. PC	0,07465	6,65E+08	1	-9,29E+10	9,71E+09	-9,16E+10	-3,65E+10
3. PC	-0,17632	-0,00013	-9,29E+10	1	2,37E+10	0,00017	2,42E+10
4. PC	-0,15149	-2,32E+10	9,71E+09	2,37E+10	1	0,00023	-3,05E+10
5. PC	-0,03213	-0,00020	-9,16E+10	0,00017	0,00023	1	0,00020
6. PC	0,18984	-2,22E+10	-3,65E+10	2,42E+10	-3,05E+10	0,00020	1

Table 12.11: Correlation matrix (7x7) of the Envisat band and the six principal components by using the six multi-spectral bands of ASTER

Dimension []	1. PC	2. PC	3. PC	4. PC	5. PC	6. PC
1. PC	0,37680	-0,55112	0,14387	-0,20861	-0,69998	-0,00974
2. PC	0,42432	-0,53750	-0,00199	-0,15244	0,69858	-0,14071
3. PC	0,55844	0,56975	0,50763	-0,31207	0,04827	0,07820
4. PC	0,55145	0,23319	-0,50314	0,48005	-0,12799	-0,37622
5. PC	0,24824	-0,05712	-0,18664	0,27113	0,04680	0,90807
6. PC	0,01984	0,15844	-0,65850	-0,72932	-0,03330	0,08867

Table 12.12: Eigen Matrix (6x6) of the six principal components by using all six multi-spectral bands of ASTER

	Eigenvalues []
1. PC	2480.32925
2. PC	729.19655
3. PC	80.22828
4. PC	41.00730
5. PC	15.27769
6. PC	4.04288

Table 12.13: Eigenvalues vector of the principal components by using all four multi-spectral bands of SPOT 5

12.6 Results of the pixel-based classification approach

Pixel-based classification result of the optical SPOT 5 data (Supervised classification)

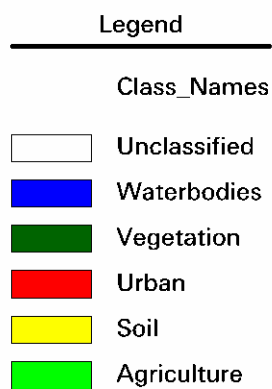
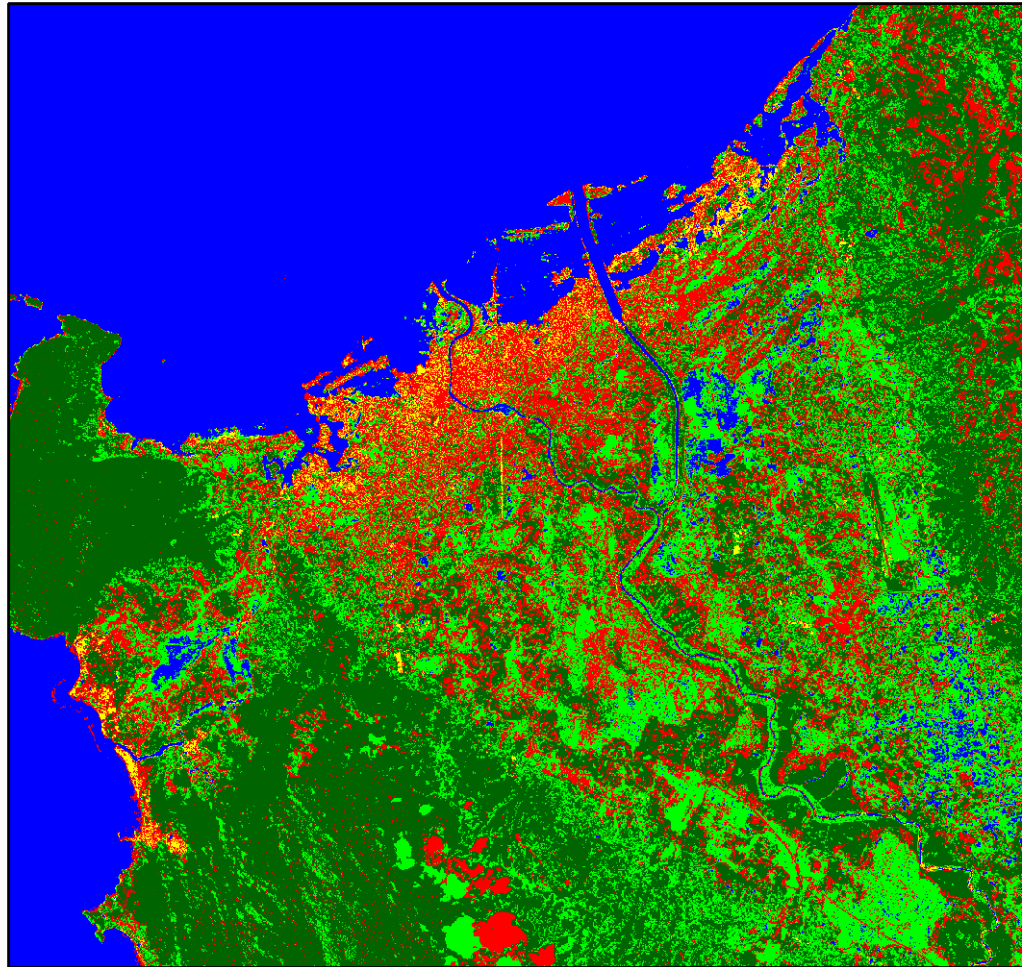


Figure 12.13: Pixel-based classification result of the optical SPOT 5 data by using the supervised classification

Pixel-based classification result of the optical SPOT 5 data (Supervised and knowledge-based classification)

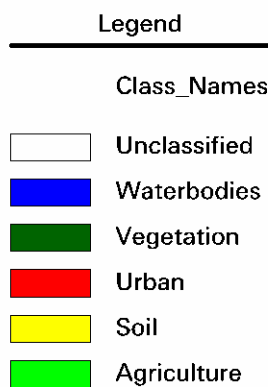
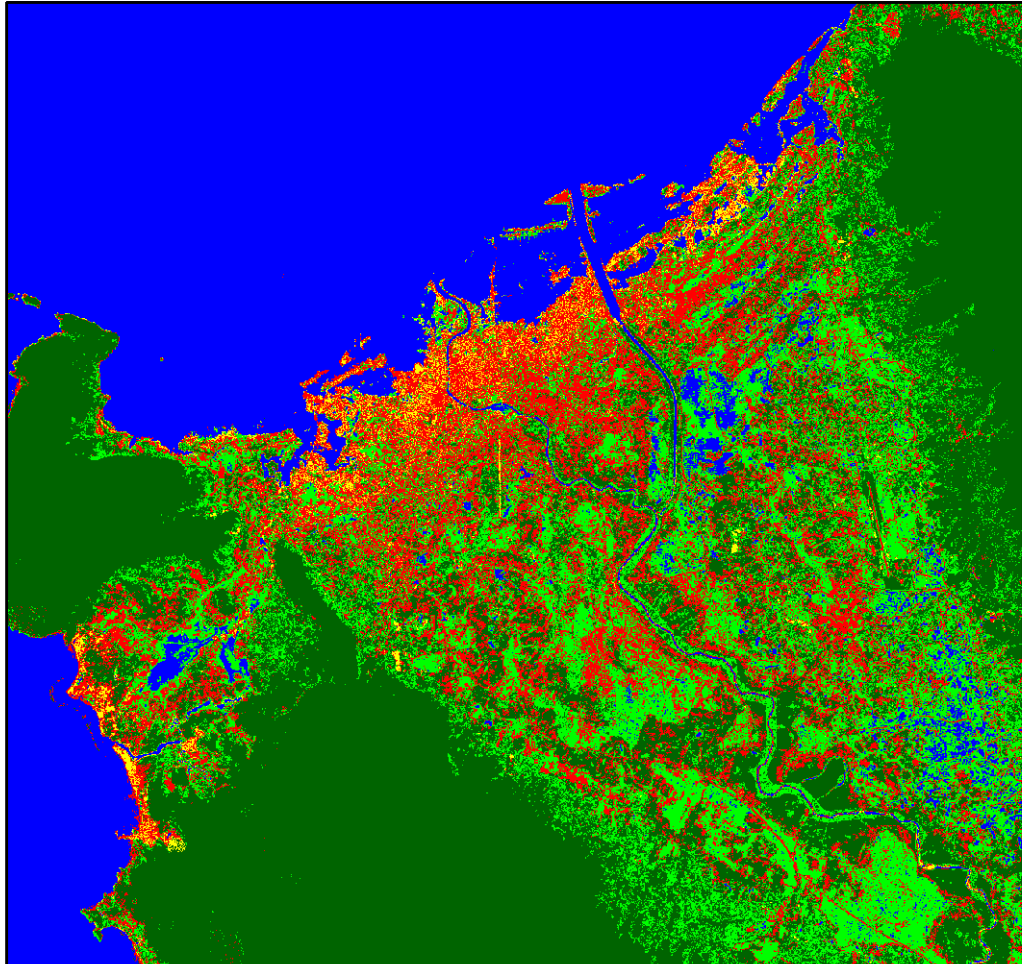


Figure 12.14: Pixel-based classification result of the optical SPOT 5 data by using supervised and knowledge-based classification

Pixel-based classification result of the Multiplicative method (Supervised and knowledge-based classification)

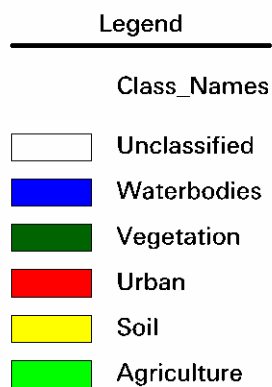
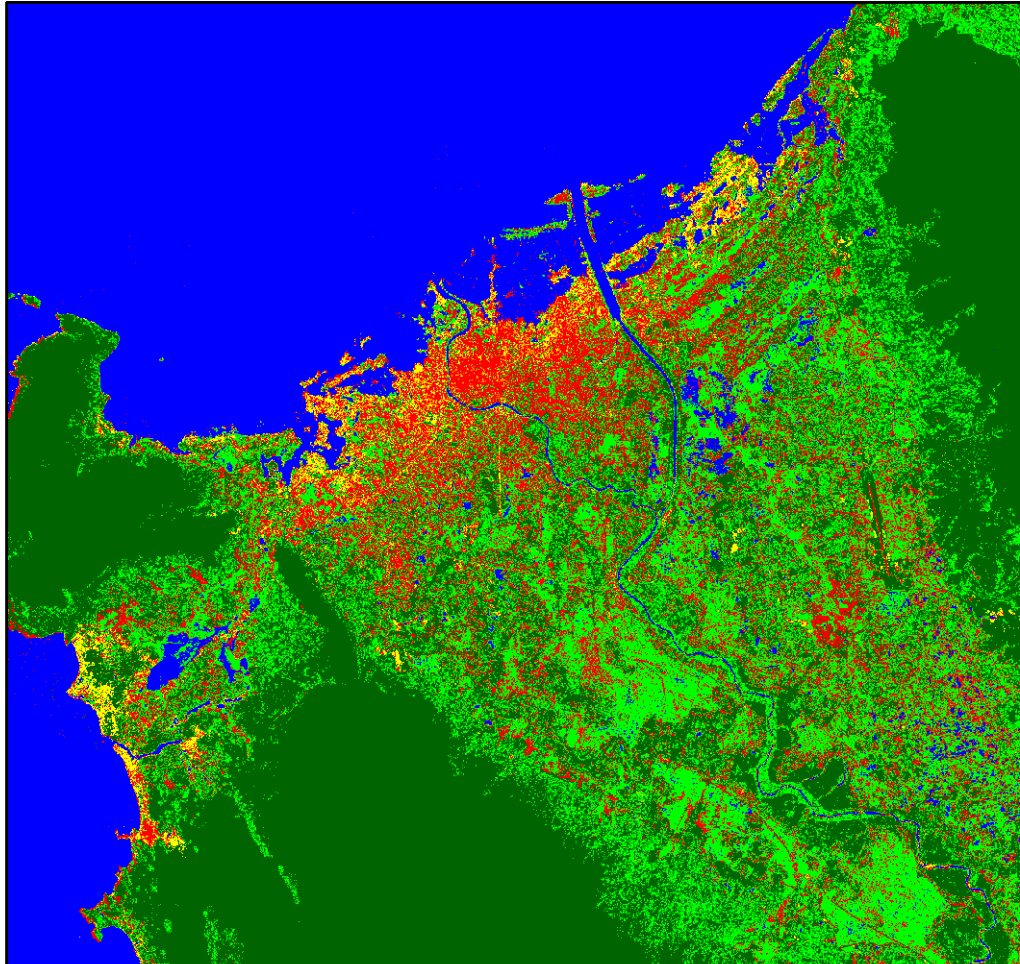


Figure 12.15: Pixel-based classification result of the Multiplicative method by using supervised and knowledge-based classification

Pixel-based classification result of the PCA Transform

(Supervised and knowledge-based classification)

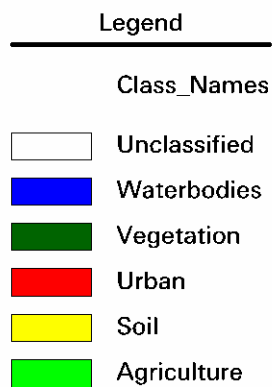
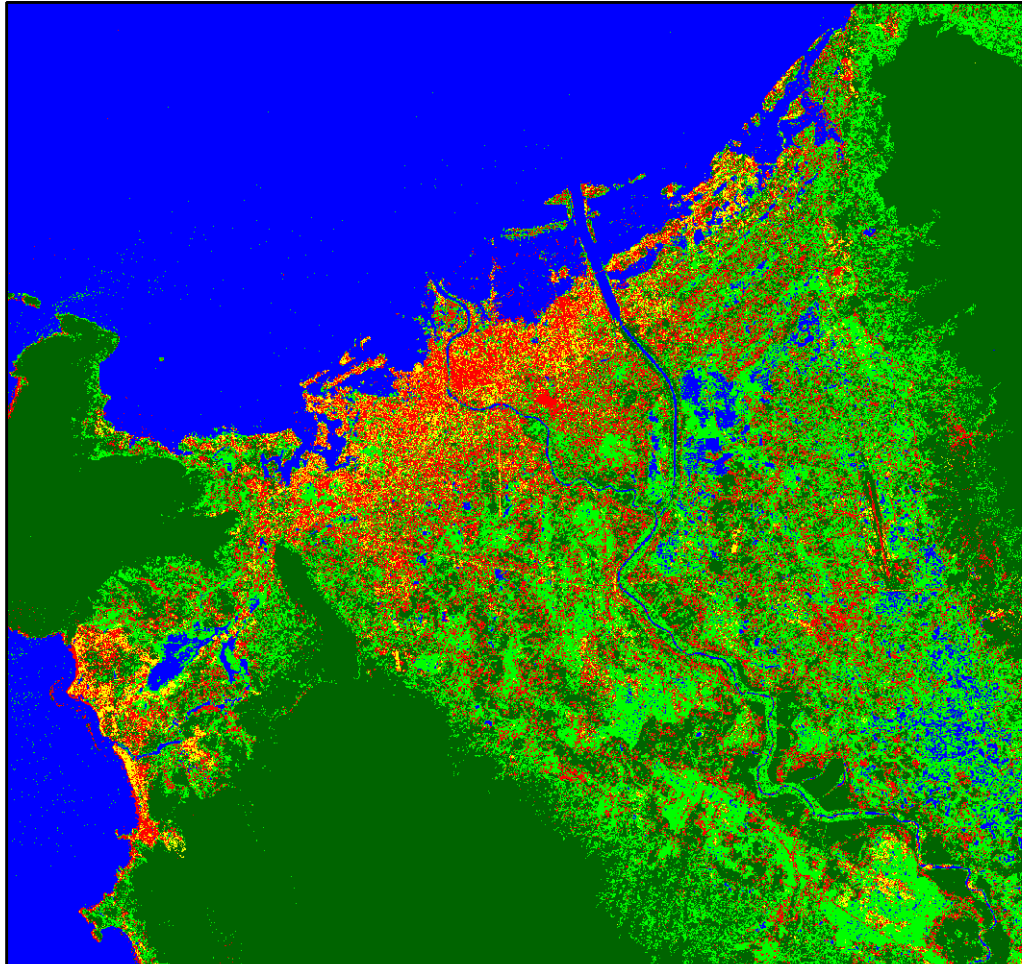
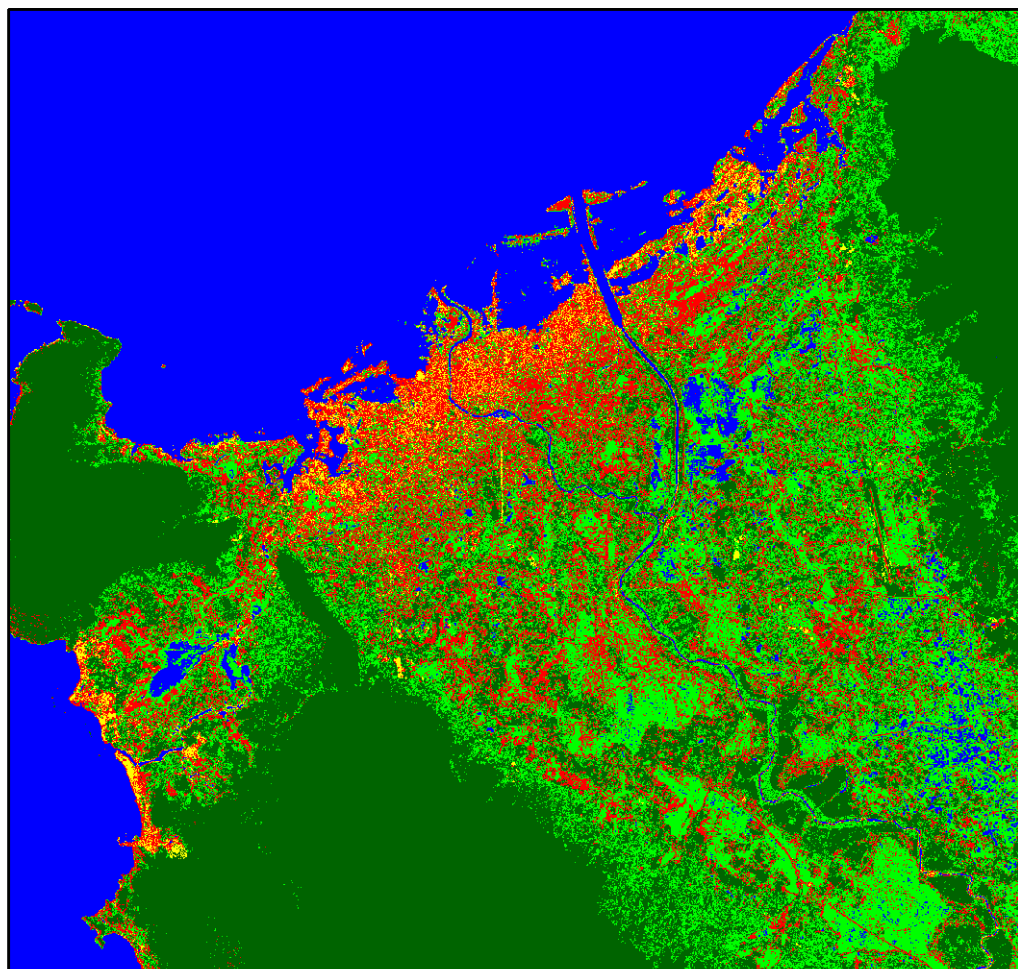


Figure 12.16: Pixel-based classification result of the PCA Transform by using supervised and knowledge-based classification

Pixel-based classification result of the Ehlers Fusion

(Supervised and knowledge-based classification)

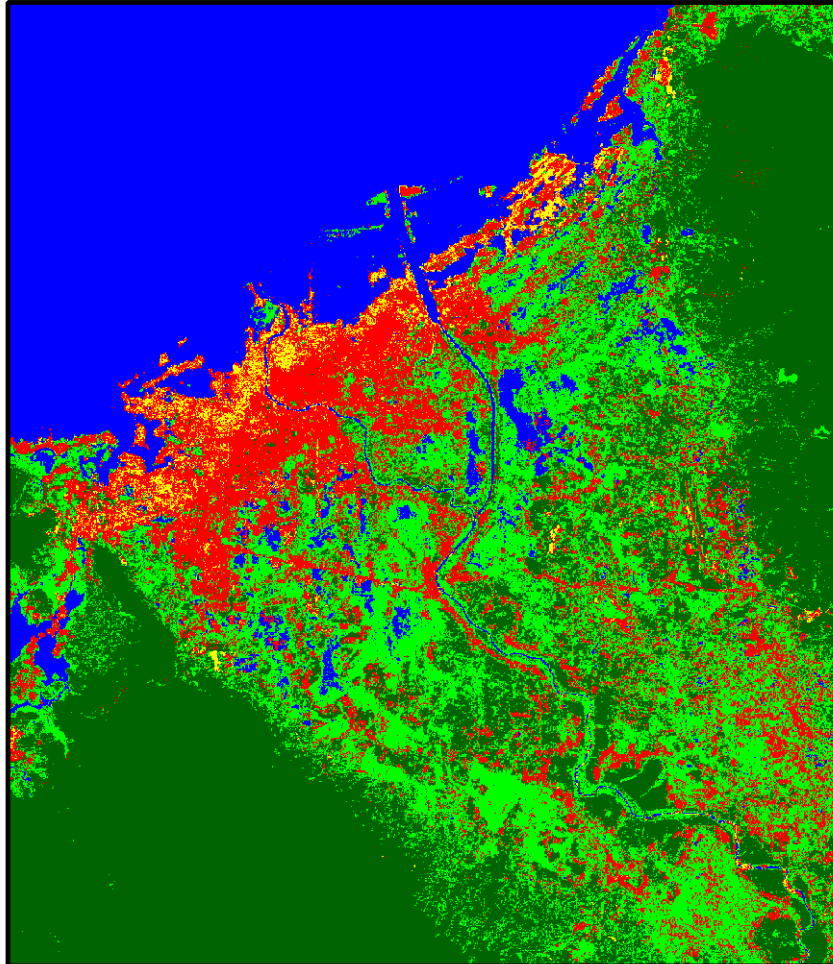


Legend

Class_Names	
	Unclassified
	Waterbodies
	Vegetation
	Urban
	Soil
	Agriculture

Figure 12.17: Pixel-based classification result of the Ehlers Fusion by using supervised and knowledge-based classification

Pixel-based classification result of the optical ASTER data (Supervised and knowledge-based classification)



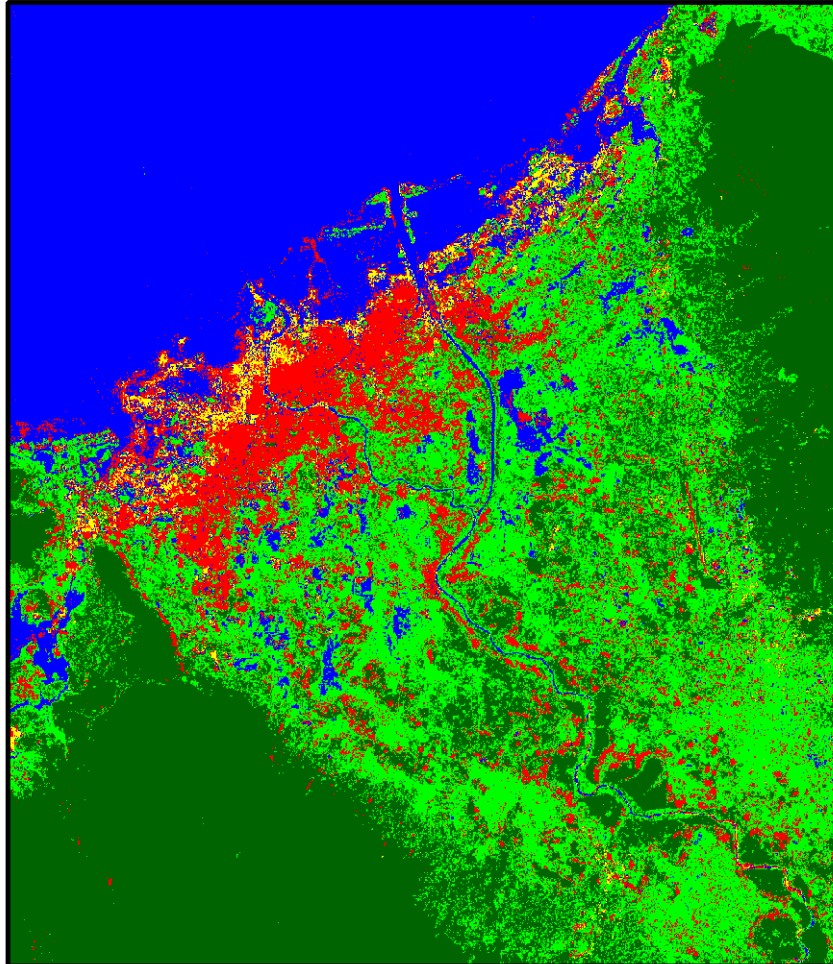
Legend

Class_Names	
	Unclassified
	Waterbodies
	Vegetation
	Urban
	Soil
	Agriculture

Figure 12.18: Pixel-based classification result of the optical ASTER data by using supervised and knowledge-based classification

Pixel-based classification result of the PCA Transform

(Supervised and knowledge-based classification)



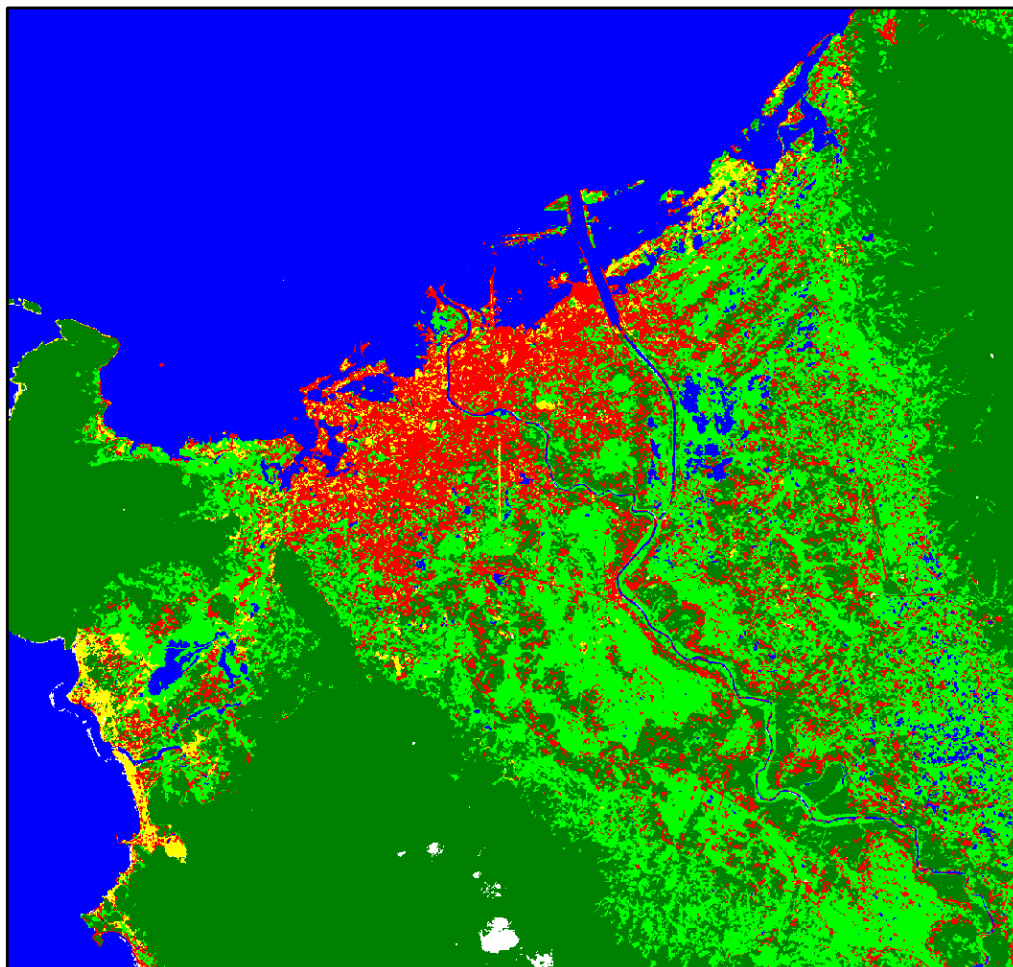
Legend

Class_Names	
	Unclassified
	Waterbodies
	Vegetation
	Urban
	Soil
	Agriculture

Figure 12.19: Pixel-based classification result of the PCA Transform by using supervised and knowledge-based classification

12.7 Results of the object-based classification approach

Object-based classification result of the optical SPOT 5 data (Supervised classification)

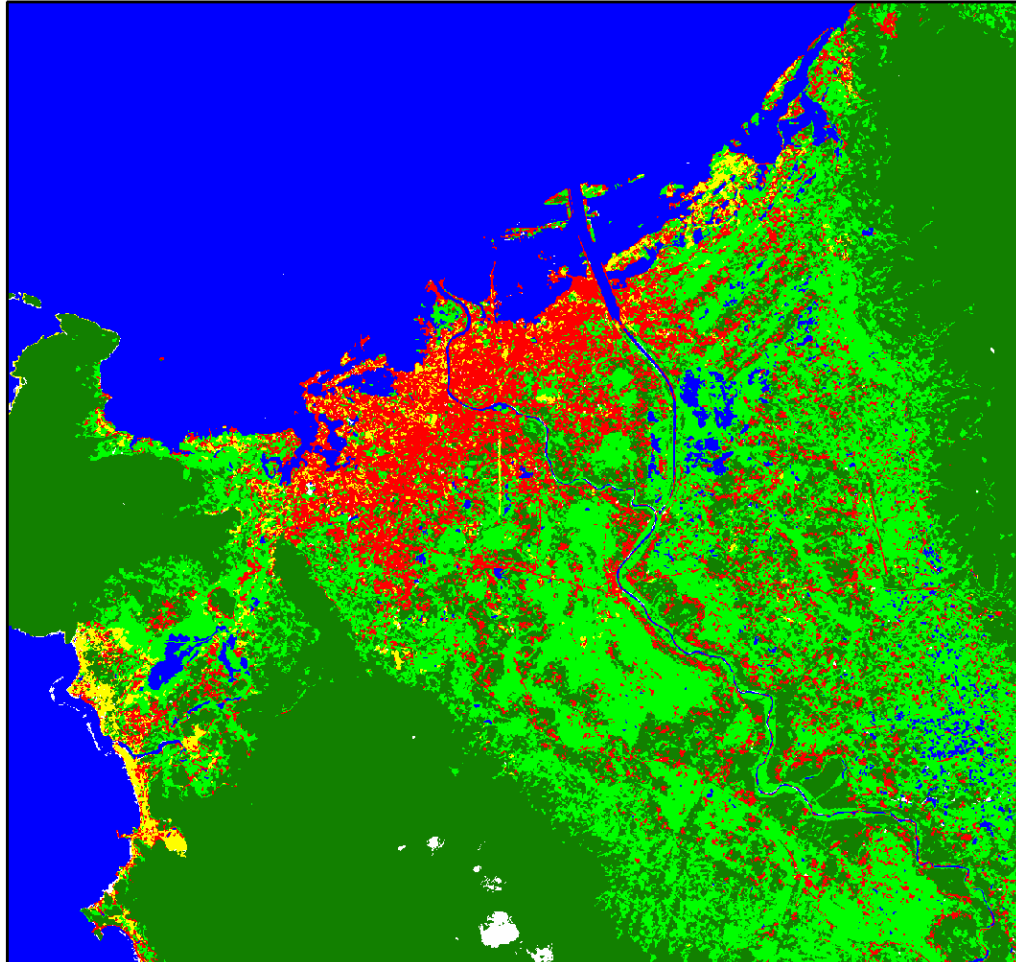


Legend

Class_Names	
	Unclassified
	Waterbodies
	Vegetation
	Urban
	Soil
	Agriculture

Figure 12.20: Object-based classification result of the optical SPOT 5 data by using the supervised classification

Object-based classification result of the optical SPOT 5 data (Supervised and knowledge-based classification)



Legend

Class_Names	
	Unclassified
	Waterbodies
	Vegetation
	Urban
	Soil
	Agriculture

Figure 12.21: Object-based classification result of the SPOT 5 data by using supervised and knowledge-based classification

Object-based classification result of optical SPOT 5 and Radarsat data (Supervised and knowledge-based classification by using additional texture features for all categories)

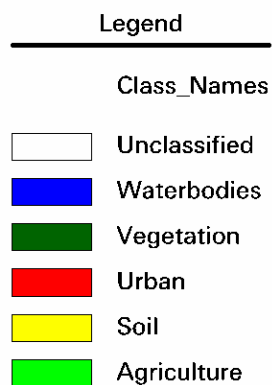
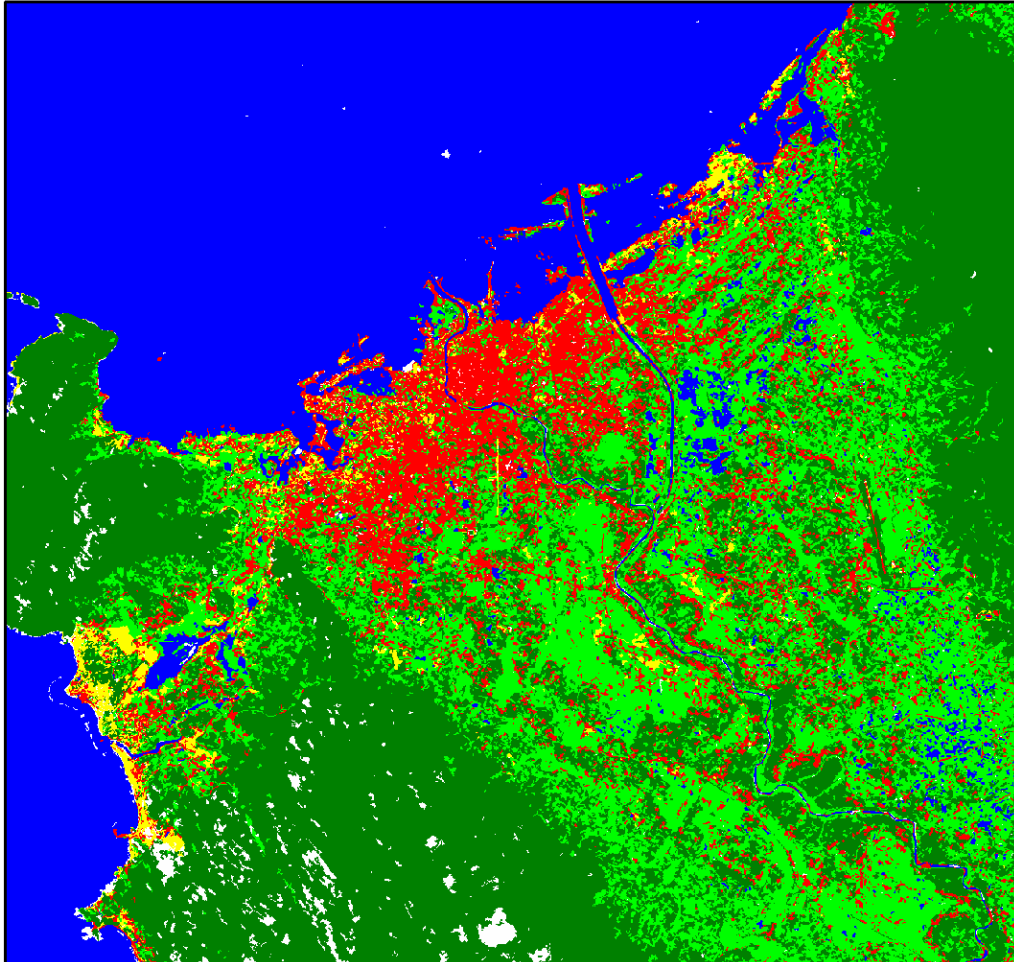
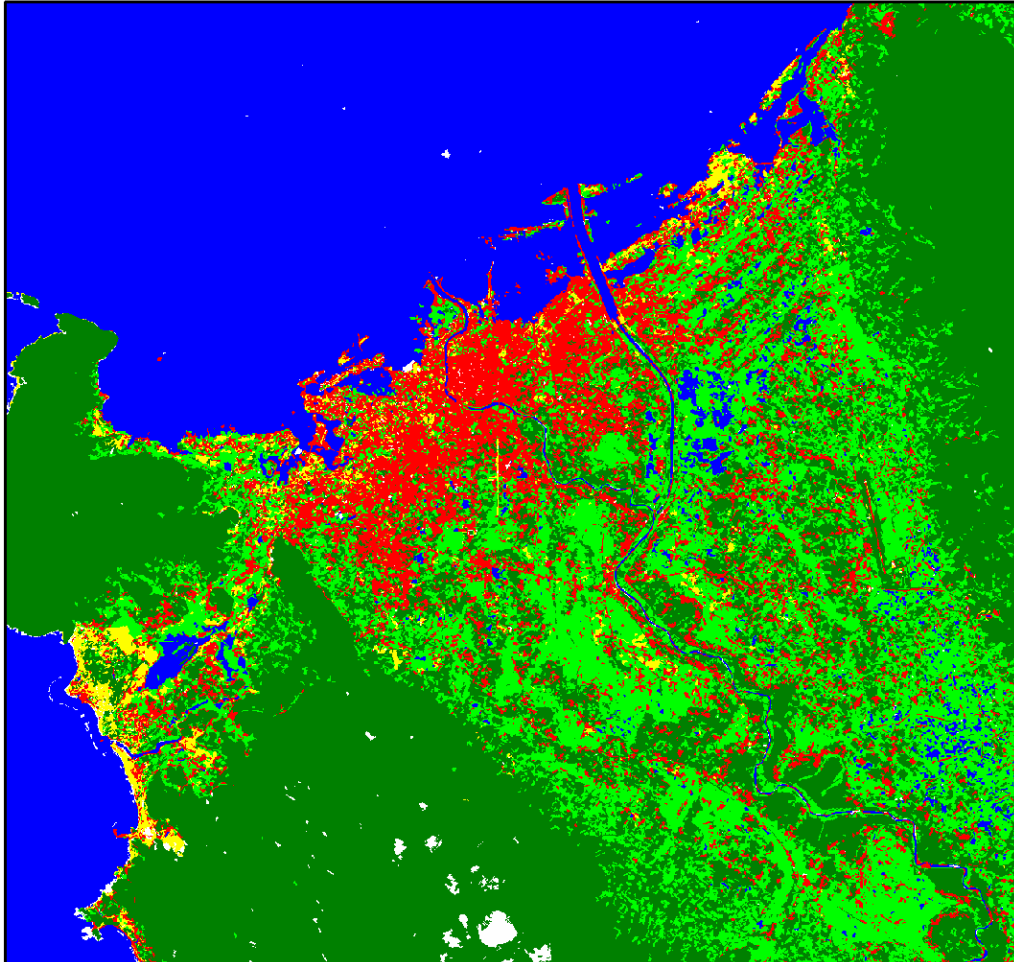


Figure 12.22: Object-based classification result of the SPOT 5 and Radarsat data by using supervised and knowledge-based classification with additional texture features

Object-based classification result of optical SPOT 5 and Radarsat data

(Supervised and knowledge-based classification
by using additional texture features without Vegetation)



Legend

Class_Names	
	Unclassified
	Waterbodies
	Vegetation
	Urban
	Soil
	Agriculture

Figure 12.23: Object-based classification result of the SPOT 5 and Radarsat data by using supervised and knowledge-based classification with additional texture features without the category vegetation

Object-based classification result of optical SPOT 5 and Radarsat data (Supervised and knowledge-based classification by using local knowledge-based radar features)

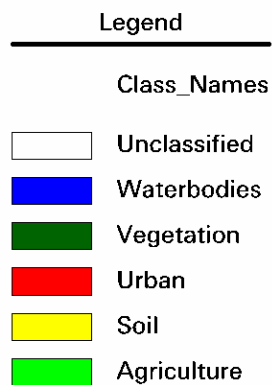
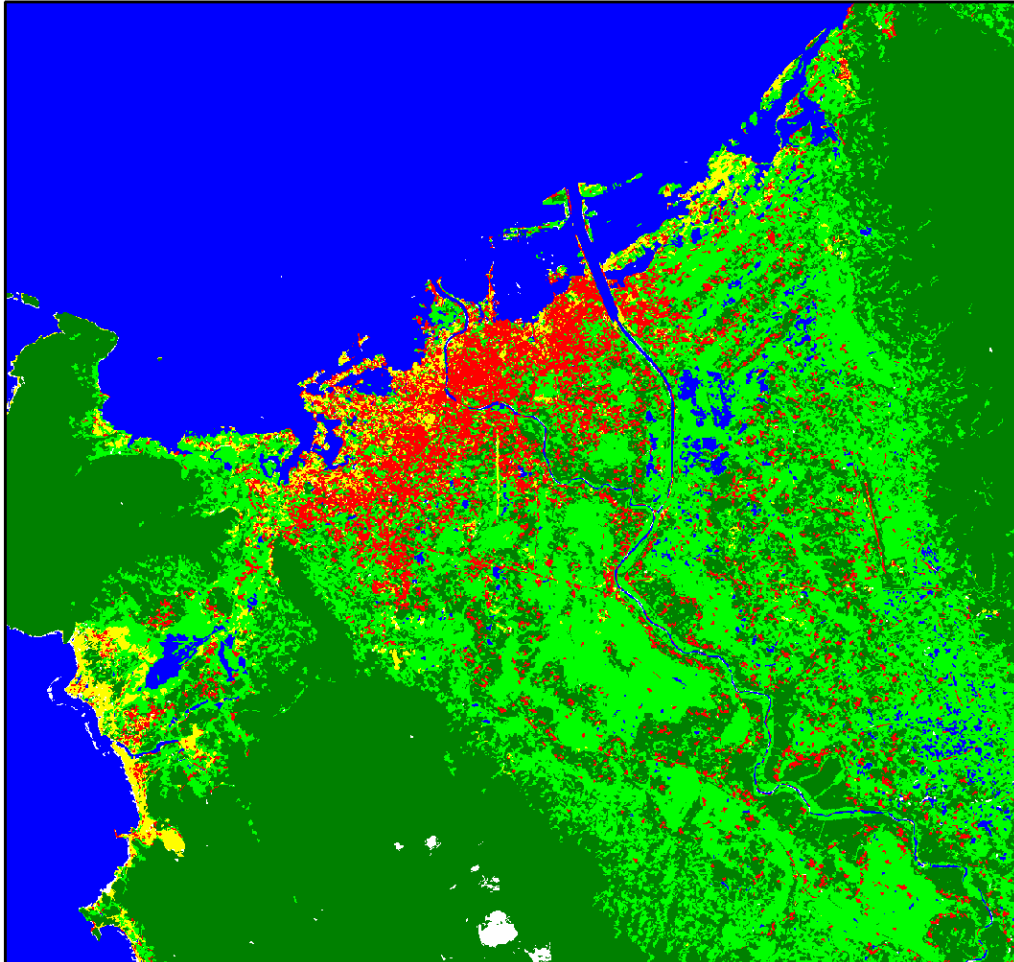


Figure 12.24: Object-based classification result of the SPOT 5 and Radarsat data by using supervised and knowledge-based classification with additional local radar features in case of the categories Waterbodies, Soil and Urban

Object-based classification result of the optical ASTER data (Supervised and knowledge-based classification)

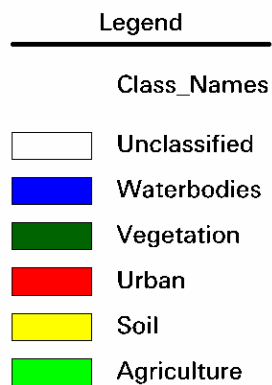
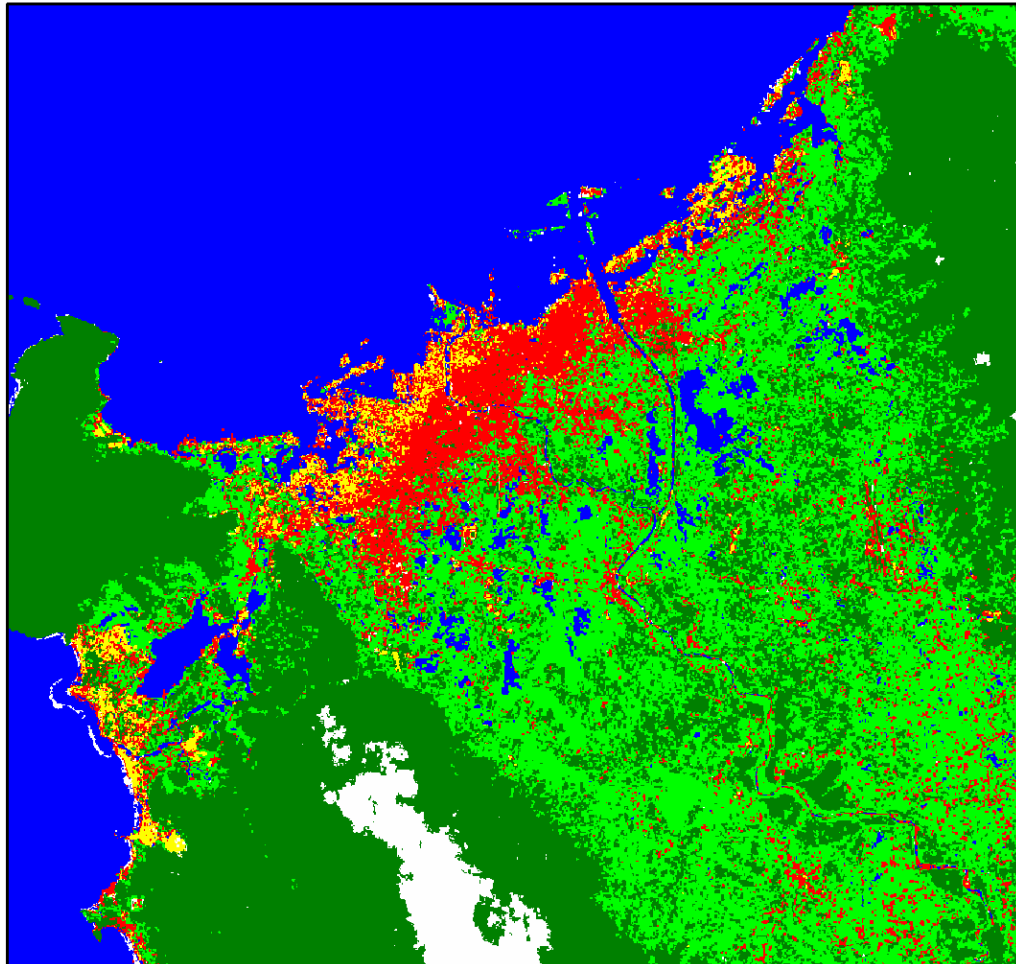


Figure 12.25: Object-based classification result of the ASTER data by using supervised and knowledge-based classification

Object-based classification result of optical ASTER and Envisat data (Supervised and knowledge-based classification by using additional texture features without Vegetation)

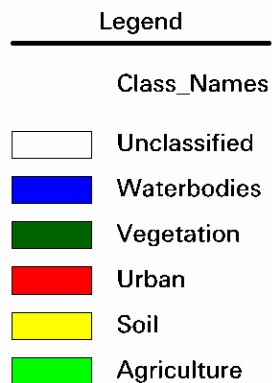
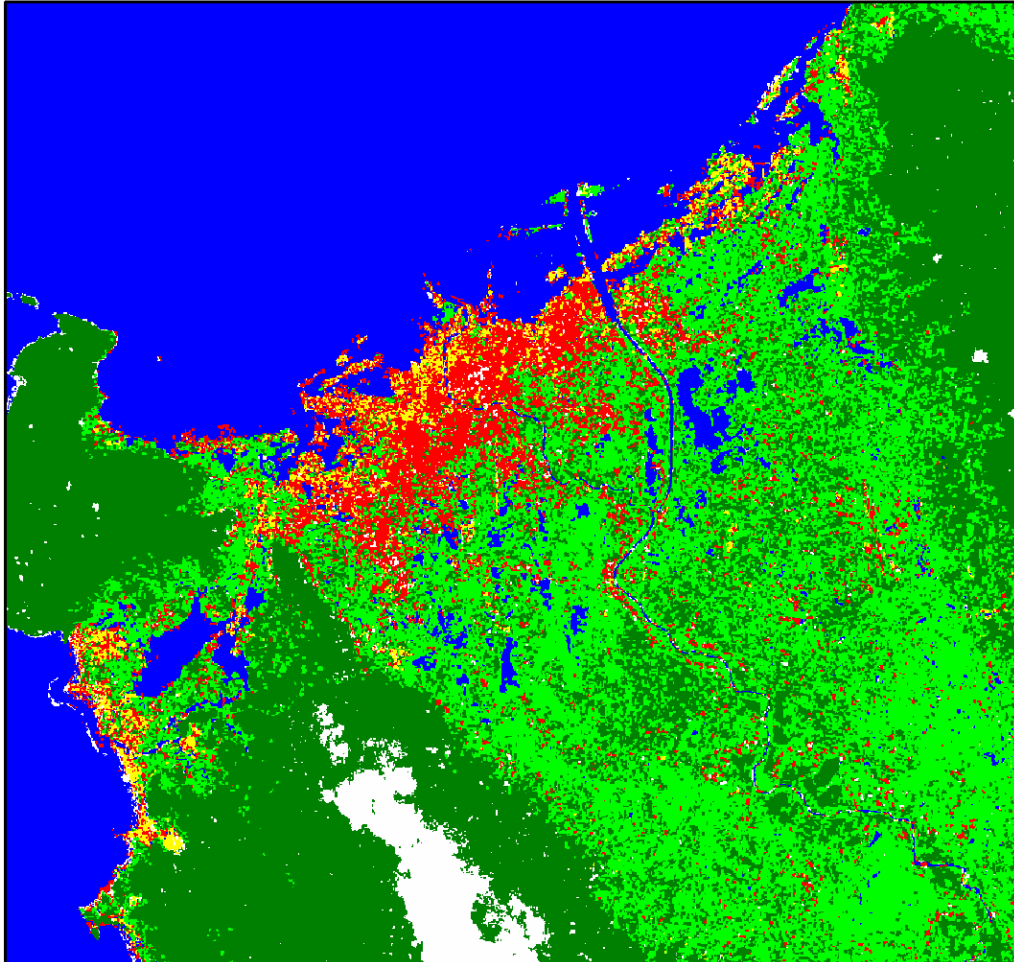


Figure 12.26: Object-based classification result of the ASTER and Envisat data by using supervised and knowledge-based classification with additional texture features without the category vegetation and the class Ocean

12.8 Knowledge-based rules of the object-based classification

Classes (sorted spectrally)	Layer information				Shape information					
	DEM [m]	Slope [°]	Ratio NDVI []	Ratio SWIR/NIR []	Asym. []	Distance to X left border [Pixel]	Distance to Y bottom border [Pixel]	Distance to border [Pixel]	Distance to Ocean [Pixel]	Distance to Urban [Pixel]
Agriculture	< 100		-0.1 < X < 1							
Mixed Farm.	< 100		0 < X < 1			> 330				
Paddy (other)	< 60	< 2	-0.1 < X < 1			> 330				
Soil	< 220		< 0.2	> 1						
Gravel	< 15		< 0.2	> 1					400	
Sand	< 60		< 0.2	> 1						
Limestone	< 220		< 0.2	> 1		< 4000	< 3500			
Urban	< 60		< 0.5	> 0.8						
Urb. (dense)	< 25		< 0.1	> 1		1450 < X < 3650	1900 < Y < 3650			
Urb. (sparse)	< 60		< 0.5	> 0.8		> 330				
Urb. (destr.)	< 15		< 0.1	> 0.8		> 330			400	
Airport	15 < X < 25	< 2	-0.1 < X < 0.2	> 1		4500 < X < 4720	2000 < Y < 2600			
Vegetation			> 0							
Veg. (dense)			> 0	< 0.65						
Veg. (mixed)			> 0	0.65 < X < 0.9						
Veg. (sparse)			> 0	0.9 < X < 1.1						
Slash & Burn	> 20		> 0	> 1.1						
Park, sport	< 25		> 0			> 330				50
Waterbodies	< 60		< 0	0 < X < 1.4						
Ocean	< 10		< 0	0 < X < 1.4		< 4500		1800		
River	< 60		< 0	0 < X < 1.4	0 < X < 1	> 570				
Flooding	< 10		< 0	0 < X < 1.4		< 4500			400	
Paddy (wet)	< 60	< 2	< 0	0 < X < 1.4		> 330				

Table 12.14: Knowledge-based rules of the object-based classification by using the first data set (SPOT 5 and Radarsat, Pixel size: 5 m)

Classes (sorted spectrally)	Layer information				Shape information					
	DEM [m]	Slope [°]	Ratio NDVI []	Ratio SWIR/NIR []	Asym. []	Distance to X left border [Pixel]	Distance to Y bottom border [Pixel]	Distance to border [Pixel]	Distance to Ocean [Pixel]	Distance to Urban [Pixel]
Agriculture	< 100		-0.1 < X < 1							
Mixed Farm.	< 100		0 < X < 1			> 110				
Paddy (other)	< 60	< 2	-0.1 < X < 1			> 110				
Soil	< 220		< 0.2	> 1						
Gravel	< 15		< 0.2	> 1					135	
Sand	< 60		< 0.2	> 1						
Limestone	< 220		< 0.2	> 1		< 1335	< 1165			
Urban	< 60		< 0.5	> 0.8						
Urb. (dense)	< 25		< 0.1	> 1		465 < X < 1215	635 < Y < 1215			
Urb. (sparse)	< 60		< 0.5	> 0.8		> 110				
Urb. (destr.)	< 15		< 0.1	> 0.8		> 110			135	
Airport	15 < X < 25	< 2	-0.1 < X < 0.2	> 1		1500 < X < 1575	665 < Y < 865			
Vegetation			> 0							
Veg. (dense)			> 0	< 0.55						
Veg. (mixed)			> 0	0.55 < X < 0.9						
Veg. (sparse)			> 0	0.9 < X < 1.1						
Slash & Burn	> 20		> 0	> 1.1						
Park, sport	< 25		> 0			> 110				17
Waterbodies	< 60		< 0	0 < X < 1.4						
Ocean	< 10		< 0	0 < X < 1.4		< 1500		600		
River	< 60		< 0	0 < X < 1.4	0 < X < 1	> 190				
Flooding	< 10		< 0	0 < X < 1.4		< 1500			135	
Paddy (wet)	< 60	< 2	< 0	0 < X < 1.4		> 110				

Table 12.15: Knowledge-based rules of the object-based classification by using the first data set (ASTER and Envisat, Pixel size: 15 m)

12.9 Confusion Matrices of the Object-based approach with 17 classes

User \ Reference	AP	AM	UD	US	UR	UP	UA	SL	SS	SG	VD	VM	VS	VB	WO	WR	WF	Sum
Paddy	1858418	68266	30186	37336	2145	3263	1339	1299	1022	5313	5231	50679	54971	12365	1159	24862	57848	2286445
Mixed Farm.	17459	172643	1423	12352	257	7084	7	931	0	11	9781	76764	70514	2482	0	407	0	418936
Urb. (dense)	68164	3844	308768	72426	32189	1842	808	9378	4426	25179	289	1062	9770	1177	1223	8749	20254	407328
Urb. (sparse)	129184	5360	56701	241312	1393	430	0	971	187	2220	4558	10417	2289	310	72	1791	630	523192
Urb. (destr.)	50	96	6666	5119	30354	232	22	1664	6467	4949	0	0	1752	209	0	0	19	50774
Park	2607	5352	389	846	562	2670	251	154	76	2	21	254	18256	1577	0	15	0	45960
Airport	74024	144	3892	191	165	0	3765	591	26	5393	0	0	429	0	0	16	999	5305
Limestone	670	91	6406	3083	3775	311	23	5397	12922	2589	100	198	533	0	6	75	191	24045
Sand	252	172	988	2106	2891	49	24	2515	32470	227	7	369	1658	0	0	0	0	59652
Gravel	5619	116	25048	6604	20817	584	292	8096	2042	43314	0	39	1121	277	77	0	1	120268
Veg. (dense)	5801	22714	90	4675	0	0	0	0	0	0	351913	161596	944	40	0	5	0	699299
Veg. (mixed)	13071	111042	841	27611	0	331	0	47	0	0	278510	459092	33341	2020	0	84	21	811316
Veg. (sparse)	20450	21950	695	1676	1013	2797	188	457	351	96	130	4038	109026	26367	0	9	0	182767
Slash & Burn	16581	729	370	1098	845	208	271	56	260	179	4	915	20582	199391	0	0	0	232812
Ocean	0	0	0	0	0	0	0	0	0	0	0	0	0	0	6930516	7414	103334	7078061
River	2090	80	31	0	0	0	0	0	5	12	0	0	51	0	4528	63268	201953	175873
Flooding	11822	0	0	0	0	0	0	0	0	0	0	0	0	0	39379	38390	787263	950128
Unclassified	99	787	446	208	1459	3	0	78	435	25	14	3	57	0	334	590	785	17420
Sum	2226361	413386	442940	416643	97865	19804	6990	31634	60689	89509	650558	765426	325294	246215	6977294	145675	1173298	
Accuracy []																		
Producer	0.83473	0.41763	0.69709	0.57918	0.31016	0.13482	0.53863	0.17061	0.53501	0.48391	0.54094	0.59988	0.33516	0.80982	0.99330	0.43431	0.67098	
User	0.83875	0.46395	0.54213	0.52708	0.52699	0.08083	0.04200	0.14839	0.74254	0.37979	0.64244	0.49577	0.57611	0.82567	0.98427	0.23259	0.89783	
KIA Per Class	0.80389	0.40183	0.68433	0.56505	0.30733	0.13279	0.53567	0.16846	0.53358	0.47970	0.52237	0.57163	0.32611	0.80651	0.98660	0.42317	0.64915	
Overall	0.823																	
KIA	0.752																	

Table 12.16: Confusion Matrix of the object-based classification result with optical SPOT 5 data without additional knowledge-based information

Diploma Thesis: Landcover Mapping of Banda Aceh, Indonesia, using Optical and SAR Satellite Imagery

User \ Reference	AP	AM	UD	US	UR	UP	UA	SL	SS	SG	VD	VM	VS	VB	WO	WR	WF	Sum
Paddy	2018288	38809	32318	41552	2693	4295	1794	140	737	7867	4368	26749	40154	3822	542	12897	49420	2286445
Mixed Farm.	20535	193966	1644	15907	287	7224	28	1949	80	25	12140	90264	69254	4274	0	1336	23	418936
Urb. (dense)	3627	81	296314	37595	28103	416	0	0	8	19071	0	4	554	0	0	9014	12541	407328
Urb. (sparse)	117821	8686	74336	269602	5166	1268	399	3985	1778	5219	2355	8450	8208	1464	433	7698	6324	523192
Urb. (destr.)	5	39	5123	5139	27125	310	0	654	6558	5682	0	0	133	0	0	0	6	50774
Park	5625	7168	807	1940	2651	4046	458	62	552	64	26	278	22162	106	0	15	0	45960
Airport	978	0	0	0	0	0	3979	0	0	0	0	0	348	0	0	0	0	5305
Limestone	242	2	390	22	563	0	0	15655	6599	0	8	73	14	0	428	4	45	24045
Sand	575	12	3965	4564	4926	69	47	3812	39224	970	0	24	1375	83	0	0	6	59652
Gravel	4006	255	26184	6533	23395	770	0	3918	3286	49910	0	40	1321	0	384	154	112	120268
Veg. (dense)	5804	21456	0	873	0	0	0	0	0	0	480918	189536	598	0	0	114	0	699299
Veg. (mixed)	20782	124038	900	31491	0	337	0	138	0	56	150447	441409	40031	1203	35	387	62	811316
Veg. (sparse)	8276	16031	219	927	432	1066	14	346	5	132	247	7632	120998	26427	6	9	0	182767
Slash & Burn	316	1520	0	207	0	0	271	521	41	350	0	878	19883	208825	0	0	0	232812
Ocean	84	0	0	0	0	0	0	0	5	0	0	0	0	0	6932528	11396	134048	7078061
River	4131	123	29	0	0	0	0	0	0	54	0	0	33	0	973	59643	110887	175873
Flooding	12361	0	0	0	0	0	0	0	36	0	0	0	0	0	39709	40466	857556	950128
Unclassified	2905	1200	711	291	2524	3	0	454	1780	109	49	89	228	11	2256	2542	2268	17420
Sum	2226361	413386	442940	416643	97865	19804	6990	31634	60689	89509	650558	765426	325294	246215	6977294	145675	1173298	
Accuracy []																		
Producer	0.90654	0.46921	0.66897	0.64708	0.27717	0.20430	0.56924	0.49488	0.64631	0.55760	0.73924	0.57668	0.37197	0.84814	0.99358	0.40943	0.73089	
User	0.88272	0.46299	0.72746	0.51530	0.53423	0.08803	0.75005	0.65107	0.65755	0.41499	0.68771	0.54407	0.66203	0.89697	.979439	0.33913	0.90257	
KIA Per Class	0.88844	0.45295	0.65912	0.63347	0.27455	0.20170	0.56908	0.49402	0.64481	0.55379	0.72562	0.55082	0.36371	0.84559	0.98711	0.40196	0.71143	
Overall	0.853																	
KIA	0.793																	

Table 12.17: Confusion Matrix of the object-based classification result with optical SPOT 5 data with additional knowledge-based information

Diploma Thesis: Landcover Mapping of Banda Aceh, Indonesia, using Optical and SAR Satellite Imagery

User \ Reference	AP	AM	UD	US	UR	UP	UA	SL	SS	SG	VD	VM	VS	VB	WO	WR	WF	Sum
Paddy	1720640	34298	35070	30890	6806	1451	395	116	665	10407	6054	21743	17513	2095	0	7615	31881	1927639
Mixed Farm.	29109	125874	1254	11955	2147	5212	292	1401	16	264	10804	60357	58053	6229	49	2160	36	315212
Urb. (dense)	2447	134	283614	37954	17092	226	0	0	0	9298	0	4	181	0	0	8476	14975	374401
Urb. (sparse)	161742	10762	96104	282541	12791	1501	50	5336	1302	10951	2427	11124	7085	1700	381	9103	11039	625939
Urb. (destr.)	98	39	8004	5720	33441	490	0	1148	7907	11749	0	0	208	0	0	0	58	68862
Park	5521	26390	1256	2407	1516	5443	627	301	1828	209	67	3258	32156	221	0	4	0	81204
Airport	0	0	0	0	0	0	4189	0	0	0	0	0	519	0	0	0	0	4708
Limestone	589	0	500	129	1096	0	0	13084	8893	0	82	30	105	0	72	0	25	24605
Sand	613	249	3012	3306	8619	272	247	2052	33123	1917	0	20	1256	84	0	36	125	54931
Gravel	27925	455	7634	3073	9507	986	0	3348	2467	43394	0	29	1777	0	278	95	416	101384
Veg. (dense)	10493	22944	0	850	0	0	0	0	0	0	519325	221439	920	0	24	298	2597	778890
Veg. (mixed)	37730	160461	476	27513	7	746	0	199	0	46	111299	435824	43380	1517	35	753	36	820022
Veg. (sparse)	23312	29611	2537	8359	460	3399	177	705	176	237	429	10752	137596	25048	0	449	0	243247
Slash & Burn	965	1138	0	728	0	0	969	955	123	375	0	682	24252	209310	0	0	0	239497
Ocean	1047	0	0	0	0	0	0	0	58	0	0	0	18	0	5953136	32210	400002	6386471
River	9642	180	0	0	40	0	0	0	0	39	0	0	0	0	12548	53407	65433	141289
Flooding	3095	0	0	0	0	0	0	0	40	0	0	0	0	0	1000791	26783	593633	1624342
Unclassified	191393	851	3479	1218	4343	78	44	2989	4091	623	71	164	275	11	9980	4286	53042	276938
Sum	2226361	413386	442940	416643	97865	19804	6990	31634	60689	89509	650558	765426	325294	246215	6977294	145675	1173298	
Accuracy []																		
Producer	0.77285	0.30450	0.64030	0.67814	0.34171	0.27484	0.59928	0.41361	0.54578	0.48480	0.79828	0.56939	0.42299	0.85011	0.85322	0.36662	0.50595	
User	0.89262	0.39933	0.75751	0.45139	0.48562	0.06703	0.88976	0.53176	0.60299	0.42802	0.66675	0.53148	0.56566	0.87396	0.93215	0.37799	0.36546	
KIA Per Class	0.73685	0.28858	0.63048	0.66317	0.33840	0.27064	0.59915	0.41258	0.54400	0.48107	0.78647	0.54278	0.41285	0.84752	0.73152	0.36020	0.44157	
Overall	0.742																	
KIA	0.648																	

Table 12.18: Confusion Matrix of the object-based classification result with SPOT 5 by integrating global Radarsat information by using additional texture features

Diploma Thesis: Landcover Mapping of Banda Aceh, Indonesia, using Optical and SAR Satellite Imagery

User \ Reference	AP	AM	UD	US	UR	UP	UA	SL	SS	SG	VD	VM	VS	VB	WO	WR	WF	Sum
Paddy	2097276	34145	60087	99311	6726	3077	1580	239	575	8273	3792	21221	27753	2726	540	12762	54632	2434715
Mixed Farm.	23106	188683	3227	24987	1595	7551	42	2846	156	188	12387	96964	78494	4491	0	1818	43	446578
Urb. (dense)	2433	13	287875	37534	16847	377	0	0	0	10424	0	4	247	0	0	5579	9806	371139
Urb. (sparse)	35870	3703	48111	186297	232	397	14	931	0	754	1435	4918	1635	173	96	2268	2318	289152
Urb. (destr.)	5	39	6892	5109	28618	374	0	654	6490	7802	0	0	326	0	0	0	6	56315
Park	3505	5519	1385	4672	997	4415	769	140	294	4	43	225	19714	233	0	15	0	41930
Airport	0	0	0	0	0	0	4056	0	0	0	0	0	867	0	0	0	0	4923
Limestone	415	2	987	317	840	0	0	16668	7170	0	56	94	156	0	435	4	25	27169
Sand	693	286	4620	5429	6572	224	89	4327	40000	1630	0	36	1661	518	0	10	1	66096
Gravel	2270	515	26583	11325	31759	1149	0	4134	3476	58769	39	22	1836	0	216	437	982	143512
Veg. (dense)	8012	23189	0	810	0	0	0	0	0	0	517388	220495	893	0	0	399	0	771186
Veg. (mixed)	24899	135167	897	35292	0	448	0	121	0	56	115009	412147	37870	1599	44	580	62	764191
Veg. (sparse)	9958	18557	1277	4143	540	1779	79	385	27	299	356	8377	130196	26708	0	210	11	202902
Slash & Burn	371	1748	0	538	0	0	339	547	41	552	0	834	23239	209601	0	0	0	237810
Ocean	84	0	0	0	0	0	0	0	5	0	0	0	18	0	6932637	9729	122883	7065356
River	1357	181	4	0	25	0	0	0	0	270	0	0	33	0	885	63526	81663	147944
Flooding	13442	0	0	86	22	0	0	0	36	31	0	0	0	0	40001	44229	897601	995448
Unclassified	2665	1639	995	793	3092	13	22	642	2419	457	53	89	356	166	2440	4109	3265	23215
Sum	2226361	413386	442940	416643	97865	19804	6990	31634	60689	89509	650558	765426	325294	246215	6977294	145675	1173298	
Accuracy []																		
Producer	0.94202	0.45643	0.64992	0.44714	0.29242	0.22293	0.58026	0.52690	0.65909	0.65657	0.79530	0.53845	0.40024	0.85129	0.99360	0.43608	0.76502	
User	0.8614	0.42251	0.77565	0.64429	0.50818	0.10529	0.82389	0.61349	0.60518	0.40951	0.67090	0.53932	0.64167	0.88138	0.98122	0.42939	0.90171	
KIA Per Class	0.92991	0.43864	0.64045	0.43555	0.28958	0.22062	0.58011	0.52599	0.65749	0.65304	0.78345	0.51199	0.39148	0.84874	0.98716	0.43010	0.74716	
Overall	0.857																	
KIA	0.779																	

Table 12.19: Confusion Matrix of the object-based classification result with SPOT 5 by integrating local Radarsat information by using additional texture features

Diploma Thesis: Landcover Mapping of Banda Aceh, Indonesia, using Optical and SAR Satellite Imagery

User \ Reference	AP	AM	UD	US	UR	UP	UA	SL	SS	SG	VD	VM	VS	VB	WO	WR	WF	Sum
Paddy	188761	5512	1291	10945	478	152	72	29	439	489	6133	10059	2110	193	141	2086	4548	233438
Mixed Farm.	8816	18107	326	4226	31	656	19	297	34	50	5018	17350	9752	4457	3	386	20	69548
Urb. (dense)	44	11	31561	3218	664	165	0	0	3	869	0	9	4	0	0	127	37	36712
Urb. (sparse)	18017	1250	10340	22337	727	348	159	496	385	1365	178	390	2460	628	316	2817	1902	64115
Urb. (destr.)	103	5	708	550	3991	21	0	49	1565	1384	2	12	131	0	20	15	94	8650
Park	533	137	667	803	0	514	50	13	78	1	3	26	483	0	0	3	0	3311
Airport	0	0	0	0	0	0	422	0	0	0	0	0	471	0	0	0	0	893
Limestone	3	6	18	44	20	0	0	1004	77	0	0	7	6	0	9	0	0	1194
Sand	5	6	272	292	770	5	3	635	2261	404	6	40	111	80	0	15	22	4927
Gravel	105	42	3475	2197	3412	72	0	359	1109	4845	0	4	127	0	19	408	410	16584
Veg. (dense)	8329	4644	0	96	0	4	0	7	0	0	47410	24920	693	3	30	131	5	86272
Veg. (mixed)	13782	12615	5	676	0	7	0	91	0	1	13014	29605	3209	116	10	195	11	73337
Veg. (sparse)	1701	3426	100	670	334	256	18	247	408	75	543	2450	14594	2647	0	85	0	27554
Slash & Burn	127	19	0	0	0	0	33	36	0	0	1	108	1139	19202	0	0	0	20665
Ocean	1570	0	1	0	0	0	0	0	1	26	1	0	0	0	769023	2305	22930	795857
River	3452	124	171	201	321	0	0	42	61	273	5	11	23	1	237	3768	5513	14203
Flooding	1885	6	4	0	22	0	0	0	95	30	13	7	2	0	6604	3613	93777	106058
Unclassified	122	54	347	92	64	7	2	218	242	133	55	46	845	31	757	232	1238	4485
Sum	247355	45964	49286	46347	10834	2207	778	3523	6758	9945	72382	85044	36160	27358	777169	16186	130507	
Accuracy []																		
Producer	0.76312	0.39394	0.64036	0.48195	0.368378	0.23289	0.54242	0.28498	0.33457	0.48718	0.65499	0.34811	0.40359	0.70188	0.98952	0.23279	0.71856	
User	0.80861	0.26035	0.85969	0.34839	0.46139	0.15524	0.47256	0.84087	0.45890	0.29215	0.54954	0.40368	0.52965	0.92920	0.96628	0.26530	0.88420	
KIA Per Class	0.72168	0.36581	0.63174	0.45986	0.36487	0.23127	0.54216	0.28444	0.33247	0.48170	0.63491	0.31612	0.39293	0.69790	0.97871	0.22578	0.69814	
Overall	0.798																	
KIA	0.716																	

Table 12.20: Confusion Matrix of the object-based classification result with optical ASTER data by using additional knowledge-based information

Diploma Thesis: Landcover Mapping of Banda Aceh, Indonesia, using Optical and SAR Satellite Imagery

User \ Reference	AP	AM	UD	US	UR	UP	UA	SL	SS	SG	VD	VM	VS	VB	WO	WR	WF	Sum
Paddy	153521	8481	1786	7336	447	380	160	40	271	565	6887	10022	5467	557	1	1061	640	197622
Mixed Farm.	20618	14361	822	7362	230	617	25	273	129	131	8557	19994	8511	7194	0	221	35	89080
Urb. (dense)	55	6	26606	4851	477	103	0	0	53	769	1	0	27	0	0	186	114	33248
Urb. (sparse)	3411	614	10825	17070	570	256	6	515	181	630	360	1374	702	178	424	1125	2584	40825
Urb. (destr.)	283	56	789	843	4439	37	0	288	2108	2317	7	20	441	0	83	287	955	12953
Park	926	640	796	2607	0	362	38	13	29	15	282	576	433	0	0	134	2	6853
Airport	10	0	0	0	0	0	468	0	0	0	0	0	447	0	0	0	0	925
Limestone	8	13	46	38	75	0	0	1087	194	0	0	37	18	18	25	0	0	1559
Sand	90	14	1507	904	1095	45	15	369	1247	905	2	19	207	195	8	89	142	6853
Gravel	62	70	3192	921	2709	67	0	246	1049	3534	0	10	275	0	9	601	959	13704
Veg. (dense)	13270	5574	3	190	0	8	0	21	0	0	45139	26074	909	26	13	133	3	91363
Veg. (mixed)	21147	11938	46	1311	0	32	0	67	0	4	10288	23433	3151	101	1	103	10	71632
Veg. (sparse)	4554	3374	244	1697	72	268	21	110	162	77	499	2761	13185	3138	0	109	2	30273
Slash & Burn	537	42	0	9	0	0	20	27	0	9	0	101	1102	15816	0	0	0	17663
Ocean	4467	32	31	8	119	0	0	7	91	148	6	4	7	0	763724	4037	46476	819157
River	2209	162	91	132	163	1	0	68	101	313	11	10	40	58	109	3890	4226	11584
Flooding	6297	17	5	21	121	0	0	1	210	107	9	6	14	0	11888	2400	65372	86468
Unclassified	15890	570	2497	1047	317	31	25	391	933	421	334	603	1224	77	884	1810	8987	36041
Sum	247355	45964	49286	46347	10834	2207	778	3523	6758	9945	72382	85044	36160	27358	777169	16186	130507	
Accuracy []																		
Producer	0.62065	0.31244	0.53983	0.36831	0.40973	0.16402	0.60154	0.30854	0.18452	0.35535	0.62362	0.27554	0.36463	0.57811	0.98270	0.24033	0.50091	
User	0.77684	0.16121	0.80023	0.41813	0.34270	0.05282	0.50595	0.69724	0.18196	0.25788	0.49406	0.32713	0.43554	0.89543	0.93233	0.33581	0.75603	
KIA Per Class	0.56594	0.27102	0.52986	0.35142	0.40481	0.16035	0.60131	0.30786	0.18094	0.34967	0.60033	0.24085	0.35212	0.57331	0.96377	0.23468	0.47178	
Overall	0.736																	
KIA	0.626																	

Table 12.21: Confusion Matrix of the object-based classification result with ASTER by integrating global Envisat information by using additional texture features

Diploma Thesis: Landcover Mapping of Banda Aceh, Indonesia, using Optical and SAR Satellite Imagery

User \ Reference	AP	AM	UD	US	UR	UP	UA	SL	SS	SG	VD	VM	VS	VB	WO	WR	WF	Sum
Paddy	172351	5210	1358	6828	263	138	82	36	200	396	4812	7262	2600	351	1	1128	659	203675
Mixed Farm.	14199	19007	724	6636	96	767	24	286	89	95	7146	18673	10344	4179	8	639	38	82950
Urb. (dense)	29	5	26565	4273	327	157	0	0	31	576	0	2	43	0	0	65	48	32121
Urb. (sparse)	5305	381	12366	20873	673	336	41	438	218	1113	337	979	699	501	259	902	1007	46428
Urb. (destr.)	99	19	671	681	4272	13	0	65	1799	1263	4	20	225	0	43	42	288	9504
Park	630	217	842	2097	1	455	43	7	27	15	108	214	366	38	0	7	2	5069
Airport	0	0	0	0	0	0	510	0	0	0	0	0	782	0	0	0	0	1292
Limestone	5	3	38	53	59	0	0	1073	197	0	6	12	17	0	9	0	3	1475
Sand	32	3	800	556	981	27	3	543	1922	763	2	38	120	84	5	27	51	5957
Gravel	119	116	2909	818	3324	33	0	436	1232	4906	2	13	241	0	18	834	916	15917
Veg. (dense)	7193	4369	2	100	0	4	0	11	0	0	45585	25510	856	26	17	71	2	83746
Veg. (mixed)	13828	12646	14	917	0	13	0	82	0	2	13653	29187	3056	71	12	109	11	73601
Veg. (sparse)	2779	3643	267	1415	218	227	18	153	229	112	430	2510	14511	2781	0	155	8	29456
Slash & Burn	128	19	0	6	0	0	35	18	0	9	0	117	1078	19259	0	2	0	20671
Ocean	1580	26	4	0	5	0	0	0	11	24	5	3	2	0	763876	2889	25873	794298
River	2292	179	75	100	157	2	3	30	49	242	7	7	33	0	159	4254	5357	12946
Flooding	3247	14	10	2	38	0	0	0	126	49	2	13	1	0	11732	3847	91488	110569
Unclassified	23539	107	2641	992	420	35	19	345	628	380	283	484	1186	68	1030	1215	4756	38128
Sum	247355	45964	49286	46347	10834	2207	778	3523	6758	9945	72382	85044	36160	27358	777169	16186	130507	
Accuracy []																		
Producer	0.69678	0.41352	0.53899	0.45036	0.39431	0.20616	0.65553	0.30457	0.28440	0.49331	0.62978	0.34319	0.40130	0.70396	0.98289	0.26282	0.70102	
User	0.84621	0.22914	0.82703	0.44958	0.44949	0.08976	0.39474	0.72746	0.32265	0.30822	0.54432	0.39656	0.49263	0.93169	0.96170	0.32860	0.82743	
KIA Per Class	0.65150	0.38076	0.52935	0.43359	0.39062	0.20359	0.65524	0.30392	0.28167	0.48812	0.60889	0.31085	0.38984	0.70001	0.96533	0.25668	0.67833	
Overall	0.778																	
KIA	0.689																	

Table 12.22: Confusion Matrix of the object-based classification result with ASTER by integrating global Envisat information without additional texture features